Segregating the Singular

Unraveling organelle division in malaria parasites

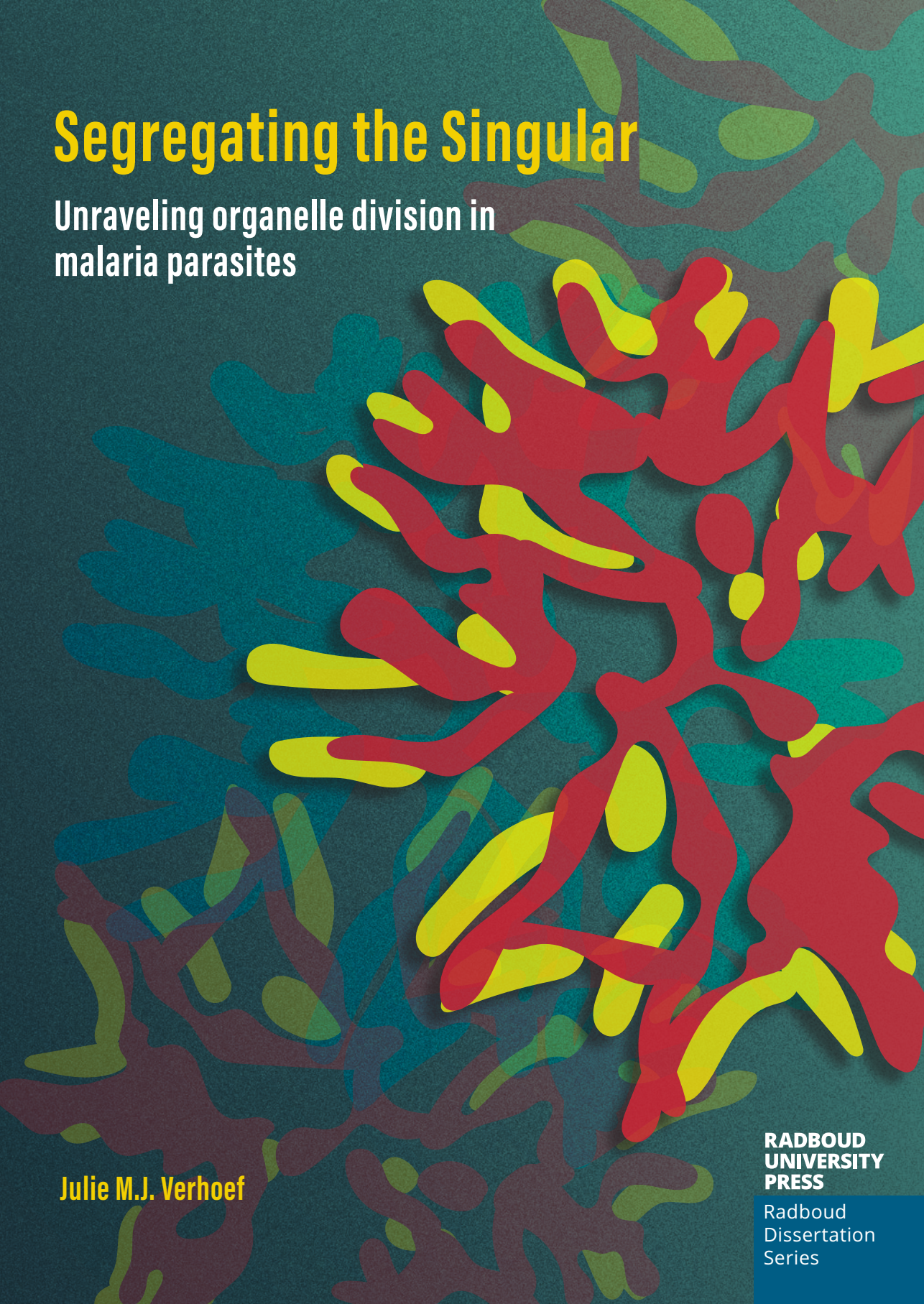

Julie M.J. Verhoef

RADBOUD UNIVERSITY PRESS

Radboud Dissertation Series

Segregating the Singular

Unraveling organelle division in malaria parasites

Julie M.J. Verhoef

Author: Julie M.J. Verhoef
Title: Segregating the Singular: Unraveling organelle division in malaria parasites

Radboud Dissertations Series
ISSN: 2950-2772 (Online); 2950-2780 (Print)

Published by RADBOUD UNIVERSITY PRESS
Postbus 9100, 6500 HA Nijmegen, The Netherlands
www.radbouduniversitypress.nl

Design: Proefschrift AIO | Annelies Lips
Cover: Proefschrift AIO | Guntra Laivacuma
Printing: DPN Rikken/Pumbo

ISBN: 9789493296893
DOI: 10.54195/9789493296893
Free download at: www.boekenbestellen.nl/radboud-university-press/dissertations

RADBOUD
UNIVERSITY
PRESS

Segregating the Singular
Unraveling organelle division in malaria parasites

Proefschrift ter verkrijging van de graad van doctor
aan de Radboud Universiteit Nijmegen
op gezag van de rector magnificus prof. dr. J.M. Sanders,
volgens besluit van het college voor promoties
in het openbaar te verdedigen op

dinsdag 11 februari 2025
om 14.30 uur precies

door

Julie Mily Jansje Verhoef
geboren op 30 april 1996
te Eindhoven

Promotor:
Prof. dr. J.T. Bousema

Copromotor:
Dr. T.W.A. Kooij

Manuscriptcommissie:
Prof. dr. A. Cambi
Prof. dr. B. Striepen (University of Pennsylvania, Verenigde Staten)
Dr. S. Absalon (Indiana University, Verenigde Staten)

Segregating the Singular
Unraveling organelle division in malaria parasites

Dissertation to obtain the degree of doctor
from Radboud University Nijmegen
on the authority of the Rector Magnificus prof. dr. J.M. Sanders,
according to the decision of the Doctorate Board
to be defended in public on

Tuesday, February 11, 2025
at 2.30 pm

by

Julie Mily Jansje Verhoef
born on April 30, 1996
in Eindhoven (the Netherlands)

Supervisor:
Prof. dr. J.T. Bousema

Co-supervisor:
Dr. T.W.A. Kooij

Manuscript Committee:
Prof. dr. A. Cambi
Prof. dr. B. Striepen (University of Pennsylvania, United States)
Dr. S. Absalon (Indiana University, United States)

Table of Contents

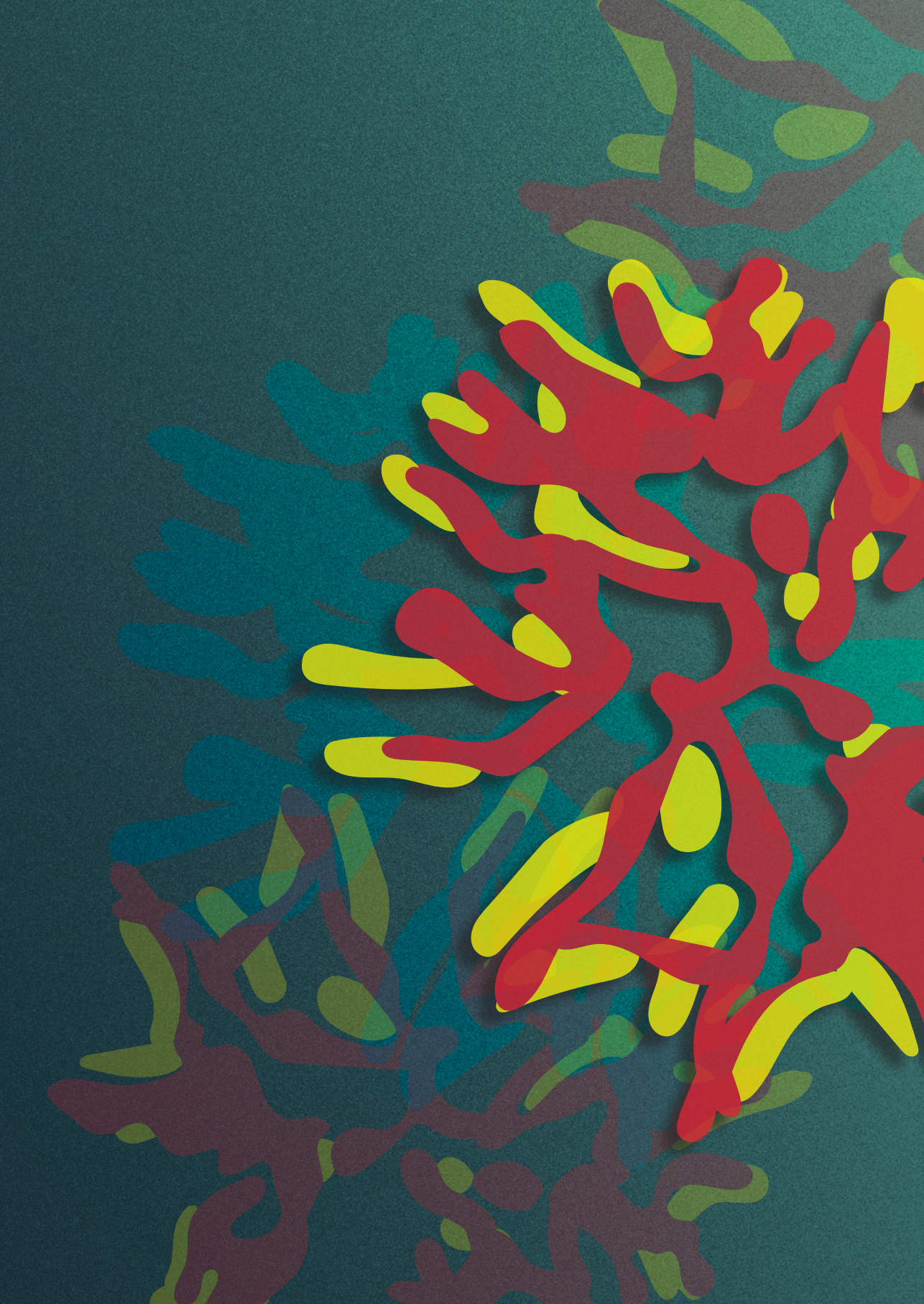

Chapter 1

Introduction

The global malaria burden

Malaria is a devastating parasitic disease caused by a unicellular eukaryote of the *Plasmodium* genus. Nearly half of the world's population lives in areas where there is risk of malaria infection[1]. In 2022, there were an estimated 249 million malaria cases and 608,000 deaths, mostly in children under 5 years old[2]. A disproportionately large part of the global malaria burden falls on African countries, with 94% of all cases and 95% of deaths. There are five *Plasmodium* species that commonly infect humans, namely *P. falciparum*, *P. vivax*, *P. ovale*, *P. malariae*, and *P. knowlesi*. *P. falciparum* and *P. vivax* are responsible for the majority of the malaria morbidity and mortality. While *P. falciparum* is dominant in sub-Saharan Africa and New Guinea, *P. vivax* is widely spread in South-East-Asia and the Americas[2].

The *Plasmodium* life cycle

Plasmodium parasites have a complex life cycle that includes invasion of different hosts and different cell types within the host (Figure 1). When an infected mosquito bites the human skin, parasites known as sporozoites are injected with the mosquito's saliva[3]. Motile sporozoites migrate actively to the blood and are transported to the liver. Here, the sporozoites invade hepatocytes, where they expand, proliferate and form tens of thousands of daughter merozoites in a single infected cell over a ~7 day period for *P. falciparum*. The merozoites are formed within a meroblasts, sub compartments created by large parasite membrane invaginations, in which 10 to 1000 merozoites are formed synchronously by budding[4,5]. When merozoites are fully formed, they are released into the blood where they will invade red blood cells (RBCs). *P. vivax* and *P. ovale* can form dormant liver-stage hypnozoites, which can persist for months or years and can eventually activate to re-establish a blood-stage infection[6]. A merozoite enters a RBC through a complex, multi-step invasion process[7]. Here, the parasite replicates in a 48-hour asexual replication cycle, progressing through three morphologically distinct stages: ring, trophozoite and schizont. Up to 40 merozoites are formed within a single schizont, which egress from their host cell into the blood stream to invade new RBCs. While liver-stage infection is clinically silent, the exponential growth of asexual blood-stage parasites causes clinical pathogenesis. The parasite derives energy from anaerobic glycolysis of host glucose to lactic acid, which can lead to hypoglycemia and lactic acidosis[8]. Anemia is caused by the sequestration of infected and uninfected RBCs, clearance by the spleen, and destruction of RBCs due

to parasite egress[9]. Sequestration of infected RBCs in the brain capillaries can cause brain microthrombi and brain swelling, leading to cerebral malaria.

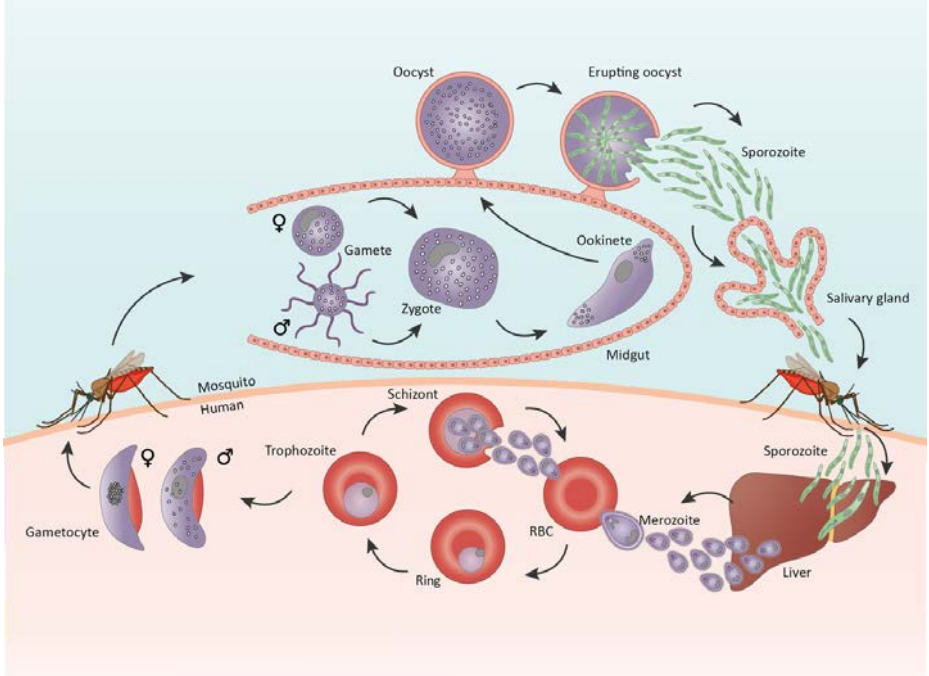

Figure 1. *Plasmodium falciparum* life cycle (with permission adapted from Inklaar et al.[17]). Sporozoites enter the skin through a mosquito bite, where they actively migrate to a blood vessel. Parasites travel through the blood to the liver, where they traverse and invade hepatocytes. Here, parasites expand and proliferate, forming thousands of daughter merozoites within an infected cell. When fully matured, merozoites are released into the blood, where they invade red blood cells (RBCs). The parasite replicates asexually within a 48-hour cycle, going through ring, trophozoite and schizont stages. During schizogony, daughter merozoites are formed and released from the host cell to invade new RBCs. Some parasites differentiate in the transmissible, sexual-stage gametocytes. When taken up by a bloodmeal of the mosquito, gametocytes become activated and the male microgametes fertilize the female macrogamete. The fertilized zygote develops into a motile ookinete stage, which traverses the mosquito midgut and settles to form an oocyst. Within the oocysts, thousands of sporozoites are formed. These sporozoites are released after full maturation, traveling to the mosquito salivary glands, where they can be injected into a new human with the next blood meal.

While asexual blood-stage parasites are unable to transmit to mosquitoes, a small proportion of parasites differentiate into non-replicating sexual-stage parasites, called gametocytes. Within a ~12-day period, *P. falciparum* gametocytes develop from stage I to mature stage V males and females[10]. Immature gametocytes sequester in the bone marrow and spleen, while mature gametocytes circulate

in the blood for approximately three weeks[11,12]. These gametocytes can be taken up by blood-feeding mosquitoes and transmit to their second host. Gametocytes become activated in the mosquito midgut by a drop in temperature, change in pH, and presence of the mosquito-derived xanthurenic acid[13,14]. While the activated female macrogamete rounds up, the male undergoes three rounds of rapid nuclear replication and produces eight flagellated microgametes in a 15-minute process called exflagellation[15]. The microgametes fertilize the female macrogamete, forming a diploid zygote. The zygote develops into a motile ookinete which crosses the midgut epithelium and enters the basal lamina. Here it settles to form an immotile oocyst. The oocyst undergoes growth and replication to produce thousands of sporozoites over a 10–12-day period[16]. When fully matured, sporozoites are released from the oocyst and travel via the hemolymph to the salivary glands. The mosquito can then inject sporozoites into the skin when taking a new blood meal, repeating the life cycle.

Challenges in malaria elimination

Major progress has been made in the fight against malaria since the beginning of the millennium. Between 2000 and 2014, there was an overall decrease in number of global malaria cases from 243 to 230 million[2]. Following this success, the Global Technical Strategy (GTS) has set the ambitious goal of a reduction of 90% in malaria incidence and mortality, and elimination in at least 35 countries by 2030[18]. However, in 2015-2019 the malaria incidence and number of deaths plateaued[2]. In 2020, there was a large increase in malaria cases (244 million), mainly due to disrupted services during the COVID-19 pandemic. If this current trajectory continues, it is highly unlikely that global targets will be achieved. Therefore, there is an urgent need to accelerate malaria elimination. However, there are several major hurdles in achieving malaria eradication.

Insecticide resistance

Malaria elimination programs rely heavily on vector control strategies, such as insecticide-treated nets (ITNs) and indoor residual praying (IRS). Modelling suggests that 75% of the decrease in malaria incidence from 2000 to 2015 can be attributed to these vector control strategies[2]. However, since the first report of insecticide resistance in the *Anopheles* mosquito in 1950, insecticide resistance has spread rapidly across numerous malaria-endemic regions, undermining the efficacy of these crucial malaria control strategies[19]. Out of the 88 malaria endemic countries, 78 countries have detected resistance to at least one class of insecticide and 19

countries have confirmed resistance to all four classes of insecticides in at least one site[2]. There are two primary mechanisms responsible for insecticide resistance: increased metabolic detoxification of insecticides, caused by gene overexpression or amplification, and structural mutation of detoxification enzymes, such as P450[20,21]; and decreased sensitivity of target proteins, such as sodium channels and GABA receptors, through structural mutations[21–23]. Strategies that could prevent the further spread of insecticide resistance include: development of new insecticides with novel modes of action; agreements between public health and agricultural sectors to rotationally use insecticides to avoid resistance; and development of resistance detection markers that could detect early stages of resistance when it could be managed more easily[24].

Vaccine development

One of the main challenges in malaria elimination is the difficulty in development of efficacious vaccines. Vaccination is one of the most cost-effective health interventions[25]. However, different vaccination strategies, including pre-erythrocytic, blood-stage, and transmission blocking vaccines have resulted in limited success in clinical trials[26]. The currently two approved malaria vaccines target the clinically silent pre-erythrocytic stage and are based on a fragment of the surface circumsporozoite protein (CSP). RTS,S/AS01 has been recommended by the WHO since October 2021 and is currently been rolled out in 12 African countries[2]. Although vaccine efficacy wanes over time[27], WHO estimates a reduction of 30% severe malaria cases in vaccinated children[28]. Since October 2023, the R21/Matrix-M vaccine became the second WHO recommended vaccine, which uses an additional adjuvant and has a promising efficacy of >70% [29]. The effects of implementing both vaccines in malaria-endemic countries remains to be seen.

The effect of climate change on malaria transmission

The WHO has declared climate change as the single biggest health threat facing humanity[30,31]. The consequences of climate change affect mostly low-income countries where malaria remains a large threat, but proportionally contribute the least to climate change. Temperature, rainfall and humidity influence mosquito survival, larval development, parasite development, and vector competence[32–37]. Therefore, changes in climate can greatly affect malaria transmission. Extreme weather events, such as flooding, can result in malaria epidemics, while severe droughts can suppress transmission. Although the exact consequences are hard to predict, there is more and more evidence that climate change will cause the further spread of malaria. For example, in the African highlands increased temperature has led to the expansion of malaria and extreme monsoon rainfall in Pakistan caused

flooding and a large malaria epidemic[38,39]. Other consequences of climate change, such as economic insecurity, food scarcity, or decreased availability of drinking water could have a more indirect effect on malaria because of decreased access to health care and increased cost and difficulties of malaria elimination programs[2]. It is therefore more important than ever to have the right toolbox at hand for malaria elimination and ensure sustainable and resilient malaria responses in the face of climate change.

Resistance to current anti-malarial drugs

Since the discovery of the first synthetic antimalarial drug chloroquine in the 1940s, a recurring pattern has emerged of drug development, wide implementation, and the emergence of resistance. Trying to prevent the spread of chloroquine-resistance, sulfadoxine/pyrimethamine replaced chloroquine as first line treatment in the 1970s. Nevertheless, chloroquine-resistant parasites spread to Africa in the 1980s, causing a dramatic rise in malaria deaths[40]. Sulfadoxine/pyrimethamine resistance was also quick to emerge, becoming widespread in many malaria-endemic regions by the early 2000s[41]. Subsequently, combination therapy, such as artemisinin combination therapy (ACT), has become the prominent treatment strategy to reduce the risk of resistance. ACT was introduced as the first-line treatment for malaria in the early 2000s and played a crucial role in reducing malaria cases between 2000 and 2015[2,42]. Artemisinin, a key component of ACTs, acts rapidly through activation by Fe^{2+}-heme and presumably causing alkylation of heme, proteins, and lipids, thereby causing oxidative stress and cellular damage[43]. However, due to its rapid metabolization, a long-lasting partner drug is required to ensure complete parasite clearance[44]. Despite the success of ACTs, partial resistance to artemisinin has emerged in Asia and several African countries, resulting in slower parasite clearance from the bloodstream[2,44–47]. Mutations in the gene encoding for Kelch-like protein 13 (*kelch13*) have been associated with slower clearance by artemisinin and ACTs[48–50]. Emerging resistance to ACT partner drugs has led to ACT treatment failures in the Greater Mekong subregion[2,51]. The increasing threat of the spread of drug resistance underscores the urgent need for improved treatment strategies and the development of new antimalarial compounds with novel modes of action.

Two endosymbiotic organelles as promising drug targets

A novel antimalarial drug must be highly effective, safe, well-tolerated, and ideally feature a unique mechanism of action to prevent resistance. To minimize adverse

reactions, the drug target should be parasite-specific and absent in the host. *Plasmodium* parasites possess two distinctive organelles of endosymbiotic origin, the mitochondrion and the apicoplast, which serve as promising drug targets. Both organelles contain their own genomes. The mitochondrion is believed to have a monophyletic origin, tracing back to a common ancestor shared with alpha-proteobacteria, indicating a single evolutionary event in eukaryotic history[52]. Despite this common ancestry, mitochondrial evolution has resulted in significant variation in their genomes, regulation, and function across species, reflecting adaptations to host-specific needs. Consequently, the *Plasmodium* mitochondrion is highly different from its human host counterpart on a molecular and functional level[53]. The apicoplast, on the other hand, is a non-photosynthetic plastid organelle unique to intracellular parasites of the phylum Apicomplexa, acquired through secondary endosymbiosis of a red alga that had previously engulfed a cyanobacterium[54]. The prokaryotic origins of both organelles, the absence of the apicoplast in the human host, and the high divergence of the mitochondrion make them attractive targets for parasite-specific drug development. Their distinct origins and functionalities present unique opportunities for targeted interventions.

Mitochondrion

It has become clear that the *Plasmodium* mitochondrion differs greatly from the well-described mitochondrion of its human host. The *Plasmodium* parasite mitochondrion harbors a unique, minimalistic mitochondrial DNA (mtDNA) of 6 kb encoding for only three proteins (COX1, COX3 and CYTB) and scrambled fragments of ribosomal RNA[55]. These proteins are all components of the electron transport chain (ECT), which is highly important for ATP production in other model eukaryotes. However, asexual blood-stage *P. falciparum* parasites rely heavily on cytoplasmic glycolysis for their ATP production and the ECT is merely required for ubiquinone recycling to sustain *de novo* pyrimidine biosynthesis[56]. Interestingly, the parasite mitochondrion in asexual blood stages (ABS) lacks the inner mitochondrial membrane (IMM) folds where ECT and ATP synthase complexes normally accumulate, also known as cristae[57]. Sexual blood-stage parasites on the other hand do have cristae and a high abundance of ECT complexes. Metabolomic approaches show a shift in carbon metabolism in gametocytes from glycolysis to increased tricarboxylic acid (TCA) cycle activity[58,59]. Mitochondrial respiration is essential for male gametogenesis and mosquito stage transmission, as shown by existing antimalarials targeting mitochondrial energy metabolism[60–62]. The ECT in *P. falciparum* is highly different from the pathway in its human host[57] (Figure 2). For example, parasites lack a canonical complex I and compensate this activity by a bacterial-like type II NADH, ubiquinone oxidoreductase[63]. It is therefore

not surprising that the ECT is a validated drug target of several anti-malarial compounds. Atovaquone is the first clinically approved drug targeting the parasites mitochondrion by acting as a ubiquinone analogue, targeting the cytochrome bc1 complex of the ECT[64,65]. Although atovaquone is a highly potent anti-malarial, resistance is quick to arise when used as a monotherapy[66]. Therefore, atovaquone is often used in the synergistic combination with proguanil in the form of Malarone for malaria treatment[67]. Other set of compounds targeting the cytochrome bc1 complex are endochin-like quinolones (ELQs)[68]. One of these, ELQ-331, has now been selected as a clinical candidate[69]. Another interesting mitochondrial drug target is DHODH, a mitochondrial enzyme that is critical in the pyrimidine biosynthesis pathway[56]. DSM265 is a promising drug with multistage, single dose efficacy, targeting DHODH and is now in clinical development[70,71]. Similarly to atovaquone, resistance to DHODH inhibitors arises quickly and they will therefore require partner drugs to reduce risk of the spread of resistance[72].

The *Plasmodium* mitochondrion houses several metabolic pathways that are crucial for parasite survival, including iron-sulphur cluster synthesis, cardiolipin synthesis, mtDNA replication, etc. Some metabolic pathways that are present in the mitochondria of other well-described model organisms, such as steroid biosynthesis and β-oxidation of fatty acids and portions of amino acids, are not present in *Plasmodium* mitochondria[53]. Other pathways, such as ubiquinone biosynthesis and heme biosynthesis, are shared between the mitochondrion and the apicoplast in *Plasmodium* parasites.

Apicoplast

In the 1970s, scientists used electron microscopy to study apicomplexan parasites and found a unique organelle that was different from the mitochondrion[73]. Several decades later it was confirmed that this organelle was a plastid harboring its own 35 kb circular genome and the "apicoplast" was born[74–76]. The apicoplast genome retains genes necessary for its function and maintenance. This includes genes encoding for a complete set of ribosomal RNAs and transfer RNAs, transcription and translational machinery, and metabolic enzymes[74]. Due to the prokaryotic-like gene expression in the apicoplast, antibiotics targeting DNA replication, transcription, and translation in bacteria also kill *Plasmodium* parasites[77,78]. Parasites treated with apicoplast-targeting drugs produce viable merozoites that can infect new RBCs. However, these newly infected parasites fail to divide and produce daughter cells[79,80]. This is referred to as the 'delayed death' phenomenon.

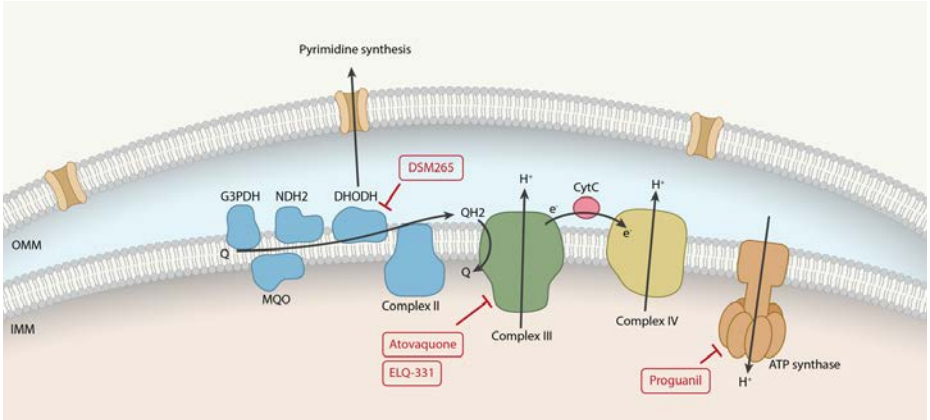

Figure 2. Mitochondrial electron transport chain (ECT) with associated drug targets. Schematic representation of the ECT and the inner- and outer mitochondrial membranes (IMM, OMM, respectively). Drugs targeting respiratory chain proteins are shown in red. Reduced ubiquinone (QH_2) is generated by five dehydrogenases: glycerol-3-phosphate dehydrogenase (G3PDH), malate:quinone oxidoreductase (MQO), type II NADH:quinone oxidoreductase (NDH2) dihydroorotate dehydrogenase (DHODH) and succinate dehydrogenase, also known as complex II. DHODH is essential for pyrimidine synthesis and is inhibited by DSM265. QH_2 is oxidized by complex III, which is inhibited by atovaquone and ELQ-331. Electrons are transferred from complex III to cytochrome C, which is oxidized by complex IV. Complex III and complex IV both pump protons into the intermembrane space, generating a proton gradient. ATP synthase normally uses the proton gradient to generate ATP from ADP, although this process is not a significant ATP source in ABS. ATP synthase can also work in reverse, hydrolyzing ATP to pump protons, which might be the target of proguanil.

The apicoplast houses four important metabolic pathways, including biosynthesis of fatty acid, isoprenoid, heme, and Fe-S clusters[78,81]. Unlike the type-I fatty acid synthesis pathway in humans, the fatty acid synthesis pathway in the *Plasmodium* apicoplast employs a bacterial-like type II fatty acid synthase enzyme[82]. Antibiotics, such as thiolactomycin target this pathway and kill *Plasmodium* parasites. Heme is used by the parasite as a prosthetic group for cytochromes and can be derived from hemoglobin, as well as *de novo* biosynthesis. During mosquito and liver stages, biosynthesis of heme is essential and can be targeted by succinylacetone[83]. The isoprenoid biosynthesis pathway is also an attractive drug target, as it has greatly diverged from the human counterpart[84]. The antibiotic fosmidomycin targets this pathway and is used in clinical setting as an adjuvant drug in combination with other antimalarials[85]. Parasites treated with fosmidomycin can be chemically rescued by supplementation of isopentenyl pyrophosphate (IPP), an isoprenoid precursor[86]. Parasites cultured under these conditions lose their apicoplast genome and protein import function, while still being able to grow indefinitely, highlighting the importance of this pathway for parasite survival.

Mitochondrion and apicoplast division during parasite replication

Malaria parasites have a complicated life cycle, during which three different proliferation stages occur to generate haploid daughter parasites. In the 48-h intraerythrocytic replication cycle, *P. falciparum* parasites replicate through a process called schizogony. During this process, asynchronous nuclear division results in a nongeometric nuclear expansion, followed by a final round of division and the simultaneous segmentation of up to 40 daughter merozoites[87]. The second stage of proliferation occurs in the mosquito vector. Several thousands of sporozoites are formed within a single oocyst in a process called sporogony. Parasite proliferation occurs through endopolygeny-like replication where multiple rounds of DNA replication are followed by internal budding[88]. The last proliferation stage occurs in the liver, where up to 90,000 daughter merozoites are generated from a single sporozoite. Liver-stage parasites replicate through schizogony which is similar to schizogony in the ABS, but on a much larger scale[89]. The final round of nuclear division and merozoite segmentation happens in sub compartments created by large membrane invaginations[5].

In contrast to human cells, which can contain hundreds of mitochondria per cell, *Plasmodium* parasites possess only a singular mitochondrion and apicoplast. Ensuring the precise division and segregation of these essential organelles to each daughter cell is crucial for parasite survival. This organelle division process diverges greatly from binary division in the human host, where hundreds of mitochondria are divided and distributed over two daughter cells. In *Plasmodium* parasites, a single mitochondrion and apicoplast need to be divided over tens, to tens of thousands of daughter cells in a highly orchestrated manner. However, very little is known about how this process happens in detail, and which proteins are involved.

Objectives and outline of this thesis

The malaria parasite harbors two unique endosymbiotic organelles, that are crucial for the parasite and form an attractive drug target. Division and segregation of these single organelles is crucial for parasite survival, but poorly understood. The main aim of the studies in this thesis is to further investigate the processes of mitochondrial and apicoplast division and distribution in the *P. falciparum* parasite and to identify key proteins involved in this process.

In **chapter 2: Organelle dynamics in apicomplexan parasite**, an extensive overview of our current understanding of organelle dynamics and molecular mechanisms underlying organelle division is given. Organelle dynamics in two important apicomplexan parasites, *Toxoplasma gondii* and *P. falciparum*, are described in detail with a clear focus on the mitochondrion and apicoplast. Molecular mechanisms underlying organelle division and distribution in model organisms are discussed and current knowledge of these mechanisms in apicomplexan parasites is summarized. Knowledge gaps in this process in *P. falciparum* are discussed, hypotheses regarding potential fission scenarios are formulated, and new potential division proteins are proposed for future examination.

In **chapter 3: Detailing organelle division and segregation in *P. falciparum***, several advanced imaging approaches were used to capture mitochondrial and apicoplast division during schizogony in ABS. A parasite line harboring a novel mitochondrial marker was generated and used to capture mitochondrial dynamics throughout the *Plasmodium* life cycle. High-resolution fluorescent imaging and focused ion-beam scanning electron microscopy (FIB-SEM) approaches were used to visualize mitochondrial and apicoplast division steps. The extremely close interaction and sequential division of these organelles were described and the role of centriolar plaques (centrosome equivalent in *P. falciparum*) in apicoplast segregation were highlighted. These findings are summarized in a new, detailed model for mitochondrial and apicoplast division and segregation.

In **chapter 4: The role of stomatin-like protein (STOML) in *P. falciparum***, a potential mitochondrial fission protein that belongs to a protein family involved in membrane organization was characterized. Deletion of STOML led to a significant growth defect in ABS, while sexual development remained unaffected. Localization of STOML on puncta on mitochondrial branching points and endings of mitochondrial branches suggests a potential role in mitochondrial dynamics. STOML was shown to resides in a large supercomplex with FtsH metalloprotease.

Predicted AlphaFold structures of STOML and multimeric STOML complexes showed high similarity with the bacterial HflK/C family member, which forms a large multimeric barrel structure around the bacterial FtsH homolog, indicating that a similar scenario might apply to the STOML-FtsH complex in *P. falciparum*.

In **chapter 5: general discussion**, the findings of the previous chapters are extensively discussed. These findings are put into perspective and future outlook is discussed.

References

1. Rabinovich, R. N. *et al.* malERA: An updated research agenda for malaria elimination and eradication. *PLoS Med.* **14**, 1–17 (2017).
2. WHO. *World malaria report 2023*. (2023).
3. Frischknecht, F. & Matuschewski, K. Plasmodium sporozoite biology. *Cold Spring Harb. Perspect. Med.* **7**, 1–14 (2017).
4. Shears, M. J. *et al.* Proteomic Analysis of Plasmodium Merosomes: The Link between Liver and Blood Stages in Malaria. *J. Proteome Res.* **18**, 3404–3418 (2019).
5. Burda, P.-C. *et al.* A Plasmodium plasma membrane reporter reveals membrane dynamics by live-cell microscopy. *Sci. Rep.* **7**, 9740 (2017).
6. Markus, M. B. The hypnozoite concept, with particular reference to malaria. *Parasitol. Res.* **108**, 247–252 (2011).
7. Cowman, A. F., Tonkin, C. J., Tham, W. H. & Duraisingh, M. T. The Molecular Basis of Erythrocyte Invasion by Malaria Parasites. *Cell Host Microbe* **22**, 232–245 (2017).
8. Daily, J. P. *et al.* Distinct physiological states of Plasmodium falciparum in malaria-infected patients. *Nature* **450**, 1091–1095 (2007).
9. Moxon, C. A., Gibbins, M. P., McGuinness, D., Milner, D. A. & Marti, M. New Insights into Malaria Pathogenesis. *Annu. Rev. Pathol. Mech. Dis.* **15**, 315–343 (2020).
10. Liu, Z., Rooks, M.. & Garrett, W.. Gametocytogenesis in malaria parasites: commitment, development and regulation. *Future Microbiol.* **176**, 139–148 (2011).
11. Gardiner, D. L. & Trenholme, K. R. Plasmodium falciparum gametocytes: Playing hide and seek. *Ann. Transl. Med.* **3**, 8–10 (2015).
12. Smalley, M. E. & Sinden, R. E. Plasmodium falciparum gametocytes their longevity and infectivity. *Parasitology* **74**, 1–8 (1977).
13. Billker, O., Shaw, M. K., Margos, G. & Sinden, R. E. The roles of temperature, pH and mosquito factors as triggers of male and female gametogenesis of Plasmodium berghei in vitro. *Parasitology* **115**, 1–7 (1997).
14. Billker, O. *et al.* Identification of xanthurenic acid as the putative inducer of malaria development in the mosquito. *Lett. to Nat.* **392**, 289–292 (1998).
15. Yahiya, S. *et al.* Live-cell fluorescence imaging of microgametogenesis in the human malaria parasite Plasmodium falciparum. *PLoS Pathog.* **18**, 1–23 (2022).
16. Meis, J. F. G. M., Wismans, P. G. P., Jap, P. H. K., Lensen, A. H. W. & Ponnudurai, T. A scanning electron microscopic study of the sporogonic development of Plasmodium falciparum in Anopheles stephensi. *Acta Trop.* **50**, 227–236 (1992).
17. Inklaar, M. R., Barillas-Mury, C. & Jore, M. M. Deceiving and escaping complement – the evasive journey of the malaria parasite. *Trends Parasitol.* **38**, 962–974 (2022).
18. Patouillard, E., Griffin, J., Bhatt, S., Ghani, A. & Cibulskis, R. Global investment targets for malaria control and elimination between 2016 and 2030. *BMJ Glob. Heal.* **2**, 1–11 (2017).
19. Riveron, J. M. *et al.* Insecticide Resistance in Malaria Vectors: An Update at a Global Scale. in *Towards Malaria Elimination - A Leap Forward* (2018). doi:10.5772/intechopen.78375.
20. Chandor-Proust, A. *et al.* The central role of mosquito cytochrome P450 CYP6Zs in insecticide detoxification revealed by functional expression and structural mode. *Biochem. J.* **455**, 75–85 (2013).

21. Liu, N. Insecticide resistance in mosquitoes: Impact, mechanisms, and research directions. *Annu. Rev. Entomol.* **60**, 537–559 (2015).
22. Ffrench-Constant, R. H., Rocheleau, T. A., Steichen, J. C. & Chalmers, A. E. A point mutation in a Drosophila GABA receptor confers insecticide resistance. *Nature* **363**, 449–451 (1993).
23. Rinkevich, F. D., Du, Y. & Dong, K. Diversity and Convergence of Sodium Channel Mutations Involved in Resistance to Pyrethroids. *Pestic Biochem Physiol* **23**, 1–7 (2008).
24. World Health Organization. *Global plan for insecticide resistance management*. (2012).
25. Ehreth, J. The global value of vaccination. *Vaccine* **21**, 596–600 (2003).
26. Duffy, P. E. & Patrick Gorres, J. Malaria vaccines since 2000: progress, priorities, products. *npj Vaccines* **5**, 1–9 (2020).
27. RTSS Clinical Trials Partnership. Efficacy and safety of RTS,S/AS01 malaria vaccine with or without a booster dose in infants and children in Africa: Final results of a phase 3, individually randomised, controlled trial. *Lancet* **386**, 31–45 (2015).
28. World Health Organization. WHO recommends groundbreaking malaria vaccine for children at risk. (2021).
29. Datoo, M. S. *et al.* Efficacy of a low-dose candidate malaria vaccine, R21 in adjuvant Matrix-M, with seasonal administration to children in Burkina Faso: a randomised controlled trial. *Lancet* **397**, 1809–1818 (2021).
30. Lee, H. *et al. Climate Change 2023: Synthesis Report. Contribution of Working Groups I, II and III to the Sixth Assessment Report of the Intergovernmental Panel on Climate Change*. *IPCC* doi: 10.59327/IPCC/AR6-9789291691647.001 (2023).
31. World Health Organization. Climate change. https://www.who.int/news-room/fact-sheets/detail/climate-change- and-health (2023).
32. Nissan, H., Ukawuba, I. & Thomson, M. Climate-proofing a malaria eradication strategy. *Malar. J.* **20**, 1–16 (2021).
33. Caminade, C., McIntyre, K. M. & Jones, A. E. Impact of recent and future climate change on vector-borne diseases. *Ann. N. Y. Acad. Sci.* **1436**, 157–173 (2019).
34. Bayoh, M. N. & Lindsay, S. W. Temperature-related duration of aquatic stages of the Afrotropical malaria vector mosquito Anopheles gambiae in the laboratory. *Med. Vet. Entomol.* **18**, 174–179 (2004).
35. Mordecai, E. A. *et al.* Optimal temperature for malaria transmission is dramatically lower than previously predicted. *Ecol. Lett.* **16**, 22–30 (2013).
36. Shapiro, L. L. M., Whitehead, S. A. & Thomas, M. B. Quantifying the effects of temperature on mosquito and parasite traits that determine the transmission potential of human malaria. *PLoS Biol.* **15**, 1–21 (2017).
37. Beck-Johnson, L. M. *et al.* The effect of temperature on Anopheles mosquito population dynamics and the potential for malaria transmission. *PLoS One* **8**, (2013).
38. Stern, D. I. *et al.* Temperature and malaria trends in highland East Africa. *PLoS One* **6**, 4–12 (2011).
39. Otto, F. E. L. *et al.* Climate change increased extreme monsoon rainfall, flooding highly vulnerable communities in Pakistan. *Environ. Res. Clim.* **2**, 025001 (2023).
40. Trape, J. F. *et al.* Impact of chloroquine resistance on malaria mortality. *Comptes Rendus l'Academie des Sci. - Ser. III* **321**, 689–697 (1998).
41. Roper, C. *et al.* Antifolate antimalarial resistance in southeast Africa: A population-based analysis. *Lancet* **361**, 1174–1181 (2003).

42. Bhatt, S. *et al.* The effect of malaria control on Plasmodium falciparum in Africa between 2000 and 2015. *Nature* **526**, 207–211 (2015).
43. Tilley, L., Straimer, J., Gnädig, N. F., Ralph, S. A. & Fidock, D. A. Artemisinin Action and Resistance in Plasmodium falciparum. *Trends Parasitol.* **32**, 682–696 (2016).
44. Dondorp, A. M. *et al.* Artemisinin Resistance in Plasmodium falciparum malaria. *N. Engl. J. Med.* **361**, 455–467 (2009).
45. Noedl, H. *et al.* Evidence of Artemisinin-Resistant Malaria in Western Cambodia. *N. Engl. J. Med.* **359**, 2619–2620 (2008).
46. Blasco, B., Leroy, Di. & Fidock, D. A. Antimalarial drug resistance: Linking Plasmodium falciparum parasite biology to the clinic. *Nat. Med.* **23**, 917–928 (2017).
47. Uwimana, A. *et al.* Emergence and clonal expansion of in vitro artemisinin-resistant Plasmodium falciparum kelch13 R561H mutant parasites in Rwanda. *Nat. Med.* **26**, 1602–1608 (2020).
48. Ariey, F. *et al.* A molecular marker of artemisinin-resistant Plasmodium falciparum malaria. *Nature* **505**, 50–55 (2014).
49. Miotto, O. *et al.* Genetic architecture of artemisinin-resistant Plasmodium falciparum. *Nat. Genet.* **47**, 226–234 (2015).
50. Straimer, J. *et al.* K13-propeller mutations confer artemisinin resistance in Plasmodium falciparum clinical isolates. *Science* **347**, 428–431 (2015).
51. Dhorda, M., Amaratunga, C. & Dondorp, A. M. Artemisinin and multidrug-resistant Plasmodium falciparum - a threat for malaria control and elimination. *Curr. Opin. Infect. Dis.* **34**, 432–439 (2021).
52. Gray, M. W., Burger, G. & Lang, B. F. Mitochondrial evolution. *Mitochondria* **183**, (1999).
53. Lamb, I. M., Okoye, I. C., Mather, M. W. & Vaidya, A. B. Unique Properties of Apicomplexan Mitochondria. *Annu. Rev. Microbiol.* **77**, 541–560 (2023).
54. Lim, L. & McFadden, G. I. The evolution, metabolism and functions of the apicoplast. *Philos. Trans. R. Soc. Lond. B. Biol. Sci.* **365**, 749–763 (2010).
55. Vaidya, A. B., Akella, R. & Suplick, K. Sequences similar to genes for two mitochondrial proteins and portions of ribosomal RNA in tandemly arrayed 6-kilobase-pair DNA of a malarial parasite. *Mol. Biochem. Parasitol.* **35**, 97–107 (1989).
56. Painter, H. J., Morrisey, J. M., Mather, M. W. & Vaidya, A. B. Specific role of mitochondrial electron transport in blood-stage Plasmodium falciparum. *Nature* **446**, 88–91 (2007).
57. Evers, F. *et al.* Composition and stage dynamics of mitochondrial complexes in Plasmodium falciparum. *Nat. Commun.* **12**, 3820 (2021).
58. MacRae, J. I. *et al.* Mitochondrial metabolism of sexual and asexual blood stages of the malaria parasite Plasmodium falciparum. *BMC Biol.* **11**, (2013).
59. Srivastava, A. *et al.* Stage-Specific Changes in Plasmodium Metabolism Required for Differentiation and Adaptation to Different Host and Vector Environments. *PLoS Pathog.* **12**, 1–30 (2016).
60. Sparkes, P. C. *et al.* Mitochondrial ATP synthesis is essential for efficient gametogenesis in Plasmodium falciparum. *bioRxiv* (2024).
61. Fowler, R. E., Billingsley, P. F., Pudney, M. & Sinden, R. E. Inhibitory action of the anti-malarial compound atovaquone (566C80) against Plasmodium berghei ANKA in the mosquito, Anopheles stephensi. *Parasitology* **108**, 383–388 (1994).
62. Fowler, R. E., Sinden, R. E. & Pudney, M. Inhibitory activity of the anti-malarial atovaquone (566C80) against ookinetes, oocysts, and sporozoites of Plasmodium berghei. *J. Parasitol.* **81**, 452–458 (1995).

63. Biagini, G. A., Viriyavejakul, P., O'neill, P. M., Bray, P. G. & Ward, S. A. Functional characterization and target validation of alternative complex I of Plasmodium falciparum mitochondria. *Antimicrob. Agents Chemother.* **50**, 1841–1851 (2006).

64. Peters, J. M. *et al.* Mutations in cytochrome b resulting in atovaquone resistance are associated with loss of fitness in Plasmodium falciparum. *Antimicrob. Agents Chemother.* **46**, 2435–2441 (2002).

65. Fry, M. & Pudney, M. Site of action of the antimalarial hydroxynaphthoquinone, 2-[trans-4-(4'-chlorophenyl) cyclohexyl]-3- hydroxy-1,4-naphthoquinone (566C80). *Biochem. Pharmacol.* **43**, 1545–1553 (1992).

66. Looareesuwan, S. *et al.* Clinical studies of atovaquone, alone or in combination with other antimalarial drugs, for treatment of acute uncomplicated malaria in Thailand. *Am. J. Trop. Med. Hyg.* **54**, 62–66 (1996).

67. Looareesuwan, S. *et al.* Malarone(TM) (atovaquone and proguanil hydrochloride): A review of its clinical development for treatment of malaria. *Am. J. Trop. Med. Hyg.* **60**, 533–541 (1999).

68. Nilsen, A. *et al.* Quinolone-3-diarylethers: A new class of antimalarial drug. *Sci. Transl. Med.* **5**, (2013).

69. Karunakaran, D. *et al.* European Journal of Pharmaceutical Sciences Long-acting intramuscular injections of ELQ-331, an antimalarial agent. *Eur. J. Pharm. Sci.* **198**, 106795 (2024).

70. Llanos-Cuentas, A. *et al.* Antimalarial activity of single-dose DSM265, a novel plasmodium dihydroorotate dehydrogenase inhibitor, in patients with uncomplicated Plasmodium falciparum or Plasmodium vivax malaria infection: a proof-of-concept, open-label, phase 2a study. *Lancet Infect. Dis.* **18**, 874–883 (2018).

71. Phillips, M. A. *et al.* A long-duration dihydroorotate dehydrogenase inhibitor (DSM265) for prevention and treatment of malaria. *Sci. Transl. Med.* **7**, (2015).

72. White, J. *et al.* Identification and Mechanistic Understanding of Dihydroorotate Dehydrogenase Point Mutations in Plasmodium falciparum that Confer in Vitro Resistance to the Clinical Candidate DSM265. *ACS Infect. Dis.* **5**, 90–101 (2019).

73. Kilejian, A. Circular mitochondrial DNA from the avian malarial parasite Plasmodium lophurae. *BBA Sect. Nucleic Acids Protein Synth.* **390**, 276–284 (1975).

74. Wilson, R. J. M. (lain. *et al.* Complete gene map of the plastid-like DNA of the malaria parasite Plasmodium falciparum. *J. Mol. Biol.* **261**, 155–172 (1996).

75. Köhler, S. *et al.* A plastid of probable green algal origin in Apicomplexan parasites. *Science* **275**, 1485–1489 (1997).

76. McFadden, G. I., Reith, M. E., Munholland, J. & Lang-Unnasch, N. Plastid in human parasites. *Nature* vol. 381 482 (1996).

77. Goodman, C. D., Su, V. & McFadden, G. I. The effects of anti-bacterials on the malaria parasite Plasmodium falciparum. *Mol. Biochem. Parasitol.* **152**, 181–191 (2007).

78. Low, L. M., Stanisic, D. I. & Good, M. F. Exploiting the apicoplast: apicoplast-targeting drugs and malaria vaccine development. *Microbes Infect.* **20**, 477–483 (2018).

79. Dahl, E. L. & Rosenthal, P. J. Multiple antibiotics exert delayed effects against the Plasmodium falciparum apicoplast. *Antimicrob. Agents Chemother.* **51**, 3485–3490 (2007).

80. Dahl, E. L. & Rosenthal, P. J. Apicoplast translation, transcription and genome replication: targets for antimalarial antibiotics. *Trends Parasitol.* **24**, 279–284 (2008).

81. Chakraborty, A. Understanding the biology of the Plasmodium falciparum apicoplast; an excellent target for antimalarial drug development. *Life Sci.* **158**, 104–110 (2016).

82. Waller, R. F. *et al.* A type II pathway for fatty acid biosynthesis presents drug targets in Plasmodium falciparum. *Antimicrob. Agents Chemother.* **47**, 297–301 (2003).

83. Ke, H. *et al.* The heme biosynthesis pathway is essential for Plasmodium falciparum development in mosquito stage but not in blood stages. *J. Biol. Chem.* **289**, 34827–34837 (2014).

84. Jomaa, H., Wiesner, J. & Sanderbrand, S. Inhibitors of the nonmevalonate PW. *Science* **285**, 1573–1576 (1999).

85. Missinou, M. A. *et al.* Fosmidomycin for malaria. *Lancet* **360**, 1941–1942 (2002).

86. Yeh, E. & DeRisi, J. L. Chemical rescue of malaria parasites lacking an apicoplast defines organelle function in blood-stage Plasmodium falciparum. *PLoS Biol.* **9**, e1001138 (2011).

87. Francia, M. E. & Striepen, B. Cell division in apicomplexan parasites. *Nat. Rev. Microbiol.* **12**, 125–136 (2014).

88. Araki, T. *et al.* Three-dimensional electron microscopy analysis reveals endopolygeny-like nuclear architecture segregation in Plasmodium oocyst development. *Parasitol. Int.* **76**, 102034 (2020).

89. Roques, M., Bindschedler, A., Beyeler, R. & Heussler, V. T. Same, same but different: Exploring Plasmodium cell division during liver stage development. *PLoS Pathog.* **19**, 1–22 (2023).

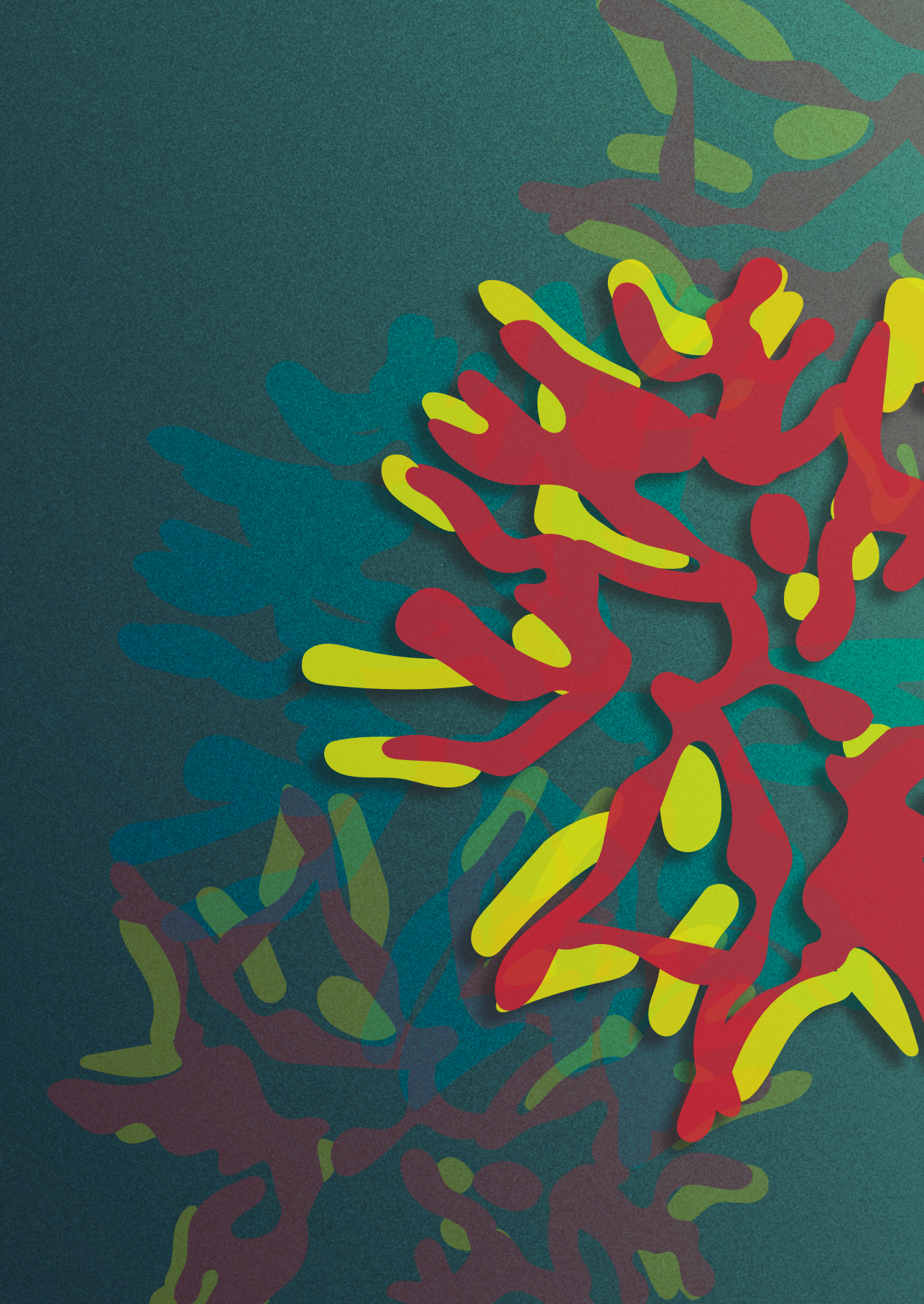

Chapter 2

Organelle dynamics in apicomplexan parasites

Julie M.J. Verhoef[1], Markus Meissner[2] & Taco W.A. Kooij[1*]

[1] Department of Medical Microbiology, Radboudumc Center for Infectious Diseases, Radboud Institute for Molecular Life Sciences, Radboud University Medical Center, PO Box 9101, 6500 HB Nijmegen, Netherlands.

[2] Division of Parasitology, Institute for Infectious Diseases and Zoonoses, Faculty for Veterinary Medicine, Ludwig-Maximilians-Universität München, 80539 München, Germany

mBio 2021. PMID:34425697

Abstract

Apicomplexan parasites, such as *Toxoplasma gondii* and *Plasmodium falciparum*, are the cause of many important human and veterinarian diseases. While *T. gondii* tachyzoites replicate through endodyogeny, during which two daughter cells are formed within the parental cell, *P. falciparum* replicates through schizogony, where up to 32 parasites are formed in a single infected red blood cell and even thousands of daughter cells during mosquito- or liver-stage development. These processes require a tightly orchestrated division and distribution over the daughter parasites of one per cell organelles such as the mitochondrion and apicoplast. Although proper organelle segregation is highly essential, the molecular mechanism and the key proteins involved remain largely unknown. In this review, we described organelle dynamics during cell division in *T. gondii* and *P. falciparum* and summarize the current understanding of the molecular mechanisms underlying organelle fission in these parasites and introduce candidate fission proteins.

Introduction

Members of the phylum Apicomplexa are single-cell, intracellular parasites that can cause many important human and veterinarian diseases, including malaria, toxoplasmosis, and cryptosporidiosis, affecting millions of people every year. These unique eukaryotes have a fascinating biology, which enables them to grow and thrive within other eukaryotes and clearly distinguishes them from other pathogens such as viruses and bacteria. Apicomplexan parasites have complex life cycles, which in large part constitute an obligate intracellular replication cycle. In many cases, this often rapid increase of parasite numbers goes hand in hand with inflammation and tissue damage and is a result of a short replication cycle and very efficient cell division. During the 48 h intraerythrocytic replication cycle of *Plasmodium falciparum*, a causative agent of malaria, one parasite can generate up to 32 merozoites, each capable of invading another red blood cell. Moreover, liver-stage *P. falciparum* can generate up to 40,000 merozoites from a single sporozoite in seven days, highlighting the extremely fast replication capability of these parasites[1]. In contrast to the familiar binary division of mammalian, plant, fungal, and bacterial cells, apicomplexan parasites replicate by *de novo* assembly of daughter cells within the parental cell. Depending on the number of newly formed parasites and the timing of nuclear division, this process is called schizogony, endodyogeny, or endopolygeny[2].

Both intracellular replication of *P. falciparum* within host erythrocytes and hepatocytes and extracellular replication of the oocyst in the mosquito vector happen via **schizogony**. During schizogony, asynchronous nuclear division results in a non-geometric expansion, after which a final round of nuclear division leads to the coordinated segmentation of daughter cells[2]. Although it was previously thought this last round of nuclear division happens in a synchronous manner, a recent study from Rudlaff *et al.* demonstrated this happens asynchronously[3]. *Toxoplasma gondii*, the causative agent of toxoplasmosis, replicates via **endodyogeny** during tachyzoite stage. During this process, DNA replication is immediately followed by the assembly of two daughter cells within the parental parasite[2]. **Endopolygeny** is a mode of replication that is used by parasites such as *Sarcocystis neurona*. These parasites undergo multiple rounds of mitosis without nuclear division, resulting in a polyploid nucleus. Only during daughter cell assembly, the last round of mitosis is followed by nuclear division and the packaging of haploid nuclei in the daughter parasites[2,4]. During these processes, parasites need to have extensive spatial and temporal control to ensure proper segregation of organelles and distribution of genetic material over daughter cells.

Like almost all eukaryotes, apicomplexan parasites contain a nucleus, endoplasmic reticulum (ER), and Golgi complex. However, they also harbor a specialized set of secretory organelles, including the rhoptries, micronemes, and dense granules, which are important for parasite invasion and establishment of parasitophorous vacuole (PV). These organelles are formed *de novo* during late intracellular stages[5]. Additionally, Apicomplexa possess an inner membrane complex (IMC) located directly beneath the plasma membrane. The IMC consists of flattened membrane sacs called alveoli and plays an important role in parasite replication, motility, and host cell invasion[6]. Furthermore, Apicomplexa harbor two singular organelles of endosymbiotic origin, the mitochondrion and a plastid organelle called the apicoplast, which both have their own reduced genomes[7]. The apicomplexan mitochondrion differs greatly from their host mitochondria on molecular and functional level[8]. One striking difference is that *P. falciparum* asexual blood stages use their electron transport chain primarily for pyrimidine biosynthesis, rather than ATP synthesis, manifesting in the loss of cristae[9,10]. The apicoplast was acquired by secondary endosymbiosis of a red alga but has lost its photosynthetic capacity[11,12]. This organelle is characterized by four membranes and plays a key role in major metabolic pathways, such as generation of isoprenoid, fatty acids, and heme[13]. The essentiality of the mitochondrion and apicoplast in apicomplexan parasites is demonstrated by the fact that these organelles are well-established drug targets[14,15]. A recent subcellular atlas of the *Toxoplasma* proteome confirmed a significant overrepresentation of essential functions in these endosymbiotic organelles[16,17].

As each individual parasite harbors only a single mitochondria and apicoplast, it is highly important that they are properly divided and distributed over daughter cells during cell division. Unlike organelle fission in mammalian, yeast, and plant cells, almost nothing is known about organelle fission in apicomplexan parasites. Other eukaryotic cells often harbor multiple mitochondria that are able to rapidly change in size, shape, and position. They undergo continuous fission and fusion events to adapt to energy needs of the cell[18]. In contrast, organelle division in apicomplexan parasites it tightly linked to cell division and spontaneous fusion or fission events have not been observed[5,19,20]. Although loop formation of the mitochondrion in *T. gondii* and *P. falciparum* could suggest the presence of self-fusion events, no components of a fusion machinery have been identified, indicating fusion of the individual organelles is redundant in these parasites[19,20]. In this review, we will describe organelle dynamics during cell division of the most commonly studied apicomplexan parasites, *P. falciparum* and *T. gondii*, with a focus on the apicoplast and mitochondrion. Furthermore, we will summarize the current understanding of the molecular mechanisms underlying organelle fission in these parasites and introduce candidate

fission proteins. Finally, we propose possible fission scenarios during schizogony and speculate about future directions to unravel these essential processes.

Organelle dynamics during cell division

During eukaryotic cell division, the cytoskeleton, membranes, and organelles change dramatically. In order to be fully functional, each daughter cell must be equipped with a complete set of organelles. A dividing cell is faced with the challenge of partitioning many different organelles that can vary in size, per-cell number, shape, and location. In mammalian cell division, larger and more complex organelles, such as the ER, Golgi and nuclear envelope must be extensively remodeled and disassembled before being distributed and reformed[18]. Smaller organelles that occur in larger numbers per cell, such as mitochondria, are fragmented prior to their distribution during cell division[21]. Unlike mammalian and plant cells, apicomplexan parasites harbor only one of each of their endosymbiotic organelles that demonstrate highly dynamic structures during the replication cycle. Organelles linked to the endomembrane system, such as ER, Golgi, and secretory organelles are distributed over daughter cells using a combination of *de novo* synthesis and recycling. However, endosymbiotic organelles need to replicate their genomes and undergo division, similarly to their bacterial ancestors. Organelle division is tightly coupled to cell division and happens in a highly organized and consecutive manner.

Structural of organelles during *Toxoplasma gondii* replication

During endodyogeny in *T. gondii*, individual organelles are divided and distributed equally in assembling daughter parasites in a tightly synchronized manner. The division process starts with fission of the Golgi and migration of the centrosome from the apical to the basal side of the nuclear envelope (Fig 1A). After duplication, the centrosomes return to the apical side of the nucleus[5,22]. The importance of this migration is not yet understood. At the same time, the single Golgi apparatus of the parasite undergoes lateral elongation and medial fission[5,22,23]. After Golgi fission, centrosomes localize at the inner ends of the divided Golgi. The apicoplast also associates with the centrosomes and undergoes lateral extension[5,24]. The scaffold of the two daughter cells, consisting of the conoid, IMC, and subpellicular microtubules, start to form and encapsulate the Golgi. The opposite ends of the elongated apicoplast are drawn into the growing daughter cells. The organelle remains associated with the centrosomes, resulting in a U-shape structure[24,25]. Next, the apicoplast undergoes medial fission and both daughter apicoplasts are packed in the assembling daughter cells. The mitochondrion typically has a lasso shape structure associating with the periphery of the parasite[19,26]. During G1 and apicoplast

elongation stages, the apicoplast and mitochondrion transiently associate with each other[5]. At the start of daughter IMC formation, the mitochondrion starts to form branches at multiple locations along its length. The ER forms a network-like structure with extensions from the nuclear envelope[5,27]. As the daughter scaffold elongates, DNA replication is completed and the nucleus lobulates. Following nuclear division, the ER enters the forming daughter scaffolds from the basal side together with the nucleus. Remarkably, the mitochondrion is completely excluded from the developing daughter cells, until very late during cell division. Once initiated, the entry of the mitochondrial extensions into the daughter cells is very fast. Here, the lasso shaped form of the mitochondrion is re-established, but the newly formed mitochondria remain attached at the basal part for an unknown period of time[5,28]. Ultimately, daughter mitochondria are separated at the basal part. Finally, maternal organelles and structures, such as micronemes, rhoptries, the IMC, and plasma membrane are almost quantitatively recycled from the parental to the daughter parasites[29]. This recycling process depends on a highly dynamic F-actin network that organizes the residual body and connects individual parasites to ensure equal distribution of maternal organelles to the forming daughter cells[29,30]. Indeed, while earlier studies suggested a relatively minor role of the parasites acto-myosin system during replication and focused on its role in gliding motility and host cell invasion, recent findings demonstrate that actin and unconventional myosins, such as MyoF, play crucial roles in organelle recycling, apicoplast segregation and organization of the parasites endomembrane system[30–33].

Structural changes of organelles during *P. falciparum* replication

In contrast to the relatively straightforward cell division of *T. gondii* where the parental cell segments into two daughter cells, the process of schizogony in *P. falciparum* is more complex. During erythrocytic schizogony of *P. falciparum*, up to 32 daughter parasites can be formed in a single parental cell. Consequently, organelles undergo drastic morphological changes and complicated fission patterns (Fig 1B). In early ring-stage parasites, the ER has a simple crescent shape around the nucleus[20]. The single Golgi apparatus of the parasite localizes closely to the ER and the nucleus[34]. The apicoplast has a rounded shape, while the mitochondrion is typically slightly elongated and has a tubular form[20]. As the parasite develops into a trophozoite, the ER forms extensions into the cytosol and around the food vacuole. The mitochondrion elongates further through the cytoplasm and starts to form branches, while the apicoplast mostly retains its rounded shape. During these earlier stages of parasite development, the apicoplast and mitochondrion often localize in close proximity to each other. In contrast to *T. gondii*, *P. falciparum* parasites lack canonical centrosomes. They organize their mitotic spindle from

a centriolar plaque, which is embedded in the nuclear envelope[35]. The centriolar plaque duplicates and migrates to opposite sides of the nucleus prior to nuclear division[36]. This pattern repeats itself coincident with the asynchronous nuclear division. Similar to *T. gondii*, the Golgi apparatus also duplicates prior to nuclear division. Only after the onset of nuclear division in early schizonts, the apicoplast elongates and the mitochondrion starts to form a more complex branched structure[20,37]. The ER forms a highly branched mesh-like network and further multiplication of the Golgi occurs[34,38]. As the apicoplast branches out, the number of contact points with the mitochondrion increases. The apicoplast divides during late stage schizogony prior to mitochondrial division[3]. Daughter apicoplasts associate with the smaller branches of the mitochondrion. The mitochondrion only divides very late during schizogony and segregates as a pair with the apicoplast into the new daughter merozoites. How and when the ER is divided and distributed during schizogony, remains largely unexplored. In newly formed merozoites, the ER has again a crescent-like shape around the nucleus, while the apicoplast is rounded and the mitochondrion has a slightly elongated tubular structure[20].

Interestingly, similar apicoplast and mitochondrial fission patterns have been observed in liver-stage parasites, but on a much larger scale with simultaneous formation of tens of thousands of merozoites[39]. During the extremely fast rounds of nuclear division in liver-stage parasites, the apicoplast and mitochondrion become extensively elongated and branched structures. The apicoplast divides with surprising synchronicity along its length while remaining closely associated with the mitochondrion, which forms finger-like structures. Similar to intraerythrocytic schizogony, during hepatic schizogony the apicoplast always divides prior to the mitochondrion. Shortly before formation of the daughter parasites, the mitochondrion divides in a similarly synchronous manner.

Organelle contact sites

During the cell division process of both *T. gondii* and *P. falciparum*, there are several moments of membrane contact between different organelles. Interestingly, in human cells association between the ER and mitochondrion is needed for the initial step of mitochondrial division[40]. The ER tubules wrap around the mitochondria and facilitate actin-myosin mediated mitochondrial constriction. This pre-constriction step is required to decrease the mitochondrial diameter by approximately half, allowing the mitochondrial division machinery to be recruited. Recently, these mitochondrial-ER contact sites have also been implicated in phospholipid and calcium transfer during division, suggesting that these contact sites also present a signaling platform for metabolite exchange that facilitates membrane remodeling and division[41,42].

Although membrane contact points between the mitochondrion and ER in *T. gondii* and *P. falciparum* have not been reported, close association between the apicoplast and extensions of the ER has been observed in these parasites[43–45]. Association of other four-membrane-bound plastids with the ER has also been observed in heterokont, haptophyte, and cryptomonad algae[46]. In plants, contact sites between the chloroplast and the ER are indicated to be involved in lipid transport[47]. Apicoplast-ER contact sites in apicomplexan parasites might also play a role in lipid distribution, which is needed for membrane remodeling and organelle dynamics[43]. So far there is no evidence that ER tubules physically wrap around the apicoplast to mediate apicoplast constriction, however, this remains largely unexplored.

The apicoplast and mitochondrion in *T. gondii* and *P. falciparum* divide subsequently while they have several transient contact sites. These contact sites have been observed with fluorescent and electron microscopy during both intraerythrocytic as well as hepatic schizogony[20,39,44,48]. It has been suggested that organelle contact facilitates metabolic exchanges, important for the biosynthesis pathway of heme, isoprenoid, iron-sulfur clusters, and fatty acids[44,48–53]. The contact points between these organelles might also represent a mechanism to ensure that every daughter parasite receives only one of each organelle[20,39]. Since apicoplast and mitochondrial fission happen in two subsequent steps, it is also possible that these contact sites allow exchange of a putatively shared fission machinery involved in the division of both organelles. However, so far this theory remains unexplored.

Figure 1. Schematic overview of organelle morphology during endodyogeny in T. gondii and schizogony in *P. falciparum*. A) Replication cycle of *T. gondii* tachyzoites. 1) Mature parasite. 2) Lateral elongation of the Golgi and migration and duplication of the centrosome at the basal site of the nucleus. 3) Centrosomes migrate back to the apical side of the nucleus and associate with the Golgi, which undergoes medial fission. The apicoplast also associates with the centrosomes and undergoes lateral extension. Budding is initiated with the formation of the IMC of daughter parasites. 4) Further formation of the IMC scaffold. Apicoplast remains associated with the centrosomes resulting in a U-shape. Nucleus and surrounding ER start to divide and enter the daughter parasites. 5) Fission of the apicoplast and nucleus with the ER. IMC scaffold encapsulates divided organelles. Extensions of the mitochondrion enter the daughter parasites. Degradation of parental secretory organelles and IMC. 6) Daughter parasites emerge, formation of the secretory organelles, establishment of the mitochondrial lasso, formation of the basal body. Only at the very last moment of division, mitochondria are separated at the basal end. B) Asexual replication of P. falciparum in red blood cells. 1) Ring-stage parasite. 2) Elongation of the mitochondrion and division of the CP and Golgi. ER forms extensions into the cytosol. 3) Further elongation and branching of the mitochondrion and apicoplast. Further replication of the Golgi and CP. Replication and expansion of the ER surrounding the dividing nuclei. 4) Apicoplast divides and associates with mitochondrial branches. Last round of nuclear division. 5) Mitochondrial division and formation of the daughter parasites. 6) Egress of merozoites from the red blood cell. Yellow, rhoptries; ochre, conoid; green, apicoplast; red, mitochondrion; light blue, nucleus; dark blue, ER; purple, Golgi apparatus; orange, centrosome (A) or centriolar plaque (CP) (B); gray, IMC.

>

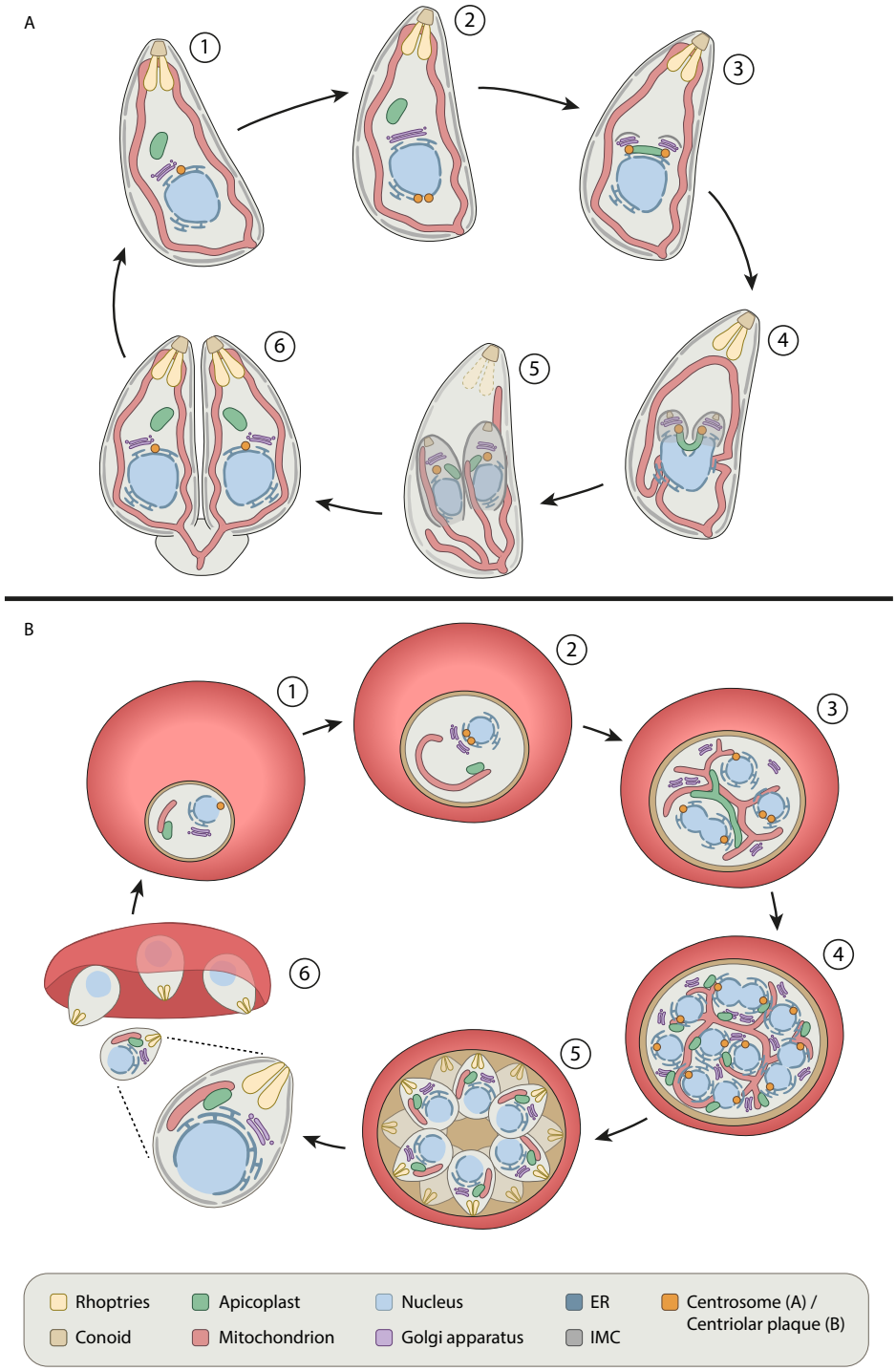
A
1
2
3
4
5
6
B
1
2
3
4
5
6
Rhoptries
Conoid
Apicoplast
Mitochondrion
Nucleus
Golgi apparatus
ER
IMC
Centrosome (A) /
Centriolar plaque (B)

Mechanisms of endosymbiotic organelle segregation

Distribution of endosymbiotic organelles

While the unusual morphology of apicomplexan parasites suggests the presence of rather unique machineries and proteins, other aspects of organelle division and distribution during the formation of daughter cells appear a common theme throughout the eukaryotic kingdom. Thus, distribution of divided organelles in eukaryotic cells typically involves coordinated remodeling of actin and the microtubule cytoskeleton. Microtubules and microtubular dynamics are critical for daughter cell assembly[31]. Interestingly, cell division is coordinated by a homolog of the striated rootlet fiber of algal flagella, striated fiber assemblins that are only expressed during division and connect the centrosome with the microtubule organization centers of the developing daughter cells, thereby defining the symmetry axis for division. Furthermore, centrosomes are tightly linked with the apicoplast, which is thought to be required for proper segregation during cytokinesis and allows to distribute apicoplasts evenly among daughter parasites[24]. In contrast, until recently the multiple roles of the parasites acto-myosin system during replication remained obscure, since the organization and functions of the actin cytoskeleton in apicomplexan parasites remained elusive due to the lack of adequate reagents to visualize F-actin and *in vitro* data that suggested that only short filaments can be formed in an unusual, isodesmic polymerization mechanism[54]. However, recent studies clarified that apicomplexan actin is well capable of forming long filaments of up to 30 µm in a cooperative polymerization mechanism, as seen for canonical actins[55,56]. Furthermore, with the application of the actin chromobody it was possible to visualize F-actin in *T. gondii* and *P. falciparum* and to explain surprising effects caused by disruption of F-actin dynamics or parasite myosins[30,33,57–60].

As in other eukaryotes, parasite actin plays crucial roles during parasite division and is involved in recycling of maternal organelles as well as apicoplast inheritance. Interestingly, the unconventional myosin F (MyoF) appears the central motor protein for these diverse functions. Ablation of *Tg*MyoF leads to loss of the apicoplast and affects the dynamic, positioning and movement of organelles of the endomembrane system[33,59,61]. To date, the exact function of MyoF and actin during apicoplast segregation is unknown. Interestingly, depletion of the actin nucleator Formin-2, which is localized close to the apicoplast, leads to a similar defect in apicoplast segregation in both, *T. gondii* and *P. falciparum*[57]. Importantly, the acto-myosin system appears to act downstream of apicoplast fission, since individual parasites can possess several, while others do not obtain a single apicoplast, upon interference with the acto-myosin system.

While the role of actin, striated fiber assemblins and microtubules in division and segregation of the apicoplast is well documented, their role in mitochondrial segregation is still obscure and requires further analysis.

Table 1. Overview of conserved endosymbiotic organelle fission proteins in *T. gondii* and *P. falciparum*.

Protein	Function	*T. gondii* homolog	*P. falciparum* homolog
Drp1, Dnm2 (human), Dnm1 (yeast), Drp3A/B (plant), Drp5B (alga)	Dynamin related protein, formation contractile ring	DrpA (TGME49_267800), DrpB (TGME49_321620), DrpC (TGME49_270690)	DYN2 (PF3D7_1037500), DYN1 (PF3D7_1145400), DYN3 (PF3D7_1218500)
hFis1, yFis1	Drp1/Dnm1 adaptor protein	Fis1 (TGME49_263323)	Fis1 (PF3D7_1325600)
Mff/MiD49/MiD51 (human)	Drp1 adaptor protein	NA	NA
Mdv1/Caf4 (yeast)	Dnm1 adaptor protein	NA	NA
FtsZ complex (plants/alga)	Formation Z-ring	NA	NA
MDR1, PDR1 (plants/alga)	Formation MD/PD ring	NA	NA
INF2/Spire1C (human)	ER-mediated constriction of the mitochondrion	NA	NA

Ancestral and eukaryotic division machinery

Mitochondria and plastids both have an endosymbiotic ancestry. It is widely accepted that mitochondria originate from primary endosymbiosis of an ancestral alphaproteobacterium. The apicoplast, being surrounded by four membranes, is the result of a secondary endosymbiotic event. It originates from a red alga that in turn obtained a plastid by endosymbiosis of a cyanobacterium[51]. Some early-branching eukaryotes, such as Amoebozoa, stramenopiles, and the red alga *Cyanidioschyzon merolae*, still use a similar division machinery as their bacterial ancestors for fission of their endosymbiotic organelles[62]. Bacteria divide by oligomerization of a tubulin-like GTPase, FtsZ, at the cytosolic membrane, corresponding to the matrix side of the inner mitochondrial membrane (IMM), where a so-called Z-ring is formed (Fig 2A). Together with a dozen other conserved proteins, the Z-ring comprises the divisional machinery and mediates mid-cell constriction[63]. We searched for apicomplexan homologs by performing reciprocal blast searches in vuepatdb and ncbi protein blast databases. Confirming previous studies, our bioinformatic analysis did not show any

homologs to components of the FtsZ division machinery in Apicomplexa (Table 1), suggesting that these parasites do not harbor this bacterial-like division system[4,50].

Many eukaryotes have partially or wholly replaced the ancestral division machinery with a new dynamin-based division machinery (Fig 2A). Dynamins or dynamin-related proteins (DRPs) are large GTPases that can form ring-like oligomers (dynamin-ring) and change conformation to facilitate membrane constriction, scission, or fusion[64]. They play a key role in processes such as vesicle budding, cytokinesis and organelle division. For example, the mammalian dynamin-related protein 1 (Drp1) and yeast dynamin-related GTPase Dnm1 mediate mitochondrial fission.

Dynamins and their central role in organelle division

All members of the dynamin superfamily have a similar architecture; a large GTPase domain, a middle domain (MD), and a downstream GTPase effector domain (GED)[64]. Three DRPs were identified in *T. gondii* (*Tg*DrpA-C) and *P. falciparum* (*Pf*DYN1-3) (Table 1). *Tg*DrpA/*Pf*DYN2 and *Tg*DrpB/*Pf*DYN1 have the typical DRP architecture, while *Tg*DrpC/*Pf*DYN3 is apicomplexan-specific and lacks both the GED and MD domains[65,66]. Surprisingly, *Tg*DrpC which lacks the two domains that are normally involved in the oligomerization and regulation of the GTPase activity, has recently been indicated to be involved in mitochondrial fission in *T. gondii*[28]. *Tg*DrpC localizes in puncta in the cytoplasm and concentrates at the mitochondrion constriction site during the last steps of cell division, similar to localization of well-studied DRPs in other systems[28,67–69]. Conditional knockdown of *Tg*DrpC showed that this protein is essential for parasite replication and significantly affects morphology of the mitochondrion, apicoplast, IMC, and Golgi[28,69]. Additionally, *Tg*DrpC has been shown to interact with proteins that are homologous to proteins involved in vesicle transport[69]. However, expression of a dominant-negative form of *Tg*DrpC resulted in impaired mitochondrial segregation and permanent mitochondrial interconnection, suggesting a role in mitochondrial division[28]. It is still unclear if *Tg*DrpC actually forms a dynamin-ring that mediates mitochondrial constriction or if it plays a more indirect role in mitochondrial fission. Although the *P. falciparum* ortholog *Pf*DYN3 is predicted to be essential[70], expression data do not unanimously support a role in mature asexual blood stages but appear rather variable across different studies (https://plasmodb.org). Thus, it still remains to be determined if *Pf*DYN3 plays a role in mitochondrial fission or has additional functions.

*Tg*DrpB is thought to be involved in the biogenesis of secretory organelles in *T. gondii*. Conditional ablation of *Tg*DrpB resulted in the parasites that lack micronemes and rhoptries, and were unable to escape or invade the host cells[66].

*Tg*DrpB is possibly involved in formation of vesicles for the secretory pathway that form the secretory organelles. The *P. falciparum* homolog *Pf*DYN1 is essential for parasite survival and is suggested to play a role in vesicle budding during hemoglobin uptake[71–73].

In plants and algae, plastid division relies on the combined action the ancestral Z-ring and the eukaryotic dynamin-ring, and it is structurally and functionally highly similar to the mitochondrial division machinery[74]. A similar division machinery is used by some heterokonts that acquired their plastids via secondary endosymbiosis and therefore harbor four plastid membranes[75]. However, apicomplexan parasites lack homology to both the FtsZ division system and the plant and alga dynamin division system (ARC5 and Dnm2, respectively). This suggests that Apicomplexa have lost the primary chloroplast division machinery and developed a new mechanism for the division of the apicoplast that is different from the division machinery of previously studied plastids[25,76].

Phylogenetic analysis has shown that *Tg*DrpA and *Pf*DYN2 are distinct from chloroplast division proteins and cluster together with other DRPs, such as human Drp1, that are involved in fission of the outer mitochondrial membrane (OMM)[76]. Surprisingly, Van Dooren *et al*. have shown that *Tg*DrpA is involved in apicoplast fission in *T. gondii*[25]. Overexpression of a non-functional *Tg*DrpA resulted in severe growth defects of the parasite and impaired apicoplast segregation. Additionally, *Tg*DrpA localizes to the apicoplast fission point during endodyogeny, where a potential dynamin-ring can be expected[25]. This would mean that the apicoplast uses a unique plastid division machinery that is highly similar to the mitochondrial dynamin-based division machinery. Although *Pf*DYN2 has been shown to have GTPase activity *in vitro*, it remains to be determined if it has a role in apicoplast division in *P. falciparum*[76]. An interesting observation entered as a comment by Ellen Yeh in PlasmoDB (http://plasmodb.org) lends support for roles beyond apicoplast fission. She noted that, while knockdown of this protein results in growth inhibition, this inhibition was not rescued by IPP as would be expected when *Pf*DYN2 would function at the apicoplast exclusively.

Besides the FtsZ and dynamin rings, EM studies have identified another electron-dense specialized ring structure at the division site of plastids and mitochondria in numerous photosynthetic eukaryotes[77–79]. The plastid-division (PD) ring comprises of two or three types of specialized electron dense ring structures: (i) the outer PD ring, which forms the main skeletal structure of the plastid division machinery and consists of a ring-shaped bundle of nanofilaments on the cytosolic

side of the organelle membrane[79]; (ii) the inner PD ring, which is formed on the inside of the inner plastid membrane; and (iii) an intermediate PD ring, which has been observed in the intermembrane space of *C. merolae* and the green alga *N. bacillaris*[80,81]. Although the conservation of the middle PD ring is less clear, the outer and inner PD rings have been found in many members of the plant kingdom and have been observed at division sites of multiple types of plastids, including proplastids, amyloplasts, and chloroplasts[82]. In some lineages of heterokonts, which harbor a four-membrane plastid of secondary endosymbiosis, an outer PD ring has been observed[83,84]. However, it remains unclear if other secondary endosymbiotic plastids, including the apicoplast also harbor this PD-ring for their organelle division. Interestingly, in lower eukaryotes a counterpart of the PD ring was found in mitochondrial division[79,85]. This mitochondrial division (MD) ring also consists of an inner MD ring located at the matrix side of the IMM and an outer MD ring at the cytosolic side of the OMM. In contrast to the PD ring, MD rings have so far only been identified in early branching eukaryotes, although some studies in yeast and human cells also identified electron dense structures at the mitochondrial division site[86,87].

Both the PD and MD rings have been shown to consists of polyglucan filaments that form a belt-like structure[88,89]. Plastid-Dividing Ring 1 (PDR1) is a glycosyltransferase protein in *C. merolae* that is embedded in the polyglucan filaments of the outer PD ring at the plastid division site and is thought to play an important role in the elongation of the glucan chain. The recently identified mitochondrial analogue Mitochondrion-Dividing Ring 1 (MDR1) has little sequence similarity with PDR1[89]. However, MDR1 and PDR1 both harbor a glycosyltransferase domain that belongs to the type-8 subgroup of the glycosyltransferase family and they have homologous functions in plastid and mitochondrial division. PDR1 orthologues have been identified in other land plants, but it remains unclear if it is conserved in other eukaryotes or apicomplexan parasites. Further studies are needed to investigate if apicomplexan parasites harbor a PD-ring in their apicoplast division machinery.

Adaptor proteins, recruiters of the organelle division machinery

DRPs are recruited to the site of fission by adaptor proteins that associate with the organelle membrane (Fig 2A)[90,91]. After recruitment of DRPs, the multimeric DRP structures are assembled and the dynamin ring is formed. Although DRPs are well conserved, adaptor proteins are highly variable between different eukaryotes and are not related by primary amino acid sequence, predicted secondary structure, or domain composition[90]. Several mitochondrial adaptor proteins have been identified in human (Mff, MiD49, MiD51, Fis1) and yeast (Mdv1, Caf4, Fis1) (Table 1). Interestingly, the membrane anchored Fis1 is the only mitochondrial adaptor protein

that is highly conserved among eukaryotes that contain mitochondria. In yeast, Fis1 is the only known membrane bound adaptor protein and is essential for the membrane recruitment of the other fission proteins Mdv1 and Caf4, which in turn recruit the mitochondrial fission machinery (Fig 2B)[92,93]. Conversely, there is redundancy in the role of human Fis1 where Drp1 recruitment can be facilitated by the other adaptor proteins, Mff, MiD49, and MiD51 (Fig 2B)[94,95]. Overexpression of human Fis1 leads to mitochondrial fragmentation, indicating a role in mitochondrial dynamics[96]. Although *T. gondii* and *P. falciparum* lack homologs to other mitochondrial adaptor proteins, both parasites harbor a Fis1 ortholog (Table 1)[28,97]. Fis1 is a relatively small protein of approximately 16 kDa and contains two tetratricopeptide domains, a C-terminal transmembrane domain and a small C-terminal tail[97,98]. N-terminal tagging of Fis1 in *T. gondii* and *P. falciparum* confirmed its mitochondrial localization, which depends on its C-terminal transmembrane domain and the C-terminal tail. Conditional knockdown or knockout of Fis1 in *T. gondii* and *P. falciparum* did not result in a growth defect nor affect mitochondrial morphology[28,97]. This suggests that Fis1 is dispensable and does not play an essential role in mitochondrial fission in these parasites. However, *T. gondii* parasites lacking Fis1 were less susceptible to the polyether ionophore monensin, which induces morphological changes of the mitochondrion as a result of constrictions in the OMM[98]. Additionally, mislocalization of Fis1 to the cytoplasm by the truncation of the C-terminal transmembrane domain in *T. gondii* caused significant alterations in mitochondrial morphology. These results indicate a role for Fis1 in mitochondrial morphology and suggest that Fis1 might interact with other proteins that are critical for mitochondrial morphology, which are pulled away from their action site upon Fis1 mislocalization. Jacobs *et al.* identified a novel OMM protein interacting with Fis1 in *T. gondii*, which they named the lasso maintenance factor 1 (LMF1). *LMF1* disrupted parasites show significant growth defect, altered mitochondrial morphology and failure of proper mitochondrial segregation during endodyogeny[98]. LMF1 might be localized to the mitochondrion by protein-protein interaction with Fis1, where it might be directly or indirectly involved in the recruitment of the fission machinery. Additionally, knockout of *LMF1* resulted in sperm-like and collapsed mitochondrial morphologies, which could be due to the loss of contact sites between the mitochondrion and the IMC. However, further research is needed to confirm these roles of LMF1 in mitochondrial morphology and division. We were not able to identify an *LMF1* ortholog in *P. falciparum*.

It is clear that our understanding of the proteins and mechanisms involved in mitochondrial fission in apicomplexan parasites is very limited. As the role of Fis1 is dispensable, it is likely that there are other, as yet unidentified adaptor proteins in apicomplexan parasites that are essential for the recruitment of the division machinery.

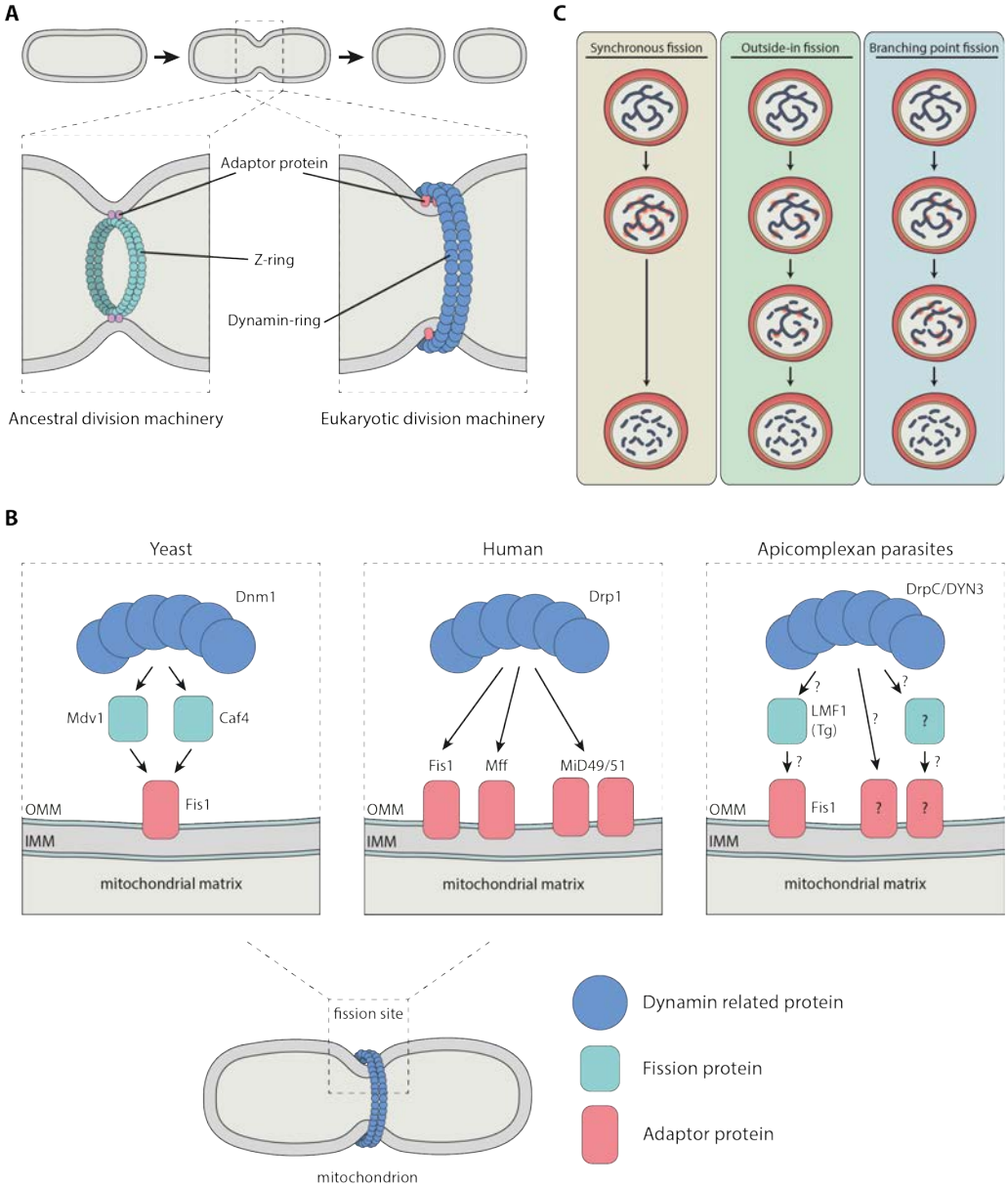
A
Adaptor protein
Z-ring
Dynamin-ring
Ancestral division machinery
Eukaryotic division machinery
C
Synchronous fission
Outside-in fission
Branching point fission
B
Yeast
Dnm1
Mdv1
Caf4
Fis1
OMM
IMM
mitochondrial matrix
Human
Drp1
Fis1
Mff
MiD49/51
OMM
IMM
mitochondrial matrix
Apicomplexan parasites
DrpC/DYN3
LMF1
(Tg)
?
Fis1
OMM
IMM
mitochondrial matrix
fission site
mitochondrion
Dynamin related protein
Fission protein
Adaptor protein

< **Figure 2. Schematic representations of organelle division mechanisms.** A) Endosymbiotic organelle division machineries. Endosymbiotic organelles are divided by the ancestral FtsZ-based division machinery where the Z-ring forms beneath the inner organelle membrane and/or the eukaryotic dynamin-based division machinery in which the dynamin ring forms at cytosolic side of the outer organelle membrane. B) Adaptor proteins recruit the mitochondrial division machinery in yeast, human, and apicomplexan parasites. In yeast, the membrane anchored Fis1 recruits adaptor proteins Mdv1 and Caf4, which in turn recruit Dnm1 to form the constrictive ring. In human cells, multiple membrane anchored adaptor proteins, including Fis1, Mff, and MiD49/51 are able to recruit Drp1 and form the division machinery. In apicomplexan parasites, the function of Fis1 in the recruitment of the division machinery is dispensable, indicating the existence of other essential adaptor proteins. Additionally, in T. gondii LMF1 seems to bind to Fis1 and might be directly or indirectly involved in the recruitment of the division machinery. C) Three possible scenarios for mitochondrial and apicoplast fission during schizogony. In the synchronous fission scenario, many fission points will occur simultaneously, resulting in an instant division of the organelle in daughter organelles. In the outside-in fission scenario, the fission points will be formed at the endings of the network-like organelle and daughter organelles will be formed by fission from the endings to the center. In the branching point fission scenario, fission points occur at the branching points of the organelle network, generating smaller fragments.

Conclusions and perspectives

Apicomplexan parasites have two different endosymbiotic organelles but harbor only one of each. The mitochondrion and apicoplast are both essential for parasite development. This makes proper division and distribution over daughter cells essential. Parasites utilize fission machineries to divide their mitochondrion and apicoplast that have highly diverged from their endosymbiotic ancestors and their human host. Therefore, these might form an attractive target for drug development. While some progress has been made towards a better understanding of the molecular processes involved, most of the fundamental mechanisms underlying organelle division remain elusive.

Morphological studies in both *T. gondii* and *P. falciparum* revealed that apicoplast division precedes mitochondrial division, which happens only during the final stages of cell division. In contrast to *T. gondii* that needs to divide and distribute the organelles over two daughter cells, *P. falciparum* must divide its mitochondrion and apicoplast in up to 32 fragments during blood-stage schizogony and even thousands during sporozoite and liver-stage merozoite formation. Here, we propose three possible scenarios for division of the mitochondrion and apicoplast in *P. falciparum* (Fig 2C):

i. **synchronous fission** - instant division of the organelle into daughter organelles with many simultaneous fission points at the organelle.
ii. **outside-in fission** - organelle division takes place at the ends of the network-like organelle, which are split off until the whole organelle is divided into daughter organelles.
iii. **branching point fission -** branching points of the mitochondrial network are the initial fission sites generating a few smaller fragments, which are then divided until all the daughter organelles are formed.

The ability to visualize and manipulate organelles and sub-organellar structures in high-resolution in a non-invasive manner is critical for understanding which, if any, of these scenarios apply to organelle fission in *P. falciparum*. Technological developments, such as lattice light sheet microscopy and high-resolution live imaging, together with the development of non-invasive organelle markers will enable the capturing of the process of organelle division in apicomplexan parasites in 4D.

In conclusion, the components and mechanisms of the organelle division machinery in apicomplexan parasites remain largely unknown. The endosymbiotic organelle

division machinery in eukaryotes includes at least one contractile ring, FtsZ- or dynamin-based, that mediates mid-organelle constriction. Although apicomplexan parasites lack components of the ancestral FtsZ-based division machinery, they do harbor three DRPs of which two have been indicated to be involved in apicoplast or mitochondrial division. Further studies are needed to verify the function of these proteins in organelle division. In contrast to the DRPs, adaptor proteins that recruit the division machinery are highly variable in eukaryotes. *T. gondii* and *P. falciparum* both harbor a Fis1 homolog, which is a highly conserved and extensively studied adaptor protein in humans, yeast, plant and algae. Although its function in mitochondrial fission in these parasites needs to be verified, dispensability of this protein indicates that there are unidentified and more important adaptor proteins that are central to recruitment of the division machinery. Despite a gradually expanding experimental genetics toolbox, ever better imaging resolution, e.g. the successful implementation of expansion microscopy[99] and FIB-SEM[3], and novel proteomics-based approaches to study protein-protein interaction and protein complexes[10,100]. The studying of such short-lived interactions will remain a significant challenge. Nevertheless, the search for the apicomplexan endosymbiotic organelle division machinery or machineries continues. Understanding the molecular basis of the organelle division machinery in apicomplexan parasites will enable a better understanding of this fascinating and essential process.

Acknowledgments

We thank all the investigators who have contributed to this body of knowledge, some of whom were not cited due to space limitations. JMJV was supported by an individual Radboudumc Master-PhD grant, TWAK by the Netherlands Organisation for Scientific Research (NWO-VIDI 864.13.009). MM is supported by the German research foundation (DFG ME 2675/6-1).

References

1. Nilsson, S. K., Childs, L. M., Buckee, C. & Marti, M. Targeting human transmission biology for malaria elimination. *PLoS Pathog.* **11**, e1004871 (2015).
2. Francia, M. E. & Striepen, B. Cell division in apicomplexan parasites. *Nat. Rev. Microbiol.* **12**, 125–136 (2014).
3. Rudlaff, R. M., Kraemer, S., Marshman, J. & Dvorin, J. D. Three-dimensional ultrastructure of Plasmodium falciparum throughout cytokinesis. *PLoS Pathog.* **16**, e1008587 (2020).
4. Vaishnava, S. *et al.* Plastid segregation and cell division in the apicomplexan parasite Sarcocystis neurona. *J. Cell Sci.* **118**, 3397–3407 (2005).
5. Nishi, M., Hu, K., Murray, J. M. & Roos, D. S. Organellar dynamics during the cell cycle of Toxoplasma gondii. *J. Cell Sci.* **121**, 1559–1568 (2008).
6. Kono, M., Prusty, D., Parkinson, J. & Gilberger, T. W. The apicomplexan inner membrane complex. *Front. Biosci.* **18**, 982–992 (2013).
7. Wilson, R. J. & Williamson, D. H. Extrachromosomal DNA in the Apicomplexa. *Microbiol. Mol. Biol. Rev.* **61**, 1–16 (1997).
8. Vaidya, A. B. & Mather, M. W. Mitochondrial evolution and functions in malaria parasites. *Annu. Rev. Microbiol.* **63**, 249–267 (2009).
9. Painter, H. J., Morrisey, J. M., Mather, M. W. & Vaidya, A. B. Specific role of mitochondrial electron transport in blood-stage Plasmodium falciparum. *Nature* **446**, 88–91 (2007).
10. Evers, F. *et al.* Composition and stage dynamics of mitochondrial complexes in Plasmodium falciparum. *Nat. Commun.* **12**, 3820 (2021).
11. Roos, D. S. *et al.* Origin, targeting, and function of the apicomplexan plastid. *Curr. Opin. Microbiol.* **2**, 426–432 (1999).
12. Janouskovec, J., Horák, A., Oborník, M., Lukes, J. & Keeling, P. J. A common red algal origin of the apicomplexan, dinoflagellate, and heterokont plastids. *Proc. Natl. Acad. Sci. U. S. A.* **107**, 10949–10954 (2010).
13. McFadden, G. I. & Yeh, E. The apicoplast: now you see it, now you don't. *Int. J. Parasitol.* **47**, 137–144 (2017).
14. Goodman, C. D., Buchanan, H. D. & McFadden, G. I. Is the mitochondrion a good malaria drug target? *Trends Parasitol.* **33**, 185–193 (2017).
15. Kennedy, K., Crisafulli, E. M. & Ralph, S. A. Delayed death by plastid inhibition in apicomplexan parasites. *Trends Parasitol.* **35**, 747–759 (2019).
16. Barylyuk, K. *et al.* A comprehensive subcellular atlas of the Toxoplasma proteome via hyperLOPIT provides spatial context for protein functions. *Cell Host Microbe* **28**, 752-766.e9 (2020).
17. Sidik, S. M. *et al.* A genome-wide CRISPR screen in Toxoplasma identifies essential Apicomplexan genes. *Cell* **166**, 1423-1435.e12 (2016).
18. Carlton, J. G., Jones, H. & Eggert, U. S. Membrane and organelle dynamics during cell division. *Nat. Rev. Mol. Cell Biol.* **21**, 151–166 (2020).
19. Ovciarikova, J., Lemgruber, L., Stilger, K. L., Sullivan, W. J. & Sheiner, L. Mitochondrial behaviour throughout the lytic cycle of Toxoplasma gondii. *Sci. Rep.* **7**, 42746 (2017).
20. van Dooren, G. G. *et al.* Development of the endoplasmic reticulum, mitochondrion and apicoplast during the asexual life cycle of Plasmodium falciparum. *Mol. Microbiol.* **57**, 405–419 (2005).

21. Jongsma, M. L. M., Berlin, I. & Neefjes, J. On the move: organelle dynamics during mitosis. *Trends Cell Biol.* **25**, 112–124 (2015).
22. Hartmann, J. *et al.* Golgi and centrosome cycles in Toxoplasma gondii. *Mol. Biochem. Parasitol.* **145**, 125–127 (2006).
23. Pelletier, L. *et al.* Golgi biogenesis in Toxoplasma gondii. *Nature* **418**, 548–552 (2002).
24. Striepen, B. *et al.* The plastid of Toxoplasma gondii is divided by association with the centrosomes. *J. Cell Biol.* **151**, 1423–1434 (2000).
25. van Dooren, G. G. *et al.* A novel dynamin-related protein has been recruited for apicoplast fission in Toxoplasma gondii. *Curr. Biol.* **19**, 267–276 (2009).
26. Melo, E. J., Attias, M. & De Souza, W. The single mitochondrion of tachyzoites of Toxoplasma gondii. *J. Struct. Biol.* **130**, 27–33 (2000).
27. Hager, K. M., Striepen, B., Tilney, L. G. & Roos, D. S. The nuclear envelope serves as an intermediary between the ER and Golgi complex in the intracellular parasite Toxoplasma gondii. *J. Cell Sci.* **112**, 2631–2638 (1999).
28. Melatti, C. *et al.* A unique dynamin-related protein is essential for mitochondrial fission in Toxoplasma gondii. *PLoS Pathog.* **15**, e1007512 (2019).
29. Periz, J. *et al.* A highly dynamic F-actin network regulates transport and recycling of micronemes in Toxoplasma gondii vacuoles. *Nat. Commun.* **10**, 4183 (2019).
30. Periz, J. *et al.* Toxoplasma gondii F-actin forms an extensive filamentous network required for material exchange and parasite maturation. *Elife* **6**, e24119 (2017).
31. Shaw, M. K., Compton, H. L., Roos, D. S. & Tilney, L. G. Microtubules, but not actin filaments, drive daughter cell budding and cell division in Toxoplasma gondii. *J. Cell Sci.* **113**, 1241–1254 (2000).
32. Drewry, L. L. & Sibley, L. D. Toxoplasma actin is required for efficient host cell invasion. *MBio* **6**, e00557 (2015).
33. Carmeille, R., Schiano Lomoriello, P., Devarakonda, P. M., Kellermeier, J. A. & Heaslip, A. T. Actin and an unconventional myosin motor, TgMyoF, control the organization and dynamics of the endomembrane network in Toxoplasma gondii. *PLoS Pathog.* **17**, e1008787 (2021).
34. Struck, N. S. *et al.* Re-defining the Golgi complex in Plasmodium falciparum using the novel Golgi marker PfGRASP. *J. Cell Sci.* **118**, 5603–5613 (2005).
35. Gerald, N., Mahajan, B. & Kumar, S. Mitosis in the human malaria parasite Plasmodium falciparum. *Eukaryot. Cell* **10**, 474–482 (2011).
36. Arnot, D. E., Ronander, E. & Bengtsson, D. C. The progression of the intra-erythrocytic cell cycle of Plasmodium falciparum and the role of the centriolar plaques in asynchronous mitotic division during schizogony. *Int. J. Parasitol.* **41**, 71–80 (2011).
37. Stanway, R. R., Witt, T., Zobiak, B., Aepfelbacher, M. & Heussler, V. T. GFP-targeting allows visualization of the apicoplast throughout the life cycle of live malaria parasites. *Biol. cell* **101**, 415–430 (2009).
38. Struck, N. S. *et al.* Spatial dissection of the cis- and trans-Golgi compartments in the malaria parasite Plasmodium falciparum. *Mol. Microbiol.* **67**, 1320–1330 (2008).
39. Stanway, R. R. *et al.* Organelle segregation into Plasmodium liver stage merozoites. *Cell. Microbiol.* **13**, 1768–1782 (2011).

40. Tilokani, L., Nagashima, S., Paupe, V. & Prudent, J. Mitochondrial dynamics: overview of molecular mechanisms. *Essays Biochem.* **62**, 341–360 (2018).
41. Kameoka, S., Adachi, Y., Okamoto, K., Iijima, M. & Sesaki, H. Phosphatidic acid and cardiolipin coordinate mitochondrial dynamics. *Trends Cell Biol.* **28**, 67–76 (2018).
42. Chakrabarti, R. *et al.* INF2-mediated actin polymerization at the ER stimulates mitochondrial calcium uptake, inner membrane constriction, and division. *J. Cell Biol.* **217**, 251–268 (2018).
43. Tomova, C. *et al.* Membrane contact sites between apicoplast and ER in Toxoplasma gondii revealed by electron tomography. *Traffic* **10**, 1471–1480 (2009).
44. Hopkins, J. *et al.* The plastid in Plasmodium falciparum asexual blood stages: a three-dimensional ultrastructural analysis. *Protist* **150**, 283–295 (1999).
45. Tonkin, C. J., Struck, N. S., Mullin, K. A., Stimmler, L. M. & McFadden, G. I. Evidence for Golgi-independent transport from the early secretory pathway to the plastid in malaria parasites. *Mol. Microbiol.* **61**, 614–630 (2006).
46. Gibbs, S. P. The route of entry of cytoplasmically synthesized proteins into chloroplasts of algae possessing chloroplast ER. *J. Cell Sci.* **35**, 253–266 (1979).
47. Wang, Z. & Benning, C. Chloroplast lipid synthesis and lipid trafficking through ER-plastid membrane contact sites. *Biochem. Soc. Trans.* **40**, 457–463 (2012).
48. Kobayashi, T. *et al.* Mitochondria and apicoplast of Plasmodium falciparum: behaviour on subcellular fractionation and the implication. *Mitochondrion* **7**, 125–132 (2007).
49. Ralph, S. A. *et al.* Tropical infectious diseases: metabolic maps and functions of the Plasmodium falciparum apicoplast. *Nat. Rev. Microbiol.* **2**, 203–216 (2004).
50. van Dooren, G. G., Stimmler, L. M. & McFadden, G. I. Metabolic maps and functions of the Plasmodium mitochondrion. *FEMS Microbiol. Rev.* **30**, 596–630 (2006).
51. Lim, L. & McFadden, G. I. The evolution, metabolism and functions of the apicoplast. *Philos. Trans. R. Soc. Lond. B. Biol. Sci.* **365**, 749–763 (2010).
52. Seeber, F. & Soldati-Favre, D. Metabolic pathways in the apicoplast of apicomplexa. *Int. Rev. Cell Mol. Biol.* **281**, 161–228 (2010).
53. Nagaraj, V. A. & Padmanaban, G. Insights on Heme Synthesis in the Malaria Parasite. *Trends Parasitol.* **33**, 583–586 (2017).
54. Skillman, K. M. *et al.* The unusual dynamics of parasite actin result from isodesmic polymerization. *Nat. Commun.* **4**, 2285 (2013).
55. Kumpula, E.-P. *et al.* Apicomplexan actin polymerization depends on nucleation. *Sci. Rep.* **7**, 12137 (2017).
56. Lu, H., Fagnant, P. M. & Trybus, K. M. Unusual dynamics of the divergent malaria parasite PfAct1 actin filament. *Proc. Natl. Acad. Sci. U. S. A.* **116**, 20418–20427 (2019).
57. Stortz, J. F. *et al.* Formin-2 drives polymerisation of actin filaments enabling segregation of apicoplasts and cytokinesis in Plasmodium falciparum. *Elife* **8**, e49030 (2019).
58. Andenmatten, N. *et al.* Conditional genome engineering in Toxoplasma gondii uncovers alternative invasion mechanisms. *Nat. Methods* **10**, 125–127 (2013).
59. Jacot, D., Daher, W. & Soldati-Favre, D. Toxoplasma gondii myosin F, an essential motor for centrosomes positioning and apicoplast inheritance. *EMBO J.* **32**, 1702–1716 (2013).
60. Whitelaw, J. A. *et al.* Surface attachment, promoted by the actomyosin system of Toxoplasma gondii is important for efficient gliding motility and invasion. *BMC Biol.* **15**, 1 (2017).
61. Heaslip, A. T., Nelson, S. R. & Warshaw, D. M. Dense granule trafficking in Toxoplasma gondii requires a unique class 27 myosin and actin filaments. *Mol. Biol. Cell* **27**, 2080–2089 (2016).

62. Leger, M. M. *et al.* An ancestral bacterial division system is widespread in eukaryotic mitochondria. *Proc. Natl. Acad. Sci. U. S. A.* **112**, 10239–10246 (2015).

63. Mahone, C. R. & Goley, E. D. Bacterial cell division at a glance. *J. Cell Sci.* **133**, jcs237057 (2020).

64. Praefcke, G. J. K. & McMahon, H. T. The dynamin superfamily: universal membrane tubulation and fission molecules? *Nat. Rev. Mol. Cell Biol.* **5**, 133–147 (2004).

65. Fukushima, N. H., Brisch, E., Keegan, B. R., Bleazard, W. & Shaw, J. M. The GTPase effector domain sequence of the Dnm1p GTPase regulates self-assembly and controls a rate-limiting step in mitochondrial fission. *Mol. Biol. Cell* **12**, 2756–2766 (2001).

66. Breinich, M. S. *et al.* A dynamin is required for the biogenesis of secretory organelles in Toxoplasma gondii. *Curr. Biol.* **19**, 277–286 (2009).

67. Bleazard, W. *et al.* The dynamin-related GTPase Dnm1 regulates mitochondrial fission in yeast. *Nat. Cell Biol.* **1**, 298–304 (1999).

68. Smirnova, E., Griparic, L., Shurland, D. L. & van der Bliek, A. M. Dynamin-related protein Drp1 is required for mitochondrial division in mammalian cells. *Mol. Biol. Cell* **12**, 2245–2256 (2001).

69. Heredero-Bermejo, I. *et al.* TgDrpC, an atypical dynamin-related protein in Toxoplasma gondii, is associated with vesicular transport factors and parasite division. *Mol. Microbiol.* **111**, 46–64 (2019).

70. Zhang, M. *et al.* Uncovering the essential genes of the human malaria parasite Plasmodium falciparum by saturation mutagenesis. *Science* **360**, eaap7847 (2018).

71. Li, H. *et al.* Isolation and functional characterization of a dynamin-like gene from Plasmodium falciparum. *Biochem. Biophys. Res. Commun.* **320**, 664–671 (2004).

72. Zhou, H., Gao, Y., Zhong, X. & Wang, H. Dynamin like protein 1 participated in the hemoglobin uptake pathway of Plasmodium falciparum. *Chin. Med. J. (Engl).* **122**, 1686–1691 (2009).

73. Milani, K. J., Schneider, T. G. & Taraschi, T. F. Defining the morphology and mechanism of the hemoglobin transport pathway in Plasmodium falciparum-infected erythrocytes. *Eukaryot. Cell* **14**, 415–426 (2015).

74. Yoshida, Y. Insights into the Mechanisms of Chloroplast Division. *Int. J. Mol. Sci.* **19**, (2018).

75. Miyagishima, S. Mechanism of plastid division: from a bacterium to an organelle. *Plant Physiol.* **155**, 1533–1544 (2011).

76. Charneau, S. *et al.* Characterization of PfDYN2, a dynamin-like protein of Plasmodium falciparum expressed in schizonts. *Microbes Infect.* **9**, 797–805 (2007).

77. Miyagishima, S., Takahara, M. & Kuroiwa, T. Novel filaments 5 nm in diameter constitute the cytosolic ring of the plastid division apparatus. *Plant Cell* **13**, 707–721 (2001).

78. Kuroiwa, H., Mori, T., Takahara, M., Miyagishima, S. & Kuroiwa, T. Chloroplast division machinery as revealed by immunofluorescence and electron microscopy. *Planta* **215**, 185–190 (2002).

79. Yoshida, Y. & Mogi, Y. How do plastids and mitochondria divide? *Reprod. Syst. Sex. Disord.* **68**, 45–56 (2019).

80. Miyagishima, S. *et al.* Identification of a triple ring structure involved in plastid division in the primitive red alga Cyanidioschyzon merolae. *Microscopy* **47**, 269–272 (1998).

81. Sumiya, N., Hirata, A. & Kawano, S. Multiple FtsZ ring formation and reduplicated chloroplast DNA in Nannochloris bagillaris (Chlorophyta, Trebouxiophyceae) under phosphate-enriched culture. *J. Phycol.* **44**, 1476–1489 (2008).

82. Kuroiwa. The primitive red algae Cyanidium caldarium and Cyanidioschyzon merolae as model system for investigating the dividing apparatus of mitochondria and plastids. *Bioessays* **20**, 344–354 (1998).

83. Hashimoto, H. Electron-opaque annular structure girdling the constricting isthmus of the dividing chloroplasts of Heterosigma akashiwo (Raphidophyceae, Chromophyta). *Protoplasma* **197**, 210–216 (1997).

84. Hashimoto, H. The ultrastructural features and division of secondary plastids. *J. Plant Res.* **118**, 163–172 (2005).

85. Kuroiwa *et al.* Structure, function and evolution of the mitochondrial division apparatus. *Biochim. Biophys. Acta* **1763**, 510–521 (2006).

86. Yoon, Y., Krueger, E. W., Oswald, B. J. & McNiven, M. A. The mitochondrial protein hFis1 regulates mitochondrial fission in mammalian cells through an interaction with the dynamin-like protein DLP1. *Mol. Cell. Biol.* **23**, 5409–5420 (2003).

87. Ingerman, E. *et al.* Dnm1 forms spirals that are structurally tailored to fit mitochondria. *J. Cell Biol.* **170**, 1021–1027 (2005).

88. Yoshida, Y. *et al.* Chloroplasts divide by contraction of a bundle of nanofilaments consisting of polyglucan. *Science* **329**, 949–953 (2010).

89. Yoshida, Y. *et al.* Glycosyltransferase MDR1 assembles a dividing ring for mitochondrial proliferation comprising polyglucan nanofilaments. *Proc. Natl. Acad. Sci. U. S. A.* **114**, 13284–13289 (2017).

90. Bui, H. T. & Shaw, J. M. Dynamin assembly strategies and adaptor proteins in mitochondrial fission. *Curr. Biol.* **23**, 891–899 (2013).

91. Miyagishima, S.-Y. Chloroplast division: A handshake across membranes. *Nat. plants* **3**, 17025 (2017).

92. Mozdy, A. D., McCaffery, J. M. & Shaw, J. M. Dnm1p GTPase-mediated mitochondrial fission is a multi-step process requiring the novel integral membrane component Fis1p. *J. Cell Biol.* **151**, 367–380 (2000).

93. Koppenol-Raab, M. *et al.* A targeted mutation identified through pKa measurements indicates a postrecruitment role for Fis1 in yeast mitochondrial fission. *J. Biol. Chem.* **291**, 20329–20344 (2016).

94. Palmer, C. S. *et al.* Adaptor proteins MiD49 and MiD51 can act independently of Mff and Fis1 in Drp1 recruitment and are specific for mitochondrial fission. *J. Biol. Chem.* **288**, 27584–27593 (2013).

95. Koirala, S. *et al.* Interchangeable adaptors regulate mitochondrial dynamin assembly for membrane scission. *Proc. Natl. Acad. Sci. U. S. A.* **110**, E1342–E1351 (2013).

96. Stojanovski, D., Koutsopoulos, O. S., Okamoto, K. & Ryan, M. T. Levels of human Fis1 at the mitochondrial outer membrane regulate mitochondrial morphology. *J. Cell Sci.* **117**, 1201–1210 (2004).

97. Maruthi, M., Ling, L., Zhou, J. & Ke, H. Dispensable role of mitochondrial fission protein 1 (Fis1) in the erythrocytic development of Plasmodium falciparum. *mSphere* **5**, e00579-20 (2020).

98. Jacobs, K., Charvat, R. & Arrizabalaga, G. Identification of Fis1 interactors in Toxoplasma gondii reveals a novel protein required for peripheral distribution of the mitochondrion. *MBio* **11**, e02732-19 (2020).

99. Bertiaux, E. *et al.* Expansion microscopy provides new insights into the cytoskeleton of malaria parasites including the conservation of a conoid. *PLoS Biol.* **19**, e3001020 (2021).

100. Hillier, C. *et al.* Landscape of the Plasmodium interactome reveals both conserved and species-specific functionality. *Cell Rep.* **28**, 1635–1647 (2019).

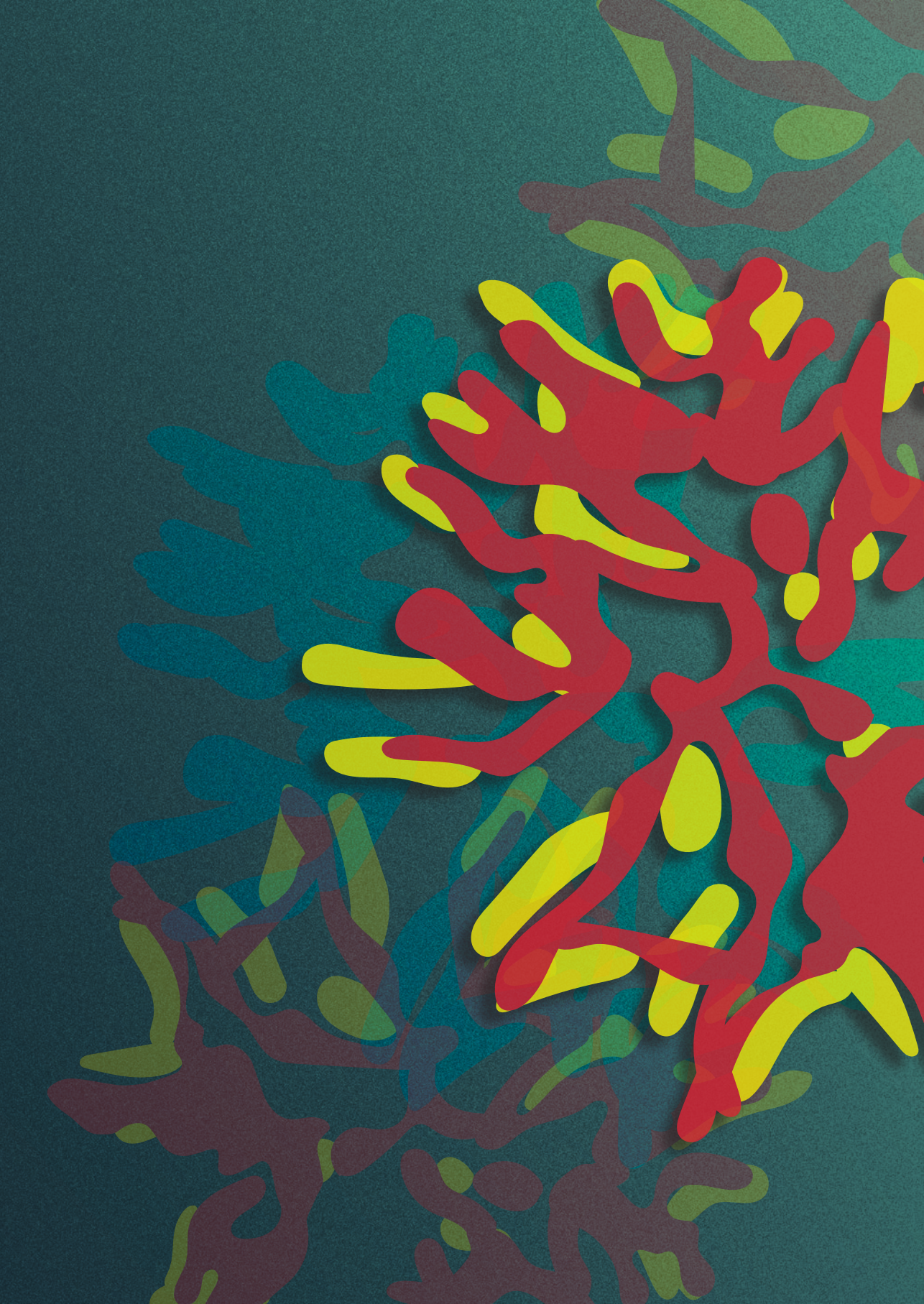

Chapter 3

Detailing organelle division and segregation in *Plasmodium falciparum*

Julie M.J. Verhoef[1], Cas Boshoven[1], Felix Evers[1], Laura J. Akkerman[1], Barend C.A. Gijsbrechts[1], Marga van de Vegte-Bolmer[1], Geert-Jan van Gemert[1], Akhil B. Vaidya[2], Taco W.A. Kooij[1*]

[1] Department of Medical Microbiology, Radboudumc Center for Infectious Diseases, Radboud University Medical Center, Nijmegen, The Netherlands

[2] Center for Molecular Parasitology, Institute for Molecular Medicine and Infectious Disease, Department of Microbiology and Immunology, Drexel University College of Medicine, Philadelphia, USA

Journal of Cell Biology 2024. PMID: 39485315

Abstract

The malaria causing parasite, *P. falciparum*, replicates through a tightly orchestrated process termed schizogony, where approximately 32 daughter parasites are formed in a single infected red blood cell and thousands of daughter cells in mosquito or liver stages. One-per-cell organelles, such as the mitochondrion and apicoplast, need to be properly divided and segregated to ensure a complete set of organelles per daughter parasites. Although this is highly essential, details about the processes and mechanisms involved remain unknown. We developed a new reporter parasite line that allows visualization of the mitochondrion in blood and mosquito stages. Using high-resolution 3D-imaging, we found that the mitochondrion orients in a cartwheel structure, prior to stepwise, non-geometric division during the last stage of schizogony. Analysis of focused ion beam scanning electron microscopy (FIB-SEM) data confirmed these mitochondrial division stages. Furthermore, these data allowed us to elucidate apicoplast division steps, highlighted its close association with the mitochondrion, and showed putative roles of the centriolar plaques (CPs) in apicoplast segregation. These observations form the foundation for a new detailed mechanistic model of mitochondrial and apicoplast division and segregation during *P. falciparum* schizogony and pave the way for future studies into the proteins and protein complexes involved in organelle division and segregation.

Introduction

Malaria is a devastating parasitic disease causing an estimated 249 million cases resulting in approximately 608,000 deaths in 2022, especially in children under 5 years old[1]. *Plasmodium falciparum* is the most virulent parasite species causing malaria. Continued emergence of resistant parasites to antimalarial drugs is a major problem for global malaria control and necessitates continued development of novel antimalarials.

The malaria parasite harbors a unique mitochondrion that differs greatly from the human mitochondrion at a molecular and functional level[2]. While the most prominent role of the mitochondrion in humans is respiration and consequent energy conversion, in the disease-causing asexual blood stages of *P. falciparum* the respiratory chain appears to be exclusively essential to support pyrimidine biosynthesis[3]. It is only during preparation for transition to the mosquito vector where sexual reproduction takes place, that canonical mitochondrial functions such as the tricarboxylic acid cycle (TCA) cycle and the oxidative phosphorylation (OXPHOS) pathway become more abundant and critical[4,5]. Because of these differences, it is not surprising that this organelle is the drug target of several anti-malarial compounds, such as atovaquone, DSM265, proguanil and ELQ300[6,7].

Host and stage transitions are commonplace in the complicated life cycle of *Plasmodium* parasites. During erythrocytic asexual replication, one parasite is segmented into approximately 32 merozoites through a tightly orchestrated process called schizogony. Cell division happens on a much larger scale in mosquito and liver stages, where one parasite is divided into thousands or even tens of thousands of daughter parasites. During *P. falciparum* cell division, the single parasite mitochondrion needs to be properly divided and distributed among the daughter cells[9]. During parasite development in asexual blood stages, the tubular mitochondrion elongates and forms a large, branched network that stretches throughout the parasite[10]. Only during the final stages of schizogony, once nuclear division is completed, does the mitochondrion undergo rapid fission[11]. The apicoplast, another essential single copy organelle of secondary endosymbiotic origin, forms a comparable branched network, but divides prior to mitochondrial fission during blood- and liver-stage replication[10,12]. To produce viable offspring, the parasite has to ensure that each daughter parasite has a complete set of these organelles. However, so far a detailed view of these processes and the mechanisms involved is lacking.

We aimed to capture the process of mitochondrial division in these multinucleated cells in detail using different imaging methods. However, this comes with several

challenges. Firstly, imaging the small-sized parasites (1-7 µm diameter), and the even smaller organelles within the parasites, requires the use of super-resolution imaging techniques. Secondly, visualization of the mitochondrion requires a specific fluorescent marker or dye. Mitochondrial dyes, such as Rhodamine123 and MitoTracker™, have been widely used in the field[13]. These dyes rely on membrane potential to enter the mitochondrion and are therefore also used as a viability marker[14]. However, eight of these dyes were tested in a drug screen all showing IC50 values below 1µM with three, Mito Red, $DiOC_6$, and Rhodamine B being highly active against *P. falciparum* with IC50 values below 30 nM[15,16]. Additionally, in our hands MitoTracker signal can be diffuse, and therefore limit the resolution that is needed for the visualization of mitochondrial fission. Hence, we aimed to develop a reporter parasite line which harbors a fluorescent mitochondrial marker that allows imaging of this organelle in live and fixed conditions in all life-cycle stages of *P. falciparum*. To do this, we deployed a similar strategy that has been used successfully in the rodent model *Plasmodium berghei*[17,18]. The targeting signal of the known mitochondrial protein HSP70-3 was fused with a fluorescent protein and integrated in a silent intergenic locus (SIL)[19]. Expression of this mitochondrial-localized fluorescent protein allowed visualization of the organelle during imaging of asexual, sexual and mosquito stages. Using high resolution confocal microscopy, we were able to make a detailed 3D map of different mitochondrial fission stages during schizogony in asexual blood stages. Focused ion beam scanning electron microscopy (FIB-SEM) image stacks from Evers *et al.* were used to confirm these mitochondrial fission stages with high detail[20]. This also allowed us to study apicoplast division and highlighted the potential role of the centriolar plaques (CPs) in apicoplast segregation. These different microscopic approaches empowered us to put forward a detailed model for mitochondrial and apicoplast division and distribution during the final stages of schizogony.

Results

To acquire a detailed understanding of mitochondrial fission and distribution, we set out to capture this process throughout the *Plasmodium* life cycle by combining different microscopy approaches. We stained mature blood-stage wild-type *P. falciparum* NF54 strain parasites with two different MitoTracker dyes and used these to visualize the mitochondrion in fixed confocal imaging. Surprisingly, both MitoTracker dyes showed a discontinuous, punctate staining pattern (Figure 1A). FIB-SEM studies have confirmed the prevailing notion that the mitochondrion is a single, branched network during these schizont stages[20]. While this observation

may arise from crosslinking of the MitoTracker dyes to specific proteins and aggregations thereof resulting from the fixation process, we concluded that the punctate staining pattern is likely an artifact and consequently limits our ability to dissect and visualize the process mitochondrial fission. To address this, we developed a new fluorescent mitochondrial marker that can be used for imaging live and fixed samples (Figure S1).

Design and generation of a new mitochondrial marker parasite line

We designed a mitochondrial marker that consists of the promotor and mitochondrial targeting sequence of the gene encoding the mitochondrial heat shock protein 70 (HSP70-3, PF3D7_1134000), fused to an mScarlet red fluorescent protein (Figure S1A). HSP70-3 was selected based on its high and consistent expression profile throughout the whole life cycle and has been successfully used for the same purpose in *P. berghei*[17,18]. We aimed to stably integrate this fluorescent marker in the *P. falciparum* genome, without affecting any normal biological processes and parasite growth throughout the parasite life cycle. Selection of the new integration site, SIL7, is described extensively in Supplemental Information S1. The integration plasmid was transfected into NF54 parasites together with two different Cas9 guide plasmids directed at the SIL7 site. Successful integration of the mitochondrial marker and absence of WT parasite contaminations were confirmed by integration PCR (Figure S1B). A growth assay showed no difference in growth of the mitochondrial reporter line, MitoRed, compared to WT parasites in asexual blood stages (Figure S1C).

Characterization of the MitoRed parasite line

To visualize the mitochondrial marker, asexual blood-stage MitoRed parasites were fixed and used for fluorescent imaging. The fluorescent signal was well preserved after fixation and no antibody staining was required for mitochondrial visualization in all asexual blood stages (Figure 1B). To assess whether the punctate mitochondrial morphology observed after MitoTracker staining was an imaging artifact or a morphological aberration caused by the dye, we stained MitoRed parasites with three different MitoTracker dyes. Discontinuous, punctate mitochondria were observed in all MitoRed parasites stained with MitoTracker, while this was not observed in unstained MitoRed parasites (Figure 1C). The effect was less pronounced during live imaging of MitoTracker stained parasites (Figure S2). While there is an obvious imaging artifact following fixation of MitoTracker-stained blood-stage *P. falciparum* parasites, the altered MitoRed signal in the presence of the dye might even suggest possible changes in mitochondrial morphology.

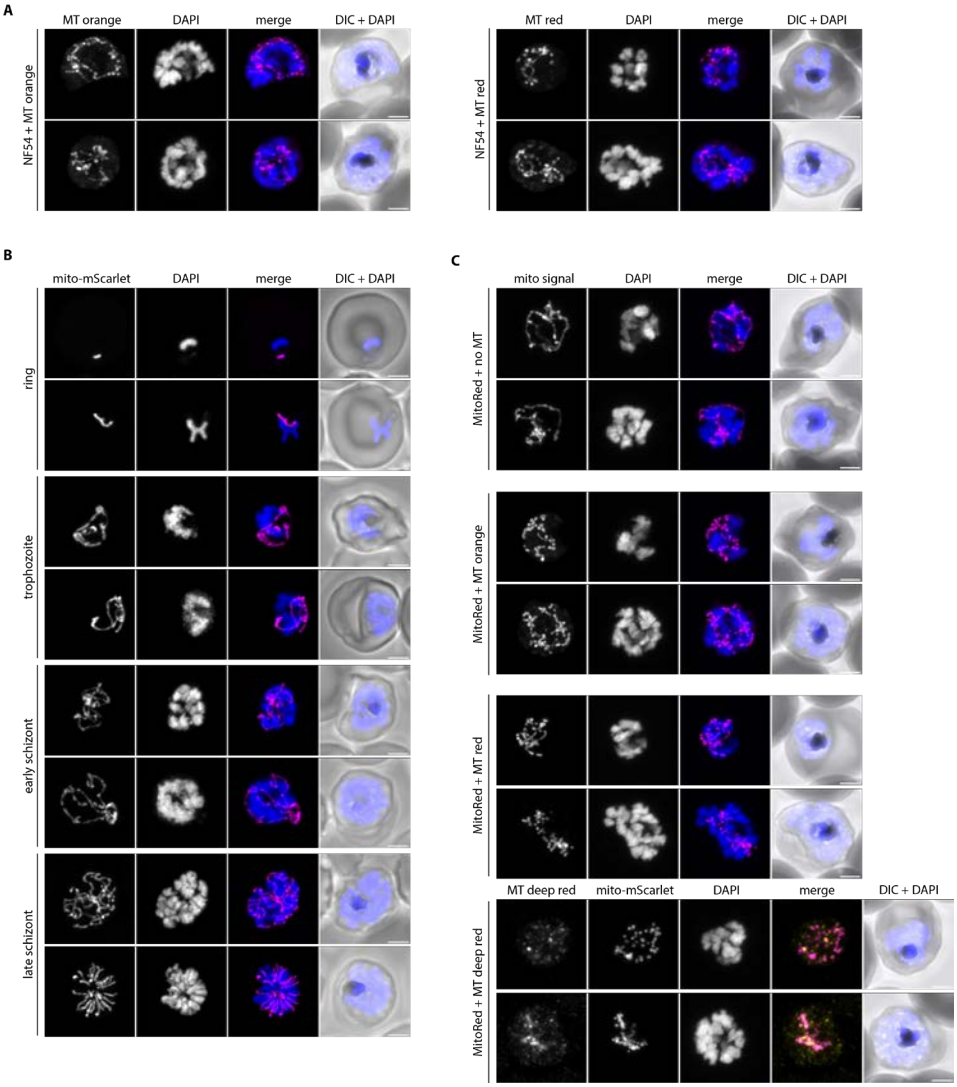

Figure 1. Comparison of MitoTracker and a new mitochondrial marker for fluorescence imaging. A) Fluorescent imaging of WT parasites stained with MitoTracker Orange CMTMRos (MT orange) or MitoTracker Red CMXRos (MT red). B) Fluorescence microscopy of MitoRed. The mito-mScarlet signal was observed in all asexual life-cycle stages including rings, trophozoites, early and late schizonts. No antibody staining was used and fluorescent signal observed is exclusively the mito-mScarlet signal. C) Fluorescence microscopy of MitoRed, either unstained (no MT) or stained with MT orange, MT red or MitoTracker Deep Red FM (MT deep red). Mito signal is the combined MitoTracker and mito-mScarlet signal that is observed in this channel. DAPI (blue) is used to visualize DNA and DIC (differential interference contrast) for general cellular context. All images are maximum intensity projections of Z-stacks (41 slices, 150 nm interval) taken with Airyscan confocal microscope. Scale bars, 2 µm.

Mitochondrial dynamics during gametocyte development and activation

To study mitochondrial dynamics throughout the malaria parasite life cycle, MitoRed parasites were induced to form gametocytes, which were fixed for microscopy on day 5, 7, 10, and 13 post induction. Parasites were stained for α tubulin to distinguish male and female gametocytes in stage IV and V. For each stage, between 11-19 parasites were imaged over two independent experiments and described observations were consistent over all analyzed parasites. In stage II and III gametocytes, the mitochondrion appears as a small knot that increases slightly in size when gametocytes become more mature (Figure 2A). This is consistent with our FIB-SEM data[20]. Evers *et al*. also showed that gametocytes have multiple mitochondria already from early gametocyte development onwards. Although light microscopy does not provide the resolution or ability to show membrane boundaries to distinguish the multiple mitochondria in stage II and III gametocytes, in stage IV gametocytes we could clearly observe separate mitochondria in both male and female gametocytes (Figure 2A, Figure S3A). There is no clear difference in stage IV gametocytes between male and female mitochondria. However, in stage V gametocytes the mitochondria in males appear slightly more dispersed, while the female mitochondria remain compact (Figure 2A, Figure S3B). Data from Evers *et al.* support this and showed consistently smaller volume and more loosely packed mitochondria in males compared to females[20]. When gametocytes are taken up by the mosquito via a blood meal, they are activated and transform into extracellular male and female gametes. While the female gametocyte develops into a single macrogamete, male gametocytes form up to eight flagellated microgametes. This transformation is triggered by a temperature drop, an increase in pH, and xanthurenic acid present in the mosquito midgut[21]. Upon *in vitro* activation, the difference between male and female mitochondria becomes more evident. Mitochondria in females remain in a compact knot while the parasite rounds up (Figure 2B). Interestingly, in males the mitochondria become smaller and more dispersed, and sometimes round up to small bean-like structures (Figure 2B, Figure 2D). This process already starts 2 min after activation. While this particular activation experiment was performed on a gametocyte culture that did not exflagellate for unclear reasons, it was repeated twice, and very similar results were found in exflagellating males (n=19) (Figure 2C). There was no significant difference between number of exflagellation events in MitoRed parasites compared to NF54 parasites (Figure S4A). An association of mitochondria with flagella is not uncommon and can also be observed in *e.g.* kinetoplastids, such as *Trypanosoma* and *Leishmania spp*, where the mitochondrion resides at the base of the flagellum, and in human sperm cells, where the mitochondrion wraps around the base of the

flagellum to provide energy for flagellar movement[22]. We found close apposition of the dispersed mitochondria to the axonemal tubulin in all 19 exflagellating males that were analyzed (Figure S4B, S4C).

Mitochondrial dynamics in mosquito stages

In the mosquito midgut, the male microgamete seeks out a female gamete for fertilization. After fertilization, the zygote takes one day to transform into a motile ookinete, which can traverse the midgut epithelium and differentiate into an oocyst. This oocyst expands and motile sporozoites are formed within the oocyst. When fully matured, the oocyst will burst and sporozoites will egress, spread through the hemolymph system, and invade the mosquito salivary glands. During oocyst development, the parasite mitochondrion has to expand enormously and then be divided over thousands of daughter sporozoites. However, very little is known about mitochondrial dynamics and only few studies have visualized the mitochondrion during these stages[17,23,24].

To explore if MitoRed parasites develop normally in the mosquito and to visualize mitochondrial morphology, mature MitoRed gametocytes were fed to *Anopheles stephensi* mosquitoes. One day after the feed, the mosquito blood bolus was extracted and stained with anti-*Pf*s25 conjugated antibodies to visualize ookinetes by live microscopy. We distinguished different stages of ookinete maturation as described by Siciliano *et al.*[25]. Due to the resolution limit of light microscopy, it was difficult to tell if there were one or multiple mitochondria as observed in gametocyte stages. Since we did not find evidence for the presence of multiple mitochondria in these ookinete development stages, we will refer to it as "the mitochondrion" in the coming paragraph, although we cannot rule out the presence of multiple mitochondria. During earlier stages of ookinete development (II), when ookinetes have a short protuberance attached to the round body, the mitochondrion resides in the round body (Figure 3A, 3B). When the protuberance starts to elongate further, one elongated mitochondrial branch stretches out and reaches into the protuberance. In stage III ookinetes, the mitochondrion stretches out further into the growing protuberance, spiraling out from the round body. We could not find clear stage IV ookinetes where the protuberance is at its full length, which could be explained by the swift development from stage IV to V ookinetes as was observed by Siciliano *et al.*[25]. However, in the mature stage V ookinetes, the mitochondrion appears as a tight knot in the main parasite body.

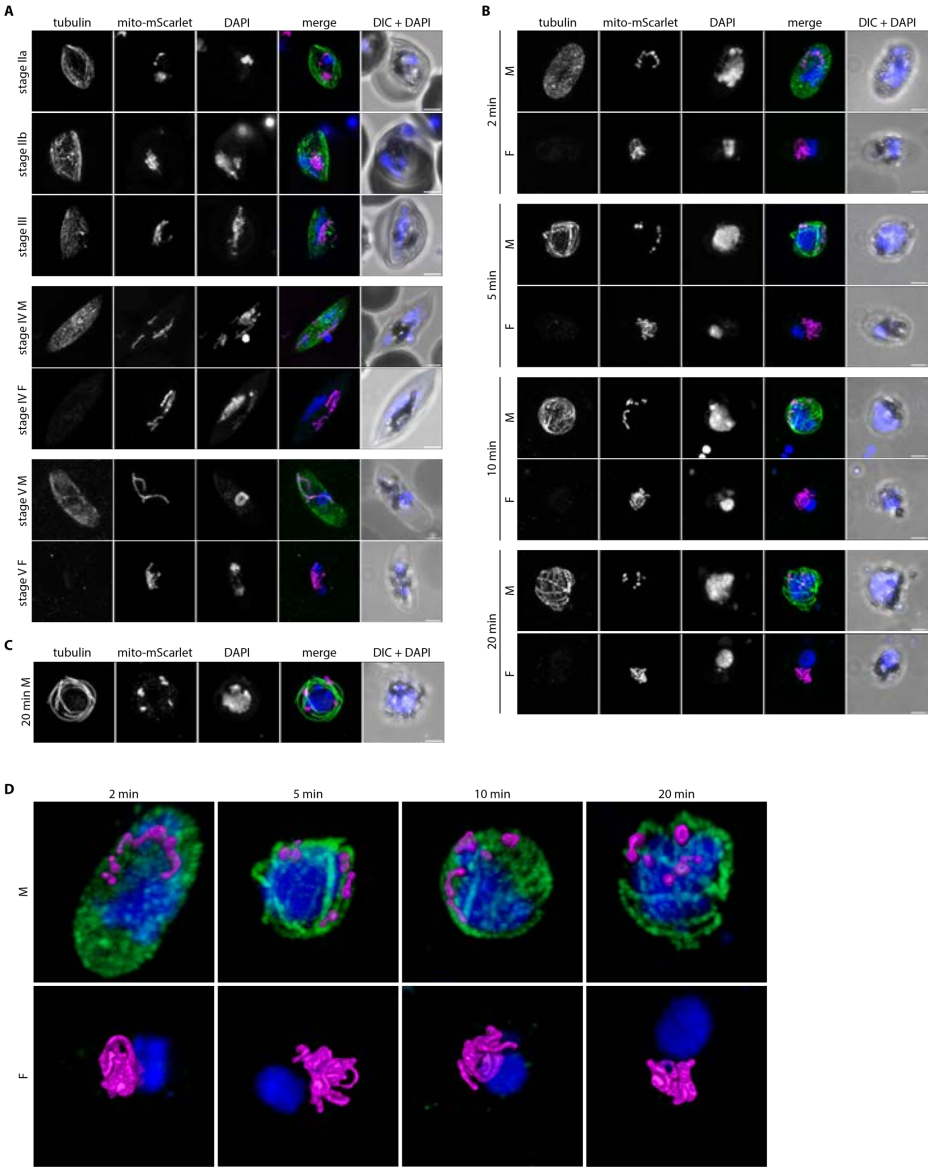

Figure 2. Mitochondrial dynamics during gametocyte development and activation. A) Immunofluorescence assay on MitoRed gametocytes stages IIa, IIb, III, IV, and V, stained with anti-β-tubulin (green) and DAPI (DNA, blue). The mito-mScarlet signal is shown in magenta. In stage IV and V, male (M) and female (F) gametocytes are distinguished based on the intensity of the tubulin signal (males high, females low). B) Immunofluorescence assay on MitoRed parasites during different stages of gametocyte activation (2, 5, 10 and 20 min after activation). C) Immunofluorescence assay on MitoRed exflagellating male gamete 20 min after activation. A-C) Images are maximum intensity projections of Z-stacks (41 slices, 150 nm interval) taken with an Airyscan confocal microscope. Scale bars, 2 µm. D) 3D visualization of male and female MitoRed parasites 2, 5, 10, and 20 min after activation. The mito-mScarlet fluorescent signal is segmented based on manual thresholding.

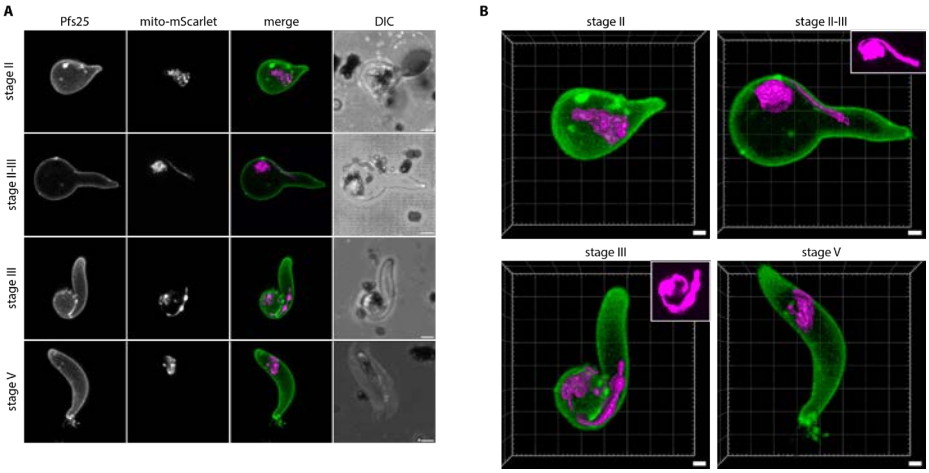

Figure 3. Mitochondrial dynamics during ookinete development. A) Live imaging of MitoRed ookinetes one day after mosquito feed. Different stages of ookinete maturation (II – V) were distinguished based on description by Siciliano et al.[25]. Cells were stained with an Alexa fluor 488 conjugated anti-Pfs25 antibody to visualize parasite outline (green). Images are maximum intensity projections of Z-stacks (30 slices, 185 nm interval) taken with an Airyscan confocal microscope. Scale bars, 2 µm. B) 3D visualization of different ookinete maturation stages. The mito-mScarlet fluorescent signal is segmented based on manual thresholding. Two smaller images in upper right corner of stage II-III and stage III are crops of the mitochondrial fluorescent signal with increased brightness and contrast. Scale bars, 1 µm.

At day 7, 10, and 13 after infection, mosquitoes from a feed with an infection rate of 100% and an average of 5 oocysts/mosquito were dissected and midguts were used for live confocal microscopy. At day 7, small oocysts (~10 µm diameter) were observed with a branched mitochondrial network stretched out throughout the cell (Figure S5A). Segmentation of the fluorescent signal based on manual thresholding indicated that the mitochondrion consisted of one continuous structure. Day 10 oocysts were much larger (~35 µm diameter) and the mitochondrial mesh-like network appeared more organized, also localizing to areas directly below the oocyst wall (Figure S5B). At day 13, oocysts of various sizes were observed. Some large oocysts (~70 µm diameter) showed a highly organized mitochondrial network, where mitochondrial branches were organized in a radial fashion around a central organizational point (Figure S5C). We named these points mitochondrial organization centers (MOCs). At least tens of these MOCs could be observed per cell. Some smaller oocysts (~35 µm diameter) at day 13 showed structures that looked like beginning MOCs (Figure S5D). However, several small oocysts showed a dispersed, globular mitochondrial signal, which we interpreted as unhealthy or dying parasite (Figure S5E). While several free sporozoites were observed in dissected midguts and salivary glands on day 16 (data not shown), we never observed an oocyst containing fully mature sporozoites with a divided

mitochondrion or an infected salivary gland on day 16 and 21 after infection. This indicates that sporozoites are produced and released into the hemocoel, however, they have a health defect that prevents them from infecting the salivary glands. Possibly the mitochondrial marker or the integration in the SIL7 locus causes issues for sporozoite development. We conclude that the MitoRed line is a great tool for mitochondrial visualization in asexual blood stages, gametocytes stages, and mosquito stages up until late oocysts (Supplemental Information S1) but that for studies later in the life cycle other tools need to be developed and tested.

Mitochondrial division during schizogony in asexual blood stages

Next, we aimed to use MitoRed for live visualization of mitochondrial division during schizogony in asexual blood stages. The biggest advantage of live imaging is that one parasite can be followed over time to capture mitochondrial fission events chronologically. Unfortunately, this proved to be challenging. All parasites imaged in several experiments for a duration exceeding 60 min exhibited significant morphological alterations, including mitochondrial swelling, fragmentation, and formation of vesicle-like structures, which indicate an unhealthy or dying parasite (Figure S6A). Additionally, we frequently observed parasites egressing from their red blood cells (RBCs) after approximately 45 min of imaging, indicating that imaged parasites are unhealthy (Figure S6B). Optimizing imaging conditions by reducing laser power, increasing time interval, better temperature control, and gassing of the imaging chamber with low oxygen mixed gas (3% O_2, 4% CO_2), did not improve parasite health during imaging. Therefore, we decided to go for a fixed imaging approach to capture mitochondrial division in asexual blood stages.

To capture mitochondrial fission, MitoRed parasites were tightly synchronized and fixed between 32-36 and 36-40 hours after invasion. In our culture system, MitoRed parasites have a replication cycle of approximately 40 hours, so we captured the last eight hours of schizont maturation before merozoite egress from the RBC. In order to distinguish the precise stage of schizont maturation, we included an anti-GAP45 antibody staining. Glideosome associated protein 45 (GAP45) is an inner membrane complex (IMC) protein and is important for RBC invasion[26,27]. IMC formation starts at the apical end of a developing merozoite during schizogony and continues to develop until it fully encapsulates the daughter merozoite with its own IMC membrane[28,29]. We used the stage of IMC formation and therefore merozoite segmentation as a marker for the maturity and age of the schizonts. Based on IMC and DNA staining, we differentiated four stages of schizont maturation: pre-segmentation (n=6), early-segmentation (n=9), mid-segmentation (n=15), and late-segmentation (n=10, Figure 4).

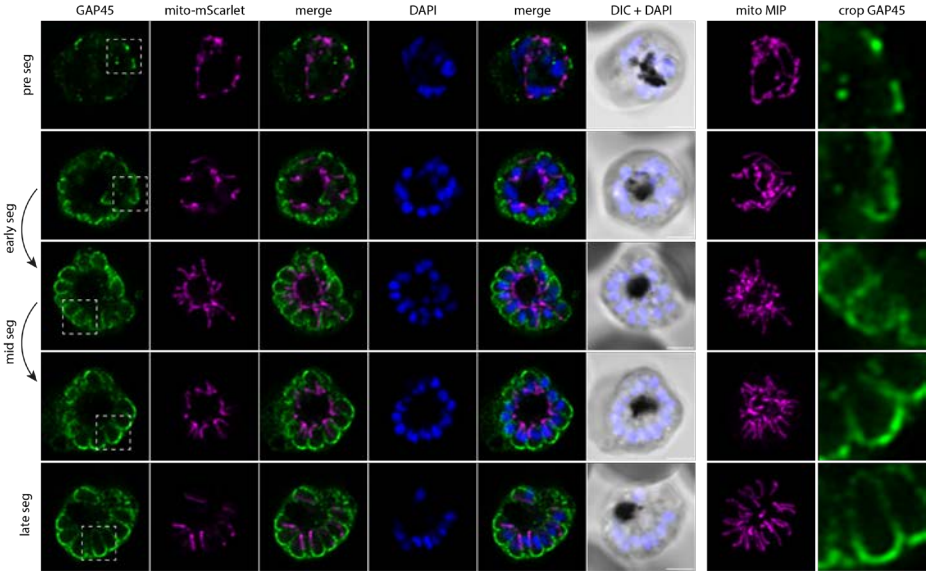

Figure 4. Mitochondrial fission in asexual blood-stage parasites. Immunofluorescence assay on MitoRed schizonts stained with anti-GAP45 antibody (green) to visualize IMC and DAPI (DNA, blue). The mito-mScarlet signal is shown in magenta. Four different stages of schizont maturity are distinguished: pre-segmentation (pre seg), schizonts still undergo nuclear division (nuclei are large and irregularly shaped) and there is no, or very little IMC staining without clear curvature. Early-segmentation (early seg), schizonts have (almost completely) finished nuclear division (nuclei are small and round), there is a clear IMC signal that has a curved shape at the apical end of the forming merozoites but is less than half-way formed. Mid-segmentation (mid seg), the IMC of the segmenting merozoites in these schizonts is more than half-way formed, but there is still a clear opening at the basal end of the merozoite. Late-segmentation (late seg), in these schizonts the IMC seems to be completely formed with no clear opening at the basal end of the forming merozoites. Images are single slices of a Z-stack taken with an Airyscan confocal microscope. Images of the mito-mScarlet signal in the seventh column are maximum intensity projections (MIPs) (41 slices, 150 nm interval). Images in the eighth column are crops of the GAP45 signal depicted in the first column, indicated by the dotted-line areas. Scale bars, 2 µm.

We generated and classified Z-stack images of 40 schizonts, which allowed us to reconstruct a timeline of mitochondrial fission. During pre- and early-segmentation stages, the branched mitochondrial network stretches throughout the parasite. Only at the end of early-segmentation stages, when the IMC is approximately halfway formed, the mitochondrion is oriented around the food vacuole in the center of the parasite with its branches pointing outwards in a radial fashion, creating a "cartwheel"-like structure (Figure 4). As the IMC progresses further and schizonts enter the mid-segmentation stage, this mitochondrial cartwheel structure is divided into smaller fragments, which maintain their radial branch orientation into the segmenting merozoites. Only when IMC formation appears complete, did we observe

mitochondria that are entirely divided and distributed over the daughter merozoites. This highlights the extremely late timing of this process. These mitochondrial division stages were confirmed in a second, independent 3D imaging experiment (Figure S7).

To further quantify the numbers and sizes of mitochondria and to create 3D renderings of the mitochondrial network throughout segmentation, we utilized threshold-based masking of the fluorescent signal (Figure 5). During pre- and early-segmentation stages, the mitochondrial network consists of one large fragment (between 7-14 μm^3), often with 1-3 smaller fragments (<1.5 μm^3) (Figure 5AI, 5AII). As evident from our FIB-SEM data (Figure S10A), the mitochondrion features constricted regions, characterized by notably reduced diameters. Hence, the smaller fragments observed during these stages are likely not autonomous but caused by the reduced fluorescent marker intensity in the constricted regions. At the end of early-segmentation stages when the IMC is almost halfway formed, the mitochondrial network starts to orient itself in a radial fashion around the center of the parasite (Figure 5AII), consistent with the 2D image analysis (Figure 4). During mid-segmentation stages, the radial mitochondrial branches elongate further into the developing merozoites, and the large mitochondrial fragment is divided in smaller fragments at the center of the cartwheel structure (Figure 5AIII). There is a slight increase in number of mitochondrial fragments per parasite, specifically the "intermediate" sized mitochondrial fragments of 1-4 μm^3. Only in the last stage of merozoite segmentation, there is a big increase in the number of mitochondrial fragments (Figure 5C). Of note, there appears to be no correlation between this number and the number of nuclei in the parasites (Figure 5B, 5C). A likely technical explanation is the limited Z-resolution of light microscopy and the different nuclear and mitochondrial segmentation methods. When mitochondrial fragments are located closely above each other, the limited Z-resolution in combination with threshold-based masking can cause the adjacent fragments to appear as one continuous structure. Therefore, the number of mitochondrial fragments per schizonts will be underestimated in these late schizont stages. The nuclei on the other hand were segmented through an automated (spherical) object detection algorithm which does not have this problem. Even when the IMC formation appears to be completed based on the GAP45 staining, only 20% of cells appear to have concluded mitochondrial fission as indicated by exclusively containing homogenously small sized mitochondrial fragments (<1.0 μm^3) (Figure 5AIV). During the late segmentation stage, some parasites still have a large mitochondrial fragment of more than 5 μm^3, while others only have small and intermediate sized mitochondrial fragments (Figure 5D). This suggest that division of the mitochondrial cartwheel structure into small fragments is a fast, stepwise process that does not happen in a 2^n progression and happens only in the final moments of merozoite segmentation.

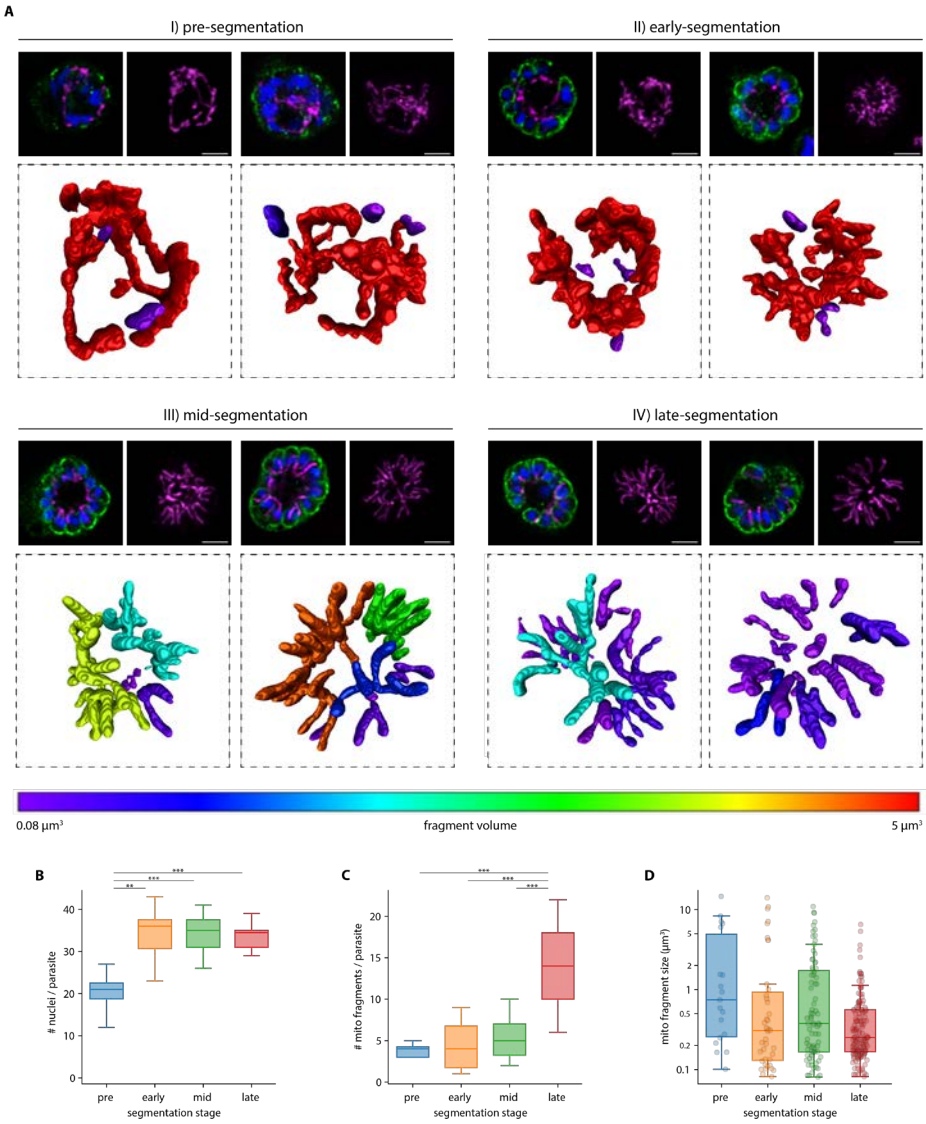

Figure 5. 3D analysis of mitochondrial fission stages during schizogony. A) 3D visualization of mitochondrial segmentations based on thresholding of the mito-mScarlet signal in Arivis image analysis software. Smaller images in top row are a single slice of the Z-stack with anti-GAP45 labelling (IMC, green), DAPI (DNA, blue) and mito-mScarlet (magenta), and a maximum intensity projection of the mito-mScarlet signal. The larger bottom picture is a 3D visualization of the segmented mitochondrial signal. The color of the mitochondrial fragment represents the size of this fragment, as is shown in the color bar at the bottom. Two representative parasites are depicted for each of the four segmentation stages defined in Figure 4. Scale bars, 2 µm. B) Boxplot indicating the number of nuclei per parasite in the different segmentation stages. **, $p<0.01$; ***, $p < 0.001$. C) Boxplot indicating the number of mitochondrial fragments per parasite in the different segmentation stages. ***, $p < 0.001$. D) Boxplot indicating the size of the mitochondrial fragments in the different segmentation stages.

Visualization of mitochondrial and apicoplast division using volume electron microscopy

Although the use of light microscopy allowed us to reconstruct mitochondrial fission in good temporal resolution, its limited spatial resolution and reliance on indirect staining leaves some questions unanswered. Our recent volume electron microscopy study detailed parasite organelle structures at a nanometer resolution bringing many new insights to the light[20]. Here, we reused the underlying FIB-SEM data, which besides gametocytes also contains asexual blood-stage parasites from different stages, to examine mitochondrial fission with high resolution. Asexual parasites in different stages of schizogony were selected and organelles including nuclei, mitochondrion, and apicoplast were segmented for 3D rendering (detailed description per parasite in Tables S2 and S3). The mitochondrion and apicoplast can be recognized by their tubular shape in addition to the double membrane of the mitochondrion and the thicker appearance of the four membranes of the apicoplast. In line with the results from our light microscopy experiments, the mitochondrion is a large, branched network stretched throughout the cell in early schizont stages before segmentation has started (Figure 6, Movie 1). The apicoplast is also a branched network, however, it is much smaller than the mitochondrion (Table S2). The apicoplast network is divided into smaller fragments of different sizes when nuclear division is still ongoing and IMC formation has started (Figure 7, Table S3, Movie 4). When nuclear division is finishing and the IMC envelops part of the nucleus, apicoplast division is completed (Figure 6, Movie 5). The mitochondrion starts to orient its branches in a radial fashion towards the developing merozoites. When nuclear division is completely finished and the IMC envelops most of the nucleus, the mitochondrion forms a clear cartwheel structure with its branches pointing into the developing merozoites (Movie 6). During late segmentation stages, where only a small opening is connecting the merozoite to the residual body, the mitochondrion is divided into smaller fragments of various sizes (Movie 7). While some mitochondrial fragments have a volume comparable with the mitochondria in a fully segmented parasite (0.016 - 0.036 μm^3), other fragments are still 2-4 times that volume (FigureS8).* These larger mitochondrial fragments have several branches that are pointing into developing merozoites but are still connected to each other outside the merozoites. In an almost fully segmented schizont, where most merozoites are fully developed and only few merozoites are still connected to the residual body through a small opening, the mitochondrial division is completed and the number of mitochondrial fragments is the same as the number of merozoites (Movie 8). These findings corroborate our light microscopy data and confirm the mitochondrial division stages, position of relevant structures not stained in light microscopy, and timing of mitochondrial and apicoplast division during schizogony.

** Note: The volumes measured in the FIB-SEM data differ greatly from the volumes measured in the 3D fluorescent microscopy data. This can be explained by the limited spatial resolution of fluorescent microscopy because of the diffraction of light. The diffraction limit of the confocal Airyscan microscope that was used is ~120 nm in lateral direction and ~350 nm in axial direction. The diameter of the mitochondrion in asexual blood-stage parasites is ~140 nm, which is at the edge of the resolution limit. Therefore, the volume measurements of thresholding-based segmentation of the fluorescent signal are not very accurate and quickly over-estimate the volume. These volume estimations should merely be used to compare relative volumes of mitochondrial fragments. The FIB-SEM data has a resolution of 5 nm in lateral direction and 15 nm in axial direction, which allows much more precise visualization of organelles and volume measurements.*

Interaction between mitochondrion and apicoplast in late stage schizonts

During schizogony, the mitochondrion and apicoplast show different moments of close association. Prior to apicoplast division, the mitochondrion and apicoplast have several apposition sites, which have also been described by Evers *et al.*[20] (Figure S9A and S9B). It remains unclear if these close associations represent true membrane contact sites that facilitate the exchange of metabolites or lipids between the organelles, or if these are merely random due to the limited space in the parasite. When apicoplast division is finished, the endings of the mitochondrial branches reach towards the basal endings of the apicoplasts (Figure S9D). Subsequently, the branches of the mitochondrial cartwheel structure align with the apicoplast over its entire length (Figure S9C and S9D). This close alignment remains when mitochondrial division is complete.

Bulbous mitochondrial structures with double membrane invaginations

The parasite mitochondrion does not have a consistent diameter during schizogony. While some parts have a very small diameter other areas of the mitochondrion are more bulbous (Figure S10A). These bulbous parts often contain double membrane invaginations of various size and shape (Figure S10C, S10D, S10F). These bulbous invagination structures (bulins) are found in all schizont stages and vary greatly in shape, size, and location in the mitochondrial network. In early stage schizonts, bulins can be found at branching points and in the middle of a continues branch of the mitochondrial network (Figure S10D, S10F). However, during mid-segmentation stages, when the mitochondrion is oriented in its typical cartwheel structure, bulins are consistently observed at the base of a mitochondrial branch near the merozoite entrance (Figure 6, Figure S10D, S10F). These merozoite-entrance bulins were found in all eight mid-segmentation stage schizonts from two independent experiments (example shown in Movie 9). Bulbous areas at the base of mitochondrial branches are also observed with fluorescent microscopy (Figure S10B). This, and the specific location of bulins, makes them unlikely an artifact of fixation or sample preparation

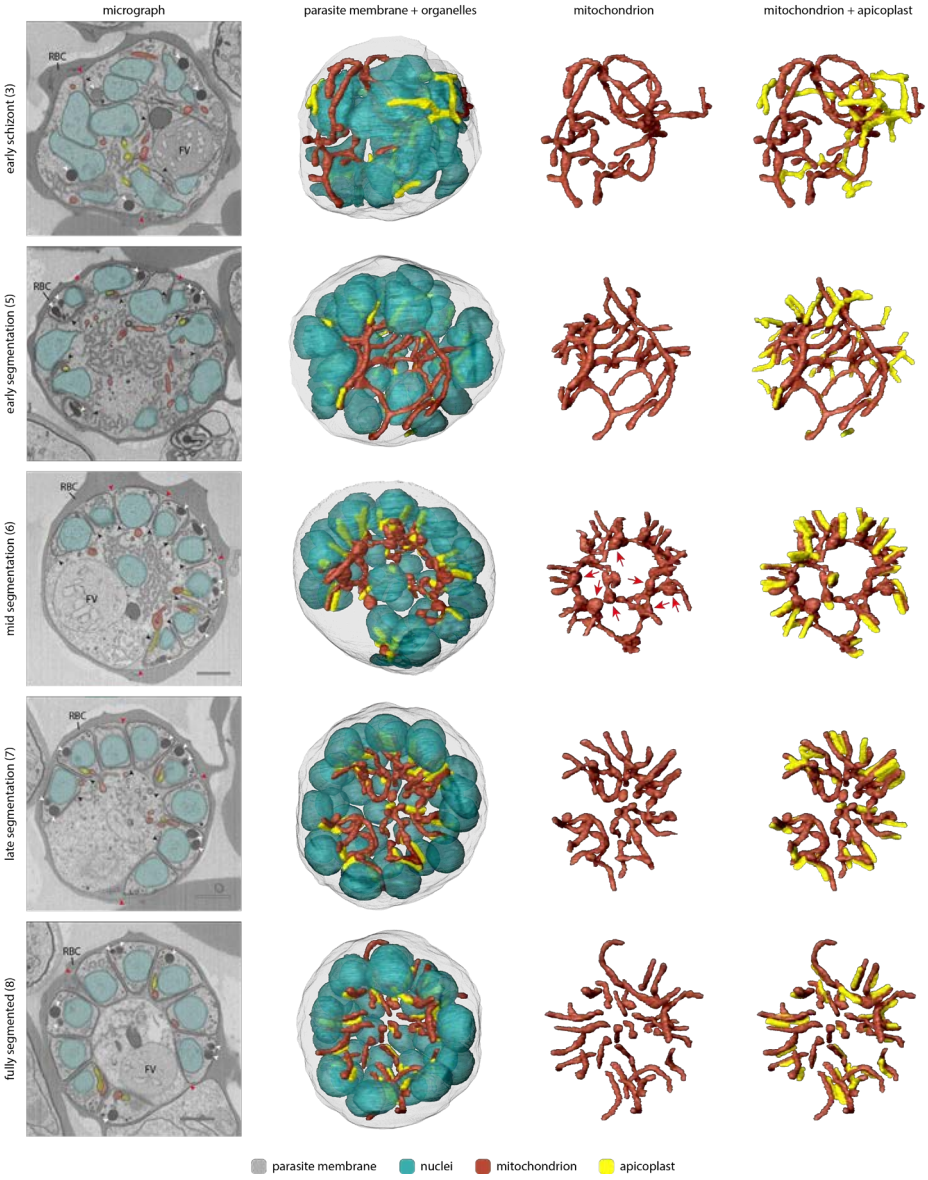

Figure 6. 3D rendering of mitochondrion and apicoplast during different stages of schizogony. First column contains representative micrograph images from different schizont stages. The numbers between brackets indicate the parasite ID number and detailed information can be found in table S2 and S3. The red blood cell (RBC) and food vacuole (FV) are indicated by their abbreviations. Rhoptries are indicated by white arrowheads, parasitophorous vacuole membrane is indicated by red arrowheads, and parasite membrane invaginations are indicated by black arrowheads. Scale bars, 1 µm. The second, third, and fourth column contain 3D renderings of parasite membrane (gray, 5% transparency), nuclei (teal, 50% transparency), mitochondrion (red), and apicoplast (yellow). Red arrows indicate merozoite entrance bulins.

for the FIB-SEM, although this cannot be ruled out completely. Bulins that reside at the entrance of a forming merozoite during the cartwheel phase are typically characterized by contact with the basal end of the divided apicoplast, and a small constriction right above the bulin where the mitochondrial branch enters the merozoite (Movie 10). Bulbous areas at the base of the mitochondrial branches are also observed with fluorescent microscopy (Figure S10B). In late-segmentation schizonts, we observed small bulins at the base of a divided mitochondrial fragment or at the entrance of a merozoite when the mitochondrial branch was not yet divided (Figure S10D, S10F). Sporadically, we also found bulins in the apicoplast (Figure S10E). The significance and function of these bulins remain to be explored, but it is tempting to speculate about a possible role in organelle division.

Centriolar plaques associate with apicoplast but not mitochondrion during organelle segregation

In mammalian cells, segregation of organelles is coordinated by microtubules that arise from the centrosomes, or so-called microtubule organizational centers (MTOCs). *Plasmodium* parasites lack canonical centrosomes but organize their mitotic spindle from a structure called the centriolar plaque (CP), which is embedded in the nuclear envelope[30,31]. Expansion microscopy studies from Liffner *et al.* have suggested an association of the CPs with both the mitochondrion and the apicoplast during schizogony, suggesting their involvement in organelle segregation[32]. In our FIB-SEM images, we can distinguish the CP by electron dense coffee filter-shaped regions in the nucleus (Figure 7A). In an early schizont that still lacks IMC or rhoptries, nuclei contain one or two CPs, which are oriented to the periphery of the parasite. 3D renderings show no direct association between the CPs and the mitochondrion or apicoplast (Figure 7B, Movie 1). Although the distances between the mitochondrion and CPs (average 616 nm, SD 235 nm) in this early schizont are significantly smaller than the apicoplast-CPs distances (average 1350 nm, SD 260 nm), there is no direct interaction between the mitochondrion and CPs since the smallest CP-mitochondrion distance measured is 332 nm. The significant difference can be explained by the fact that the apicoplast is located in the center of the parasite, while the mitochondrion is larger and stretched throughout the whole cell leading to coincidental closer proximity to the peripheral CPs. In slightly later stage schizonts where IMC and rhoptry formation has started, all nuclei contain either two CPs, or one CP that is dividing. A portion of the CPs associated with the apicoplast, specifically with the endings of apicoplast branches (Movie 2). When the IMC is developed slightly further, all CPs associate with the apicoplast over the total length of the peripherally localized apicoplast network (Movie 3). While two CPs from the same nucleus usually associate with one apicoplast branch

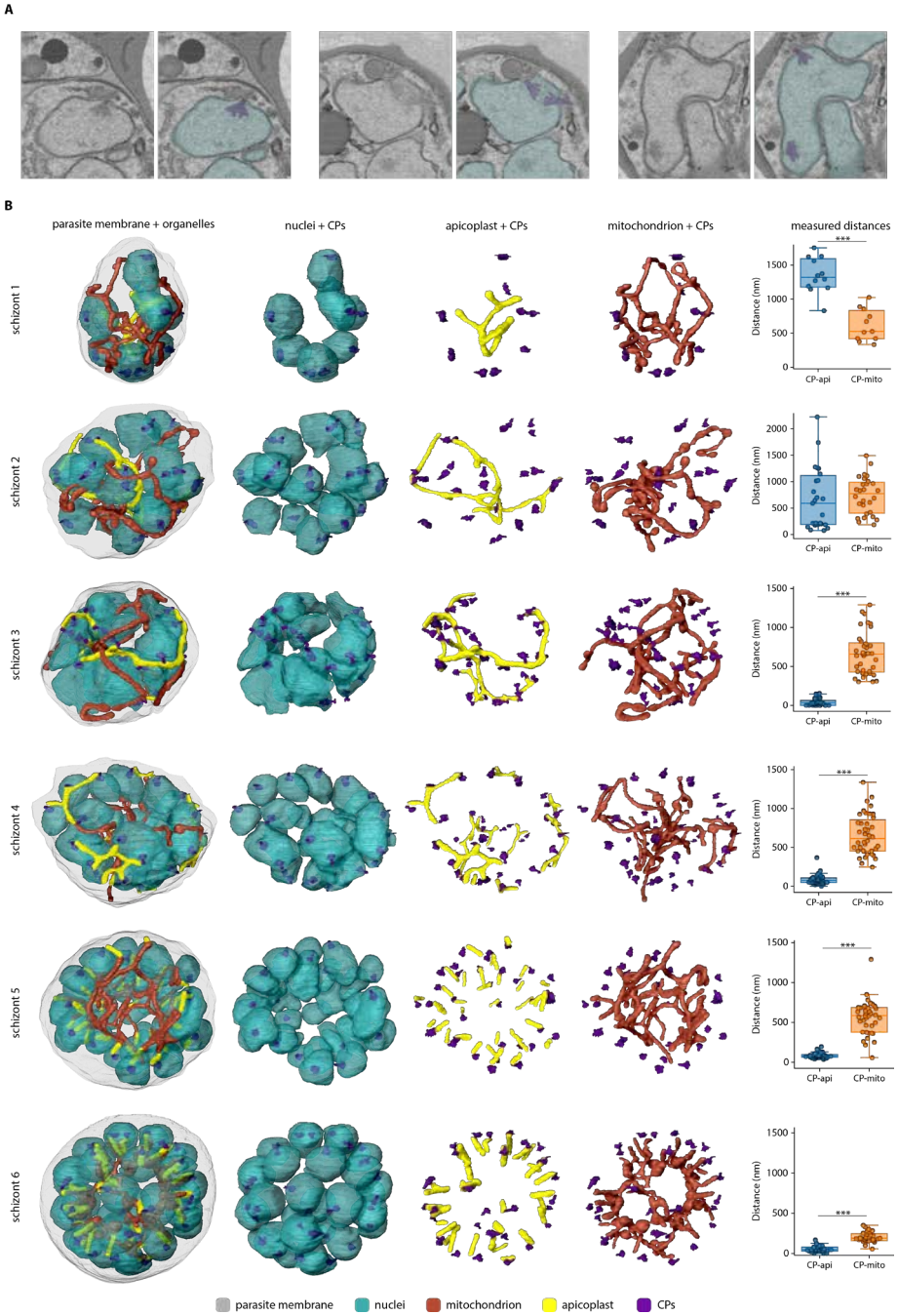

Figure 7. Association of apicoplast and not the mitochondrion with centriolar plaques during schizont development. A) Micrographs of nuclei (teal) with centriolar plaques (CPs, purple). B) 3D rendering of nuclei (teal), apicoplast (yellow), mitochondrion (red), CPs (purple), and parasite membrane (gray, 5% opacity). Parasite ID numbers are indicated on the left side of the micrograph images. Right column shows measured distances between CPs and closest point to the apicoplast or mitochondrion. ***, $p < 0.001$.

(Figure S11A), sometimes these associate with completely different branches of the apicoplast network (Figure S11B). Furthermore, the distances between the CPs and apicoplast are significantly smaller (42 nm average, SD 46 nm) compared to those measured in earlier stages as well as to the unchanged CP-mitochondrion distances (663 nm average, SD 274 nm) (Figure 7B). The association between CPs and apicoplast continues during and after apicoplast division (Movie 4-7). After apicoplast division, each apicoplast fragment is associated with one CP at its peripheral end (53 nm average distance, SD 37 nm) (Movie 5). During mid-segmentation stages, the endings of the mitochondrial branches are close to the CPs (202 nm average distance, SD 65 nm) (Movie 6). However, this seems to be a result of the close association of the mitochondrion with the apicoplast, rather than a direct interaction between the mitochondrion and the CPs. In a fully segmented schizont, the CPs were much smaller and did not show a clear extranuclear compartment (Movie 8). This close and very consistent association between the apicoplast and the CP, suggest an important role in apicoplast segregation, while the mitochondrion likely deploys different mechanisms to accomplish its proper distribution over the forming merozoites.

Discussion

In contrast to most eukaryotes, the fast-replicating *P. falciparum* asexual blood-stage parasites harbor only a single mitochondrion. Consequently, proper division and distribution of this organelle during schizogony is crucial to ensure all daughter cells receive a mitochondrion. Here, we visualized the poorly understood mitochondrial dynamics in blood and mosquito stages using a new parasite line with a fluorescent mitochondrial marker and super-resolution 3D imaging methods. During blood-stage schizogony, a cartwheel structure is formed and divided into smaller, unequally sized mitochondrial fragments in a stepwise process. Final division into single mitochondria happens during the last stage of merozoite segmentation. These division steps were cross validated by analyzing available FIB-SEM data with nanometer resolution. This also allowed us to reconstruct apicoplast division and its interactions with the mitochondrion. Finally, we showed that the apicoplast but not the mitochondrion associates with the CPs during merozoite formation.

To date, the visualization of *Plasmodium* mitochondria has largely relied on MitoTracker dyes. However, these dyes are toxic at nanomolar concentrations[15,16] and our data suggest that they may alter mitochondrial morphology (Figure 1). We developed a reporter parasite line harboring a fluorescent mitochondrial marker

that shows a more continuous and less punctate staining pattern compared to MitoTracker dyes and is compatible with live and fixed imaging without necessitating antibody labeling. Unfortunately, MitoRed is not well suited for long-term time lapse imaging (>1h) since parasites showed various signs of poor health, probably due to phototoxicity. While expansion microscopy is currently not feasible with MitoRed, addition of a linear epitope tag would make this marker compatible with the required denaturation step.

In line with our earlier observations, we demonstrated multiple mitochondria in gametocyte stages[20]. As discussed by Evers *et al.*, there are several possible reasons for the emergence of multiple mitochondria in gametocytes, such as adaptation to a metabolically varied environment, distribution mechanism of mtDNA, or management of reactive oxygen species. We expand upon these observations by also imaging gametocytes during activation. In males, mitochondria become more dispersed while female mitochondria remain in a tight knot. One possible explanation for this is that mitochondria in males are distributed to specific locations in the cell to provide energy locally for certain processes. In sperm cells, the mitochondrion resides at the base of the flagellum to provide energy for flagellar movement[22]. While we observed close apposition of the mitochondria with axonemal tubulin in some activated males using light microscopy (Fig. S4), this was not consistently observed in all males, and we lack the resolution to prove real association. Another explanation could be that the parasite undergoes a form of mitophagy as a source for proteins, lipids, and nucleotides required for the rapid nuclear division and microgamete formation. Even though mitophagy has not been studied in *Plasmodium*, some homologues of the general autophagy pathway have been identified[33]. Autophagy as a survival mechanism was described for *P. falciparum* and *T. gondii* under starvation conditions[34,35]. In *T. gondii*, the fragmentation of the mitochondrion was reversed by using the established autophagy inhibitor 3-methyl adenine[34]. Alternatively, the distribution of the mitochondria could merely be a consequence of the nuclear expansion in the cell.

Mitochondrial dynamics during mosquito stages is poorly understood and to our knowledge studies have thus far been restricted to *P. berghei*[17,23,24,36]. Here, we visualized the mitochondrion in *P. falciparum* during mosquito stages for the first time. In early oocyst stages, the mitochondrion resembles the extensively branched network from asexual blood-stage schizonts. During oocyst development, the mitochondrial network organizes into multiple MOCs that resemble the cartwheel structure observed in asexual blood stages. Although these mitochondrial observations should be interpreted with care since oocysts did not form salivary

gland populating sporozoites and might therefore not be representing healthy oocysts (see the supplement for a more extensive discussion), in *P. berghei* liver-stage schizonts, a very similar mitochondrial organization was observed in sub-compartments created by large membrane invaginations[12,37]. Similar sub-compartments are present during oocyst development[37]. Based on apicoplast visualizations in *P. berghei* and our observations of the formation of MOCs during oocyst stages, mitochondrial and apicoplast dynamics in these sub-compartments in both oocyst and liver stages resemble the dynamics of these organelles in blood-stage schizogony[12,38,39].

Although the use of new imaging techniques, such as expansion microscopy and 3D volume EM, have revealed new insights in mitochondrial dynamics, many questions about the timing and organization of mitochondrial division remained unanswered[11,32]. In an earlier literature review, we proposed three possible mitochondrial division models: synchronous fission, outside-in fission, or branching point fission[9]. Here, we used a new mitochondrial marker and advanced imaging techniques, such as Airyscan confocal microscopy, to reconstruct mitochondrial fission during schizogony. The use of volume EM provided the resolution required to verify our fluorescence-based mitochondrial fission model while simultaneously shedding light on the division of the second endosymbiotic organelle, the apicoplast. This allows us to propose a new, detailed model of the organellar division and segregation (Figure 8).

In this model, we describe the cartwheel orientation of the mitochondrion, its non-geometric 2^n division, the late timing of division, and its association with the apicoplast. The apicoplast divides when nuclear division is still ongoing and merozoite segmentation has just started. Similar to the mitochondrion, its division does not happen in a geometric 2^n progression, but different sized apicoplast fragments are observed in a mid-division stage. The timing and orientation of the apicoplast-mitochondrion appositions, suggest a potential role of the apicoplast in mitochondrial segregation. However, doxycycline treated parasites, that have lost their apicoplast and are chemically rescued by isopentenyl pyrophosphate supplementation, can still produce viable merozoites, suggesting that association with the apicoplast is not essential for mitochondrial segregation[40]. The specific types of membrane contact between both endosymbiotic organelles, whether these consist of direct physical contacts, membrane fusions or tethering proteins, may vary and remain to be explored. However, EM tomography data from Sun *et al*. show there are hints of connecting structures between the mitochondrion and apicoplast in areas where the distance between the organelles is very small and

similar to the distance between the inner and outer membranes of the organelles themselves in merozoites, suggesting physical link between the organelles.

In other eukaryotic models, mitochondrial fission is facilitated by adaptor proteins on the cytoplasmic side of the outer mitochondrial membrane that recruit dynamin GTPases, which in turn oligomerize to form a constrictive ring around the organelle[9]. The only conserved adaptor protein in *P. falciparum*, Fission 1 (Fis1), is dispensable in asexual blood stages precluding an essential role in mitochondrial fission during schizogony[41]. Malaria parasites also harbor three dynamin-related proteins[9]. As the timing of the apicoplast division precedes that of the mitochondrion, it is conceivable that (parts of) the same dynamin-based machinery may be reused for mitochondrial fission. Indeed, in a recent pre-print *P. falciparum*, dynamin 2 (*Pf*DYN2) was shown to mediate both apicoplast and mitochondrial fission[42]. Which other proteins comprise the mitochondrial division machinery in *P. falciparum* remains to be explored.

Their morphological features, timing of appearance, and specific location at the entrance of the developing merozoite during mid-segmentation stages suggests that the bulbous invagination structures, or bulins, could play a role in mitochondrial fission. A role in the distribution of certain components – e.g. mitochondrial DNA, proteins, or protein complexes – to the branches of the mitochondrial cartwheel structure that enter the merozoite is also conceivable. However, in earlier stages, bulins are also found at branching points or in continuous parts of the mitochondrion and apicoplast, perhaps suggesting possible roles in more general membrane remodeling of the organellar network.

We also observed CPs, the *P. falciparum* analogue of the centrosome, which function as microtubule organizing centers and are important for mitosis and cell cycle regulation[43,44]. In *T. gondii*, the centrosome associates with the apicoplast and ensures correct segregation of the organelle during daughter cell formation[45,46]. Recent expansion microscopy data suggested interaction of the CP with both the apicoplast and the mitochondrion in *P. falciparum*[32]. From the onset of IMC and rhoptry formation, we observed close apposition of the CPs and apicoplast, but not the mitochondrion (Figure 8). This CP-apicoplast association continues during and after apicoplast division, indicating a role of the CPs in apicoplast segregation. In other apicomplexan parasites, such as *Toxoplasma gondii* and *Sarcocystis neurona*, centrosomes have also been indicated to be involved in apicoplast organization and distribution during cell division[45,47]. The initial absence of CP-apicoplast association and the later association of two CPs from one nucleus

with separate apicoplast branches suggests an active recruitment strategy. Motor proteins facilitate intracellular transport of organelles along the cytoskeleton in multicellular eukaryotes. While dynein and kinesin facilitate organelle transport along microtubules, myosin motor proteins transport organelles along actin filaments to specific locations in the cell[48]. Previous studies have shown a critical role of F-actin and myosin F in the inheritance of the apicoplast in *P. falciparum* and *T. gondii*[49–52]. In *T. gondii* parasites that lack myosin F, the apicoplast fails to associate with centrosomes[53]. Therefore, we hypothesize that myosin facilitates recruitment of the apicoplast branches over the actin filaments to the CPs. Although the mitochondrion is close to the CPs in late segmentation stages, the distance is always significantly bigger than the apicoplast-CP distance. Additionally, mitochondrial branches reach much further into the merozoites when fully segmented, compared to the apicoplast. Furthermore, conditional knockout of *PfACT1* (actin-1) did not alter mitochondrial morphology in asexual blood-stage schizogony[49]. Therefore, it remains questionable if the mitochondrial branches are recruited to the CP via a similar mechanism as the apicoplast.

Volume EM is a powerful tool to study biological questions as it allows the visualization of complex, connecting structures and gives spatial and cellular context. Here, we reused available FIB-SEM data, which contains sexual and asexual blood-stage malaria parasites from many different stages of intra-erythrocytic development. Future reinterrogation of the data could facilitate in answering other biological questions that are beyond the scope of this paper, such as rhoptry biogenesis and development of the apical complex.

In this study, we have developed a reporter parasite line harboring a fluorescent mitochondrial marker – integrated in a new genomic locus – that can be used for mitochondrial visualization in blood and early mosquito stages. This allowed us to visualize mitochondrial division in unprecedented detail and describe the relative timing and of mitochondrial fission and segregation using high-resolution confocal microscopy and FIB-SEM image analysis. Combined with new insights in apicoplast division, mitochondrial and apicoplast interactions, and association of the apicoplast with the CP during schizogony, this allowed us to propose a new, detailed model of apicoplast and mitochondrial division during schizogony. These findings pave the way to home in on the molecular mechanisms underpinning mitochondrial and apicoplast division and segregation.

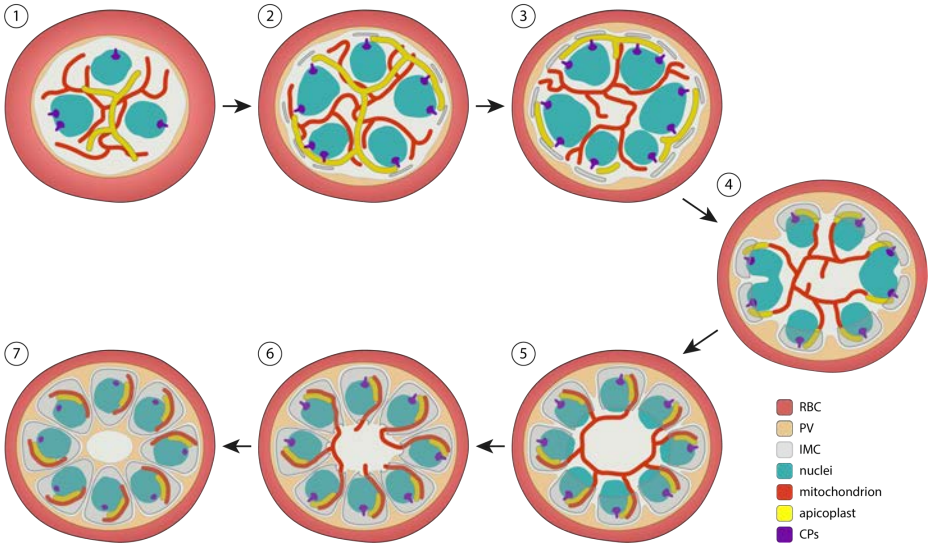

Figure 8. Schematic model for mitochondrial and apicoplast division and segregation in *P. falciparum* during schizogony. (1) Nuclear division is ongoing, while inner membrane complex (IMC) formation has not started and both the mitochondrion and apicoplast are branched networks. The apicoplast localizes more to the center of the cell, while the mitochondrion is stretched throughout the whole cell. (2) When IMC formation starts, the apicoplast branches associate with the centriolar plaques (CPs) at the periphery of the parasite. (3) The apicoplast divides in a non 2^n progression, while it keeps its interaction with the CPs. (4) When nuclear division is finishing, apicoplast division is completely finished. The apical end of the apicoplast fragments associate with the CPs, while mitochondrial branches associate with the basal end of the apicoplast fragments. (5) The IMC develops further and envelops large parts of the nuclei. The mitochondrion orients itself in a cartwheel structure, while its branches align with the apicoplast fragments. (6) IMC formation is almost finished, and just a small opening connects the merozoites to the residual body. The mitochondrion divides in a non 2^n progression. The apicoplast still associates with the CPs and aligns with mitochondrial branches/fragments. (7) Merozoite segmentation is complete, the apicoplast loses its clear association with the CPs since they become smaller and do not have a clear extra nuclear compartment anymore. The mitochondrion is fully divided and still aligns with the apicoplast. Red blood cell (RBC), parasitophorous vacuole (PV).

Materials and Methods

P. falciparum culture and transfections

P. falciparum NF54 and MitoRed parasites were cultured in RPMI1640 medium supplemented with 25 mM HEPES, 10% human type A serum and 25 mM $NaHCO_3$ (complete medium). Parasites were cultured in 5% human RBCs type O (Sanquin, the Netherlands) at 37°C with 3% O_2 and 4% CO_2. For transfection, 60 µg of homology-directed repair plasmid was linearized by overnight digestion, precipitated, and transfected with 60 µg Cas9 plasmid using ring transfection[54,55]. Briefly, a ring-

stage sorbitol synchronized parasite culture was transfected with the plasmids by electroporation (310 V, 950 µF). Five hours after transfection, parasites were treated with 2.5 nM WR99210 for five days. Success of transfection was assessed by integration PCR (Fig S1, Table S1).

Plasmid constructs

To generate the base SIL7 reporter plasmid (pRF0057) the 5′ and 3′ homology regions for SIL7 were amplified from genomic NF54 DNA (Table S1) and cloned into the pBAT backbone[19] with NgoMIV and AleI (5′) and BmgBI and AatII (3′). For the final MitoRed repair plasmid, first the mScarlet sequence was amplified from p1.2RhopH3-HA-mScarlet (a kind gift from Prof. Alan Cowman)[56] (Table S1). The mScarlet sequence was cloned into pRF0077 (empty tagging plasmid with PBANKA_142660 bidirectional 3′UTR) with AflII and EcoRI restriction sites, generating pRF0078 intermediate plasmid. The HSP70-3 promotor (prom) and targeting sequence (t.s.) sequence was cloned into pRF0078 with EcoRI and NheI restriction sites, generating pRF0079 intermediate plasmid. The whole mitochondrial marker (HSP70-3 prom + t.s. + mScarlet) was cloned from pRF0079 into pRF0057 with EcoRI and AflII restriction sites, generating pRF0191, the final repair plasmid. CRISPR-Cas9 guide plasmids targeting two different sites in the SIL7 region were generated. Guide oligonucleotides were annealed and cloned into pMLB626 plasmid (a kind gift from Marcus Lee)[57] using BbsI restriction enzyme, generating the two final guide plasmids (Table S1).

Growth assay

NF54 WT and MitoRed parasites were synchronized using 63% Percoll centrifugation. Late-stage parasites were isolated from the Percoll gradient and added to fresh RBCs. Four hours later, a 5% sorbitol synchronization was performed, which allowed only young rings that just invaded a new RBC to survive. Ring-stage parasites were counted and three independent cultures of 0.05% parasitemia were set up for each parasite line. Every 24 hours, 10 µl culture was taken and fixed in 100 µl 0.25% glutaraldehyde in PBS up until day 5. To prevent overgrowth, parasite cultures were cut back 1/50 after samples were taken on day 3. Before readout, fixative was taken of, and parasite DNA was stained with 1:10,000 SYBR Green in PBS. Parasitemia was determined by measuring SYBR Green positive cells with a Cytoflex flow cytometer (Beckman Coulter Cytoflex) using the 488 nm laser. Final parasitemia on day 4 and 5 was adjusted for the 1/50 dilution factor, explaining why final parasitemia can reach more than 100%.

Immunofluorescence assays and fixed fluorescence imaging

Immunofluorescence assays were performed on asexual and sexual blood-stage parasites, using the same fixation and staining protocols. Asexual blood-stage parasites were usually synchronized with 5% sorbitol to get them in the preferred stage for imaging. For tight synchronization, late-stage parasites were isolated with 63% Percoll centrifugation and added to fresh RBCs. Four hours later, a 5% sorbitol was performed to select for young rings. Parasites were settled on a poly-L-lysine coated coverslip for 20 min at 37°C. Parasites were fixed (4% EM-grade paraformaldehyde, 0.0075% EM-grade glutaraldehyde in PBS)[58] for 20 min and permeabilized with 0.1% Triton X-100 for 10 min. Samples were blocked with 3% bovine serum albumin (BSA) (Sigma-Aldrich) in PBS for 1 h. Primary and secondary antibody incubations were performed for 1 h in 3% BSA. The nucleus was visualized by staining with 1 µM DAPI in PBS for 1 h. PBS washes were performed between different steps. Parasites were mounted with Vectashield (Vector Laboratories). Images were taken with a Zeiss LSM880 or LSM900 Airyscan microscope with 63x oil objective with 405, 488, 561, 633 nm excitations. Images were Airyscan processed before analysis with FIJI software. MitoTracker stainings (including MitoTracker™ Orange CMTMRos, Red CMXRos, Deep Red FM, all from Thermo Fisher Scientific) were done before settling and fixation by incubation of the parasites with 100 nM MitoTracker for 30 min at 37°C, followed by a wash with complete media. The IMC protein GAP45 was labeled using the anti-GAP45 rabbit antibody (1:5000) (a kind gift from Julian Rayner)[27] and goat anti-rabbit AlexaFluor 488 antibody (1:500, Invitrogen). Alfa-tubulin was labeled with an anti-alfa tubulin mouse antibody (1:500, Thermo Fisher Scientific) and chicken anti-mouse AlexaFluor 488 antibody (1:400, Invitrogen). 3D visualization and quantifications were done in Arivis 4D Vision software. For mitochondrial measurements, threshold-based segmentation was used. For nuclei, blob-finder function was used for segmentation. Number of segmented objects and volume of objects was determined automatically in Arivis software.

Gametocyte generation and mosquito feeds

Gametocyte cultures were maintained in a semi-automatic culturing system with media changes twice a day[59]. MitoRed gametocytes used for imaging were induced by Albumax supplementation. A mixed asexual blood-stage culture of 1% was set up and maintained in medium supplemented with 2.5% Albumax II (Thermo Fisher Scientific) without human serum for four days[60]. After four days, parasites were cultured in complete medium again for further gametocyte development. For mosquito feeding, MitoRed gametocytes were stress induced through asexual overgrowing. A mixed asexual blood-stage culture of 1% was set up and maintained for 2 weeks. At day 15 after gametocyte induction, gametocytes were

fed to *Anopheles stephensi* mosquitoes (Sind-Kasur Nijmegen strain)[61]. 24 hours after feeding, several mosquitoes were dissected, and blood bolus was obtained for live imaging of ookinetes.

Live imaging of asexual blood-stage parasites

Sorbitol-synchronized MitoRed and NF54 schizonts were stained with 0.5 µg/ml Hoechst 33342 (Invitrogen, H3570) for 30 min at 37°C for nuclear staining. MitoTracker stainings (including MitoTracker™ Orange CMTMRos, Red CMXRos, Deep Red FM, Rhodamin123, all from Thermo Fisher Scientific) were done by incubation of the parasites with 100 nM MitoTracker or 1 µg/ml Rhodamin123 for 30 min at 37°C, followed by a wash with complete medium. Stained parasites were diluted 1:40 in complete medium and settled for 20 min at 37°C in a poly-L-lysine coated µ-slide 8-well imaging chamber (Ibidi). Unbound cells were washed away with phenol red free complete medium in which cells were also kept during imaging. Parasites were imaged on a Zeiss LSM880 Airyscan microscope with 37°C heated stage table and 63x oil objective. Images were Airyscan processed before analysis with FIJI software.

Live imaging of mosquito-stage parasites

Ookinetes were obtained from the blood bolus of infected mosquitoes 24 hours after feeding. Ookinetes were stained by mouse monoclonal anti-*Pf*s25 conjugated antibody (made in house, final concentration 15µg/ml). Stained sample was applied on a glass slide and covered with a glass coverslip. The sample was immediately imaged on a Zeiss LSM880 Airyscan microscope with 63x oil objective. Mosquito midguts were dissected at day 7, 10, and 13 after infection and put on a glass slide in PBS covered with a glass coverslip. Samples were imaged immediately on a Zeiss LSM880 or LSM900 microscope with 63x oil objective. Oocysts were identified based on their fluorescent mitochondrion and round shape in the brightfield channel. All images were Airyscan processed before analysis with FIJI software. 3D segmentations and visualizations were done by manual thresholding of the fluorescent signal in Arivis 4D vision software. Salivary glands were dissected on day 13, 16, and 21 after infection and stained with mouse monoclonal anti-CSP conjugated antibody (made in house, final concentration 1µg/ml). Stained glands were applied on a glass slide and covert with a glass coverslip. Samples were imaged on a Zeiss Axioscope A1 microscope with AxioCam ICc1.

FIB-SEM image analysis

FIB-SEM image stacks were reused from Evers *et al.*[20] (EMPIAR-10392). For these stacks, gametocyte-induced iGP2 parasite cultures were MACS purified. During this

process many late-stage asexual parasites in these cultures were co-purified and fixed in the agarose blocks used for FIB-SEM imaging. Detailed sample preparation and FIB-SEM imaging methods are described in Evers *et al.*[20]. All image processing, visualizations and analysis was done in ORS Dragonfly software (2022.2). Segmentations were done by either manual segmentation or deep learning-based segmentation. Deep learning-based segmentations were manually reviewed and corrected when necessary. 3D renderings of segmented regions were converted to triangle meshes for visualization.

Acknowledgements

We thank members from the molecular malaria research group for the discussions. We also thank Aniek Garritsen for her contributions to the generation of the SIL plasmids. We do greatly appreciate the help from Chiara Andolina and Nicholas Proellochs with mosquito experiments. We would like to thank Astrid Pouwelsen, Jolanda Klaassen, Laura Pelser-Posthumus, Saskia Mulder and Jacqueline Kuhnen for breeding of mosquitoes and handling of the infected mosquitoes. We thank the Radboud Technology Center Microscopy, Radboud Technology Center flowcytometry, and Radboudumc Electron Microscopy Center for the use of their facilities. We are grateful to Alan Cowman for sharing the p1.2RhopH3-HA-mScarlet plasmid and Julian Rayner for sharing the anti-GAP45 antibody. J.M.J.V. is supported by an individual Radboudumc Master-PhD grant. A.B.V. is supported by an NIH grant (R01 AI028398).

References

1. WHO. *World malaria report 2023*. (2023).
2. Vaidya, A. B. & Mather, M. W. Mitochondrial evolution and functions in malaria parasites. *Annu. Rev. Microbiol.* **63**, 249–267 (2009).
3. Painter, H. J., Morrisey, J. M., Mather, M. W. & Vaidya, A. B. Specific role of mitochondrial electron transport in blood-stage Plasmodium falciparum. *Nature* **446**, 88–91 (2007).
4. Ke, H. *et al.* Genetic investigation of tricarboxylic acid metabolism during the Plasmodium falciparum life cycle. *Cell Rep.* **11**, 164–174 (2015).
5. Evers, F. *et al.* Composition and stage dynamics of mitochondrial complexes in Plasmodium falciparum. *Nat. Commun.* **12**, 3820 (2021).
6. Lamb, I. M., Okoye, I. C., Mather, M. W. & Vaidya, A. B. Unique Properties of Apicomplexan Mitochondria. *Annu. Rev. Microbiol.* **77**, 541–560 (2023).
7. Goodman, C. D., Buchanan, H. D. & McFadden, G. I. Is the Mitochondrion a Good Malaria Drug Target? *Trends Parasitol.* **33**, 185–193 (2017).
8. Ruiz-Trillo, I. & de Mendoza, A. Towards understanding the origin of animal development. *Dev.* **147**, 1–7 (2020).
9. Verhoef, J. M. J., Meissner, M. & Kooij, T. W. A. Organelle dynamics in apicomplexan parasites. *MBio* **12**, (2021).
10. van Dooren, G. G. *et al.* Development of the endoplasmic reticulum, mitochondrion and apicoplast during the asexual life cycle of Plasmodium falciparum. *Mol. Microbiol.* **57**, 405–419 (2005).
11. Rudlaff, R. M., Kraemer, S., Marshman, J. & Dvorin, J. D. Three-dimensional ultrastructure of Plasmodium falciparum throughout cytokinesis. *PLoS Pathog.* **16**, e1008587 (2020).
12. Stanway, R. R. *et al.* Organelle segregation into Plasmodium liver stage merozoites. *Cell. Microbiol.* **13**, 1768–1782 (2011).
13. Linzke, M. *et al.* Live and Let Dye: Visualizing the Cellular Compartments of the Malaria Parasite Plasmodium falciparum. *Cytom. Part A* **97**, 694–705 (2020).
14. Painter, H. J., Morrisey, J. M. & Vaidya, A. B. Mitochondrial electron transport inhibition and viability of intraerythrocytic Plasmodium falciparum. *Antimicrob. Agents Chemother.* **54**, 5281–5287 (2010).
15. Joanny, F., Held, J. & Mordmüller, B. In Vitro activity of fluorescent dyes against asexual blood stages of Plasmodium falciparum. *Antimicrob. Agents Chemother.* **56**, 5982–5985 (2012).
16. Gebru, T., Mordmüller, B. & Heldb, J. Effect of fluorescent dyes on in vitro-differentiated, late-stage plasmodium falciparum gametocytes. *Antimicrob. Agents Chemother.* **58**, 7398–7404 (2014).
17. Matz, J. M., Goosmann, C., Matuschewski, K. & Kooij, T. W. A. An Unusual Prohibitin Regulates Malaria Parasite Mitochondrial Membrane Potential. *Cell Rep.* **23**, 756–767 (2018).
18. Esveld, S. L. Van *et al.* A Prioritized and Validated Resource of Mitochondrial Proteins in Plasmodium Identifies Unique Biology. *mSphere* **6**, e00614-21 (2021).
19. Kooij, T. W. A., Rauch, M. M. & Matuschewski, K. Expansion of experimental genetics approaches for Plasmodium berghei with versatile transfection vectors. *Mol. Biochem. Parasitol.* **185**, 19–26 (2012).
20. Evers, F. *et al.* Comparative 3D ultrastructure of Plasmodium falciparum gametocytes. *bioRxiv* 2023.03.10.531920 (2023).
21. Billker, O. *et al.* Identification of xanthurenic acid as the putative inducer of malaria development in the mosquito. *Lett. to Nat.* **392**, 289–292 (1998).

22. Moraes, C. R. & Meyers, S. The sperm mitochondrion: Organelle of many functions. *Anim. Reprod. Sci.* **194**, 71–80 (2018).
23. Vega-Rodríguez, J. *et al.* The glutathione biosynthetic pathway of Plasmodium is essential for mosquito transmission. *PLoS Pathog.* **5**, 16–18 (2009).
24. Sturm, A., Mollard, V., Cozijnsen, A., Goodman, C. D. & McFadden, G. I. Mitochondrial ATP synthase is dispensable in blood-stage Plasmodium berghei rodent malaria but essential in the mosquito phase. *Proc. Natl. Acad. Sci. U. S. A.* **112**, 10216–10223 (2015).
25. Siciliano, G. *et al.* Critical Steps of Plasmodium falciparum Ookinete Maturation. *Front. Microbiol.* **11**, 1–9 (2020).
26. Ridzuan, M. A. M. *et al.* Subcellular location, phosphorylation and assembly into the motor complex of GAP45 during Plasmodium falciparum schizont development. *PLoS One* **7**, (2012).
27. Jones, M. L., Cottingham, C. & Rayner, J. C. Effects of calcium signaling on Plasmodium falciparum erythrocyte invasion and post-translational modification of gliding-associated protein 45 (PfGAP45). *Mol. Biochem. Parasitol.* **168**, 55–62 (2009).
28. Rudlaff, R. M., Kraemer, S., Streva, V. A. & Dvorin, J. D. An essential contractile ring protein controls cell division in Plasmodium falciparum. *Nat. Commun.* **10**, 2181 (2019).
29. Kono, M., Prusty, D., Parkinson, J. & Gilberger, T. W. The apicomplexan inner membrane complex. *Front. Biosci.* **18**, 982–992 (2013).
30. Voß, Y., Klaus, S., Guizetti, J. & Ganter, M. Plasmodium schizogony, a chronology of the parasite's cell cycle in the blood stage. *PLoS Pathog.* **19**, 1–21 (2023).
31. Gerald, N., Mahajan, B. & Kumar, S. Mitosis in the human malaria parasite Plasmodium falciparum. *Eukaryot. Cell* **10**, 474–482 (2011).
32. Liffner, B. *et al.* Atlas of Plasmodium falciparum intraerythrocytic development using expansion microscopy. *Elife* 1–39 (2023) doi:10.1101/2023.03.22.533773.
33. Hain, A. U. P. & Bosch, J. Autophagy in Plasmodium, a multifunctional pathway? *Comput. Struct. Biotechnol. J.* **8**, e201308002 (2013).
34. Ghosh, D., Walton, J. L., Roepe, P. D. & Sinai, A. P. Autophagy is a cell death mechanism in Toxoplasma gondii Debasish. *Cell. Microbiol.* **23**, 1–7 (2012).
35. Joy, S. *et al.* Basal and starvation-induced autophagy mediates parasite survival during intraerythrocytic stages of Plasmodium falciparum. *Cell Death Discov.* **4**, (2018).
36. Saeed, S., Tremp, A. Z., Sharma, V., Lasonder, E. & Dessens, J. T. NAD (P) transhydrogenase has vital non-mitochondrial functions in malaria parasite transmission. *EMBO Rep.* **21**, 1–11 (2020).
37. Burda, P.-C. *et al.* A Plasmodium plasma membrane reporter reveals membrane dynamics by live-cell microscopy. *Sci. Rep.* **7**, 9740 (2017).
38. Stanway, R. R., Witt, T., Zobiak, B., Aepfelbacher, M. & Heussler, V. T. GFP-targeting allows visualization of the apicoplast throughout the life cycle of live malaria parasites. *Biol. cell* **101**, 415–430 (2009).
39. Roques, M., Bindschedler, A., Beyeler, R. & Heussler, V. T. Same, same but different: Exploring Plasmodium cell division during liver stage development. *PLoS Pathog.* **19**, 1–22 (2023).
40. Yeh, E. & DeRisi, J. L. Chemical rescue of malaria parasites lacking an apicoplast defines organelle function in blood-stage Plasmodium falciparum. *PLoS Biol.* **9**, e1001138 (2011).
41. Maruthi, M., Ling, L., Zhou, J. & Ke, H. Dispensable role of mitochondrial fission protein 1 (Fis1) in the erythrocytic development of Plasmodium falciparum. *mSphere* **5**, e00579-20 (2020).

42. Morano, A. A., Xu, W., Shadija, N., Dvorin, J. D. & Ke, H. The dynamin-related protein Dyn2 is essential for both apicoplast and mitochondrial fission in. *bioRxiv* (2024).
43. Arnot, D. E., Ronander, E. & Bengtsson, D. C. The progression of the intra-erythrocytic cell cycle of Plasmodium falciparum and the role of the centriolar plaques in asynchronous mitotic division during schizogony. *Int. J. Parasitol.* **41**, 71–80 (2011).
44. Simon, C. S. *et al.* An extended DNA-free intranuclear compartment organizes centrosome microtubules in malaria parasites. *Life Sci. Alliance* **4**, 1–15 (2021).
45. Striepen, B. *et al.* The plastid of Toxoplasma gondii is divided by association with the centrosomes. *J. Cell Biol.* **151**, 1423–1434 (2000).
46. van Dooren, G. G. *et al.* A novel dynamin-related protein has been recruited for apicoplast fission in Toxoplasma gondii. *Curr. Biol.* **19**, 267–276 (2009).
47. Vaishnava, S. *et al.* Plastid segregation and cell division in the apicomplexan parasite Sarcocystis neurona. *J. Cell Sci.* **118**, 3397–3407 (2005).
48. Frederick, R. L. & Shaw, J. M. Moving mitochondria: Establishing distribution of an essential organelle. *Traffic* **8**, 1668–1675 (2007).
49. Das, S., Lemgruber, L., Tay, C. L., Baum, J. & Meissner, M. Multiple essential functions of Plasmodium falciparum actin-1 during malaria blood-stage development. *BMC Biol.* **15**, 1–16 (2017).
50. Periz, J. *et al.* Toxoplasma gondii F-actin forms an extensive filamentous network required for material exchange and parasite maturation. *Elife* **6**, e24119 (2017).
51. Stortz, J. F. *et al.* Formin-2 drives polymerisation of actin filaments enabling segregation of apicoplasts and cytokinesis in Plasmodium Falciparum. *Elife* **8**, 1–34 (2019).
52. Jacot, D., Daher, W. & Soldati-Favre, D. Toxoplasma gondii myosin F, an essential motor for centrosomes positioning and apicoplast inheritance. *EMBO J.* **32**, 1702–1716 (2013).
53. Devarakonda, P. M., Sarmiento, V. & Heaslip, A. T. F-actin and myosin F control apicoplast elongation dynamics which drive apicoplast-centrosome association in Toxoplasma gondii. *MBio* **14**, (2023).
54. Wu, Y., Sifri, C. D., Lei, H. H., Su, X. Z. & Wellems, T. E. Transfection of Plasmodium falciparum within human red blood cells. *Proc. Natl. Acad. Sci. U. S. A.* **92**, 973–977 (1995).
55. Crabb, B. S. & Cowman, A. F. Characterization of promoters and stable transfection by homologous and nonhomologous recombination in Plasmodium falciparum. *Proc. Natl. Acad. Sci. U. S. A.* **93**, 7289–7294 (1996).
56. Pasternak, M. *et al.* RhopH2 and RhopH3 export enables assembly of the RhopH complex on P. falciparum-infected erythrocyte membranes. *Commun. Biol.* **5**, 1–12 (2022).
57. Lim, M. Y. X. *et al.* UDP-galactose and acetyl-CoA transporters as Plasmodium multidrug resistance genes. *Nat. Microbiol.* **1**, (2016).
58. Tonkin, C. J. *et al.* Localization of organellar proteins in Plasmodium falciparum using a novel set of transfection vectors and a new immunofluorescence fixation method. *Mol. Biochem. Parasitol.* **137**, 13–21 (2004).
59. Ponnudurai, T., Lensen, A. H. W., Meis, J. F. G. M. & Meuwissen, J. H. E. Synchronization of Plasmodium falciparum gametocytes using an automated suspension culture system. *Parasitology* **93**, 263–274 (1986).
60. Graumans, W. *et al.* AlbuMAX supplemented media induces the formation of transmission-competent P. falciparum gametocytes. *bioRxiv* 1–9 (2024).
61. Feldmann, A. M. & Ponnudurai, T. Selection of Anopheles stephensi for refractoriness and susceptibility to Plasmodium falciparum. *Med. Vet. Entomol.* **3**, 41–52 (1989).

Supplemental information

Supplemental information S1

Selection of new genomic integration sites

A previous study has described successful integration of a reporter gene into a so-called silent intergenic locus (SIL) in *P. berghei*[1]. We extended the same concept to *P. falciparum* and identified potentially suitable chromosomal breakpoints in *P. falciparum* conserved between *Plasmodium vivax* and the rodent malaria parasite lineages[2]. By using these SIL sites, we prevent the need for additional gene replacements commonly used to introduce transgenes. For instance, NF54HT-GFP-luc parasites had the GFP-luc cassette introduced in the presumed silent *Pf*s47 locus[3]. Meanwhile, it has been demonstrated that this gene can play an important role in mosquito infections[4,5]. Another commonly used integration site is the *PfRH3* pseudogene, for instance for integration of a dimerizable Cre gene[6,7]. Although *PfRH3* is transcribed and not translated in blood stages, the RH3 protein has been detected in sporozoites[8,9]. The genes flanking the SIL sites have been rearranged during the evolution of *P. falciparum* and we reasoned that there would not be any genetic constraints to keep these genes physically linked. We analyzed available data on gene expression and potential transcription start sites to target a locus that lacks any detectable (regulation of) gene expression in the *Plasmodium* life-cycle stages[10]. In addition, UTRs of the flanking genes need to remain intact.

Applying the combined criteria, we identified three loci on *P. falciparum* chromosomes 7, 12, and 14. The site on chromosome 12 (genomic location between PF3D7_121220 and PF3D7_1212100) proved very difficult to clone, with frequent plasmid rearrangements and very low plasmid yields. A total of 3 transfections targeting the site on chromosome 14 (genomic location between PF3D7_1438100 and PF3D7_143800) did not result in any transgenic parasite lines, suggesting either technical challenges or some important function of this locus in ABS parasite viability. The third SIL, termed SIL7 as it is on chromosome 7, locates between PF3D7_0715900 and PF3D7_0716000 and was used for integration of the mitochondrial marker. We generated an integration plasmid containing 5' and 3' homology regions (HRs) and the mitochondrial marker (Figure S1A).

Considerations for the use of SIL7 for stable transgene integration

Integration of the fluorescent mitochondrial marker in SIL7 did not affect parasite growth or development in blood and mosquito stages up until oocyst formation. Although we did observe several free sporozoites in our dissected mosquito

samples, we never observed sporozoites in the salivary glands. This suggests that sporozoites might have a developmental defect that prevents them from populating the salivary glands. One possible explanation could be the presence of the fluorescent mitochondrial marker, which might be toxic for this stage specifically. Even though we used an organelle-specific promoter, the high, HSP70-3 (PF3D7_1134000) promoter driven mito-mScarlet expression combined with limited resources, and possible lack of feedback loops to control protein levels could be overwhelming the small sized mitochondrion. Alternatively, integration in SIL7 might be disruptive for sporozoite development, possibly due to interference with genetic or epigenetic processes in this stage. Therefore, we conclude that SIL7 is an excellent integration site when studying blood or mosquito stages up until oocyst development, but it might not be well suited to study sporozoite or liver stages.

References

1. Kooij, T. W. A., Rauch, M. M. & Matuschewski, K. Expansion of experimental genetics approaches for Plasmodium berghei with versatile transfection vectors. *Mol. Biochem. Parasitol.* **185**, 19–26 (2012).
2. Carlton, J. M., Escalante, A. A., Neafsey, D. & Volkman, S. K. Comparative evolutionary genomics of human malaria parasites. *Trends Parasitol.* **24**, 545–550 (2008).
3. Vaughan, A. M. *et al.* A transgenic Plasmodium falciparum NF54 strain that expresses GFP-luciferase throughout the parasite life cycle. *Mol. Biochem. Parasitol.* **186**, 143–147 (2012).
4. Molina-Cruz, A., Canepa, G. E. & Barillas-Mury, C. Plasmodium P47: a key gene for malaria transmission by mosquito vectors. *Curr. Opin. Microbiol.* **40**, 168–174 (2017).
5. Molina-Cruz, A. *et al.* Plasmodium falciparum evades immunity of anopheline mosquitoes by interacting with a Pfs47 midgut receptor. *Proc. Natl. Acad. Sci. U. S. A.* **117**, 2597–2605 (2020).
6. Wilde, M. L. *et al.* Protein kinase A is essential for invasion of Plasmodium falciparum into human erythrocytes. *MBio* **10**, (2019).
7. Carrasquilla, M. *et al.* Barcoding Genetically Distinct Plasmodium falciparum Strains for Comparative Assessment of Fitness and Antimalarial Drug Resistance. *MBio* **13**, (2022).
8. Taylor, H. M. *et al.* Plasmodium falciparum homologue of the genes for plasmodium vivax and Plasmodium yoelii adhesive proteins, which is transcribed but not translated. *Infect. Immun.* **69**, 3635–3645 (2001).
9. Florens, L. *et al.* A proteomic view of the malaria parasite life cycle. *Proc. 50th ASMS Conf. Mass Spectrom. Allied Top.* **419**, 59–60 (2002).
10. PlasmoDB: An integrative database of the Plasmodium falciparum genome. Tools for accessing and analyzing finished and unfinished sequence data. The Plasmodium Genome Database Collaborative. *Nucleic Acids Res.* **29**, 66–69 (2001).

Table S1. Primer and guide RNA sequences for generation of repair and guide plasmids.

Primer name	Primer function	Sequence	Restriction site
Generation repair plasmids			
JV069	HSP70-3 prom + t.s. F	AATAAAGAATTCTTGCATGCCCCATAATTTTCAC	EcoRI
JV070	HSP70-3 prom + t.s. R	ATTAAAGCTAGCAGCATCTTCATCATATTTTCTACC	NheI
JV071	mScarlet F	AATAATGAATTCAAAGCTAGCATGGTGAGCAAGGGCGAGG	EcoRI, NheI
JV072	mScarlet R	AATAATCTTAAGTTACTTGTACAGCTCGTCCATGC	AflII
NF001	SIL7 5′HR F	AAAGCCGGCGTCGACGAAAAAAAAGAAGAGTAGAGCAGTAC	NgoMIV
NF002	SIL7 5′HR R	TAACACGTACGTGAGGTAATATAACATTGAATTTATAATACATTAC	AleI
NF003	SIL7 3′HR F	AAACCACGTCTTGGAAATGTGTAGCACTTTTTTCATTCC	BmgBI
NF004	SIL7 3′HR R	AAAGACGTCGTCGACCCTATAAAATAAAAATGATTCCAACAAAAAAG	AatII
Guide RNA sequences			
Pf0084	SIL7 guide 1 sense	TATTGTATATGTGGTAATAAATAAA	
Pf0085	SIL7 guide 1 antisense	AAACTTTATTTATTACCACATATAC	
Pf0086	SIL7 guide 2 sense	TATTGATTCAATATAATAAGGTCAA	
Pf0087	SIL7 guide 2 antisense	AAACTTGACCTTATTATATTGAATC	
Integration PCR			
NP297	Integration PCR 5′F	GCTCACCTTAAATGTTCCAC	
JV104	Integration PCR 5′R	ATTATATGTGAAAATTATGGGGCATGC	
NP190	Integration PCR 3′R	AGTCATATCCAGGAATAAACATAC	
NP298	Integration PRC 3′R	CGTTCATGCTTTCACAAGAAC	

Used abbreviations: HR = homology region, F = forward primer, R = reverse primer. Overhang for restriction sites are red, restriction sites are underlined, and gRNA sequences are blue.

Table S2. Description of segmented schizonts used in this paper.

Parasite ID	Nr of nuclei	Total nuclei volume (µm³)	Average volume nuclei (±SD) (µm³)	Nr of mito fragments	Total mito volume (µm³)	Average volume mito fragment (±SD) (µm³)	Nr of apicoplast fragments	Total apicoplast volume (µm³)	Average volume apicoplast fragment (±SD) (µm³)	Nr of CPs	Total parasite volume (µm³)
Schizont 1*	8	14.05	1.76 (0.31)	1	1.29	1.294	1	0.57	0.573	12	60.11
Schizont 2	15	18.26	1.22 (0.27)	1	1.06	1.055	1	0.37	0.372	29	74.29
Schizont 3	20	24.42	1.22 (0.21)	1	1.44	1.443	1	0.71	0.711	36	84.28
Schizont 4	23	27.48	1.19 (0.33)	1	1.33	1.334	8	0.51	0.064 (0.043)	40	98.63
Schizont 5	32	22.19	0.69 (0.24)	1	1.09	1.093	36	0.31	0.009 (0.002)	36	81.92
Schizont 6	32	19.22	0.60 (0.04)	1	1.19	1.193	31	0.52	0.017 (0.005)	32	86.14
Schizont 7	34	17.20	0.51 (0.02)	21	0.84	0.040 (0.026)	35	0.42	0.012 (0.002)	34	72.41
Schizont 8	32	18.11	0.57 (0.02)	32	0.86	0.027 (0.005)	32	0.35	0.011 (0.002)	32	78.63

*Parasite is not complete so displayed numbers might not represent the total numbers/volumes in this cell.

Table S3. Detailed textual description of segmented parasites used in this paper.

Parasite ID	Detailed description		Representative micrograph
Schizont 1	**Nuclei**	Early stage schizont with 8 nuclei, nuclear division is still ongoing, nuclei are large and irregularly shaped.	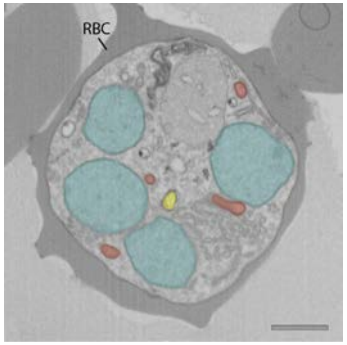
	IMC and rhoptries	No IMC formation and no rhoptries.	
	Apicoplast	The apicoplast is smaller and less complex than the mitochondrion and locates to the center of the parasite.	
	Mitochondrion	The mitochondrion is one large network stretched throughout the whole cell.	
	CPs	CPs are dividing and do not interact with the apicoplast or mitochondrion.	
Schizont 2	**Nuclei**	Schizont has 15 nuclei, nuclear division is still ongoing, nuclei are large and irregularly shaped.	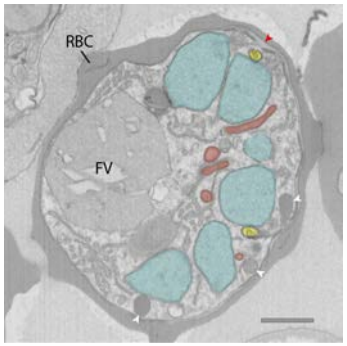
	IMC and rhoptries	IMC and rhoptry formation has started (one larger, dark rhoptry and one smaller, light rhoptry per pair).	
	Apicoplast	Apicoplast branches are more elongated, and some branches associate with a portion of the CPs.	
	Mitochondrion	The mitochondrion is one large network stretched out throughout the whole cell.	
	CPs	CPs are dividing or have divided and are localizing further apart from each other within one nucleus. Some CPs interact with the apicoplast branches.	

Table S3. Continued

Parasite ID	Detailed description		Representative micrograph
Schizont 3	**Nuclei**	Schizont has 20 nuclei, nuclear division is still ongoing, nuclei are large and irregularly shaped.	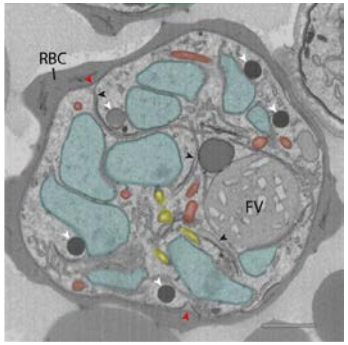
	IMC and rhoptries	Large parasite membrane invaginations, below which IMC is being formed, IMC does not yet show curvature, rhoptries are present (one larger, dark rhoptry and one smaller, light rhoptry per pair).	
	Apicoplast	Apicoplast has developed more smaller branches compared to earlier stages, the apicoplast associates with all CPs. Most of the apicoplast branches located to the periphery of the parasite.	
	Mitochondrion	The mitochondrion is one large network stretched out throughout the whole cell.	
	CPs	CP division is finished and CPs are located further apart from each other within one nucleus.	
Schizont 4	**Nuclei**	Schizont has 23 nuclei, nuclear division is still ongoing, most nuclei are large and irregularly shaped and are still dividing, some are smaller and nuclear division seems to be finished (contain only one CP).	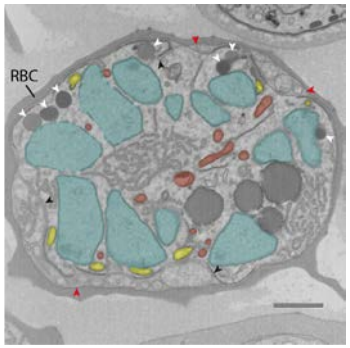
	IMC and rhoptries	Parasite membrane starts to curve around the forming merozoites, IMC is showing clear curvature, rhoptries are present below the IMC (the rhoptries from a pair are similar size, but one rhoptry is darker and the rhoptry neck is elongated further than the lighter rhoptry).	
	Apicoplast	Apicoplast is mid division and consists of 8 different-sized fragments. The apicoplast localizes completely to the periphery of the parasite. The apicoplast interacts with all CPs and each ending of an apicoplast branch is interacting with a CP.	
	Mitochondrion	The mitochondrion is one large network stretched out throughout the whole cell.	
	CPs	CP division is finished and larger nuclei that are still undergoing division contain two dispersed CPs, while the smaller nuclei that seem to have finished division contain one CP that localizes close to the apical end of the forming merozoites.	

Table S3. Continued

Parasite ID	Detailed description		Representative micrograph
Schizont 5	**Nuclei**	Schizont has 32 nuclei, nuclear division is almost finished and only four nuclei are still undergoing nuclear division (they contain two dispersed MTOCs and are larger).	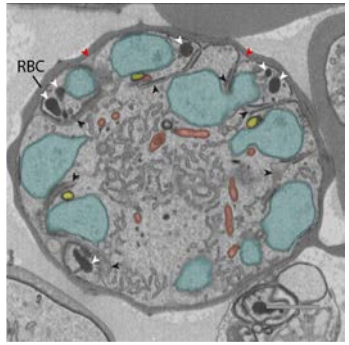
	IMC and rhoptries	Parasite membrane is curved further around the forming merozoites, IMC has developed further and is enveloping part of the nucleus. Rhoptries are present below the IMC (rhoptries of one pair now both have the same dark color and rhoptry neck has elongated, although one rhoptry is still longer than the other).	
	Apicoplast	Apicoplast division has finished and each apical apicoplast ending is associating with a CP.	
	Mitochondrion	The mitochondrion starts to orient itself in a cartwheel structure where the branches are entering the forming merozoites and are often interacting with the basal end of the apicoplast fragments.	
	CPs	CP division is finished, and most nuclei contain only one CP that is localized to the apical end of the forming merozoite.	
Schizont 6	**Nuclei**	Schizont has 32 nuclei and nuclear division is completely finished, all nuclei are small, round shaped and contain one CP.	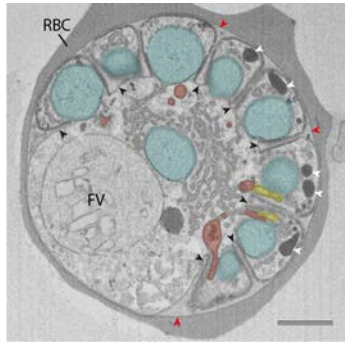
	IMC and rhoptries	IMC has developed further and envelops a large part the nucleus. Rhoptries are present at the apical end and seem to be fully developed (rhoptries from one pair have the same shape and dark color and have an elongated rhoptry neck).	
	Apicoplast	The apicoplast is completely divided and each apical apicoplast ending associates with a CP.	
	Mitochondrion	The mitochondrion is oriented in a clear cartwheel structure where the branches are entering the forming merozoites and align with the apicoplast.	
	CPs	CP division is finished, and each nucleus contains one CP that is located to the apical end of the forming merozoite.	

Table S3. Continued

Parasite ID	Detailed description		Representative micrograph
Schizont 7	**Nuclei**	Late schizont with 34 nuclei. Nuclear division is completely finished, all nuclei are small, round shaped and contain one CP.	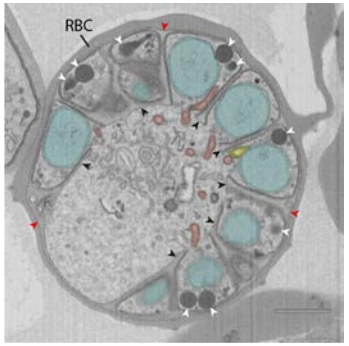
	IMC and rhoptries	IMC formation seems almost completely finished and IMC envelops the complete nucleus. Merozoites have a small basal opening through which the mitochondrion enters the parasite.	
	Apicoplast	The apicoplast is completely divided and each apicoplast ending is associate with a CP.	
	Mitochondrion	The mitochondrion is dividing and consists of 21 fragments of different sizes. The mitochondrial branches and fragments that enter the merozoite completely align with the apicoplast.	
	CPs	CP division is finished, and each nucleus contains one CP that is located to the apical end of the forming merozoite.	
Schizont 8	**Nuclei**	Late stage schizont with 32 nuclei. Nuclear division is finished, all nuclei are small, round shaped and contain one CP.	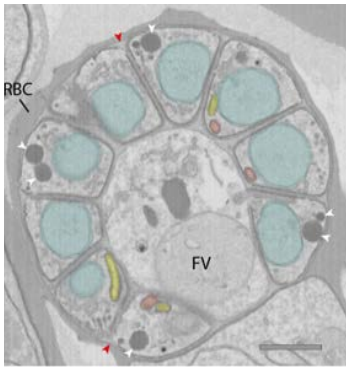
	IMC and rhoptries	IMC formation is almost finished and most merozoites are completely enveloped by parasite membrane and pinched of from the residual body. Some merozoites are still connected to the basal body and have a small opening at their apical end.	
	Apicoplast	The apicoplast is completely divided and does not clearly associate with the CP anymore.	
	Mitochondrion	The mitochondrion has completely divided and consists of 32 fragments. Each mitochondrial fragments localizes fully into a merozoite, except for two mitochondrial fragments that still enter the residual body through the small apical opening. Mitochondrial fragments align with the apicoplast fragments and are slightly longer.	
	CPs	CP division is finished, and each nucleus contains one CP that is located to the apical end of the forming merozoite. CPs don't have an extra nuclear compartment and are smaller compared to earlier stages.	

RBC and food vacuole (FV) are indicated by abbreviations. Rhoptries (white arrowhead), parasitophorous vacuole membrane (red arrowhead) and parasite membrane invagination (black arrowhead), nuclei (teal), mitochondrion (red), apicoplast (yellow).

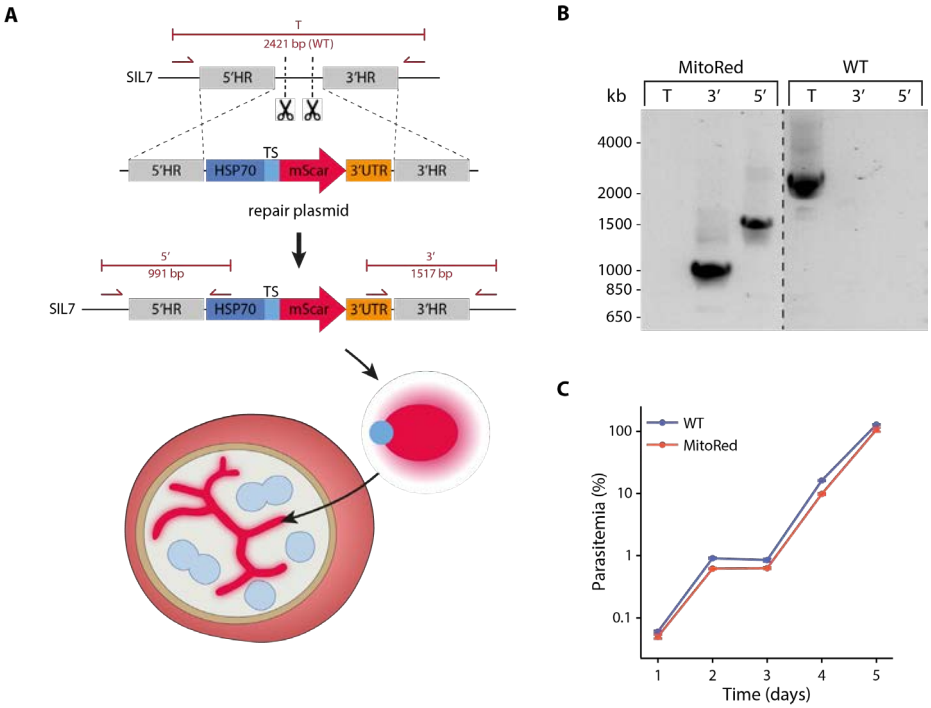

Figure S1. Generation and verification of MitoRed parasite line. A) Schematic overview of strategy to generate a parasite line harboring a fluorescent mitochondrial marker. CRISPR-Cas9 is used to create two double-strand breaks at SIL7 (indicated by scissors). A construct containing the promotor and targeting sequence of the mitochondrial protein HSP70-3 (PF3D7_1134000) fused with mScarlet is integrated by double homologous recombination. Once integrated, the mitochondrial targeted mScarlet is expressed and led to fluorescent staining of the mitochondrion. B) Diagnostic PCR of MitoRed parasite line with WT- and integration-specific primer combinations (indicated in panel A) demonstrating successful 5' and 3' integration and the absence of WT parasites in the MitoRed line. C) Growth assay showing similar growth of MitoRed and WT parasites. Three independent cultures were set up from one tightly synchronized parasite culture for both MitoRed and WT. Samples were taken over a 5-day period and parasitemia (corrected for dilution factors) was determined with flow cytometry. Error bars (note they are quite small) indicate standard deviation.

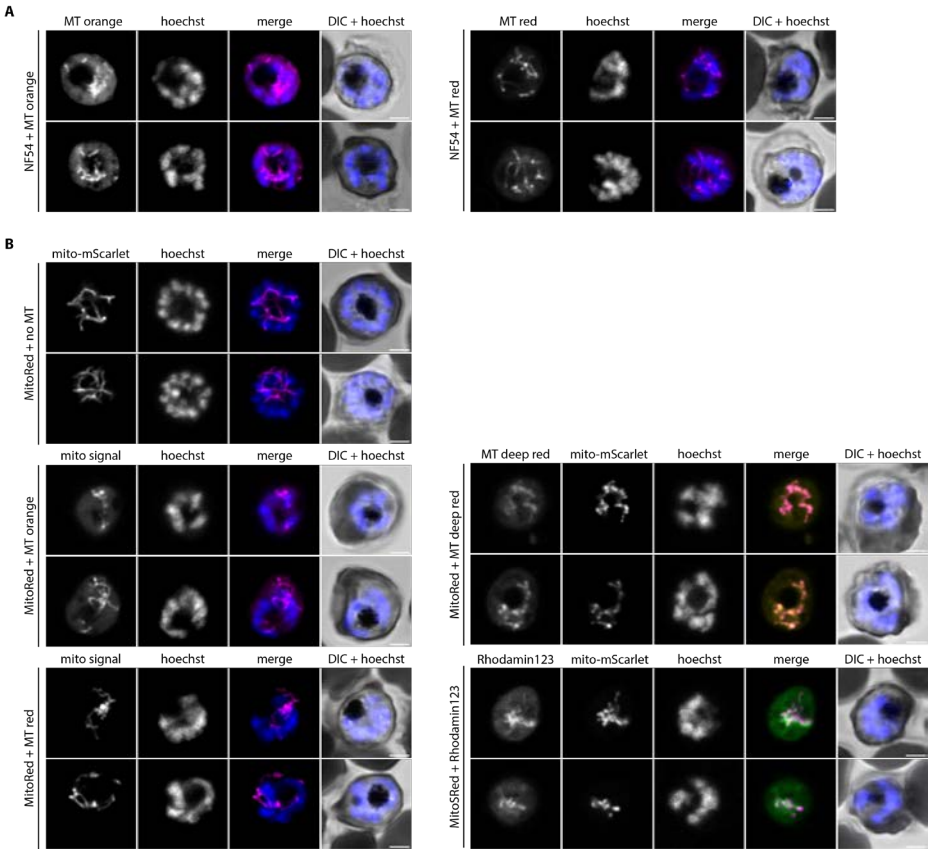

Figure S2. Comparison of MitoTracker and the mitochondrial marker for live fluorescence imaging. A) live imaging of WT parasites stained with MitoTracker Orange CMTMRos (MT orange) or MitoTracker Red CMXRos (MT red). B) Live imaging of MitoRed stained with MT orange, MT red, MitoTracker Deep Red FM (MT deep red), Rhodamin123 or without staining. Mito signal is the combined MitoTracker and mito-mScarlet signal that is observed in this channel. Parasites were stained with Hoechst 33342 to visualize DNA. All images are single slices of Z-stacks taken with Airyscan confocal microscope. Scale bars, 2 µm.

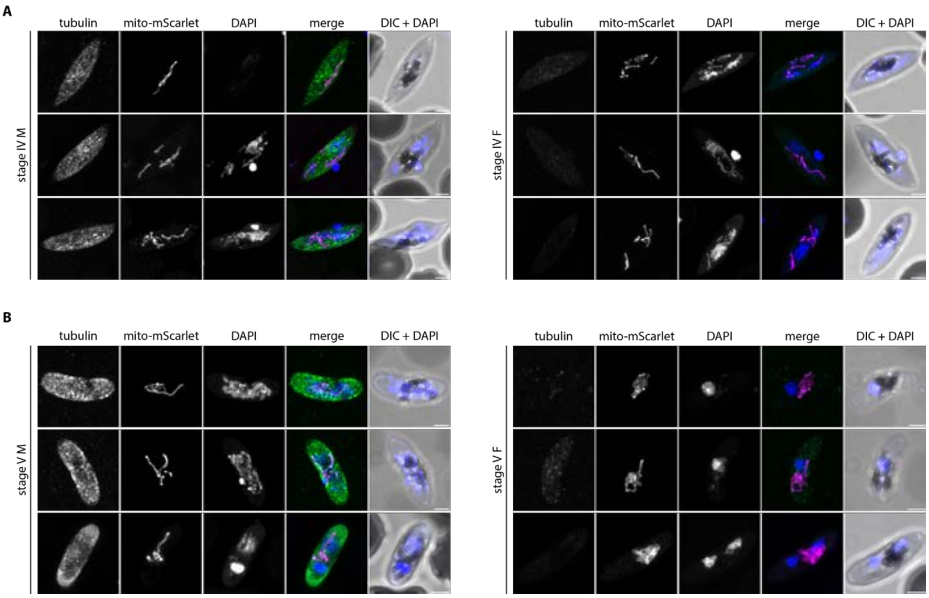

Figure S3. Mitochondrial morphology in stage IV and V male and female gametocytes. Immunofluorescence assay on male and female MitoRed gametocytes stage IV (A) and stage V (B), stained with anti-β-tubulin (green) and DAPI (blue). Male (M) and female (F) gametocytes are distinguished based on the intensity of the tubulin signal (males high, females low). Images are maximum intensity projections of Z-stacks taken with an Airyscan confocal microscope. Scale bars, 2 µm.

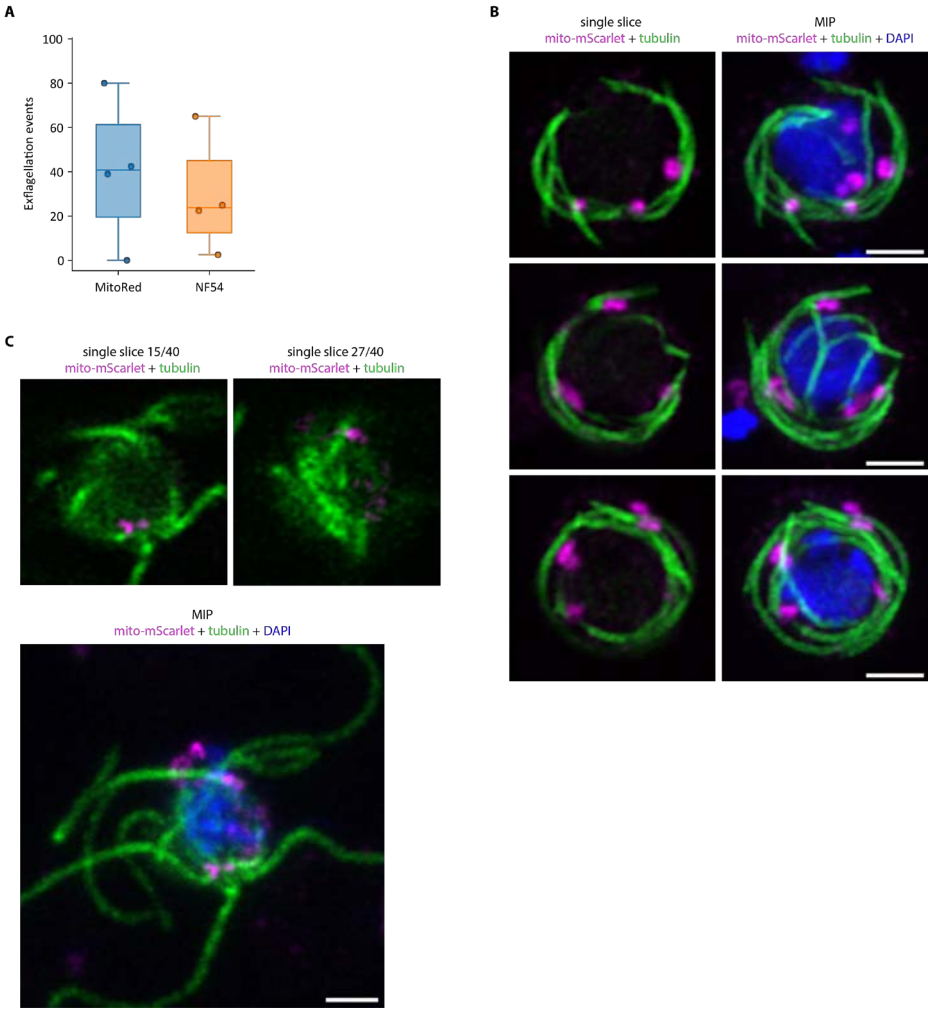

Figure S4. Mitochondrial association with axonemes in activated male gametocytes. A) Exflagellation events in MitoRed and NF54 parasites 20 min after activation in four cultures in two independent experiments. Unpaired t-test showed no significant difference. B) Three examples of activated males where the mitochondria (magenta) localize closely to the axonemal tubulin (green) in MitoRed parasites. Left images are single slices, right images are maximum intensity projections (MIPs). C) Exflagellating MitoRed male gametocyte with apposition of the mitochondria with the axonemal tubulin. Top images are single slices and crops from bottom image, which is a MIP. Scale bars, 2 µm.

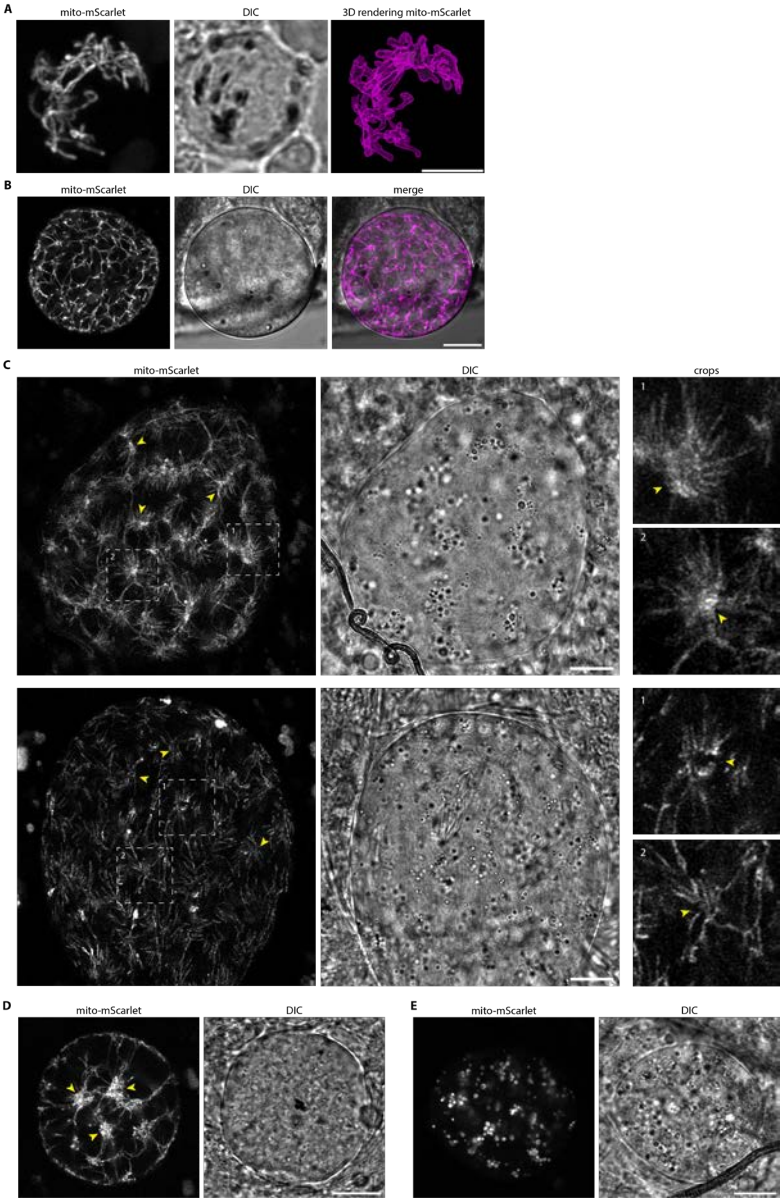

Figure S5. Mitochondrial dynamics in oocyst development. Live imaging of MitoRed oocysts on day 7 (A) day 10 (B) and day 13 (C) after mosquito infection. A) Oocyst at day 7 after infection with left image showing a maximum intensity projection of the mito-mScarlet signal. Right image shows a segmentation of the mito-mScarlet fluorescent signal by thresholding in Arivis software. Scale bar, 4 µm. C) two oocysts at day 13 after infection. Images on the right are crops of the mito-mScarlet signal of the image on the left, indicated by the dotted-line areas. Yellow arrowheads indicate mitochondrial organization centers (MOCs). D) Oocysts at day 13 showing beginning MOCs (yellow arrowheads). E) Oocyst at day 13 showing globular mitochondrial signal which could be a sign of unhealthy or dying parasites. B-E) Scale bars, 10 µm.

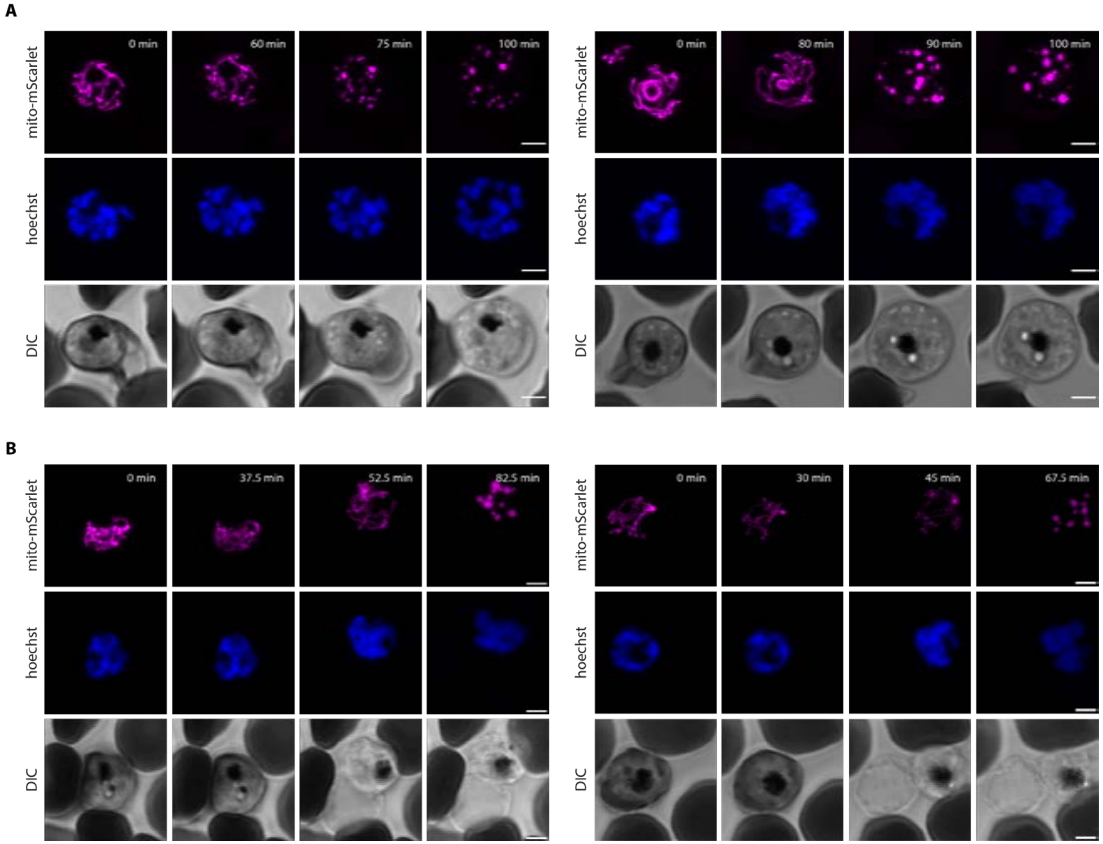

Figure S6. Time-lapse imaging of MitoRed. A) Live time-lapse imaging of MitoRed schizonts that show changes in parasite morphology. Mitochondria fall apart after approximately 75-90 minutes of imaging. B) Live time-lapse imaging of MitoRed schizonts that leave the RBC after 45-52.5 minutes of imaging. Parasites were stained with Hoechst to visualize DNA. All images are maximum intensity projections of Z-stacks taken with Airyscan confocal microscopy. Timestamps in the upper right corner represent the time points of the time-lapse experiment in minutes. Scale bars, 2 µm.

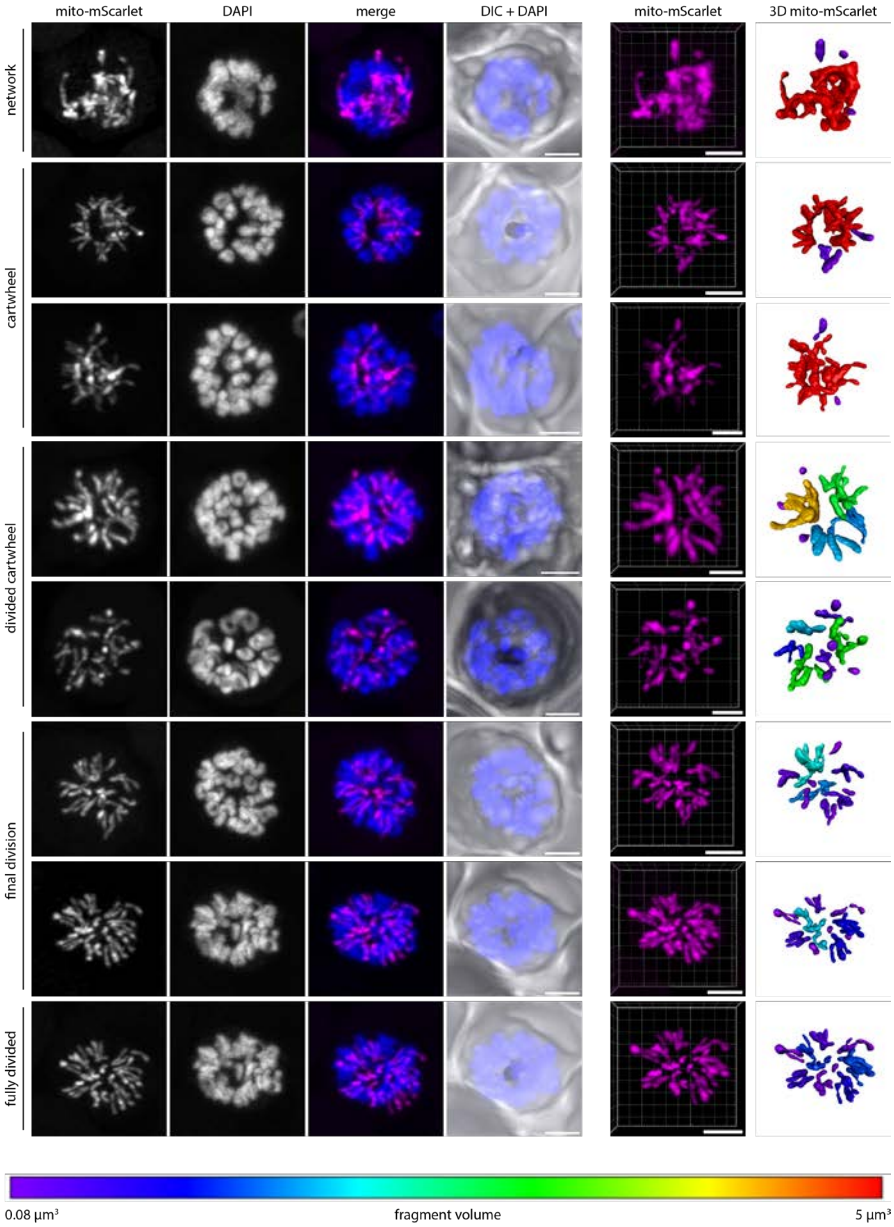

Figure S7. Mitochondrial division stages in ABS schizogony. Fluorescent imaging of MitoRed parasites in different mitochondrial division stages (described on the left). Images are representatives of the 17 parasites that were analyzed in second independent experiment. Mito-mScarlet signal is shown in magenta and DAPI (DNA) in blue. Images are maximum intensity projections of Z-stacks taken with an Airyscan confocal microscope. The fifth column shows the 3D image if the fluorescent mito-mScarlet signal, while the sixth column shows the 3D visualization of the segmented mitochondrial signal. The color of the mitochondrial fragment represents the size of this fragment, as is shown in the color bar at the bottom. Scale bars, 2 µm.

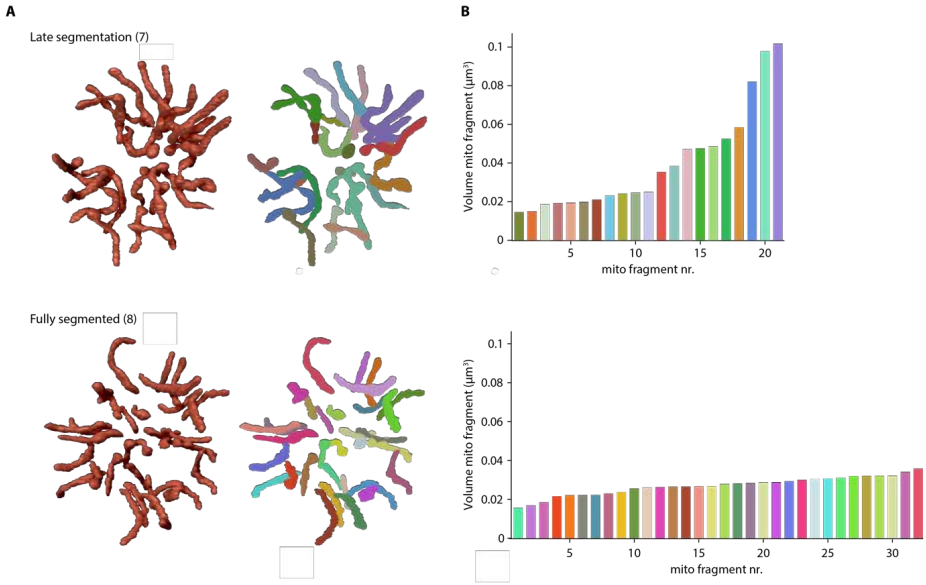

Figure S8. Shape and volume of mitochondrial fragments during final stages of schizogony. A) 3D rendering of mitochondria in a late and fully segmented schizont. The number between brackets indicates the parasite ID number (Table S3). In the right images, each mitochondrial fragment is depicted in an arbitrary color to distinguish separate and connected structures. B) Bar graphs indicating the mitochondrial fragment volumes in μm^3 and bar colors correspond to colors of the mitochondrial fragments in A.

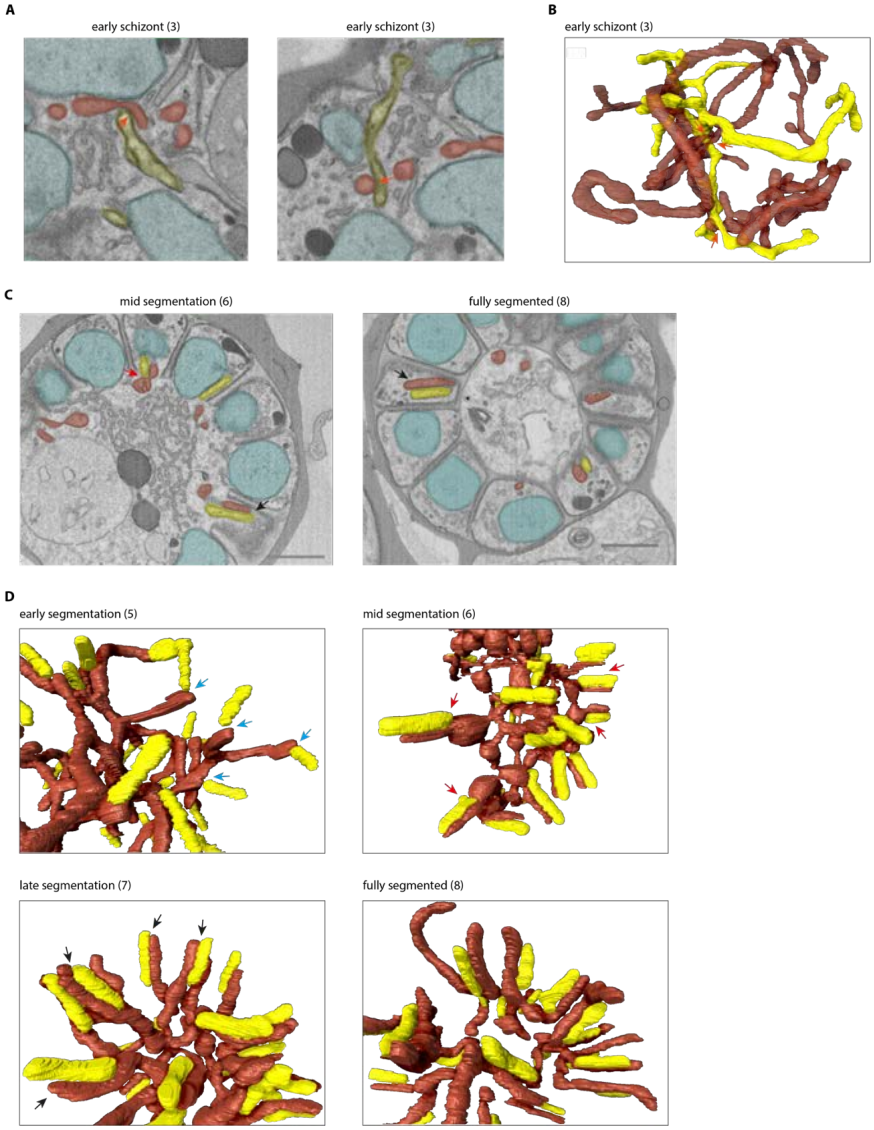

Figure S9. Interaction between mitochondrion and apicoplast in different stages of schizogony. A) Micrograph images of contact sites between the apicoplast (yellow) and mitochondrion (red) in early stage schizont, indicated by orange arrows. Nuclei are marked in teal. B) 3D rendering of mitochondrion (red, 50% opacity) and apicoplast (yellow), with contact sites indicated by orange arrows. C) Micrograph images of mid- and fully segmented schizonts showing contact sites where apicoplast and mitochondrion are aligned over the total apicoplast length (black arrows). Red arrow indicates where the basal end of the apicoplast is in contact with the bulbous part of the mitochondrion at the merozoite entrance. Scale bars, 1 µm. D) 3D rendering of apicoplast and mitochondrion in different stage schizonts. Blue arrows indicate where the basal end of an apicoplast interacts with the end of a mitochondrial branch. The number between brackets indicates schizont ID number (Table S3).

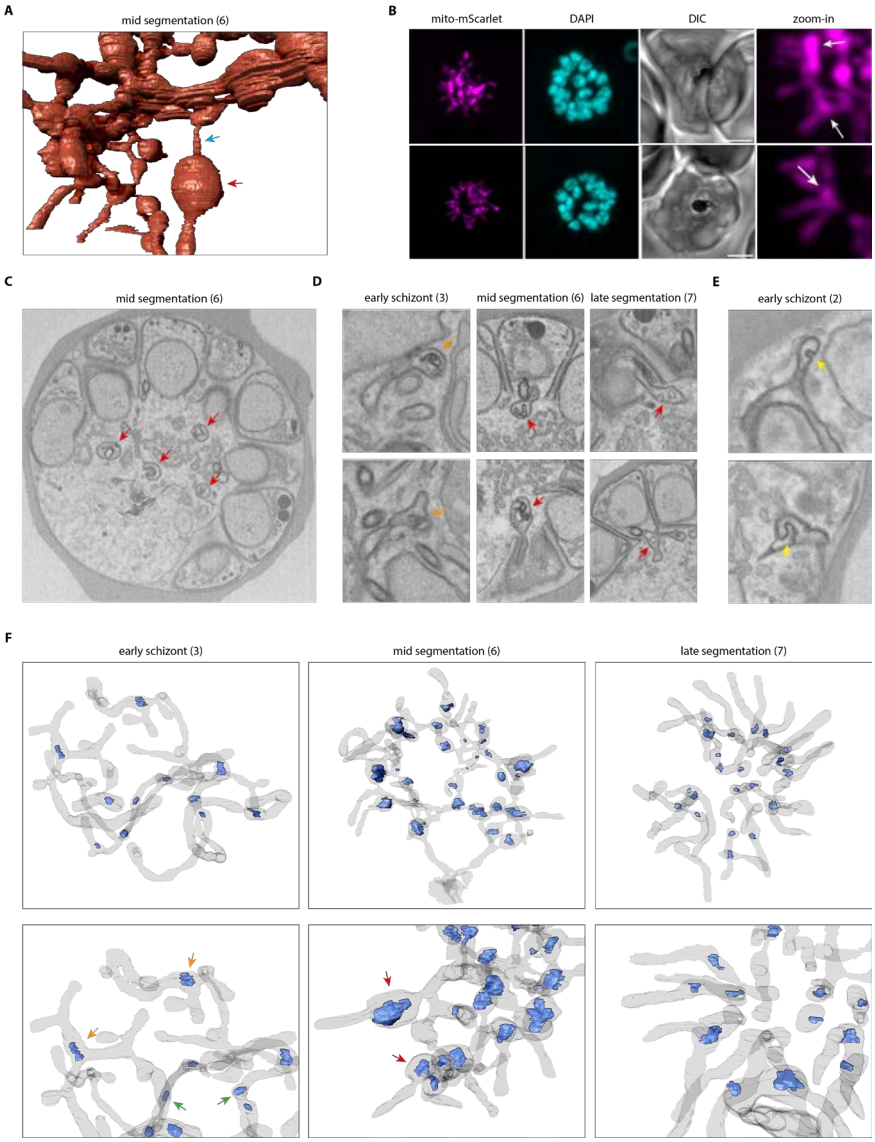

Figure S10. Bulbous membrane invagination structures (bulins) in the mitochondrion. A) 3D rendering of the mitochondrion in a mid-segmentation schizont with a thin (blue arrow) and thick (red arrow) part. B) Fluorescent microscopy of mito-mScarlet showing bulbous mitochondrial parts at the base of a mitochondrial branch. Scale bars, 2 µm. C) Micrograph image of mid-segmentation schizont showing four bulins. D) micrograph images of mitochondrial bulins in different schizont stages. E) micrograph images of apicoplast bulins (yellow arrows) in early stage schizont. F) 3D rendering of the mitochondrion (gray, 7% opacity) and membrane invaginations (blue). Red arrows indicate bulins at the base of a mitochondrial branch just outside the forming merozoite entrance. Orange arrows indicate membrane invaginations at a branching point in the mitochondrial network. Green arrows indicate membrane invaginations in the middle of a continuous mitochondrial branch. The number between brackets indicate schizont ID number (Table S3).

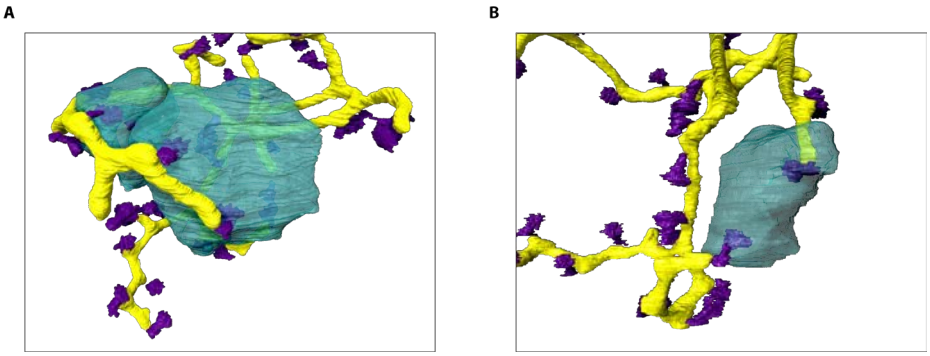

Figure S11. Different interaction between apicoplast and centriolar plaques in an early schizont (3). A) Two centriolar plaques (CPs, purple) from a single nucleus (teal) associating with one apicoplast branch (yellow). B) Two CPs from a single nucleus associating with two different apicoplast branches.

Movie legends

Movie 1. Schizont 1. Visualization of schizont 1 with parasite outline (grey), nuclei (cyan), apicoplast (yellow), mitochondrion (brown/red), centriolar plaques (purple).

Movie 2. Schizont 2. Visualization of schizont 2 with parasite outline (grey), nuclei (cyan), apicoplast (yellow), mitochondrion (brown/red), centriolar plaques (purple).

Movie 3. Schizont 3. Visualization of schizont 3 with parasite outline (grey), nuclei (cyan), apicoplast (yellow), mitochondrion (brown/red), centriolar plaques (purple).

Movie 4. Schizont 4. Visualization of schizont 4 with parasite outline (grey), nuclei (cyan), apicoplast (yellow), mitochondrion (brown/red), centriolar plaques (purple).

Movie 5. Schizont 5. Visualization of schizont 5 with parasite outline (grey), nuclei (cyan), apicoplast (yellow), mitochondrion (brown/red), centriolar plaques (purple).

Movie 6. Schizont 6. Visualization of schizont 6 with parasite outline (grey), nuclei (cyan), apicoplast (yellow), mitochondrion (brown/red), centriolar plaques (purple).

Movie 7. Schizont 7. Visualization of schizont 7 with parasite outline (grey), nuclei (cyan), apicoplast (yellow), mitochondrion (brown/red), centriolar plaques (purple).

Movie 8. Schizont 8. Visualization of schizont 8 with parasite outline (grey), nuclei (cyan), apicoplast (yellow), mitochondrion (brown/red), centriolar plaques (purple).

Movie 9. Bulins during mid-segmentation. Micrograph stacks of another mid-segmentation schizont showing merozoite-entrance bulins.

Movie 10. Detailed bulins. Micrograph stacks of schizont 6, showing two merozoite-entrance bulins, localizing at the basal end of the divided apicoplast.

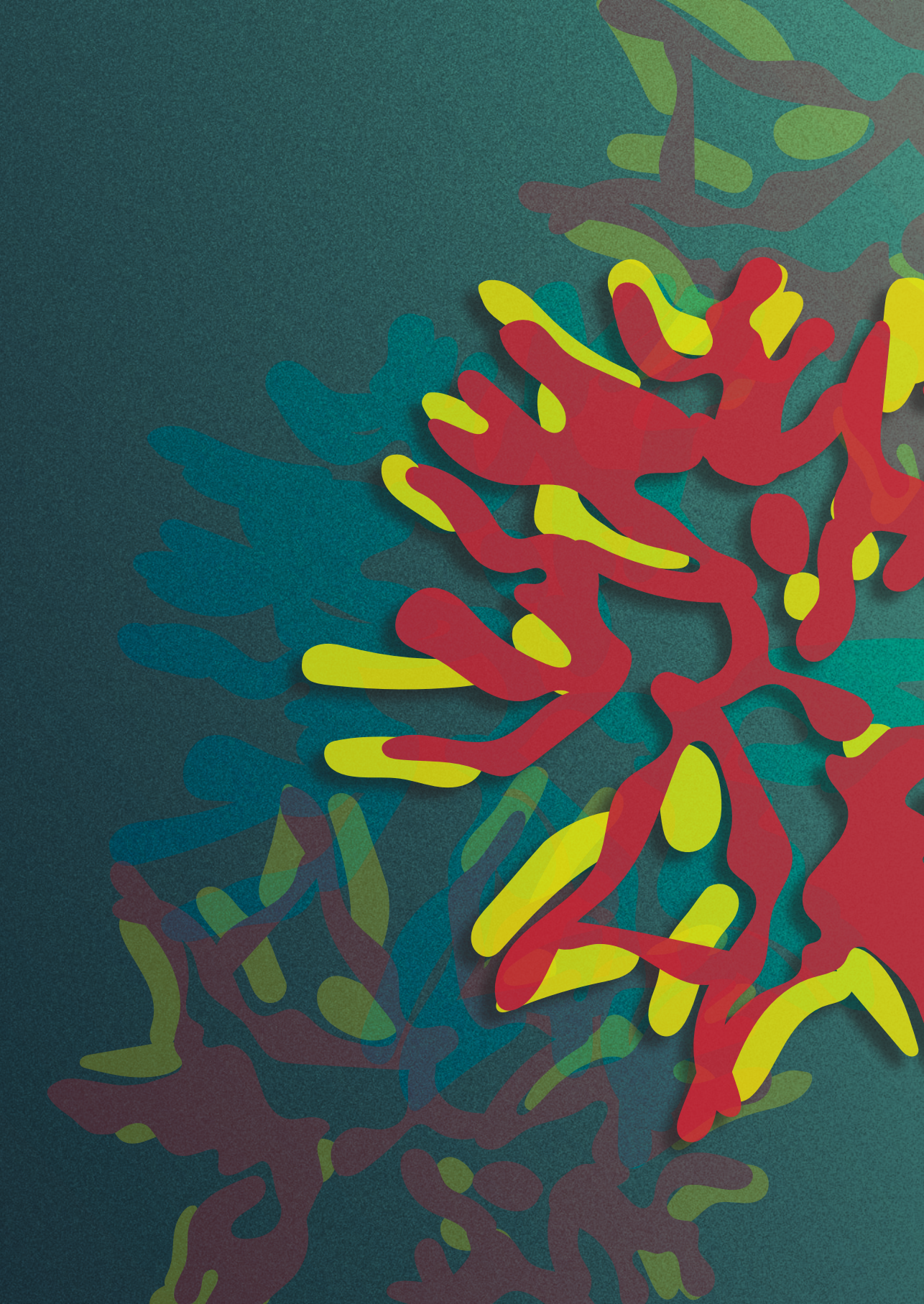

Chapter 4

The role of stomatin-like protein (STOML) in *Plasmodium falciparum*

Julie M.J. Verhoef[1], Ezra T. Bekkering[1], Cas Boshoven[1], Megan Hannon[1], Felix Evers[1], Nicholas I. Proellochs[1], Cornelia G. Spruijt[2], Taco W.A. Kooij[1]

[1]Department of Medical Microbiology, Radboudumc Center for Infectious Diseases, Radboud University Medical Center, Nijmegen, The Netherlands

[2]Department of Molecular Biology, Faculty of Science, Radboud University Nijmegen, Nijmegen, The Netherlands

Manuscript under review

Abstract

Members of the Stomatin, Prohibitin, Flotillin and HflK/C (SPFH) protein family form large membrane anchored or spanning complexes and are involved in various functions in different organelles. The human malaria causing parasite *Plasmodium falciparum* harbors four SPFH proteins, including prohibitin 1 and 2, prohibitin-like protein (PHBL), and stomatin-like protein (STOML) which all localize to the parasite mitochondrion. In the murine *Plasmodium berghei*, STOML has been shown to be essential and to localize to puncta on mitochondrial branching points in oocyst stages. In this study, we investigate the function of STOML in the human malaria parasite, *P. falciparum*. We show that deletion of *STOML* causes a significant growth defect and slower asexual blood-stage (ABS) development, while sexual-stage development remains unaffected. Parasites lacking *STOML* were not more sensitive to respiratory chain targeting drugs, rendering a function of STOML in respiratory chain assembly unlikely. Epitope tagging of endogenous STOML revealed a distinct punctate localization on branching points and endings of the ABS mitochondrial network. STOML resides in a large protein complex and pulldown experiments identified a zinc dependent metalloprotease, FtsH, as a likely interaction partner. The predicted AlphaFold structure of STOML shows high similarity with the bacterial HflK/C, which has been shown to form a large vault like structure around the bacterial FtsH hexamers. Combined, our results suggest that a similar STOML-FtsH complex localized to specific loci of *P. falciparum* mitochondria facilitate the parasite's asexual blood-stage development.

Introduction

Malaria is an infectious disease caused by *Plasmodium* parasites, which takes more than 600.000, mostly young lives annually[1]. *Plasmodium falciparum* is the most virulent malaria causing species. Resistance to current antimalaria drugs is fast to emerge, emphasizing the need for the continuous development of novel anti-malarial compounds. *Plasmodium* parasites harbor a unique mitochondrion that differs considerably from human mitochondria, which makes it a suitable drug target of antimalarial compounds such as atovaquone, DSM265, ELQ300, and proguanil[2,3].

The mitochondrion consists of an inner and outer membrane, which are both rich in large protein complexes. Indeed, the inner mitochondrial membrane (IMM) is considered one of the most protein-rich membranes in any cell-type and contains large multiprotein complexes, such as respiratory chain complexes, ATP synthase, and the mitochondrial contact site and cristae organizing system (MICOS). Similarly to all other biological membranes, the mitochondrial membranes are organized into domains of distinct protein and lipid composition[4,5]. These membrane microdomains are important for the spatial and temporal control of membrane protein complex assembly and regulation[4]. SPFH (Stomatin, Prohibitin, Flotillin and HflK/C) family proteins are enriched in eukaryotic and prokaryotic membrane microdomains of various organelles, such as plasma membrane, nucleus, endoplasmic reticulum (ER), and mitochondria[6]. The common feature of SPFH proteins is the presence of the highly conserved SPFH or Band-7 protein domain[7]. These proteins form large self-oligomerizing membrane-spanning or membrane-anchored complexes and have been indicated in a diverse set of functions[6]. A subset of SPFH proteins, including prohibitins (PHBs) and stomatin-like protein 2 (SLP2), localizes to the IMM. The two prohibitins (PHB1 and PHB2) form a large protein complex together, which has been indicated to play a role in mitochondrial protein degradation, cristae formation, mitochondrial dynamics, cell cycle regulation, and apoptosis[8–11]. SLP2 localizes to cardiolipin enriched membrane microdomains, where it interacts with and controls stability of the PHB complex[12,13]. The PHB and SLP2 complexes are both important for the formation and stability of the respiratory chain complex and mitochondrial translation[8,13–17]. They reside in large supercomplexes with metalloproteases and assert their proteolytic function through regulation of metalloprotease activity, similar to their bacterial family member HflIK/C[8,11,12,18–21].

Plasmodium parasites harbor three conserved SPFH proteins, including two prohibitins (PHB1 and PHB2) and stomatin-like protein (STOML), as well as an

unusual myzozoan-specific prohibitin-like protein (PHBL)[22]. Attempts to delete the four genes using both genome-wide screens in *P. falciparum* and the murine malaria model parasite *Plasmodium berghei*, and targeted approaches in the latter, resulted in conflicting results with only *PHB2* consistently surfacing as essential. Localization studies through fluorescent tagging of the endogenous *P. berghei* genes revealed a mitochondrial localization of three SPFH proteins throughout the *P. berghei* life cycle[22]. Although tagging of *PHB1* was unsuccessful, PHB1/2 heterodimerization is evolutionary well-conserved[15,23] and *Pf*PHB1 ranks 84th on the validated list of *Plasmodium* mitochondrial proteins[24]. Functional complementation of yeast *PHB* mutants provided further support for prohibitin heterodimerization in *P. falciparum*[25]. *Pf*PHBs were shown to be involved in stabilizing mitochondrial DNA, maintaining mitochondrial integrity, and rescuing yeast cell growth[25]. PHBL-deficient parasites failed to colonize *Anopheles* mosquitos as they arrest during ookinete development, which is correlated with depolarization of the mitochondrial membrane potential[22].

The role and importance of STOML remains unclear. Genetic screens in *P. falciparum* and *P. berghei* both suggested a dispensable role, yet targeted approaches did never yield a pure isogenic or clonal line free of wild-type parasites, indicating possible developmental issues. Interestingly, *Pb*STOML localizes to punctate foci at the parasite mitochondrion during oocyst growth, often at organellar branching points. This specific mitochondrial localization combined with the uncertainty about its importance and function drove us to further investigate the role of STOML in the human malaria causing *P. falciparum*.

In this study, we show that deletion of *STOML* in *P. falciparum* causes a significant growth delay of asexual blood stages (ABS), while sexual-stage development is not affected. *Pf*STOML localizes to punctate foci at mitochondrial branch endings and at branching points throughout ABS development. *Pf*STOML resides in a large protein complex and pulldown experiments identified metalloprotease FtsH as a likely interaction partner. We also show that the predicted AlphaFold structure of *Pf*STOML is highly similar to its bacterial family member HflK/C, which has recently been shown to form a large, oligomerized, vault structure around FtsH hexameres, this way regulating their accessibility. This suggests that a similar scenario might apply to the STOML-FtsH complex in *P. falciparum*. These results gave us novel insights into the function of STOML in *P. falciparum* and pave the way for future studies into the function of SPFH proteins and their potential as anti-malarial drug targets.

Results

Knockout of *PfSTOML* results in a significant growth defect

To study the function of *Pf*STOML (PF3D7_0318100) during ABS development, we aimed to generate *PfSTOML* knockout (KO) parasites using a targeted replacement strategy (Figure S1A). Although the first three transfection attempts were unsuccessful, we managed to generate two *PfSTOML* KO parasite lines in NF54 (*stoml*$^{-}$) and the MitoRed background (*stoml*$^{-}_{mito}$), which harbors a fluorescent mitochondrial marker (mito-mScarlet)[26]. Correct integration and the absence of unaltered wild-type (WT) NF54 or MitoRed parasite contaminations were verified by diagnostic PCR (Figure S1B). To demonstrate if *PfSTOML* KO causes a growth defect, we set up a new competition growth assay analogous to the protocol used with *Plasmodium berghei*[27]. In both *PfSTOML* KO lines, *stoml* is replaced by a *gfp* gene under the constitutive *P. falciparum* histone 2B (*Pf*H2B, PF3D7_1105100) promotor, making them green fluorescent. By mixing these with WT parasites harboring a constitutively expressed mScarlet, the relative abundance of red and green fluorescent parasites can be determined by flow cytometry and followed over time (Figure 1A). The average factor by which the red/green ratio changed from the first to the second timepoint in three independent experiments was defined as f_r. We included a control condition in which mNeonGreen expressing WT parasites (*cyto-NG*) are mixed with mScarlet expressing WT parasites (*cyto-mScarlet*) (Figure S2). We confirmed that the ratio of red and green parasites in this control culture was stable over time ($f_r = 1.0$) (Figure 1B). However, when co-culturing either of our *PfSTOML* KO lines with *cyto-mScarlet*, we found that the red/green distributions shift significantly over time ($f_r = 20.9$, $p<0.0001$). In one representative experiment, the ratio of *cyto-mScarlet* versus *stoml*$^{-}_{mito}$ parasites changes from 47: 53, to 94: 6 after one week and 99: 1 after two weeks, indicating that *stoml*$^{-}_{mito}$ grows approximately 12 times slower in a week period compared to WT in mixed culture conditions. We observed a very similar trend in *stoml*$^{-}$ mixed cultures. To test whether this growth defect is caused by lower number of viable offspring per parasite, reduced invasion, or delayed development throughout the ABS cycle, we quantified growth and analyzed stage development microscopically in two independent experiments, either every 8-16 h over an 88-h period or daily for eight days (Figure 1C, 1D, 1E). These experiments showed that *stoml*$^{-}_{mito}$ develops slower throughout the ABS replication cycle compared to MitoRed WT parasites. At the end of the first replication cycle (40 h), MitoRed WT cultures contained mostly segmented schizonts and rings, and the parasitemia has increased 6.0-fold compared to the 24 h timepoint (Figure 1D). *stoml*$^{-}_{mito}$ cultures contained mostly early schizonts and very few rings at 40 h, and the parasitemia has only increased 1.6-fold. However, at 48 h, *stoml*$^{-}_{mito}$ parasitemia

has almost "caught up" with WT parasitemia with a 4.9-fold increase compared to the 24 h timepoint. This trend of delayed ABS development continues in the next replication cycles (Figure 1E). These results indicate that *stoml*$^{-}_{mito}$ has a growth defect that is mostly caused by slower and prolonged development throughout the asexual replication cycle.

*Pf*STOML is unlikely to be involved in assembly of the respiratory chain

In other eukaryotes, STOML is thought to be involved in a variety of mitochondrial functions[13,21,28–30]. To explore if *Pf*STOML has a similar mitochondrial function in *P. falciparum*, we were curious to see if *PfSTOML* KO would alter mitochondrial dynamics. We compared mitochondrial morphology of *stoml*$^{-}_{mito}$ with MitoRed parasites and found no obvious differences throughout different stages of ABS development in two independent experiments (Figure S3). Mature *stoml*$^{-}_{mito}$ schizonts showed divided and segregated mitochondria, similarly to MitoRed WT parasites.

SLP2, the human STOML homolog, has been indicated to play an essential role in the assembly of the respiratory chain[12,28]. To test if STOML has a similar function in *P. falciparum*, we investigated if *stoml*$^{-}$ parasites would have an increased sensitivity to drugs targeting the respiratory chain. We performed drug assays with different mitochondrial drugs (including DSM1, DSM265, atovaquone, ELQ300 and proguanil) and non-mitochondrial drugs (chloroquine, DHA, MMV183) and found no difference in drug sensitivity between *stoml*$^{-}$ and WT parasites in two independent experiments (Figure S4). Energy metabolism in *P. falciparum* ABS relies heavily on glycolysis, and oxidative phosphorylation (OXPHOS) is only essential for ubiquinone recycling for pyrimidine synthesis[31]. However, in gametocytes, there is an increased TCA cycle utilization and presumably respiration[32,33]. We were therefore curious to see if *stoml*$^{-}_{mito}$ parasites could develop to mature gametocytes and gametes. We found that *stoml*$^{-}_{mito}$ parasites could develop to healthy-looking, mature gametocytes within a comparable time frame as WT parasites in three independent experiments. Mature male and female *stoml*$^{-}_{mito}$ gametocytes did not show obvious aberrations in mitochondrial morphology (Figure S5A). *Stoml*$^{-}_{mito}$ parasites were still able to exflagellate and had dispersed mitochondria after activation, similarly to what we have described for the MitoRed WT line[26] (Figure S5B). Based on these results, it is unlikely that STOML is directly involved in respiratory chain assembly in *P. falciparum*.

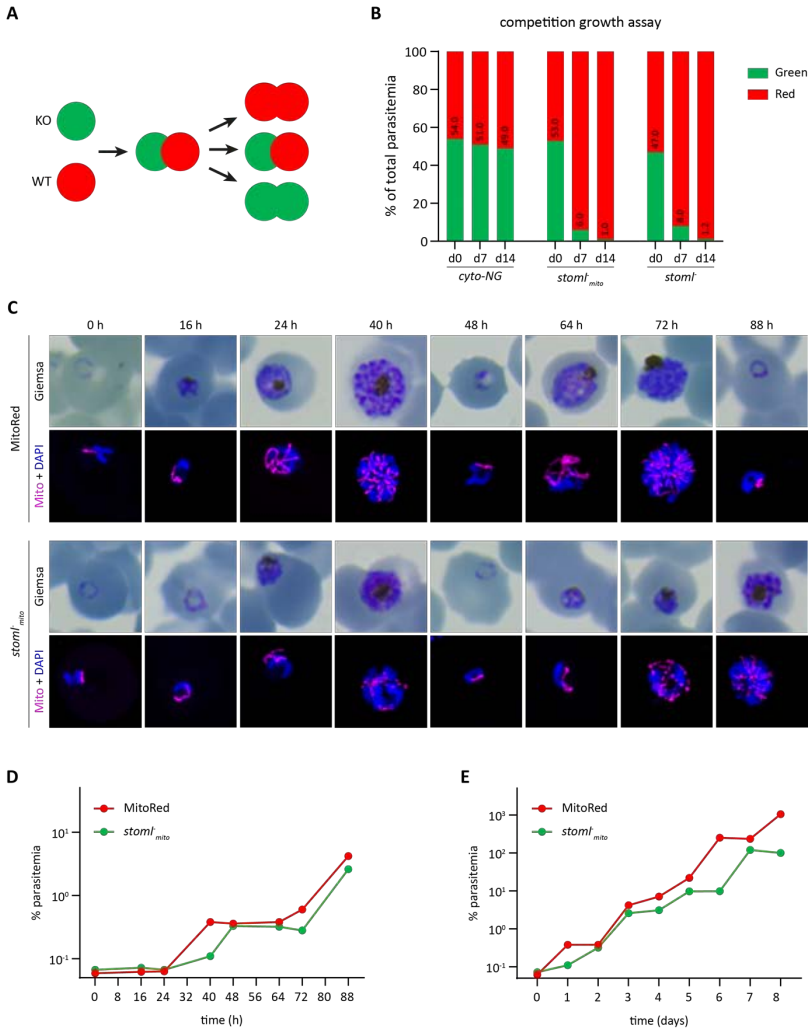

Figure 1. ABS development of stoml$^{-}_{mito}$ parasites is delayed. A) Schematic overview of the competition growth assay. PfSTOML knockout parasites expressing cytosolic GFP (green) are mixed with wild-type parasites expressing cytosolic mScarlet (red) in an approximate 1:1 ratio. Overtime, the distribution of red/green parasites is measured using flow cytometry. If PfSTOML knockout causes a growth defect, the wild-type population will grow faster, and the ratio red/green parasites will shift. B) Bar graph showing distribution of red/green parasites in the competition growth assay at day 0, day 7 and day 14. The graph shows one representative example of three independent experiments. Cyto-mScarlet parasites are mixed with green cyto-NG (control), stoml^{-}, or stoml$^{-}_{mito}$ parasites to create mixed cultures. C) Giemsa-stained thin blood smears and fluorescent images showing the mitochondrial mScarlet marker (magenta) and DNA (blue) in MitoRed (WT) and stoml$^{-}_{mito}$ parasites over time. Fluorescence microcopy images are maximum intensity projections of Z-stack confocal Airyscan images. D-E) Growth curve of parasitemia of MitoRed and stoml$^{-}_{mito}$ over time in hours (D) and days (E). In order to visualize continuous growth, we corrected for the parasitemia for the dilution factors, resulting in corrected parasitemias above 100%. The graphs show one representative experiments of two independent experiments.

*Pf*STOML localizes to specific foci at the mitochondrion during ABS development

To learn more about the function of *Pf*STOML, we analyzed its subcellular localization. To do this, we generated a transgenic parasite line, *stoml-NG*, in which *STOML* is fused with a 3HA-mNG-GlmS tag. We also integrated a mitochondrial marker cassette mito-mScarlet for protein co-localization (Figure S1A). Correct integration and the absence of WT parasite contaminations were verified by diagnostic PCR (Figure S1B). Western blot analysis of ABS parasite extract confirmed expression of the full length *Pf*STOML-3HA-NG (Figure S1C). Live fluorescent microscopy of *stoml-NG* in three independent experiments showed localization of *Pf*STOML-3HA-NG to punctate foci during ABS development (Figure 2). In ring stages, *Pf*STOML-3HA-NG localized to a single spot, close to the mitochondrion (Figure 2A). As the parasites progress to late rings and the mitochondrion elongates, *Pf*STOML-3HA-NG is consistently found in two foci that reside at both endings of the mitochondrion (Figure 2A, 2B, Movie 1). In trophozoites, the mitochondrion starts to form a branched structure and the number of *Pf*STOML-3HA-NG foci per parasite increases (Figure 2C). *Pf*STOML-3HA-NG foci are found both at endings of mitochondrial branches, as well as branching points (Figure 2A). Similar localization is found in early schizont stages, were the mitochondrion forms a complex, branched network (Figure 2A, 2B, Movie 2). The number of foci per parasite increases during schizont stages. In late schizonts, when the mitochondrial branches orient in a radial fashion prior to division, the *Pf*STOML-3HA-NG foci are found at the endings of most mitochondrial branches, although *Pf*STOML-3HA-NG signal can also be observed along mitochondrial branches (Figure 2A, 2B, Movie 3). In a fully segmented parasite that seems to have egressed form the RBC, only few *Pf*STOML-3HA-NG foci were found. This unique localization pattern is different from the homogeneous mitochondrial localization of *Pb*STOML observed in *P. berghei* ABS[22].

*Pf*STOML resides in a large protein complex with *Pf*FtsH

PHBs and STOML are found in large hetero- and homo- oligomers at the IMM in other eukaryotes, such as humans and yeast[15,21]. *P. falciparum* mitochondrial complexome profiling data showed that *Pf*STOML migrates in a large ~2 MDa protein complex on a native gel (Figure 4C)[33]. In order to identify the proteins in this complex, we performed two independent pulldown experiments (Figure 4A-B, S6). In the first experiment, late-stage *stoml-NG* parasites (24-40 h.p.i.) were lysed through saponin lysis and nitrogen cavitation, and organelle fraction was used as input for co-immunoprecipitation with anti-mNG coated magnetic beads. As a control, the same fraction was loaded on uncoated beads. 27 proteins were

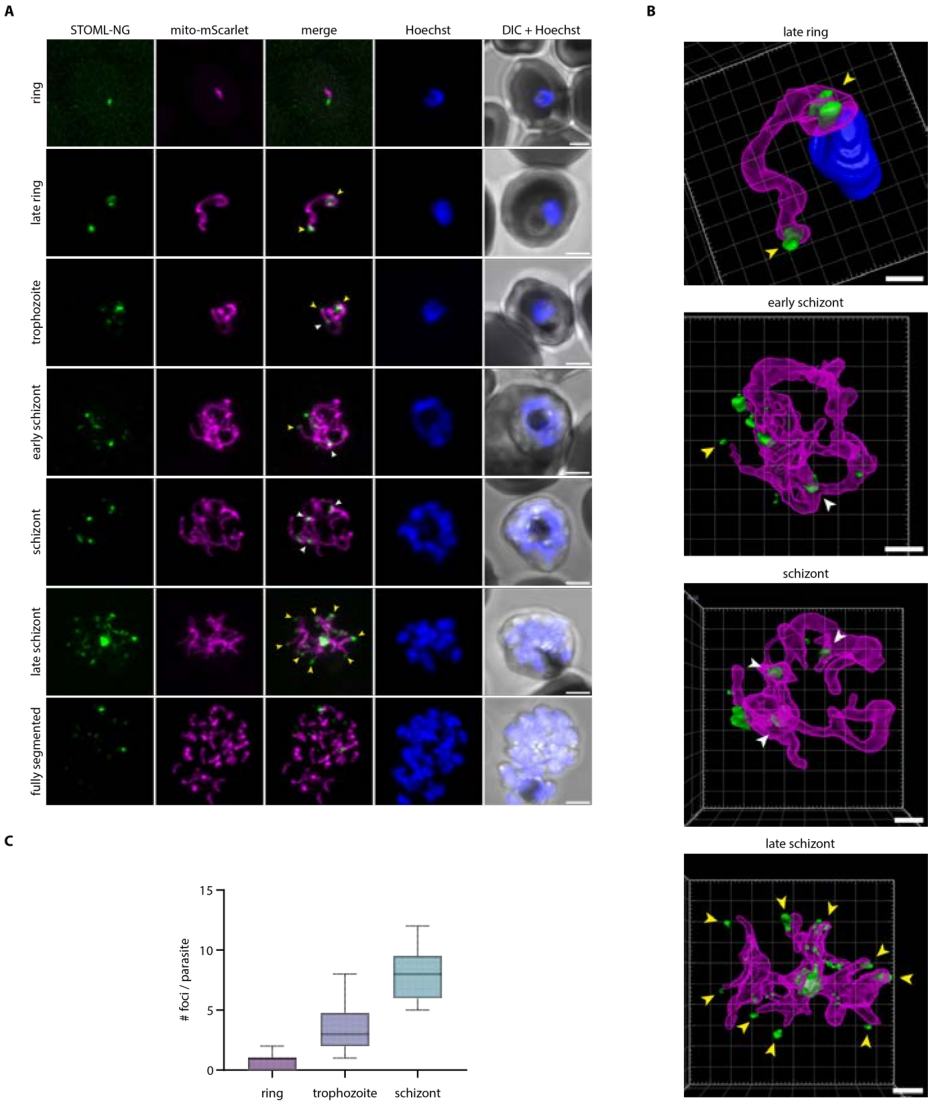

Figure 2. Localization of STOML-3HA-NG in ABS parasites. A) Live imaging of stoml-NG with PfSTOML-3HA-NG (green), mito-mScarlet mitochondrial marker (magenta), Hoechst for DNA visualization (blue) and DIC through the asexual replication cycle. Images are maximum intensity projections of Z-stack confocal Airyscan images. Arrowheads indicate PfSTOML-3HA-NG signal at mitochondrial branching points (white) or mitochondrial branch endings (yellow). Scale bars, 2 µm. B) 3D visualization of Z-stack confocal Airyscan images using Arivis 4D vision software. Fluorescent signal is segmented by manual thresholding. Arrowheads indicate STOML-NG signal at mitochondrial branching points (white) or mitochondrial branch endings (yellow). Scale bars, 1 µm. C) Boxplot indicating number of PfSTOML-3HA-NG foci per parasite in ring (n=7), trophozoite (n=12) and schizont (n=9) stages with a total of 28 parasites.

significantly enriched after pulldown with mNG beads, of which *Pf*STOML was the most significantly enriched (Figure 4A, Table S2). For the second pulldown experiment, we generated a transgenic parasite line in which *STOML* is fused with an 3HA-GlmS tag, which we termed *stoml-HA*. Correct integration and the absence of wild-type (WT) parasite contaminations were verified by diagnostic PCR (Figure S1B) and Western blot analysis confirmed expression of STOML-3HA (Figure S1C). Organelle fraction of late-stage *stoml-HA* parasites was used as input for pulldown with anti-HA coated magnetic beads and empty protein G beads were used as control. In the second experiment, 122 proteins were significantly enriched after HA pulldown (Figure S6, Table S3). Three proteins were significant hits in both pulldown experiments: STOML, an ATP-dependent zinc metalloprotease FtsH (PF3D7_1464900), and a conserved protein of unknown function (PF3D7_1306200) (Figure 4B). Although FtsH is also found in a large protein complex of ~2.5 MDa in the complexomics dataset[33], it does not perfectly comigrate with the STOML complex in ABS (Figure 4C). In gametocytes, however, FtsH and STOML comigrate at ~2.3 MDa. In contrast, PF3D7_1306200 does not comigrate with STOML in either ABS or gametocyte stages. PF3D7_1306200 is predicted to be an essential protein and is expressed in late schizonts[34,35]. It contains an AB-hydrolase domain and is thought to localize to the apicoplast. FtsH, on the other hand, is a predicted mitochondrial protein (ranking 265th with a mitochondrial prediction score of 2.1[24]) and phylogenetic analysis shows clustering with *i*-AAA proteases in the IMM[36].

SPFH proteins are known to form large protein complexes with metalloproteases, regulating their protease activity[8,18,19,21,37]. The human STOML homolog, SLP2, forms a large proteolytic complex termed the SPY complex at the inner mitochondrial membrane with rhomboid protease PARL and *i*-AAA metalloprotease YME1L[21]. SLP2 regulates the activity of YME1L, which forms homo-hexamers and is involved in degradation of unfolded or excess mitochondrial proteins[38]. In *Trypanosoma brucei*, another unicellular protozoan parasite, SLP2 can also be found in a complex with the Yme1L homolog, *Tb*Yme1[39]. A BLAST search of *h*YME1L identified *P. falciparum* FtsH as top hit with 41% identity (Figure S7).

Cryo-electron microscopy revealed that the bacterial HflK and HflC form a large, hetero-oligomeric vault structure around four membrane-anchored FtsH hexamers (Figure 5E)[19]. We compared the predicted AlphaFold[40] structure of *Pf*STOML with the bacterial HflK/C complex (Figure 5A-D). Although *Pf*STOML lacks a clear transmembrane domain, the overall predicted structure of the protein is highly similar to its bacterial family members. To further explore if *Pf*STOML could form a similar multimer barrel structure, we used AlphaFold multimer[41] to predict the

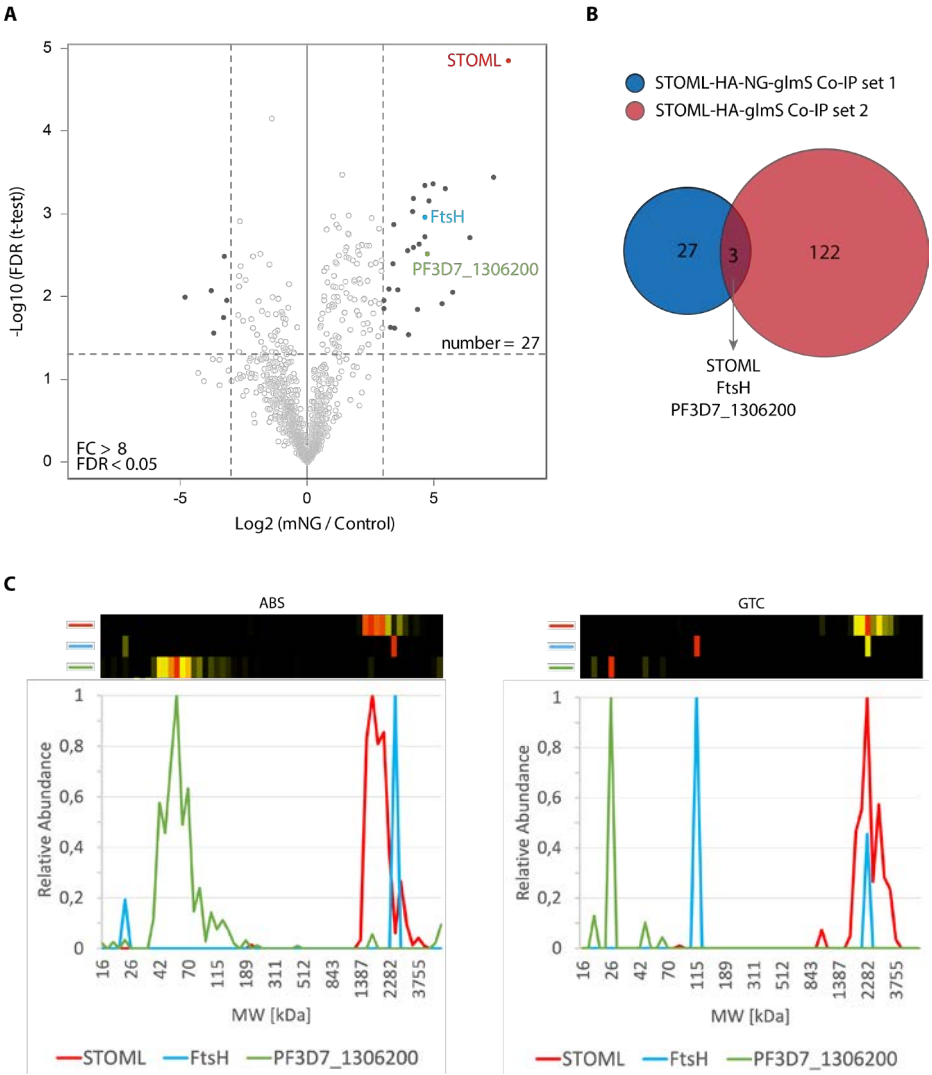

Figure 4. Identification and characterization of STOML protein complex. A) Anti-mNG co-immunoprecipitation of PfSTOML-3HA-mNG containing complexes. The volcano plot showing mean $\log_2$ fold changes (FC) and $-\log_{10}$ false discovery rate (FDR) for anti-mNG pulldown in comparison with control pulldown. Horizontal and vertical dotted lines indicate FC > 8 and FDR < 0.05 respectively. Dark dots represent enriched proteins. The number of proteins enriched in the anti-mNG pulldown compared to the control pulldown is indicated on the right. B) Overlap of enriched proteins in both anti-HA pulldown on STOML-HA and anti-mNG pulldown on STOML-mNG. C) Heatmap and graph showing migration profiles of STOML (red), FtsH (blue) and PF3D7_1306200 (green) on a blue native gel with a normalized relative abundance of 1 (red) represents the highest iBAQ value for a given protein and the molecular weight (MW) indicated on the x-axis.

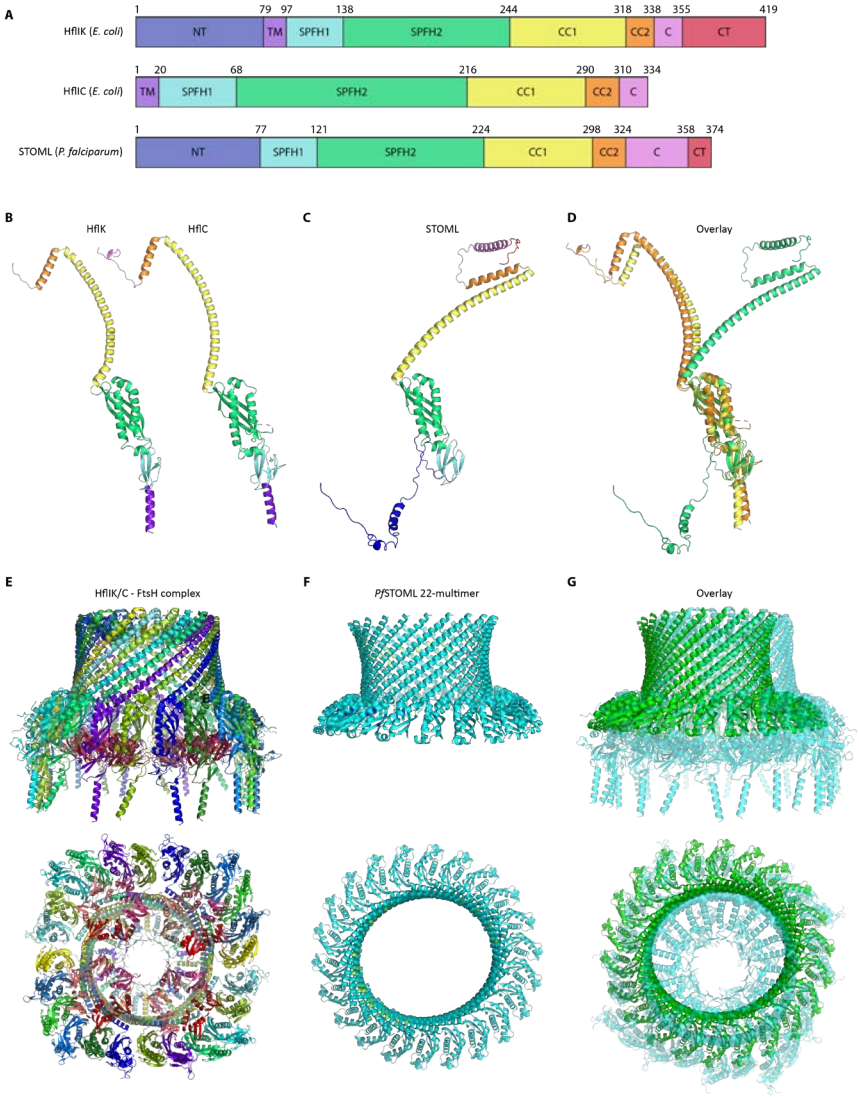

Figure 5. AlphaFold predictions of PfSTOML complex structure and comparison with the bacterial HflK/C supercomplex structures. A) Protein domains of EcHflK EcHflC, and PfSTOML, indicated are transmembrane domain (TM), SPFH1 and SPHF2 domains, long coiled-coil domain 1 (CC1), coiled-coil domain 2 (CC2), C-terminal region (CT). B) Protein structures of EcHflK and EcHflC determined by Ma et al.[19]. C) Predicted AlphaFold structure of PfSTOML. D) Overlay of EcHflK and EcHflC structures with PfSTOML AlphaFold structure. E) Cryo-EM structure of HflK/C – FtsH complex with the side view (top) and bottom view (bottom). Purple/blue-colored proteins are HflC, green/yellow-colored proteins are HflK, red/pink-colored proteins are part of the FtsH hexamers. F) Predicted AlphaFold structure of PfSTOML 22-multimer with side view (top) and top view (bottom), coloring according to model confidence with very high confidence (pLDDT > 90) dark blue, high confidence (pLDDT > 70) light blue, and low confidence (pLDDT > 50) yellow. G) Overlay of predicted AlphaFold PfSTOML 22-multimer structure (green) with HflK/C – FthsH complex (light blue) with side view (top) and top view (bottom).

*Pf*STOML 24-multimer structure (Figure S8A). We used the SPFH2 and long alpha helix domains of *Pf*STOML, as these are the best predicted parts of the *Pf*STOML structure (pLDDT>90). The *Pf*STOML 24-multimer structure was predicted to form a round, yet distorted barrel structure with the endings of the multimer structure not joining together to close the structure, which visually seemed to include too many *Pf*STOML proteins (Figure S8A). In order to estimate the correct amount of *Pf*STOML proteins in the barrel complex, we used AlphaFold multimer to predict the structure of *Pf*STOML 8-multimer structure with SPFH1, SPFH2 and long alpha helix domains (Figure S8B). We then measured the angle between the SPFH domains in the 8-multimer complex to estimate the curvature of the barrel (Figure 8SC). We found an angle of 16.5 degrees between SPFH domains, suggesting that the *Pf*STOML complex might consist of approximately 22 *Pf*STOML monomers. Indeed, AlphaFold predicts an intact, slightly oval barrel structure for a *Pf*STOML 22-multimer with SPFH2 and long alpha helix domains (Figure 5F, S8D). The predicted *Pf*STOML 22-multimer structure showed high similarity with the HflK/C-FtsH complex, indicating that STOML might form a similar supercomplex with FtsH in the IMM in *P. falciparum*.

Discussion

The SPFH protein family is a highly conserved family involved in the formation of microdomains in membranes of various organelles. Prohibitins and stomatin-like protein (STOML) are localized to the IMM and have been implicated in several mitochondrial functions, including cristae formation and assembly of the respiratory chain[11,12,14,28]. *Plasmodium* harbors four SPFH family members, including two prohibitins (PHB1 and PHB2), a prohibitin-like protein (PHBL), and STOML, which localize to the mitochondrion[22]. STOML is likely essential in *P. berghei* and localizes to foci on mitochondrial branching points during oocyst stages. In this study, we investigated the function of STOML in the human malaria causing parasite *P. falciparum*.

In contrast to the *in vivo* murine model parasite *P. berghei* in which *STOML* could not be deleted, we were able to generate two *STOML* KO lines in *P. falciparum*. *stoml*$^{-}$ parasites developed slower throughout the ABS replication cycle compared to WT parasites, indicating an important but non-essential function for *PfSTOML* under *in vitro* culture conditions. In trophozoite and schizont stages, *Pf*STOML localizes to specific foci at the mitochondrial branching points and endings of mitochondrial branches. In late schizonts, when mitochondrial branches are oriented in a radial

fashion prior to division[26], *Pf*STOML has a punctate localization at the endings of mitochondrial branches. While STOML appears to have a more uniform mitochondrial distribution in most *P. berghei* life cycle stages, *Pb*STOML localizes to foci on mitochondrial branching points in oocyst stages[22]. This specific localization suggests a potential function for *Pf*STOML in mitochondrial dynamics and/or segregation. This could explain why *PfSTOML* deletion did not affect the sexual stage development, during which parasites do not undergo cell division. On the other hand, *PfSTOML* knockout does not seem to affect mitochondrial division, and segregation (Figure S3). Therefore, the exact function of *Pf*STOML at this specific mitochondrial localization remains to be elucidated.

In human, yeast and plants, STOML has been indicated to play a role in the assembly of the respiratory chain[12,13,28]. We hypothesized that STOML might have a similar function in *P. falciparum* and that *PfSTOML* knockout would lead to an increased sensitivity to drugs targeting the respiratory chain, such as atovaquone and ELQ300. However, our data show no changes in drug sensitivity upon *PfSTOML* knockout. Additionally, $stoml^{-}_{mito}$ parasites were able to form healthy gametocytes and undergo male gametogenesis, during which mitochondrial ATP synthesis is thought to be essential[42]. This indicates that in contrast with orthologs in other eukaryotes, *Pf*STOML is not directly involved in respiratory chain assembly in *P. falciparum*.

Our mitochondrial complexomics data shows that *Pf*STOML consistently resides in a large ~2 MDa protein complex[33]. SPFH proteins are known to form large homo- or heteromeric complexes, often together with proteases[8,18]. In order to further characterize the STOML complex in *P. falciparum*, we performed two complementary STOML-pulldown experiments to identify potential interactors. Three proteins, including *Pf*STOML, *Pf*FtsH metalloprotease, and a protein of unknown function (PF3D7_1306200), were identified as significantly enriched in both pulldown experiments. PF3D7_1306200 contains an AB-hydrolase domain and is predicted to be essential[34]. Similarly to STOML, it is mostly expressed in schizont stages[35], yet the putative hydrolase is predicted to localize to the apicoplast[43] and did not show comigration with STOML on a native gel in our complexomics data[33]. Based on its predicted apicoplast localization, and the lack of comigration with *Pf*STOML on a native gel, it is unlikely that PF3D7_1306200 forms a complex with *Pf*STOML at the IMM, yet, the consistent pull down with the STOML-FtsH complex is remarkable. Particularly in the light of a recent discovery of an AB-hydrolase, ABHD16A, localized to the endoplasmic reticulum in human cell lines, that appears to regulate the recruitment of fission and fusion machineries to mitochondria by altering phospholipid composition at ER-mitochondria membrane contact sites[44].

*Pf*FtsH belongs to the AAA (ATPases Associated with various cellular Activities) metalloprotease family at the IMM, which play a role in protein surveillance by degrading non-native integral membrane proteins and membrane associated proteins such as unassembled units of the respiratory chain[45,46]. *P. falciparum* harbors three FtsH homologs[36]. Two of the *P. falciparum* FtsH homologs, including PF3D7_1464900, which we identified in our STOML pull-down, locate to the IMM, have a single transmembrane domain, and cluster with *i*-AAA FtsH homologs, which are exposed to the intermembrane space. The third homolog, *Pf*FtsH1 (PF3D7_1239700), has two transmembrane domains and clusters with *m*-AAA FtsH homologs at the IMM that are exposed to the mitochondrial matrix. *Pf*FtsH1 forms oligomeric complexes and has a punctate distribution on the mitochondrial branching points in late trophozoite and early schizont stages[36], which is similar to STOML distribution in these stages. Contradictory, another study showed that actinonin, a small molecule inhibitor, targets *Pf*FtsH1 and disrupts apicoplast biogenesis[47] and its homolog in *T. gondii* is also localized to the apicoplast[48]. Expression of *Pf*FtsH1 in *E. coli* causes defective cytokinesis, implying a potential role in organelle division. Unfortunately, Amberg-Johnsen and colleagues were unable to generate endogenously tagged knockdown parasite lines of the two *i*-AAA proteases[47]. Therefore, the exact function and substrates of FtsH in *P. falciparum* remains to be elucidated.

The interaction between STOML and PfFtsH is well-supported by evidence. Their respective human homologs, SLP2 and Yme1L, form the SPY complex[21], which is essential for the proteolytic regulation of proteins involved in mitochondrial dynamics and quality control. Yme1L also contributes to OPA1 cleavage, a mitochondrial GTPase which is involved in mitochondrial fusion and cristae formation[49,50], however, no *Plasmodium* OPA1 homolog has been identified to date. In *Trypanosoma brucei*, *Tb*SLP2 forms a large mitochondrial complex with *Tb*Yme1, which is involved in mitochondrial stress resistance[39]. Also in filamentous fungus *Neurospora crassa*, STOML2 has been found in a large complex with an *i*-AAA protease (IAP1)[51]. Furthermore, other SPFH family members are known to form large complexes with AAA+ proteases, such prohibitins with Yta10/Yta12 in yeast[8] or HflK/C with FtsH in bacteria[18]. Characterization of the HflK/C-FtsH supercomplex structure showed that HflK/C forms a 24-heteromer vault structure around four hexameric FtsH complexes at the bacterial membrane[52] (Figure 5E). Here, we show that the *Pf*STOML AlphaFold predicted structure shows high similarity with that of bacterial HflK/C. Our AlphaFold multimer predictions indicate it is likely that *Pf*STOML forms a 22-multimer barrel structure that is highly similar to the vault structure of HflK/C-FtsH supercomplex in bacteria. Although these predictions are based on modelling and therefore need to be interpreted with caution, the

high structural similarity of the *Pf*STOML 22-multimer complex with HflK/C-FtsH supercomplex, combined with our co-immunoprecipitation data, suggests that *Pf*STOML might form a similar supercomplex structure with *Pf*FtsH, possibly regulating *Pf*FtsH accessibility.

Taken together, we have demonstrated that KO of *PfSTOML* causes a significant delayed ABS development, while gametocytes develop normally. *Pf*STOML has a punctate distribution to mitochondrial branching points and endings of mitochondrial branches, but knockout of *PfSTOML* does not affect mitochondrial morphology. Knockout of *PfSTOML* did not affect sensitivity to drugs targeting the respiratory chain, suggesting that *Pf*STOML is not directly involved in respiratory chain assembly. *Pf*STOML resides in a large supercomplex with *Pf*FtsH, likely forming a large, multimeric barrel structure that regulates the accessibility of *Pf*FtsH, similar to its bacterial family members. Although the exact function of the STOML-FtsH complex in *P. falciparum* remains to be elucidated, these results could pave the way for future studies into this highly conserved protein family and their role in proteolytic processes and membrane organization.

Materials and Methods

P. falciparum culture and transfections

P. falciparum NF54 and mutant parasites lines were cultured in RPMI1640 medium supplemented with 25 mM HEPES, 10% human type A serum (Sanquin, The Netherlands) and 25 mM $NaHCO_3$ (complete medium). Parasites were cultured in 5% human RBCs type O (Sanquin, The Netherlands) at 37°C with 3% O_2 and 4% CO_2. For transfection, 60 µg of HDR plasmid was linearized by overnight digestion, precipitated, and transfected with 60 µg Cas9 plasmid using either RBC loading or ring transfection[53]. For RBC loading, plasmids were loaded into RBCs by electroporation (310 V, 950 µF) and a trophozoite parasite culture was added to the transfected RBCs. One day after transfection, parasites were treated with 2.5 nM WR99210 (Jacobus Pharmaceutical) for five days. For ring transfection, a ring-stage sorbitol synchronized parasite culture was transfected with the plasmids by electroporation (310 V, 950 µF). Five hours after transfection, parasites were treated with 2.5 nM WR99210 for five days. Success of transfection was assessed by diagnostic PCR (Figure S1). Gametocyte cultures were maintained in a semi-automatic culturing system with media changes twice a day[54]. Gametocytes were stress-induced through asexual overgrowing. A mixed asexual culture of 1% was set up and cultured for up to 2 weeks.

Plasmid constructs

To generate *STOML* KO repair plasmid, pGK plasmid was used, which contains a pBAT backbone with H2B promotor, GFP and PBANKA_142660 bidirectional 3'UTR, flanked by multiple cloning sites. 5' and 3' Homology Regions (HRs) were amplified and cloned into pGK sequentially, using XmaI + XhoI and NcoI + EcoRI restriction sites respectively, generating pRF0038 *STOML* KO repair plasmid. CRISPR-Cas9 guide plasmids targeting two different sites in *STOML* were generated. Guide oligonucleotides were annealed and cloned into pMLB626 plasmid (a kind gift from Marcus Lee) using BbsI restriction enzyme, generating the pRF0039 and pRF0040 final guide plasmids (Table S1).

To generate *STOML* tagging repair plasmid, pRF0079 empty tagging plasmid was used, containing 3HA-NG-GlmS, PBANKA_142660 bidirectional 3'UTR, and the mito-mScarlet mitochondrial marker[26]. 5' HR was generated by overlap PCR, harboring a shield mutation that prevents cutting of CRISPR-Cas9 when the construct is integrated. 5' and 3' HRs were cloned into pRF0079 using KpnI + BamHI and EcoRI + NgoMIV restriction enzymes respectively, generating pRF0166 *STOML* tagging plasmid. Because this plasmid was unsuccessful in generating mutant parasite line after three transfection attempts, we decided to clone the *DHFR* selection marker in the repair plasmid and remove it from the guide plasmid. By addition of WR after transfection, we will then directly select for parasites with integration of the *DHFR* cassette, instead of selection on the guide plasmid. The *DHFR* cassette was removed from pRF0040 guide plasmid by digestion with EcoRI and ApaI, followed by blunt end generation with DNA polymerase I (klenow), following manufacturer's instructions, and ligation. The new guide plasmid without *DHFR* was termed pRF0210. The *DHFR* cassette cloned from MLB626 plasmid into pRF0166 with SphI and EcoRI restriction enzymes, generating pRF0213 3HA-NG-GlmS tagging plasmid with mito-mScarlet and *DHFR* selection marker. Since a big fluorescent tag might interfere with protein function, we also generated a *STOML* tagging repair plasmid by removing mNG from pRF0213, generating pRF0266 3HA-GlmS tagging plasmid, using BamHI and NheI restriction enzymes.

For generation of the repair plasmids for cyto-mScarlet and cyto-mNG parasite lines (used for the competition growth assay), SIL7 reporter plasmid (pRF0057) was used[26]. *mScarlet* gene was amplified from p1.2RhopH3-HA-mScarlet (a kind gift from Prof. Alan Cowman) (Table S1) and cloned into pRF0057 using AfeI and NheI restriction enzymes, generating pRF0278 cyto-mScarlet repair plasmid. *mNeonGreen* was amplified from pRF0079 plasmid and cloned into pRF0278 with AflII and NheI restriction sites to generate pRF0290, the cyto-mNG repair plasmid. CRISPR-Cas9 guide plasmids targeting SIL7 were used[26]. All enzymes used were obtained via New England Biolabs.

Competition growth assay

For the competition growth assay, parasite lines harboring a cytosolic mScarlet or cytosolic mNG were generated by integration of cyto-mScarlet and cyto-mNG constructs in SIL7 integration site[26]. Cyto-mScarlet, Cyto-mNG, *stoml*$^{-}$ and *stoml*$^{-}_{mito}$ were synchronized by a 63% Percoll centrifugation. Late-stage parasites were isolated from the Percoll gradient and added to fresh RBCs. Four hours later, 5% sorbitol synchronization was performed, which allowed only young rings that just invaded a new RBC to survive. Ring-stage parasites were counted and diluted to each have 0.4% final parasitemia in Cyto-mScarlet + Cyto-mNG, Cyto-mScarlet + *stoml*$^{-}$, and Cyto-mScarlet + *stoml*$^{-}_{mito}$ mixed cultures. Samples for flow cytometry analysis were taken directly after set-up, at day 7 and at day 14. Samples from each mixed culture were taken and stained with 0.5 µg/ml Hoechst 33342 (Invitrogen, H3570) for 30 min at 37°C. Samples were directly analyzed on BD FACSAria™ III Cell Sorter and number of red and green parasites were counted. Data was analyzed in FlowJo (version 10.10).

Growth assay

For this growth assay, MitoRed (WT), *stoml*$^{-}$, and *stoml*$^{-}_{mito}$ parasites were synchronized by a 63% Percoll centrifugation. Late-stage parasites were isolated from the Percoll gradient and added to fresh RBCs. Four hours later, 5% sorbitol synchronization was performed, which allowed only young rings that just invaded a new RBC to survive. Ring-stage parasites were counted and diluted to 0.05% parasitemia. Samples for flow cytometry analysis and fluorescent microscopy were taken directly after setup (t=0), and then every 8, 16 or 24 h over a period of 8 days. To prevent overgrowth, parasite cultures were cut back 1/100 on day 3, and 1/50 on day 6. For flow cytometry, samples were taken and fixed in 0.25% glutaraldehyde. All samples from different time points were processed at the same time, by staining with Hoechst 33342 for 30 min at 37°C and then analyzed by flow cytometry (Beckman Coulter Cytoflex) to determine parasitemia using the 405 nm laser. Data was analyzed in FlowJo (version 10.10). Final parasitemia was adjusted for the dilution factor, explaining why final parasitemia can reach more than 100%. For fluorescent microscopy, parasite samples were processed as described in "fixed imaging" paragraph below.

Live imaging

Stoml-NG parasites were stained with Hoechst 33342 for 30 min at 37°C and settled in an 8-well imaging chamber (Ibidi) in complete media without phenol red. Parasites were imaged on a Zeiss LSM880 or LSM900 Airyscan microscope with 63x oil objective and 37°C heated stage, using 405, 488, and 561 nm excitation lasers. Images were Airyscan processed before analysis with FIJI software.

Fixed imaging

Fluorescent microscopy was performed on asexual and sexual blood-stage *stoml*$^{-}_{mito}$ parasites, using the same fixation and staining protocols. Parasites were settled on a poly-L-lysine coated coverslip for 20 min at 37°C. Parasites were fixed (4% EM-grade paraformaldehyde, 0.0075% EM-grade glutaraldehyde in PBS) for 20 min and permeabilized with 0.1% Triton X-100 for 10 min. DNA was visualized by staining with 1 µM DAPI in PBS for 1 h. PBS washes were performed between different steps. Parasites were mounted with Vectashield (Vector Laboratories). Samples were imaged with Zeiss LSM880 or LSM900 Airyscan microscope with 63x oil objective and 405, 488, and 561 nm excitation lasers. Images were Airyscan processed before analysis with FIJI software.

Co-immunoprecipitation assay

StomI-HA and *stomI-NG* parasites were synchronized with 5% sorbitol and harvested 22 h later to obtain late-stage parasites. Parasites were treated with 0.06% saponin, snap-frozen in liquid nitrogen, and stored at -80°C until further processed. Nitrogen cavitation was used for cell disruption as described[33]. On the day of the experiment, 18 pellets of 30-ml cultures per parasite line were resuspended and pooled in 25 ml ice-cold MESH-buffer (250 mM sucrose, 10 mM HEPES, 1 mM EDTA, 1× cOmplete™ EDTA-free Protease Inhibitor Cocktail (Sigma), pH 7.4). The sample was added to the pre-chilled cell disruption vessel (#4639 Parr Instrument Company) and pressurized with nitrogen gas at 1500 psi for 45 min on ice. The parasites were then sheared through slow release. The organelle-enriched fraction was obtained by differential centrifugation as described[33]. Protein concentrations were determined by Pierce™ BCA Protein Assay Kit (Thermo Scientific). Samples were solubilized with n-dodecyl-β-D-maltoside (DDM) (Sigma), using 3:1 detergent:protein (w/w) ratios. Solubilized samples were spun down at 22,000 x g at 4°C. Supernatant derived from *stomI-NG* samples were applied on ChromoTek mNeonGreen-Trap magnetic agarose beads (ChromoTek), or empty control agarose beads (ChromoTek). Supernatant from *stomI-HA* samples were applied on Pierce™ HA-tag magnetic beads (Thermofisher) or empty protein G control beads (Thermofisher). Beads were incubated at 4°C for 30 minutes with gentle agitation and then washed twice with washing buffer (PBS, 1mM EDTA, 1× cOmplete™ EDTA-free Protease Inhibitor Cocktail, 0.05% DDM) and three times with ice-cold PBS, using a magnetic stand. After washes, on bead digestion was performed as follows: beads were resuspended in 50 µl elution buffer (2M urea, 100 mM Tris-HCl pH 8.0, 10 mM DTT) and incubated for 20 minutes at 25°C while shaking. To alkylate cysteines, iodoacetamide was added to a final concentration of 50 mM. Samples were kept in the dark for 10 min at 25°C. Subsequently, 0.25 µg of sequencing grade tryspin (Promega) was added to digest

the proteins. The samples were shaken at 25°C for 2 h. The supernatants, containing the partially digested proteins, were collected and 50 µl of fresh elution buffer was added to the beads and shaken for another 5 min. Next, these supernatants were collected and combined with the first supernatant. Another 0.1 µg of trypsin was added, to stimulate overnight digestion at 25°C. The next day, samples were concentrated and purified on C18 stagetips[55]. Samples were analyzed on a Thermo Exploris 480 mass spectrometer, operated with an online Easy-nLC 1000. A gradient of buffer B (80% acetonitrile, 0.1% formic acid) was applied for 60 min. The mass spectrometer was ran in Top20 mode, while dynamic exclusion was enabled for 45 sec. Raw data was analyzed using Maxquant version 1.6.6.0[56] with a *Plasmodium* database (strain 3D7, version August 5th 2022, obtained from plasmodb.org[57]). LFQ, iBAQ and match between runs were enabled, and deamidation (NQ) was added as additional variable modification. The output was filtered using Perseus 1.5.0.15[58]. Proteins marked as potential contaminants, reverse hits, and proteins with less than 2 peptides were removed. Samples were grouped into triplicates, and proteins with less than 3 valid values in at least 1 group were removed, after which missing values were imputed using the default settings. A t-test was performed to identify specific outliers. Data was visualized using R.

Drug sensitivity assay

NF54 and *stoml*$^{-}$ parasites were used in a replication assay as described[59] to determine sensitivity to anti-malarial compounds. Briefly, parasites were diluted to 0.83% parasitemia and 3% hematocrit. Thirty microliters of diluted parasites were combined with 30 µl of compound serially diluted in dimethyl sulfoxide (DMSO) and RPMI 1640 medium to reach a final DMSO concentration of 0.1% in a total assay volume of 60 µl. Parasites were incubated at 37°C for 72 hours with mixed gas (3% O_2 and 4% CO_2). Then 30 µl of lysis buffer containing 1:15,000 SYBR Green reagent (Life Technologies), 13.3 mM Tris-HCl, 3.3 mM EDTA, 0.067% TritonX-100 and 0.0053% saponin was added and fluorescence intensity was quantified using BioTek Synergy 2 plate reader. GraphPad Prism was used for data analysis and inhibitory dose-response curves were determined with a variable slope model, in which the curve is generated with the following formula: $y = Bottom + (Top - Bottom)/(1 + 10^{(logIC50-x)*Hillslope})$.

AlphaFold structure predictions

AlphaFold multimer[41] predictions were performed using the COSMIC[2] platform (https://cosmic-cryoem.org/tools/alphafoldmultimer/). All (predicted) protein and protein complex structures and alignments were visualized using PyMOL Molecular Graphics System (version 2.5.2. Schrödinger, LLC).

Acknowledgements

We are very grateful to Prof. Akhil Vaidya for the insightful discussions. We would like to thank all members of the molecular & cellular parasitology team at Radboudumc for the insightful discussions. We would like to thank the Radboud Technology Center Microscopy for use of their microscopy facilities. We are grateful to Michiel Vermeulen and his team for providing the mass spectrometry facility and to Dick Zijlmans for proofreading the manuscript. We also thank the Radboud Technology Center Flowcytometry for the use of their flowcytometry facilities. We are grateful to Koen Dechering and Tonnie Huijs for their support with the drug sensitivity assays. We thank Marcus Lee for providing the pMLB626 CRISPR/Cas9 guide plasmid. J.M.J.V. is supported by an individual Radboudumc Master-PhD grant. A.B.V. is supported by an NIH grant (R01 AI028398).

References

1. WHO. *World malaria report 2023*. (2023).
2. Lamb, I. M., Okoye, I. C., Mather, M. W. & Vaidya, A. B. Unique Properties of Apicomplexan Mitochondria. *Annu. Rev. Microbiol.* **77**, 541–560 (2023).
3. Goodman, C. D., Buchanan, H. D. & McFadden, G. I. Is the mitochondrion a good malaria drug target? *Trends Parasitol.* **33**, 185–193 (2017).
4. Laude, A. J. & Prior, I. A. Plasma membrane microdomains: Organization, function and trafficking (Review). *Mol. Membr. Biol.* **21**, 193–205 (2004).
5. Whitelegge, J. Up close with membrane lipid-protein complexes. *Science (80-.).* **334**, 320–321 (2011).
6. Browman, D. T., Hoegg, M. B. & Robbins, S. M. The SPFH domain-containing proteins: more than lipid raft markers. *Trends Cell Biol.* **17**, 394–402 (2007).
7. Tavernarakis, N., Driscoll, M. & Kyrpides, N. C. The SPFH domain: Implicated in regulating targeted protein turnover in stomatins and other membrane-associated proteins. *Trends Biochem. Sci.* **24**, 425–427 (1999).
8. Steglich, G., Neupert, W. & Langer, T. Prohibitins regulate membrane protein degradation by the m-AAA protease in mitochondria. *Mol. Cell. Biol.* **19**, 3435–3442 (1999).
9. Merkwirth, C. & Langer, T. Prohibitin function within mitochondria: Essential roles for cell proliferation and cristae morphogenesis. *Biochim. Biophys. Acta - Mol. Cell Res.* **1793**, 27–32 (2009).
10. Oyang, L. *et al.* The function of prohibitins in mitochondria and the clinical potentials. *Cancer Cell Int.* **22**, 1–10 (2022).
11. Merkwirth, C. *et al.* Prohibitins control cell proliferation and apoptosis by regulating OPA1-dependent cristae morphogenesis in mitochondria. *Genes Dev.* **22**, 476–488 (2008).
12. Da Cruz, S. *et al.* SLP-2 interacts with prohibitins in the mitochondrial inner membrane and contributes to their stability. *Biochim. Biophys. Acta - Mol. Cell Res.* **1783**, 904–911 (2008).
13. Christie, D. A. *et al.* Stomatin-Like Protein 2 Binds Cardiolipin and Regulates Mitochondrial Biogenesis and Function. *Mol. Cell. Biol.* **31**, 3845–3856 (2011).
14. Mitsopoulos, P. *et al.* Stomatin-Like Protein 2 Is Required for In Vivo Mitochondrial Respiratory Chain Supercomplex Formation and Optimal Cell Function. *Mol. Cell. Biol.* **35**, 1838–1847 (2015).
15. Nijtmans, L. G. J. *et al.* Prohibitins act as a membrane-bound chaperone for the stabilization of mitochondrial proteins. *EMBO J.* **19**, 2444–2451 (2000).
16. He, J. *et al.* Mitochondrial nucleoid interacting proteins support mitochondrial protein synthesis. *Nucleic Acids Res.* **40**, 6109–6121 (2012).
17. Mitsopoulos, P. *et al.* Stomatin-like protein 2 deficiency results in impaired mitochondrial translation. *PLoS One* **12**, 1–13 (2017).
18. Kihara, A., Akiyama, Y. & Ito, K. A protease complex in the Escherichia coli plasma membrane: HflKC (HflA) forms a complex with FtsH (HflB), regulating its proteolytic activity against SecY. *EMBO J.* **15**, 6122–6131 (1996).
19. Ma, C. *et al.* Structural insights into the membrane microdomain organization by SPFH family proteins. *Cell Res.* **32**, 176–189 (2022).
20. Osman, C., Merkwirth, C. & Langer, T. Prohibitins and the functional compartmentalization of mitochondrial membranes. *J. Cell Sci.* **122**, 3823–3830 (2009).
21. Wai, T. *et al.* The membrane scaffold SLP2 anchors a proteolytic hub in mitochondria containing PARL and the i -AAA protease YME1L. *EMBO Rep.* **17**, 1844–1856 (2016).

22. Matz, J. M., Goosmann, C., Matuschewski, K. & Kooij, T. W. A. An Unusual Prohibitin Regulates Malaria Parasite Mitochondrial Membrane Potential. *Cell Rep.* **23**, 756–767 (2018).
23. Artal-Sanz, M. & Tavernarakis, N. Prohibitin and mitochondrial biology. *Trends Endocrinol. Metab.* **20**, 394–401 (2009).
24. Esveld, S. L. Van *et al.* A Prioritized and Validated Resource of Mitochondrial Proteins in Plasmodium Identifies Unique Biology. *mSphere* **6**, e00614-21 (2021).
25. Saini, M. *et al.* Characterization of Plasmodium falciparum prohibitins as novel targets to block infection in humans by impairing the growth and transmission of the parasite. *Biochem. Pharmacol.* **212**, 115567 (2023).
26. Verhoef, J. M. J. *et al.* Detailing organelle division and segregation in Plasmodium falciparum *bioRxiv* 2024.01.30.577899 (2024).
27. Matz, J. M. *et al.* The Plasmodium berghei translocon of exported proteins reveals spatiotemporal dynamics of tubular extensions. *Sci. Rep.* **5**, 1–14 (2015).
28. Gehl, B. & Sweetlove, L. J. Mitochondrial Band-7 family proteins: Scaffolds for respiratory chain assembly? *Front. Plant Sci.* **5**, 1–6 (2014).
29. Heredia, M. Y. & Rauceo, J. M. The spfh protein superfamily in fungi: Impact on mitochondrial function and implications in virulence. *Microorganisms* **9**, (2021).
30. Tondera, D. *et al.* SIP-2 is required for stress-induced mitochondrial hyperfusion. *EMBO J.* **28**, 1589–1600 (2009).
31. Painter, H. J., Morrisey, J. M., Mather, M. W. & Vaidya, A. B. Specific role of mitochondrial electron transport in blood-stage Plasmodium falciparum. *Nature* **446**, 88–91 (2007).
32. MacRae, J. I. *et al.* Mitochondrial metabolism of sexual and asexual blood stages of the malaria parasite Plasmodium falciparum. *BMC Biol.* **11**, (2013).
33. Evers, F. *et al.* Composition and stage dynamics of mitochondrial complexes in Plasmodium falciparum. *Nat. Commun.* **12**, 3820 (2021).
34. Zhang, M. *et al.* Uncovering the essential genes of the human malaria parasite Plasmodium falciparum by saturation mutagenesis. *Science* **360**, eaap7847 (2018).
35. Toenhake, C. G. *et al.* Chromatin Accessibility-Based Characterization of the Gene Regulatory Network Underlying Plasmodium falciparum Blood-Stage Development. *Cell Host Microbe* **23**, 557-569.e9 (2018).
36. Tanveer, A. *et al.* An FtsH protease is recruited to the mitochondrion of Plasmodium falciparum. *PLoS One* **8**, e74408 (2013).
37. Merkwirth, C. & Langer, T. Prohibitin function within mitochondria: essential roles for cell proliferation and cristae morphogenesis. *Biochim. Biophys. Acta* **1793**, 27–32 (2009).
38. Shi, H., Rampello, A. J. & Glynn, S. E. Engineered AAA+ proteases reveal principles of proteolysis at the mitochondrial inner membrane. *Nat. Commun.* **7**, 1–12 (2016).
39. Serricchio, M. & Bütikofer, P. A Conserved Mitochondrial Chaperone-Protease Complex Involved in Protein Homeostasis. *Front. Mol. Biosci.* **8**, 767088 (2021).
40. Jumper, J. *et al.* Highly accurate protein structure prediction with AlphaFold. *Nature* **596**, 583–589 (2021).
41. Evans, R. *et al.* Protein complex prediction with AlphaFold-Multimer. *BioRxiv* (2022) doi:10.1101/2021.10.04.463034v1.

42. Sparkes, P. C. *et al.* Mitochondrial ATP synthesis is essential for efficient gametogenesis in Plasmodium falciparum. *bioRxiv* (2024).
43. Boucher, M. J. *et al.* Integrative proteomics and bioinformatic prediction enable a high-confidence apicoplast proteome in malaria parasites. *PLoS Biol.* **16**, 1–29 (2018).
44. Nguyen, T. T. & Voeltz, G. K. An ER phospholipid hydrolase drives ER-associated mitochondrial constriction for fission and fusion. *Elife* **11**, 1–30 (2022).
45. Leonhard, K. *et al.* Membrane protein degradation by AAA proteases in mitochondria: Extraction of substrates from either membrane surface. *Mol. Cell* **5**, 629–638 (2000).
46. Gerdes, F., Tatsuta, T. & Langer, T. Mitochondrial AAA proteases - Towards a molecular understanding of membrane-bound proteolytic machines. *Biochim. Biophys. Acta - Mol. Cell Res.* **1823**, 49–55 (2012).
47. Amberg-Johnson, K. *et al.* Small molecule inhibition of apicomplexan FtsH1 disrupts plastid biogenesis in human pathogens. *Elife* **6**, (2017).
48. Karnataki, A., Derocher, A. E., Coppens, I., Feagin, J. E. & Parsons, M. A membrane protease is targeted to the relict plastid of toxoplasma via an internal signal sequence. *Traffic* **8**, 1543–1553 (2007).
49. Song, Z., Chen, H., Fiket, M., Alexander, C. & Chan, D. C. OPA1 processing controls mitochondrial fusion and is regulated by mRNA splicing, membrane potential, and Yme1L. *J. Cell Biol.* **178**, 749–755 (2007).
50. Guillery, O. *et al.* Metalloprotease-mediated OPA1 processing is modulated by the mitochondrial membrane potential. *Biol. Cell* **100**, 315–325 (2008).
51. Marques, I., Dencher, N. A., Videira, A. & Krause, F. Supramolecular organization of the respiratory chain in Neurospora crassa mitochondria. *Eukaryot. Cell* **6**, 2391–2405 (2007).
52. Ma, C. *et al.* Structural insights into the membrane microdomain organization by SPFH family proteins. *Cell Res.* **32**, 176–189 (2022).
53. Deitsch, K. W., Driskill, C. L. & Wellems, T. E. Transformation of malaria parasites by the spontaneous uptake and expression of DNA from human erythrocytes. *Nucleic Acids Res.* **29**, 850–853 (2001).
54. Ponnudurai, T., Lensen, A. H. W., Meis, J. F. G. M. & Meuwissen, J. H. E. Synchronization of Plasmodium falciparum gametocytes using an automated suspension culture system. *Parasitology* **93**, 263–274 (1986).
55. Rappsilber, J., Ishihama, Y. & Mann, M. Stop And Go Extraction tips for matrix-assisted laser desorption/ionization, nanoelectrospray, and LC/MS sample pretreatment in proteomics. *Anal. Chem.* **75**, 663–670 (2003).
56. Cox, J. & Mann, M. MaxQuant enables high peptide identification rates, individualized p.p.b.-range mass accuracies and proteome-wide protein quantification. *Nat. Biotechnol.* **26**, 1367–1372 (2008).
57. PlasmoDB: An integrative database of the Plasmodium falciparum genome. Tools for accessing and analyzing finished and unfinished sequence data. The Plasmodium Genome Database Collaborative. *Nucleic Acids Res.* **29**, 66–69 (2001).
58. Tyanova, S. *et al.* The Perseus computational platform for comprehensive analysis of (prote)omics data. *Nat. Methods* **13**, 731–740 (2016).
59. Schalkwijk, J. *et al.* Antimalarial pantothenamide metabolites target acetyl-coenzyme A biosynthesis in Plasmodium falciparum. *Sci. Transl. Med.* **11**, (2019).

Supplemental information

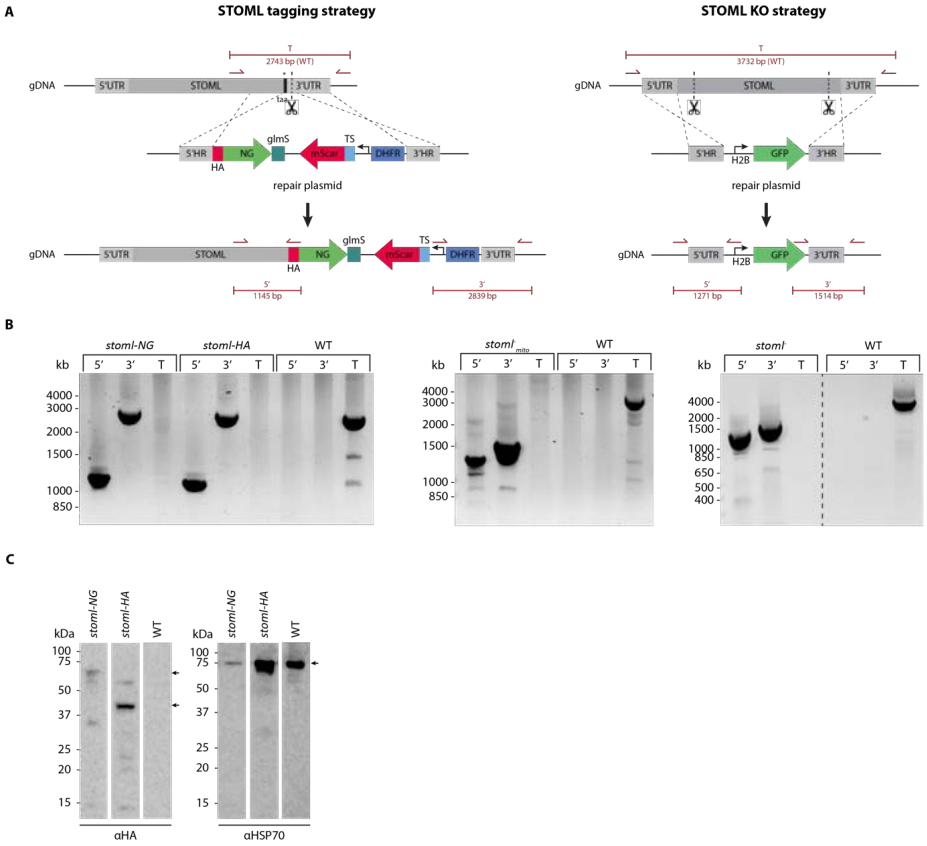

Figure S1. Generation of STOML tagging and KO parasite lines. A) Schematic overview of STOML tagging and KO strategy. For tagging of STOML with 3HA-NG-glmS or 3HA-glmS, CRISPR-Cas9 (indicated by scissors) is used to introduce a double-strand break to facilitate integration of the linear repair constructs 3HA(-NG)-glmS tag directly after STOML before the stop codon, while at the same time integrating a mito-mScarlet mitochondrial marker and a DHFR drug selection cassette. For STOML KO, two CRISPR-Cas9 introduced DNA breaks at the 5′ and 3′ of the gene will be repaired by the linearized HDR plasmid. After integration, STOML will be replaced by GFP under the control of the H2B promotor. B) Diagnostic PCR of stoml-NG, stoml-HA and stoml$^{-}_{(mito)}$ parasite lines with integration specific primer combinations (indicated in panel A), demonstrating successful 5′ and 3′ integration and the absence of WT parasites (T=total). C) Western blot analysis showing expression of STOML-3HA-NG (73 kDa) and STOML-3HA (46.6 kDa) at expected sizes using anti-HA antibody and anti-HSP70 for loading control.

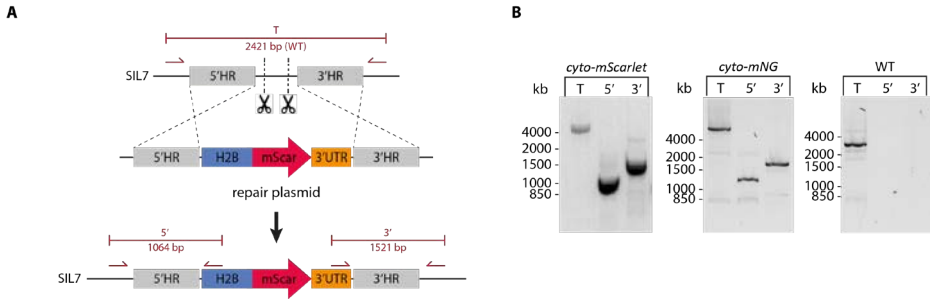

Figure S2. Generation of cyto-mScarlet and cyto-mNG parasite lines. A) Schematic overview of transfection strategy. CRISPR-Cas9 and two guides were used to generate double stranded breaks in a silent intergenic locus (SIL7), characterized in Verhoef et al.[1] (indicated by scissors). DNA breaks are repaired by double homologous recombination with a repair plasmid containing 5′ and 3′ homology regions (HRs) and mScarlet under the control of the H2B promotor and PBANKA_142660 bidirectional 3′UTR. B) Diagnostic PCR of cyto-mScarlet and cyto-mNG parasite lines with integration-specific primer combinations (indicated in panel A), demonstrating successful 5′ and 3′ integration and the absence of WT parasites (T=total).

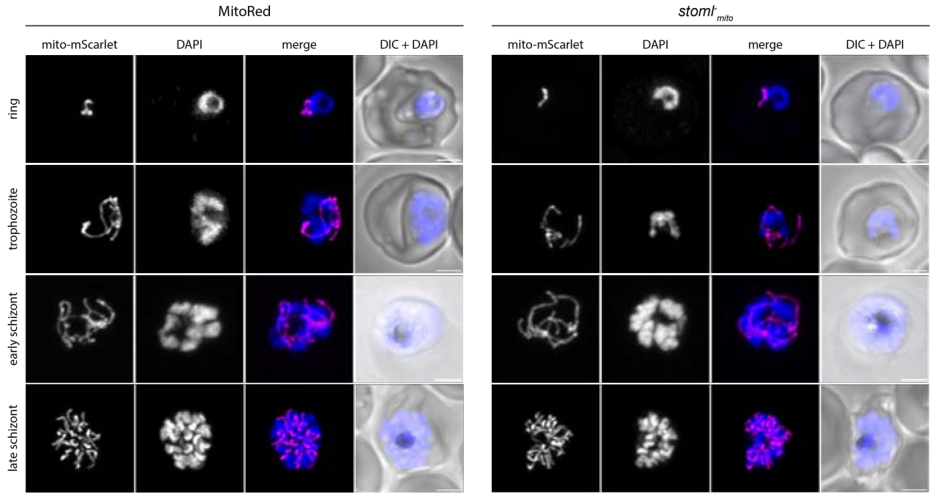

Figure S3. Mitochondrial morphology in stomI$^{-}_{mito}$ ABS parasites. Fluorescent microscopy of stomI$^{-}_{mito}$ and MitoRed (WT) parasites during ring, trophozoite, early and late schizont stages. The mito-mScarlet signal is preserved after fixation and can be observed without antibody staining. DNA was stained using DAPI. Images are maximum intensity projections of Z-stack confocal Airyscan images. Scale bars, 2 µm.

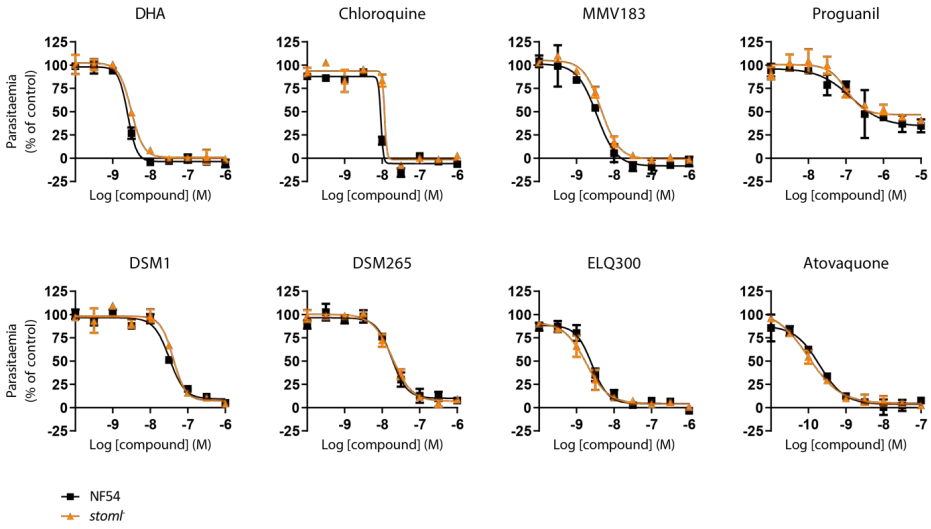

Figure S4. Sensitivity of stoml⁻ parasites to anti-malarial compounds. Drug sensitivity assay for *P. falciparum* NF54 and stoml⁻ parasites. The graphs show average values for mean parasite density relative to controls for asexual blood-stage replication assay and represent one of the two independent replicates. Error bars indicate SEM determined from two technical replicates per experiment. The data were analyzed using nonlinear regression in GraphPad Prism. Proguanil, DSM1, DSM265, ELQ300 and Atovaquone are compounds targeting the parasite mitochondrion, while DHA, chloroquine and MMV183 are non-mitochondrial compounds.

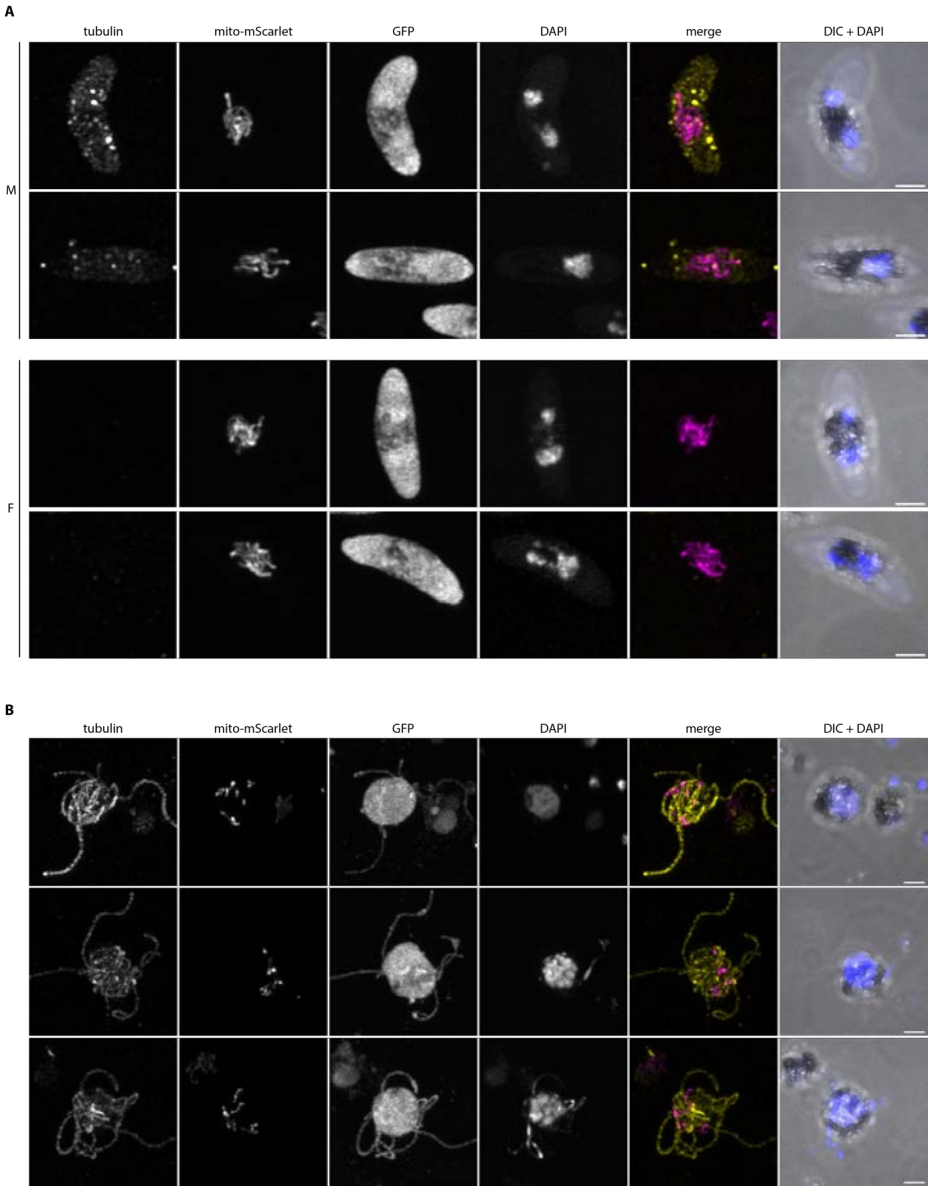

Figure S5. Stoml$^{-}_{mito}$ parasites develop to healthy gametocytes that exflagellate. A) Fluorescent microscopy on male (M) and female (F) stoml$^{-}_{mito}$ stage V gametocytes. Parasites were stained for tubulin (yellow) to distinguish male (high α-tubulin signal) from female (low α-tubulin signal) gametocytes. B) fluorescent microscopy on exflagellating stoml$^{-}_{mito}$ male gametes at 20 minutes after activation. Parasites were stained with tubulin to visualize axonemes. A-B) Visualization of mito-mScarlet mitochondrial marker (magenta), cytosolic GFP, DAPI for DNA visualization (blue) and DIC. Images are maximum intensity projections of Z-stack confocal Airyscan images. Scale bars, 2 µm.

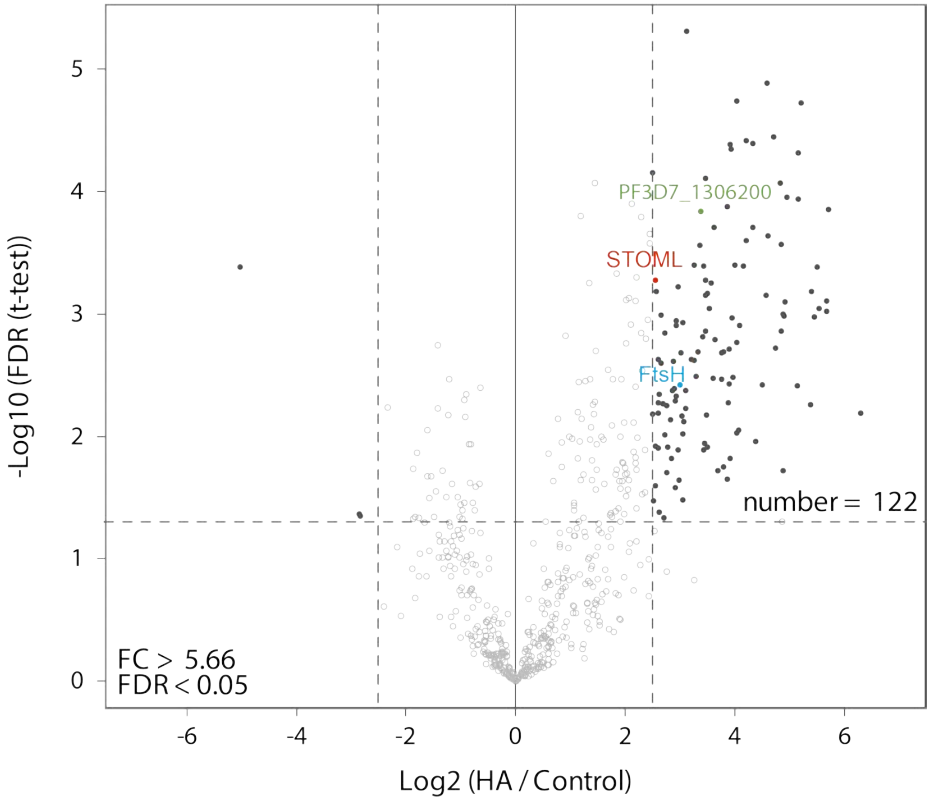

Figure S6. Identification of STOML interacting proteins with co-immunoprecipitation. Immunoprecipitation of STOML-HA containing complexes. The volcano plot showing mean $\log_2$ fold changes (FC) and $-\log_{10}$ false discovery rate (FDR) for anti-HA pulldown in comparison with control pulldown. Horizontal and vertical dotted lines indicate FC > 5.66 and FDR <0.05 respectively. Dark dots represent enriched proteins. The number of proteins enriched in the anti-HA pulldown compared to the control pulldown is indicated on the right.

```
Q96TA2|YMEL1_HUMAN      MFSLSSTVQPQVTVPLSHLINAFHTPKNTSVSLSGVSVSQNQHRDVVPEHEAPSSECMFS      60
Q8IKI9|FtsH_P.F         MLLLRNIV---------------------------ILDLKRSNKLLNINNLPKIACILN      32
                        *: * . *                            :. :: ..::  :: *.  *::.

Q96TA2|YMEL1_HUMAN      DFLTKLNIVSIGKGKIFEGYRSMFMEPAKRMKKSLDTTDNWHIRPEPFSLSIPPSLNLRD     120
Q8IKI9|FtsH_P.F         T-------------------------------------------------------R      34


Q96TA2|YMEL1_HUMAN      LGLSELKIGQIDQLVEN---------LLPGFCKGKNI------SSHWHTSHVSAQS----     161
Q8IKI9|FtsH_P.F         KGFSVLKNERLDRLKREVRNKPNDNFLILQFYKEANVHNPNEVIKHYENANYIKDESITK      94
                        *:* **  ::*:* .:         *:  * *  *:       .*:..::   :.

Q96TA2|YMEL1_HUMAN      ------FFE--NKYGNLDIFSTLRSSCLYRHHSRALQSICSDLQYWPVFIQSRGFKTLKS     213
Q8IKI9|FtsH_P.F         EYIKALVYTNKLKYTNLDNIKYDSDHNMYNK-----------------SMHDTTTNEMHS     137
                              .:    ** *** :.   .  :*.:                  ::.   : ::*

Q96TA2|YMEL1_HUMAN      RTRRLQSTSERLAETQNIAPSFV-KGFLLRDRGSDVESLDKLMKTKNIPEAHQDAFKTGF     272
Q8IKI9|FtsH_P.F         NE-----RSNNIYEGNNVNSENNYNNMSSNHSTHKVEYMDKK------RNQHPEMYSLHI     186
                        .       *:.: * :*:  .   :.:  ..   .** :**        : * : :.  :

Q96TA2|YMEL1_HUMAN      AEGFLKAQALTQKTNDSLRRTRLILFVLLLFGIYGLLKNPF---------------LSVR     317
Q8IKI9|FtsH_P.F         D----PKKPLK-----------VSVIDSNKKGLWNLLKSTIGFLILVAAGSVYMEGVSQN     231
                               : *.           : ::     *::.***. :               :* .

Q96TA2|YMEL1_HUMAN      FRTTTG-LDSAVDPVQMKNVTFEHVKGVEEAKQELQEVVEFLKNPQKFTILGGKLPKGIL     376
Q8IKI9|FtsH_P.F         VQKGIGVSNKKIIPVENVKVTFADVKGCDEVKQELEEIIDYLKNSDKFTKIGAKLPKGIL     291
                        .:.  *  :. : **:  :*** .*** :*.****:*::::*** :*** :*.*******

Q96TA2|YMEL1_HUMAN      LVGPPGTGKTLLARAVAGEADVPFYYASGSEFDEMFVGVGASRIRNLFREAKANAPCVIF     436
Q8IKI9|FtsH_P.F         LSGEPGTGKTLIARAIAGEANVPFLQASGSEFEEMFVGVGARRIRELFQAAKKHAPCIVF     351
                        * * *******:***:****:***  ******:******** ***:**: ** :***::*

Q96TA2|YMEL1_HUMAN      IDELDSVGGKRIESPMHPYSRQTINQLLAEMDGFKPNEGVIIIGATNFPEALDNALIRPG     496
Q8IKI9|FtsH_P.F         IDEIDAVGSKRSSRD-NSAVRMTLNQLLVELDGFEQNEGIVVICATNFPQSLDKALVRPG     410
                        ***:*:**.** .   :   * *:****.*:***: ***:::* *****::**:**:***

Q96TA2|YMEL1_HUMAN      RFDMQVTVPRPDVKGRTEILKWYLNKIKFDQSVDPEIIARGTVGFSGAELENLVNQAALK     556
Q8IKI9|FtsH_P.F         RLDKTIVVPLPDIKGRYEILKMYSNKIVLSKDVDLHVLSRRTVGMTGADLNNILNIAAIK     470
                        *:*  :.** **:*** **** * *** :.:.** .:::* ***::**:*:*::* **:*

Q96TA2|YMEL1_HUMAN      AAVDGKEMVTMKELEFSKDKILMGPERRSVEIDNKNKTITAYHESGHAIIAYYTKDAMPI     616
Q8IKI9|FtsH_P.F         CSVEGKKSVDMNSIEQAFDRVVVGLQRKS-PLNEEEKNITAYHEGGHTLVNFYTKGSDPV     529
                        .:*:**: * *:.:* : *::::* :*:*  :::::*.******.**::: :***.: *:

Q96TA2|YMEL1_HUMAN      NKATIMPRGPTLGHVSLLPENDRWNETRAQLLAQMDVSMGGRVAEELIFGTDHITTGASS     676
Q8IKI9|FtsH_P.F         HKATIMPRGMSLGVTWKIPISDKYSQKIKDVQSEIDILMGGLVSEEIIFGKNNVTTGCSS     589
                        :******** :** .  :* .*::.:.  :: :::*: *** *:**:***.:::***.**

Q96TA2|YMEL1_HUMAN      DFDNATKIAKRMVTKFGMSEKL--GVMTYSDTGKLSPETQSAIEQEIRILLRDSYERAKH     734
Q8IKI9|FtsH_P.F         DLQKATHIAQSLVMNYGVGINEDNISMFLHDKQNISEEMKIKIDKSIQRILLDSYNRAKN     649
                        *:::**:**: :* ::*:. :     *   *. ::* * :  *::.*: :* ***:***:

Q96TA2|YMEL1_HUMAN      ILKTHAKEHKNLAEALLTYETLDAKEIQIVLEGKKLEVR-----------------         773
Q8IKI9|FtsH_P.F         VLNQHIDELHRIASALVEYETLTSDEIKLAMQGKCDQIRKNREIKQKEYNLKDSRIS         706
                        :*: * .* :.:*.**: **** :.**::.::**  ::*
```

Figure S7. Alignment of human Yme1L amino acid sequence with *P. falciparum* FtsH. Amino acid sequence comparison of human Yme1L with P. falciparum FtsH showing 41% identity. Identical residues ("*"), residues with similar properties (":"), residues with weak similarity ("."), and amino acid numbers (on the left) are indicated.

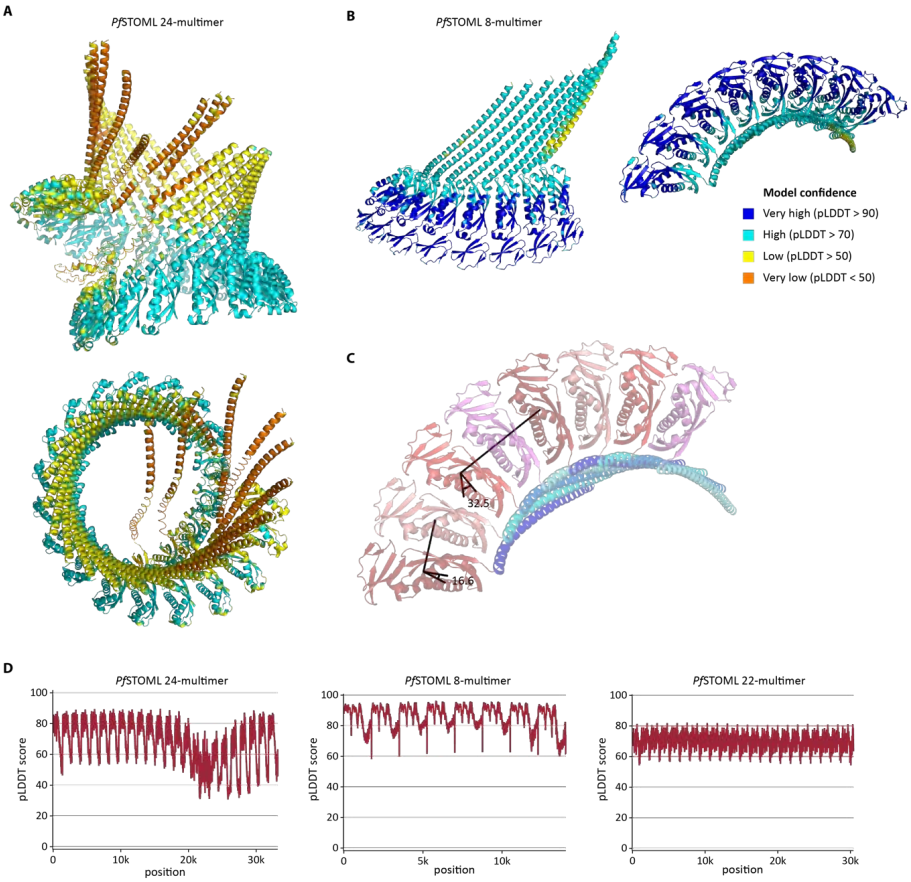

Figure S8. AlphaFold structure prediction of PfSTOML multimers. A) AlphaFold prediction of PfSTOML 24-multimer with side view (top) and top view (bottom). B) AlphaFold prediction of PfSTOML 8-multimer with side view (left) and top view (right). Coloring in A and B represent model confidence as indicated by the color legend in B. C) Top view of predicted PfSTOML 8-multimer structure, indicating the angles measured between SPFH domains of different STOML proteins in the complex. D) graphs with pLDDT scores representing model confidence of predicted PfSTOML 24, 8 and 22 multimer structures.

Table S1. Primer and guide RNA sequences for generation of repair and guide plasmids.

Primer name	Primer function	Sequence	Restriction site
STOML KO repair plasmid			
JV047	STOML KO 5'HR F	AAATATCCCGGGCCTGCTATAGATTAATTGTGTCCC	XmaI
JV048	STOML KO 5'HR R	TAATATCTCGAGGTTCATCTTCTCATGAATTTTTATCAATC	XhoI
JV049	STOML KO 3'HR F	AATATACCATGGGAACAACTAATTTGATTCAAGTTTTGC	NcoI
JV050	STOML KO 3'HR R	ATTAATGAATTCAATATACACAACTTATTTTTTATGTTTTCCC	EcoRI
STOML tagging repair plasmids			
JV084	STOML tag 5'HR F	AATTAAGGTACCGGAACCATTTAGGTTTTGTGATTATACC	KpnI
JV113	STOML tag shield R	CTCTTTCTCCTTCGCTCTGTAAAATTTCAGC	
JV114	STOML tag shield F	GCTGAAATTTTACAGAGCGAAGGAGAAAGAG	
JV085	STOML tag 5'HR R	AATAATGGATCCGTTGTTCATATCAGAATGAATTTGTTTTTG	BamHI
JV027	STOML tag 3'HR F	ATTATTGAATTCATATGAAAACAACTATATTTTTATGAAAGC	EcoRI
JV086	STOML tag 3'HR R	TTAAAAGCCGGCTATAAATTGTACGTGTATTATTCATTACTC	NgoMIV
Cyto-mScarlet and cyto-mNG repair plasmids			
JV064	mScarlet F	AATAAAGCTAGCATGGTGAGCAAGGGCGAGG	NheI
JV072	mScarlet R	AATAATCTTAAGTTACTTGTACAGCTCGTCCATGC	AflII
JV062	mNG F	AATAAAGCTAGCATGGTGAGCAAGGGCGAGGAG	NheI
JV072	mNG R	AATAATCTTAAGTTACTTGTACAGCTCGTCCATGC	AflII
Guide RNA sequences			
JV051	STOML KO G1 F	TATTGATGTATGATACCCTTTAGCT	
JV052	STOML KO G1 R	AAACAGCTAAAGGGTATCATACATC	
JV053	STOML KO/Tag G2 F	TATTGGCTGAAATTTTACAAAGTGA	
JV054	STOML KO/Tag G2 R	AAACTCACTTTGTAAAATTTCAGCC	

Table S1. Continued

Primer name	Primer function	Sequence	Restriction site
Pf0084	SIL7 guide 1 sense	TATTGTATATGTGGTAATAAATAAA	
Pf0085	SIL7 guide 1 antisense	AAACTTTATTTATTACCACATATAC	
Pf0086	SIL7 guide 2 sense	TATTGATTCAATATAATAAGGTCAA	
Pf0087	SIL7 guide 2 antisense	AAACTTGACCTTATTATATTGAATC	
Integration PCRs			
JV108	Int PCR STOML tag 5′F	AATATGGAACCGAGCTAAAGGG	
JV103	Int PCR STOML tag 5′R	CTGGAACATCGTAAGGATACGC	
JV104	Int PCR STOML tag 3′F	ATTATATGTGAAAATTATGGGGCATGC	
JV121	Int PCR STOML tag 3′R	CTCTTTTTTTTCCACTAAAATTATTATAGG	
JV061	Int PCR STOML KO 5′F	TATAGATGTGGATTATTTTACACAATTGAC	
NP50	Int PCR STOML KO 5′R	CTTAATATTGATAAGTATCATGTG	
NP49	Int PCR STOML KO 3′R	CCGAAAAAGTTAAAATTAATTTAC	
JV028	Int PRC STOML KO 3′R	ATATTAGGCGCCTATAAATTGTACGTGTATTATTCATTACTC	
NP50	Int PCR cyto-mScar 3′F	CTTAATATTGATAAGTATCATGTG	
NP298	Int PCR cyto-mScar 3′R	CGTTCATGCTTTCACAAGAAC	
NP297	Int PCR cyto-mScar 5′F	GCTCACCTTAAATGTTCCAC	
NP190	Int PCR cyto-mScar 5′R	AGTCATATCCAGGAATAAACATAC	

Used abbreviations: HR = homology region, F = forward primer, R = reverse primer. Overhang for restriction sites are red, restriction sites are underlined, and gRNA sequences are blue. The same primers are used for the integration PCR of cyto-mScarlet and cyto-mNG.

Table S2. Proteins detected in STOML-3HA-NG pulldown.

Gene ID	Annotation	Unique peptide counts	Log t-test p value	t-test difference	Mito score
PF3D7_0318100	stomatin-like protein, putative	23	4.85	7.91	11.36
PF3D7_1427300	conserved Plasmodium protein, unknown function	40	3.44	7.35	-1.62
PF3D7_1412100	mini-chromosome maintenance complex-binding protein	28	2.71	6.42	-14.59
PF3D7_0209300	2C-methyl-D-erythritol 2,4-cyclodiphosphate synthase	9	2.05	5.74	-8.09
PF3D7_0525100	acyl-CoA synthetase	69	3.30	5.43	-5.91
PF3D7_1447200	conserved protein, unknown function	13	1.91	5.29	-13.78
PF3D7_1145800	conserved Plasmodium protein, unknown function	12	3.37	4.94	-9.97
PF3D7_1211700	DNA replication licensing factor MCM5, putative	61	3.16	4.78	-7.75
PF3D7_1306200	conserved protein, unknown function	10	2.51	4.72	-8.33
PF3D7_1464900	ATP-dependent zinc metalloprotease FTSH, putative	12	2.96	4.64	2.07
PF3D7_0410900	conserved Plasmodium protein, unknown function	11	3.34	4.64	-9.67
PF3D7_0722100	protein pelota homolog, putative	14	2.73	4.63	-11.38
PF3D7_0805600	phosphatidic acid phosphatase 2	4	2.63	4.40	-7.38
PF3D7_1474600	vacuole membrane protein 1, putative	12	1.84	4.35	-11.69
PF3D7_0807000	YEATS domain-containing protein, putative	4	3.19	4.18	-8.87
PF3D7_1223800	citrate/oxoglutarate carrier protein, putative	8	2.60	4.18	1.32
PF3D7_0303400	palmitoyltransferase DHHC1	9	3.03	4.14	-13.55
PF3D7_0112200	multidrug resistance-associated protein 1	28	1.54	3.99	-8.26
PF3D7_1313800	conserved Plasmodium membrane protein, unknown function	8	2.56	3.96	-5.54
PF3D7_0104800	novel putative transporter 1, putative	11	2.08	3.58	-8.87
PF3D7_1354200	phosphoinositide phosphatase SAC1	11	1.62	3.43	-13.01

Table S2. Continued

Gene ID	Annotation	Unique peptide counts	Log t-test p value	t-test difference	Mito score
PF3D7_1108000	IWS1-like protein, putative	8	2.86	3.41	-12.46
PF3D7_0932800	importin alpha re-exporter, putative	4	2.39	3.37	-12.07
PF3D7_1355300	histone-lysine N-methyltransferase, putative	7	1.63	3.29	-12.74
PF3D7_1305300	translational activator GCN1, putative	28	2.09	3.21	-13.86
PF3D7_0908400	conserved Plasmodium protein, unknown function	4	1.95	3.03	-2.98
PF3D7_1363200	bifunctional polynucleotide phosphatase/kinase	11	1.86	3.01	-8.65

Table S3. Proteins detected in STOML-3HA pulldown.

Gene ID	Annotation	Unique peptide counts	Log t-test p value	t-test difference	Mito score
PF3D7_1451900	ribosome biogenesis protein TSR1, putative	55	2.19	6.29	-13.01
PF3D7_1129400	RNA cytosine C(5)-methyltransferase, putative	26	3.86	5.72	-13.46
PF3D7_1342000	40S ribosomal protein S6	31	3.02	5.67	-11.38
PF3D7_1415800	ribosomal RNA small subunit methyltransferase A1	28	3.11	5.67	-7.10
PF3D7_1108700	heat shock protein J2	33	3.04	5.54	-7.47
PF3D7_0503800	60S ribosomal protein L31	6	3.38	5.50	-7.95
PF3D7_1110400	RNA-binding protein, putative	44	2.98	5.45	-8.86
PF3D7_1354600	60S ribosomal protein L7-2, putative	23	3.18	5.40	-4.33
PF3D7_1021500	ATP-dependent RNA helicase ROK1, putative	31	2.26	5.39	-3.97
PF3D7_1126200	40S ribosomal protein S18, putative	19	4.72	5.22	-5.56
PF3D7_1354300	large subunit rRNA methyltransferase, putative	15	4.31	5.16	-10.57
PF3D7_0513600	deoxyribodipyrimidine photo-lyase, putative	35	3.94	5.16	-2.63
PF3D7_1022600	kelch protein K10	28	2.41	5.14	-10.14
PF3D7_1033300	conserved protein, unknown function	10	3.96	4.95	-4.62
PF3D7_1109400	essential nuclear protein 1, putative	17	3.10	4.92	-9.25
PF3D7_0217800	40S ribosomal protein S26	9	2.98	4.91	-7.47
PF3D7_0522600	magnesium transporter NIPA, putative	7	3.00	4.89	-11.69
PF3D7_1021900	PHAX domain-containing protein, putative	38	1.72	4.88	-5.31
PF3D7_1105400	40S ribosomal protein S4, putative	37	3.57	4.85	-7.90
PF3D7_1020000	RNA-binding protein 34, putative	9	2.86	4.84	-13.50
PF3D7_1476300	Plasmodium exported protein (PHISTb), unknown function	19	4.07	4.84	-6.46

Table S3. Continued

Gene ID	Annotation	Unique peptide counts	Log t-test p value	t-test difference	Mito score
PF3D7_1143400	translation initiation factor eIF-1A, putative	12	2.72	4.74	-7.90
PF3D7_0723900	RNA-binding protein, putative	17	4.44	4.72	-6.42
PF3D7_1007700	AP2 domain transcription factor AP2-I	15	3.64	4.61	-11.47
PF3D7_0510500	topoisomerase I	27	4.89	4.58	-7.79
PF3D7_1466700	60S ribosome subunit biogenesis protein NIP7, putative	10	3.15	4.57	-12.46
PF3D7_0817900	high mobility group protein B2	11	2.42	4.51	-6.30
PF3D7_0615700	THO complex subunit 4, putative	9	1.96	4.38	-6.30
PF3D7_1027300	peroxiredoxin	27	4.39	4.34	-5.21
PF3D7_1113100	protein tyrosine phosphatase	4	3.71	4.33	-5.35
PF3D7_1104200	chromatin remodeling protein	35	4.42	4.22	-7.15
PF3D7_0914600	transcription elongation factor 1, putative	3	3.60	4.21	-6.93
PF3D7_1407100	rRNA 2-O-methyltransferase fibrillarin, putative	25	3.39	4.16	-10.38
PF3D7_1323400	60S ribosomal protein L23	14	2.90	4.09	-6.90
PF3D7_0415500	nuclear cap-binding protein subunit 2, putative	14	2.05	4.08	-10.38
PF3D7_0202000	knob-associated histidine-rich protein	14	2.03	4.04	-4.33
PF3D7_0527900	ATP-dependent RNA helicase DDX41, putative	21	4.74	4.04	-11.70
PF3D7_1248700	conserved protein, unknown function	16	2.77	4.03	-12.75
PF3D7_0709700	prodrug activation and resistance esterase	11	3.40	4.00	-1.98
PF3D7_1225300	rRNA-processing protein FCF1, putative	14	2.48	3.97	-4.93
PF3D7_1216300	signal recognition particle subunit SRP19	9	2.97	3.96	-11.38
PF3D7_1302800	40S ribosomal protein S7, putative	32	4.34	3.93	-3.48

Table S3. Continued

Gene ID	Annotation	Unique peptide counts	Log t-test p value	t-test difference	Mito score
PF3D7_0520000	40S ribosomal protein S9, putative	19	4.39	3.91	-6.90
PF3D7_1460700	60S ribosomal protein L27	13	1.82	3.91	-10.57
PF3D7_0821700	60S ribosomal protein L22, putative	6	2.43	3.90	-3.35
PF3D7_1419000	conserved Plasmodium protein, unknown function	20	2.71	3.89	-4.11
PF3D7_1368200	ABC transporter E family member 1, putative	22	2.28	3.87	-7.75
PF3D7_0707200	conserved Plasmodium protein, unknown function	17	1.65	3.86	-5.74
PF3D7_0504400	ATP-dependent helicase, putative	17	3.88	3.86	-7.20
PF3D7_1317800	40S ribosomal protein S19	9	1.75	3.80	-2.35
PF3D7_1459400	conserved protein, unknown function	15	2.69	3.79	-8.65
PF3D7_1421200	40S ribosomal protein S25	14	2.47	3.77	-9.35
PF3D7_1408600	40S ribosomal protein S8e, putative	19	2.68	3.75	-6.90
PF3D7_0316800	40S ribosomal protein S15A, putative	20	1.72	3.69	-4.48
PF3D7_0930600	peptidyl-prolyl cis-trans isomerase	13	2.79	3.64	-8.65
PF3D7_0111800	eukaryotic translation initiation factor 4E, putative	5	3.71	3.62	-9.03
PF3D7_0519400	40S ribosomal protein S24	17	2.48	3.60	-7.90
PF3D7_1019400	60S ribosomal protein L30e, putative	6	3.25	3.58	-7.47
PF3D7_0721600	40S ribosomal protein S5, putative	23	3.05	3.53	-8.03
PF3D7_0214400	protein LTV1, putative	10	3.17	3.51	-6.06
PF3D7_0422400	40S ribosomal protein S19	24	1.92	3.50	-10.11
PF3D7_1407500	multifunctional methyltransferase subunit TRM112, putative	10	2.17	3.49	-13.62
PF3D7_1033600	pre-mRNA-splicing factor CEF1, putative	9	3.28	3.47	-13.78

Table S3. Continued

Gene ID	Annotation	Unique peptide counts	Log t-test p value	t-test difference	Mito score
PF3D7_0910900	DNA primase large subunit, putative	12	2.86	3.47	-2.10
PF3D7_0617800	histone H2A	10	4.11	3.46	-9.25
PF3D7_0322900	40S ribosomal protein S3A, putative	42	3.16	3.46	-6.90
PF3D7_1346100	protein transport protein SEC61 subunit alpha	7	1.94	3.46	-10.99
PF3D7_1002400	transformer-2 protein homolog beta, putative	15	1.89	3.43	-8.86
PF3D7_1133800	RNA (uracil-5-)methyltransferase, putative	25	3.39	3.43	-12.49
PF3D7_1445900	ATP-dependent RNA helicase DDX17	35	2.81	3.41	-10.57
PF3D7_1306200	conserved protein, unknown function	8	3.84	3.39	-8.33
PF3D7_1149400	Plasmodium exported protein, unknown function	8	3.56	3.37	-5.71
PF3D7_0813900	40S ribosomal protein S16, putative	21	2.69	3.33	-7.90
PF3D7_0522300	18S rRNA (guanine-N(7))-methyltransferase, putative	5	2.49	3.29	-9.13
PF3D7_1225500	small subunit rRNA processing factor, putative	5	3.40	3.25	-4.33
PF3D7_1028300	rRNA-processing protein EBP2, putative	11	2.62	3.25	-11.42
PF3D7_1452700	U1 snRNP-associated protein, putative	15	2.63	3.22	-9.03
PF3D7_1114200	GTPase-activating protein, putative	6	5.31	3.13	-7.30
PF3D7_0218400	ATP-dependent RNA helicase DDX47, putative	17	2.23	3.11	-10.57
PF3D7_1030100	pre-mRNA-splicing factor ATP-dependent RNA helicase PRP22, putative	21	2.37	3.10	-8.20
PF3D7_0813000	protein KIC7	7	2.12	3.06	-11.85
PF3D7_0831400	Plasmodium exported protein, unknown function	11	2.93	3.06	-8.95
PF3D7_1469300	pre-rRNA-processing protein PNO1, putative	13	1.48	3.06	-10.57
PF3D7_1202900	high mobility group protein B1	12	2.02	3.04	-7.95

Table S3. Continued

Gene ID	Annotation	Unique peptide counts	Log t-test p value	t-test difference	Mito score
PF3D7_0818400	rRNA-processing protein FCF1, putative	6	2.17	3.03	-10.57
PF3D7_1317400	zinc finger protein, putative	7	2.68	3.01	-5.18
PF3D7_1464900	ATP-dependent zinc metalloprotease FTSH, putative	13	2.42	3.00	2.07
PF3D7_0802000	glutamate dehydrogenase, putative	39	1.64	2.98	-9.39
PF3D7_1111000	RNA cytosine C(5)-methyltransferase NSUN2	12	3.22	2.97	-9.82
PF3D7_0316700	protein YOP1, putative	6	1.89	2.97	-7.42
PF3D7_0821000	conserved Plasmodium protein, unknown function	6	2.33	2.93	-4.56
PF3D7_0318900	conserved protein, unknown function	9	2.91	2.93	-10.11
PF3D7_0710100	conserved protein, unknown function	9	2.94	2.93	-0.03
PF3D7_0317600	40S ribosomal protein S11, putative	21	2.29	2.92	-6.69
PF3D7_1015300	methionine aminopeptidase 1b, putative	17	1.58	2.91	-14.90
PF3D7_0721300	ATP-dependent DNA helicase DDX31	9	2.39	2.89	-10.57
PF3D7_1242700	40S ribosomal protein S17, putative	17	2.61	2.88	-8.03
PF3D7_1207100	pre-rRNA-processing protein ESF1, putative	13	2.37	2.86	-10.38
PF3D7_1119200	conserved protein, unknown function	9	1.82	2.84	-9.04
PF3D7_0519700	FoP domain-containing protein, putative	19	2.14	2.82	-8.65
PF3D7_1231600	pre-mRNA-splicing factor ATP-dependent RNA helicase PRP2, putative	14	1.91	2.77	-13.78
PF3D7_1004400	RNA-binding protein, putative	27	2.25	2.76	-9.08
PF3D7_1202200	mitochondrial phosphate carrier protein	7	1.70	2.76	6.75
PF3D7_1358800	40S ribosomal protein S15	18	2.85	2.73	-6.90
PF3D7_1033200	early transcribed membrane protein 10.2	7	2.01	2.72	-4.71

Table S3. Continued

Gene ID	Annotation	Unique peptide counts	Log t-test p value	t-test difference	Mito score
PF3D7_0612900	nucleolar GTP-binding protein 1, putative	11	1.34	2.70	-10.57
PF3D7_1331800	60S ribosomal protein L23, putative	13	2.26	2.68	-7.75
PF3D7_1034200	ribosomal protein L27, putative	4	2.60	2.66	0.79
PF3D7_0516200	40S ribosomal protein S11	15	2.99	2.65	-5.08
PF3D7_0903900	60S ribosomal protein L32	13	2.34	2.63	-6.90
PF3D7_0306400	FAD-dependent glycerol-3-phosphate dehydrogenase, putative	27	1.38	2.62	6.33
PF3D7_1461200	U3 small nucleolar ribonucleoprotein protein IMP3, putative	5	2.19	2.61	-9.25
PF3D7_1008800	nucleolar protein 5, putative	16	2.27	2.61	-13.78
PF3D7_0528800	nuclear GTP-binding protein, putative	13	2.63	2.60	-8.65
PF3D7_1315400	zinc finger (CCCH type) protein, putative	6	1.90	2.60	-9.34
PF3D7_1368400	ribosomal protein L1, putative	12	3.18	2.58	-9.97
PF3D7_0318100	stomatin-like protein, putative	6	3.27	2.56	11.36
PF3D7_0503300	serine/arginine-rich splicing factor 12	10	1.92	2.56	-5.97
PF3D7_1345100	thioredoxin 2	8	1.59	2.55	-7.53
PF3D7_0621300	mRNA-binding protein PUF3	12	1.48	2.52	-9.25
PF3D7_0219400	ribosome associated membrane protein RAMP4, putative	8	4.16	2.50	-1.98
PF3D7_0208200	KRR1 small subunit processome component, putative	8	2.19	2.50	-10.25
PF3D7_1215300	10 kDa chaperonin	7	3.38	-5.02	5.62

Movie legends

Movie 1. 3D visualization of STOML-3HA-NG in late ring. 3D visualization of STOML-3HA-NG (green) and mito-mScarlet (magenta) in rings with live confocal Airyscan microscopy, using Arivis 4D vision software. Fluorescent signal is segmented by manual thresholding.

Movie 2. 3D visualization of STOML-3HA-NG in early schizont. 3D visualization of STOML-3HA-NG (green) and mito-mScarlet (magenta) in rings with live confocal Airyscan microscopy, using Arivis 4D vision software. Fluorescent signal is segmented by manual thresholding.

Movie 3. 3D visualization of STOML-3HA-NG in late schizont. 3D visualization of STOML-3HA-NG (green) and mito-mScarlet (magenta) in rings with live confocal Airyscan microscopy, using Arivis 4D vision software. Fluorescent signal is segmented by manual thresholding.

References

1. Verhoef, J. M. J. *et al.* Detailing organelle division and segregation in Plasmodium falciparum; *bioRxiv* 2024.01.30.577899 (2024).

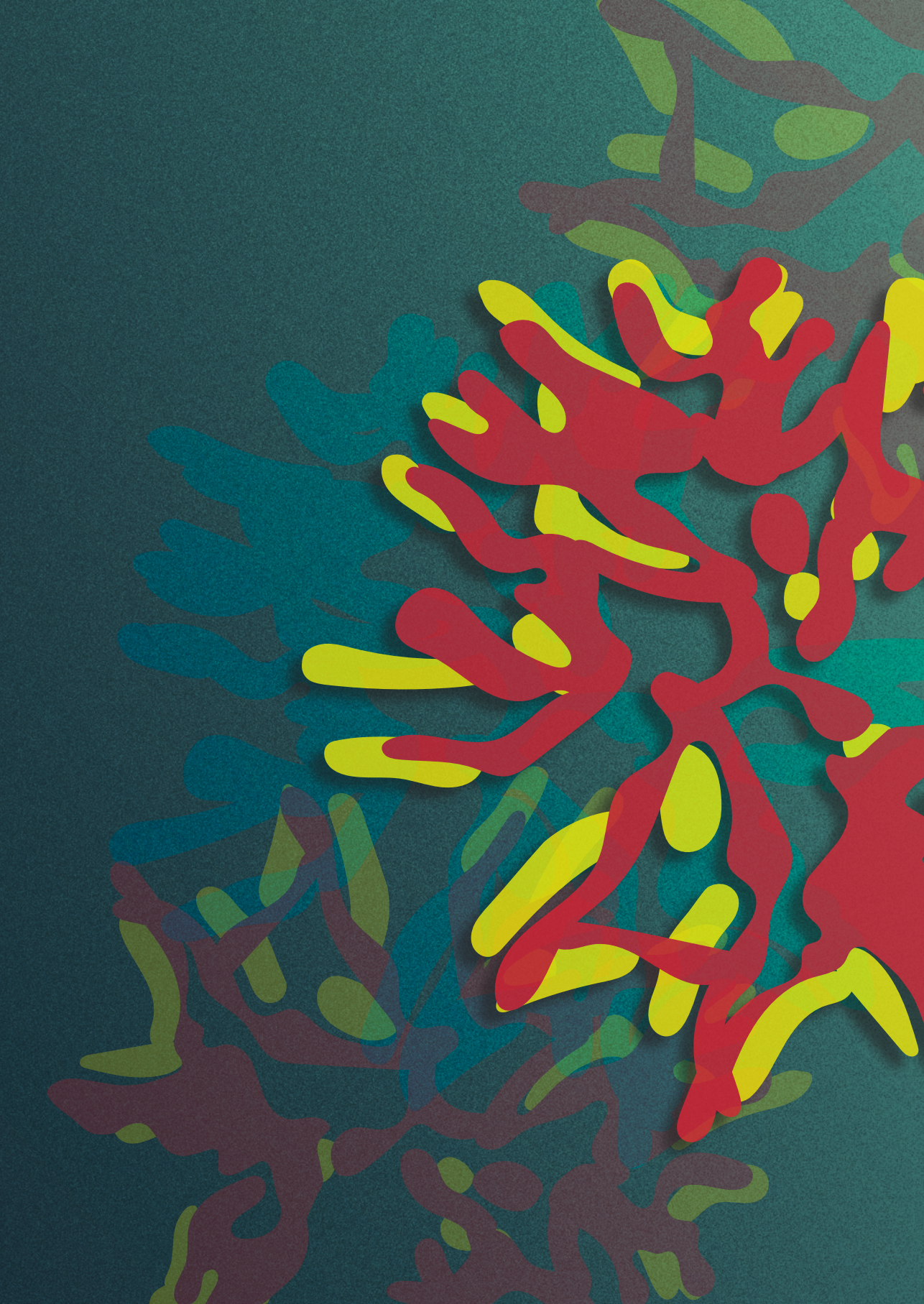

Chapter 5

General discussion

The rapid emergence of drug resistance to current antimalarial drugs necessitates the continuous development of new compounds. The malaria parasite harbors two endosymbiotic organelles, the mitochondrion and apicoplast. Both organelles are established drug targets and, due to their divergence from host organelles, present a promising landscape for the discovery of new parasite-specific compounds. During the complicated cell division process, each of these organelles needs to be properly divided and distributed over daughter parasites. This is highly essential for the parasite to ensure each daughter cell has a complete set of organelles. However, very little is known about these processes. In this thesis, I shed new light on the process of organelle division in *P. falciparum* parasites.

Trying to understand the malaria parasite

Since the discovery of the disease-causing *Plasmodium* parasite in 1880, extensive progress has been made in our understanding of the biology and pathogenesis of this parasite[1]. However, despite more than a century of research, we still understand relatively little about its complex and fascinating molecular biology with more than 50% of predicted proteins still annotated as "unknown function". This is largely due to insufficient homology to proteins with a known function as well as the presence of *Plasmodium*, apicomplexan or alveolate specific genes that have not been studied. Another group of proteins is partially annotated (e.g. "transporter", "kinase") but they remain putative and unstudied. Technological advancements, such as high-throughput sequencing and CRISPR-Cas9 genome editing have provided new insights into the parasite's genome and facilitated precise manipulation of genes to study their functions. These innovations have led to critical discoveries, such as the identification of novel drug targets or an understanding of drug resistance mechanisms. Despite these advancements, there are still several obstacles that complicate molecular malaria research. *In vitro* experiments on malaria parasites present practical challenges that make them significantly more difficult than experiments in mammalian cell systems. In the upcoming paragraphs, I will discuss three of these major challenges, their impact on my PhD research, and how new advancements could ease these issues for future studies.

A challenging life cycle

Malaria parasites have a complex life cycle, which involves multiple stages within the human and mosquito hosts. In each life cycle stage, the parasite presents unique biological characteristics to adapt to their specific and fundamentally different environments. Up until now, surprisingly little is known about the morphological

adaptations of the mitochondrion and apicoplast in each life cycle stage. There are only few studies that describe the morphology of these organelles in the human malaria parasite species *P. falciparum* in asexual and sexual blood stages[2–4] while mosquito- and liver-stage morphology has only been described in the rodent malaria species *P. berghei*[5–8]. In **chapter 3**, I visualized and described mitochondrial morphology from blood stage to mosquito stages, using a newly generated parasite line harboring a fluorescent mitochondrial marker (MitoRed). However, the stage-dependent requirements make it difficult to cultivate *P. falciparum in vitro* throughout its entire life cycle. While the blood stages of *P. falciparum* can be cultured *in vitro* in human red blood cells (RBCs), maintaining a consistent supply of fresh RBCs and human serum for parasite culture can be challenging and costly. While many laboratory *P. falciparum* strains have lost their ability to produce gametocytes due to long term cultivation and loss of specific chromosomal loci[9], sexual blood-stage cultivation is possible with gametocyte producing lines, such as NF54 or the inducible gametocyte producing (iGP) line[10]. The production of *P. falciparum* gametocytes is labor intensive, as parasites require daily media changes during their ~12 days maturation period. However, automatic culturing systems can greatly ease the work load[11]. Mosquito-stage parasite cultivation is more difficult, as they can only reliably be generated *in vivo* in *Anopheles* mosquitoes. This requires a biosafety level 2 insectary and specialized staff for the maintenance of the mosquito colonies and dissections. Mosquito infection requires the strict coordination of mature gametocyte generation and production of ready-to-infect mosquitoes for feeding. It is therefore challenging to generate high and consistent mosquito infection rates over different experiment. Hence, we were not able to directly compare infection rates of MitoRed and NF54 parasites. Enhancement of gametocyte induction protocols using Albumax supplementation could improve consistency in gametocyte production and transmission[12]. The recent development of an *in vitro* infectious sporozoite production protocol that eliminates the need for mosquitoes is a big step forward[13]. This innovation could open up new possibilities, specifically for *P. falciparum* liver-stage research which is often restricted by the availability of infectious sporozoites[14]. Researchers usually use fresh hepatocytes isolated from human livers isolated during liver surgery. However, some companies now offer fresh cryopreserved hepatocytes, providing many vials from a single donor, which is ideal for large-scale experiments and high-throughput screens. This consistency in donor hepatocytes also enhances experimental reproducibility. Although finding the most suitable hepatocyte donor for *P. falciparum* infection may require careful selection[15], availability of these resources makes it possible to study *P. falciparum* liver stages. All these factors combined make it challenging, but possible to study *P. falciparum* parasites *in vitro* throughout their complicated life cycle.

Challenges in molecular genetics

A better understanding of critical biological processes in the parasite are key for the identification of novel drug targets and understanding of drug resistance mechanisms. The ability to elucidate the functions of parasite genes and proteins relies heavily on the ability to genetically modify these genes. Although genetic modification in *Plasmodium* parasites presents unique challenges compared to well-studied model systems like *Saccharomyces cerevisiae* or HeLa cells, significant advancements have been made.

The ABS is the only life-cycle stage used to generate transgenic parasite lines, as parasites can be cultured *in vitro*, undergoing continuous asexual replication, which allows for the use of selectable markers to obtain the modified parasites of interest. The parasite's haploid genome limits genetic redundancy, meaning knockout of essential genes is lethal. To overcome this, an inducible gene deletion system, such as dimerizable Cre (DiCre)-lox, can be used. The addition of rapamycin will dimerize two Cre subunits restoring its recombinase activity and excising the *loxP*-flanked gene region[16]. Nevertheless, genomic integration of the two *loxP* sites in a Cre-expressing parasite line can be challenging and often requires multiple sequential transfections. The lack of multiple good working selection markers further complicates this.

Huge progress in genetic manipulation has been made by the development of CRISPR-Cas9, which was applied for the first time in *P. falciparum* by Ghorbal and colleagues in 2014[17]. However, the efficiency and ease of generating stable transgenic lines is still lower in *P. falciparum* compared to other well-studied model systems. There are several reasons for this lower efficiency. The extremely high AT-rich genome of *P. falciparum* with the overall AT composition of 80.6% and reaching 90% AT content in the non-coding regions complicates cloning of repair plasmids[18]. Plasmids with high AT-rich sequences are prone to recombination events when grown in bacteria and repetitive regions can cause slippage and errors during amplification or sequencing. Additionally, it is more difficult to find suitable guide RNA sequences since the number of PAM motives (NGG) in the genome is limited[19]. The lack of non-homologous end joining (NHEJ) in *Plasmodium* parasites complicates large-scale genetic screens, as parasites rely on homology-directed repair guided by a homologous template to repair double stranded DNA breaks[20]. Nevertheless, targeting vector libraries and non-targeted transposon mutagenesis enabled genome-wide screens for gene essentiality in *P. berghei*[21] and *P. falciparum,* respectively[22].

While *Plasmodium* parasites have a nuclear envelop and plasma membrane similar to mammalian cells, they also reside in a parasitophorous vacuole inside an RBC.

Therefore, there are four membranes that need to be crossed for the plasmids to reach the genomic DNA in the nucleus, which imminently makes it less efficient compared to mammalian cell transfection, where only two membranes are crossed. Electroporation of infected RBCs, merozoites, or uninfected RBCs to allow spontaneous uptake of DNA after RBC invasion are commonly used methods for transfection of *P. falciparum*[23]. However, these methods require large amounts of plasmid DNA per transfection (60 – 150 µg per plasmid)[23,24] in contrast to standard mammalian cell line transfections (0.1 – 2.5 µg per plasmid)[25]. Additionally, while *P. falciparum* parasites lack a classical RNA interference mechanism, alternative transcriptional knockdown systems, such as *glmS* ribozyme or TetR-DOZI are being successfully employed to study gene function[27].

All these factors make it significantly more challenging to study gene functions in *P. falciparum*, compared to other model eukaryotes. One of the main aims of this PhD work was to identify and characterize potential mitochondrial division proteins in *P. falciparum*. In order to do this, I aimed to generate knockout and knockdown-tagged parasite lines to study the role of proteins of interest in mitochondrial division. However, this relies completely on the generation of transgenic parasite lines, which, as described above, can be challenging. Dynamins play a central role in division of mitochondria in other model eukaryotes. Dynamins are large GTPase proteins that are recruited to the mitochondrion by adaptor proteins to form a constrictive ring around the fission site, as discussed in detail in **chapter 2**. *Pf*DYN2 and *Pf*DYN3 are the two main candidates thought to be involved in apicoplast and mitochondrial division, respectively, based on their homology in *Toxoplasma gondii*[28]. Despite numerous attempts, I was unable generate DYN2 and DYN3 knockout or knockdown-tagged parasite lines. Selection of new guide RNA sequences, placement of the selection marker in the repair plasmid instead of the guide plasmid, and the use of the Selection Linked Integration (SLI) system failed in generating transgenic parasites over a total of 26 transfections. This further demonstrates the difficulty of transgenic parasite generation in *P. falciparum*. Interestingly, other groups have been able to generate DYN2 and DYN3 tagged parasite lines. Detailed comparison of construct design and transfection protocols could be useful to identify why we were unable to generate these lines.

New, more efficient methods to study gene functions are needed to accelerate progress in understanding parasite biology. Development of new and better selection markers could improve transfection efficiency. Additionally, Ramaprasad *et al*. recently developed a frameshift-based trackable inducible knockout system (SHIFTiKO)[29]. Barcoded repair templates are used to insert *loxP* sites

around short regions in targeted genes and DiCre-mediated excision results in a tracible frameshift mutation. This strategy allows collective inducible knockout generation and phenotyping of tens of mutants simultaneously. Furthermore, the recent discovery of bridge RNAs (bRNAs) by Durrant *et al.* represent an extremely promising advancement in the field of genome engineering[30,31]. This technique uses the natural ability of IS110 insertion sequences to cut and paste themselves throughout a genome. The reprogrammable bRNA recognizes and binds both the genomic target DNA and the donor DNA, bringing these in close proximity to each other. A recombinase enzyme then recombines and re-ligates the DNA, leaving it fully intact. This mechanism is distinct from CRISPR editing, which cuts the DNA and relies on the cell's innate repair system to repair the break. Another advantage is that the bRNA system does not require a PAM motive (NGG), allowing for potential targeting of numerous sites in the AT-rich *Plasmodium* genome. Furthermore, this technique ensures precise genome editing with minimal off-target effects, as it does not tolerate mismatches. Although this technique has only been tested in *E. coli* and further studies are necessary to test its applicability in other cell systems, it holds great promise as a third-generation RNA-guided tool for precise genome editing.

Challenges in parasite visualization

During the pathogenic ABS, malaria parasites reside in RBCs which are the smallest cells of our body with a diameter of ~7 µm. Visualization of this tiny parasite and especially processes that happen within this parasite using standard imaging techniques is challenging. The resolution limit of light microscopy is primarily determined by the diffraction limit of light and is typically around 200-300 nm lateral (xy) resolution and 500-700 nm axial (z) resolution. Although this resolution allows visualization of general parasite morphology, such as large organelle structures, finer details, such as the exact localization of a protein within an organelle or the division of organelle branches remains difficult. One of the main aims of this thesis was to visualize the process of mitochondrial and apicoplast division in *P. falciparum*. The parasite mitochondrion and apicoplast have a diameter of 100-200 nm. The small size of the mitochondrial tubes and complexity of the intricate mitochondrial network make it nearly impossible to visualize organelle division with conventional light microscopy. Therefore, high- or super-resolution imaging techniques are necessary to image the organelle division process in any truly accurate way. Airyscan microscopy is an advanced imaging technique that uses an array of 32 concentric detectors which improve imaging sensitivity and resolution up to 1.7x compared to conventional confocal microscopy. The resolution advantage of this technique allowed me to visualize mitochondrial dynamics and division as described in **chapter 3**. However, with the limited Z-resolution it remains

challenging to distinguish separate mitochondrial fragments if they are spaced on top of each other in the Z dimension. Super-resolution imaging techniques such as Stimulated Emission Depletion (STED) microscopy, Photoactivated Localization Microscopy (PALM), Stochastic Optical Reconstruction Microscopy (STORM), and Structured Illumination Microscopy (SIM) can reach a resolution of 100 – 10 nm depending on the technique and have been used successfully in *P. falciparum*[32–35]. However, these techniques all require expensive, specialized microscopes and trained personnel to operate them.

Another method that overcomes the resolution limit of light microscopy is electron microscopy (EM). EM can achieve up to 0.1 nm resolution, primarily because the wavelength of electrons is much shorter than that of visible light. In 1942, EM was used for the first time to visualize *Plasmodium* parasites[36]. From then onwards, EM has had a significant impact on malaria research by providing detailed insights into the ultrastructure of *Plasmodium* parasites and their interactions with host cells. The further development of 3D or volume EM is a tremendous advancement, allowing for the visualization of complex connecting structures such as a mitochondrial network, which are extremely difficult to interpret from only single slice images. Volume EM is highlighted as one of the seven technologies to watch in 2023 by *Nature*[37]. Focused ion beam scanning electron microscopy (FIB-SEM) is a volume EM technique that uses a focused ion beam for sequential milling of a thin sample layer combined with scanning electron microscope for imaging of the exposed sample surface, allowing detailed 3D reconstructions of cellular structures. In **chapter 3**, we used FIB-SEM to verify the mitochondrial division steps during schizogony with nanometer resolution. One big advantage of this technique is that it does not require labelling and allows visualization of many different organelles and subcellular structures. Therefore, these data also revealed the apicoplast division steps, the close interaction between the apicoplast and mitochondrion, and the potential role of the centriolar plaque (CP) in apicoplast segregation. However, the downsides of this technique are the need for specialized microscope and trained personnel, high costs, time-consuming and labor-intensive data analysis, and it is low throughput.

Fortunately, the imaging field is rapidly developing. One such important advancement is expansion microscopy (ExM)[38,39]. ExM involves the isotropic expansion of a biological sample embedded in a swellable polymer gel. This allows visualization of subcellular structures beyond the diffraction limit of light microscopy, while using conventional light microscopes. ExM is now widely used in the field of molecular parasitology, and many organelles, including apicoplast and

mitochondrion have been visualized using this technique[40]. Recent developments such as iterative ExM[41] and cryo-ExM[42] further expand the boundaries and applicability of this technique. Cryo-ExM combines cryofixation with ExM, allowing significantly better preservation of membranous structures, such as the ER and mitochondrion, compared to chemical fixation methods. During this PhD trajectory, I aimed to apply cryo-ExM for the first time in *P. falciparum* for visualization of mitochondrial and apicoplast contact sites. First attempt cryo-ExM images showed indeed an improved, more continuous mitochondrial signal when stained with MitoTracker, compared to conventional ExM in *P. falciparum* schizonts (Figure 1). However, the NHS-Ester stain, which binds to amine groups of proteins and is often used to visualize general subcellular structures such as rhoptries, CPs, and basal bodies, showed a much more diffuse staining in the cryo-ExM images compared to the ExM image. Therefore, further optimalization of the protocol is needed, which was unfortunately not feasible within the timeframe of my PhD. Nevertheless, these preliminary data show a promising role for cryo-ExM in organelle visualization in *Plasmodium* parasites.

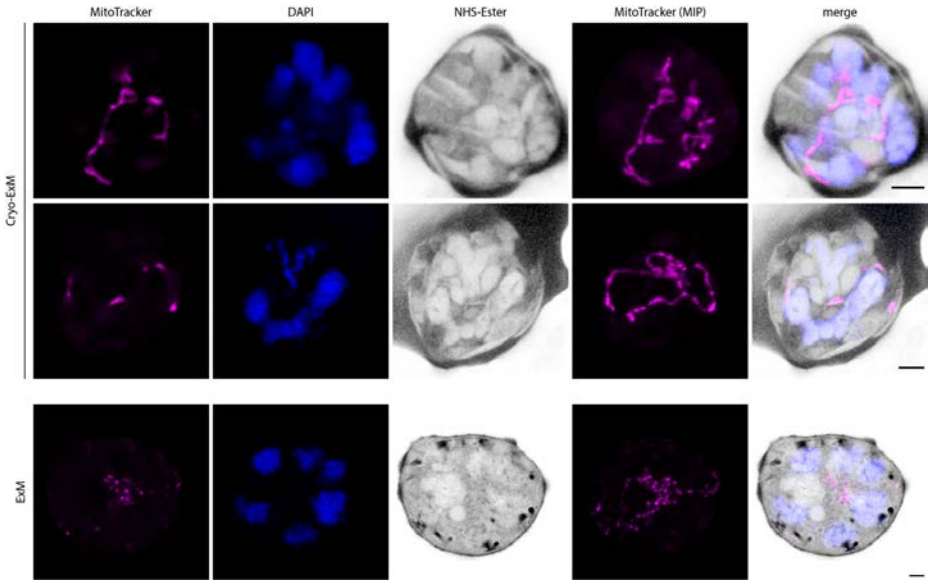

Figure 1. Mitochondrial visualization with cryo-Expansion Microscopy (cryo-ExM) in *P. falciparum* schizonts. Cryo-ExM images (top two rows) and conventional ExM images (bottom row) of *P. falciparum* schizonts stained with MitoTracker CMXRos for mitochondrial visualization, DAPI for DNA visualization, and NHS-Ester for protein visualization. Fourth column represents maximum intensity projection (MIP) of MitoTracker signal. Scale bars, 3 µm.

Development of organelle markers

One of the main aims of this research was to capture mitochondrial and apicoplast division during ABS schizogony in *P. falciparum*. This requires the visualization of these organelles for fluorescent microscopy. There are several approaches to do this, including the use of fluorescent dyes such as MitoTracker, tagging of proteins that localize to the organelle, or targeting of fluorescent proteins to the organelle. In **chapter 3**, we showed that MitoTracker dyes give a discontinuous, punctate staining pattern of the mitochondrion in blood-stage schizonts. We know from our volume EM data that the mitochondrion in these stages is one continuous intricate network. The punctate staining pattern is likely an artifact of the fixation process and limits the ability to visualize mitochondrial fission. Therefore, we developed a new mitochondrial marker using a similar approach as has been used successfully in *P. berghei*[5]. We used the promotor and targeting sequence of the gene encoding for the mitochondrial heat shock protein 70 (HSP70-3), fused to mScarlet. We assumed that by using the promotor of a known mitochondrial protein, we would prevent toxic "overloading" of the organelle with the targeted fluorescent protein. We aimed to stably integrate this marker in the *P. falciparum* genome. However, the previously used integration locus, *Pfs*47, has been shown to play a role in mosquito stages[43–45]. The *Pf*RH3 pseudogene, another frequently used integration site, has been shown to be transcribed and not translated in blood stages, while the RH3 protein has been detected in sporozoites[46–49]. Therefore, we selected a new integration site for the reporter gene, using a similar strategy as was described for *P. berghei*[50]. Three evolutionary recent chromosome break points on chromosomes 7, 12 and 14 were identified in the *P. falciparum* genome, using a bioinformatic approach comparing *Plasmodium* genomes as discussed in detail in **chapter 3**. The Silent Intergenic Locus (SIL) on chromosome 7 (SIL7) was used for integration of the mitochondrial marker, causing no developmental issues in blood-stage growth and development. However, MitoRed parasites failed to form salivary-gland-infecting sporozoites. This could be caused by the mitochondrial marker itself, which might be toxic or too highly expressed in this stage specifically. However, it is also possible that integration of a transgene, in this case the mitochondrial marker, in SIL7 might have developmental consequences during mosquito stages. Therefore, it is important to search for new SILs that allow transgenic integration and parasite development throughout the whole *Plasmodium* life cycle. Another approach to identify potential new SIL sites is to bioinformatically search for gene insertion or deletion sites by comparison of *Plasmodium* genomes. Our reasoning for this is that since these regions have been changed throughout the evolution of *P. falciparum,* integration into these sites would be harmless. Using this approach, we identified 12 new candidate loci (Table 1). Based

on the size of these regions, the presence of a good guide RNA targeting sequence, and transcriptional data, these loci were categorized as promising or possible SIL candidates. These candidates now need to be tested for their cloning and transfection efficiency, and transgenic expression. Furthermore, parasites with modified loci need to be tested for life cycle progression. Successful integration of a mitochondrial marker in Ins-32 (also known as SIL12 because of its localization on chromosome 12) has been verified, although its progression through mosquito and liver stages still needs to be confirmed. It would be ideal to have multiple SILs at our disposal that allow transgenic integration throughout the complete life cycle, so that double or triple reporter lines could be generated. This could be a useful tool for the molecular malaria research community to study processes that requires parasites with multiple fluorescent organelle markers, such as the dynamics of organelle contact sites.

Table 1. Potential new SILs based on gene insertion or deletion in the *P. falciparum* genome.

Identifier	Category	Upstream gene	Downstream gene	Size	Guide*	Comments
Ins-3	Promising	PF3D7_0606700	PF3D7_0606800	1359	+	
Ins-6	Promising	PF3D7_0617300	PF3D7_0617400	1804	+	
Ins-22	Promising	PF3D7_1219100	PF3D7_1219300	2453	+	Contains pseudogene
Ins-32	Promising	PF3D7_1240900	PF3D7_1241000	1880	+	
Ins-41	Promising	PF3D7_1312600	PF3D7_1312700	1004	+	
Ins-59	Promising	PF3D7_1473900	PF3D7_1474000	1425	+	
Del-51	Promising	PF3D7_0512400	PF3D7_0512500	2753	+	Contains pseudogene
Ins-27	Possible	PF3D7_1240000	PF3D7_1240100	633	+	Might be too small
Del-42	Possible	PF3D7_0403500	PF3D7_0403600	1100	~	
Del-61	Possible	PF3D7_0806700	PF3D7_0806800	863	~	
Del-70	Possible	PF3D7_1460100	PF3D7_1460200	999	~	
Del-76	Possible	PF3D7_1326100	PF3D7_1326200	1229	+	>3 EST alignments

* + indicates the presence of at least one guide RNA sequence with > 0.4 on-target efficiency and 1 or no off-target BLAST hits[51]. ~ indicates the guide RNA sequences present with > 0.4 on-target efficiency have > 5 off-target BLAST hits.

In order to study apicoplast division in *P. falciparum*, we applied the same strategy for the generation of an apicoplast marker parasite line. We used the promotor and targeting sequence of the gene coding for 20kDa chaperonin (CPN20), a known apicoplast protein, fused with mScarlet. We successfully integrated this apicoplast

marker into the *P. falciparum* genome. Unfortunately, expression of the marker was low, and the fluorescent signal was insufficient to study apicoplast dynamics with confocal microscopy. Therefore, we used PlasmoDB to search for other apicoplast proteins that are higher expressed and selected 60kDa chaperonin (CPN60)[52] and peptide deformylase (PDF)[53] as potential candidates. Future studies could explore if these are suitable candidates for a fluorescent apicoplast marker.

Up until now, we have used the fluorescent protein, mScarlet, for our organelle markers, as it is the brightest fluorescent protein in the Red Fluorescent Protein (RFP) spectrum and therefore well suited for live imaging[54]. However, fluorescent proteins are not compatible with ExM (discussed in previous paragraph) as this involves a denaturation step to homogenize the gel samples. The use of a linear peptide tag, such as an influenza hemagglutinin (HA) or myelocytomatosis viral oncogene (Myc) tag, would overcome this problem, as their antibody binding does not depend on a secondary or tertiary structure. However, because of the small size of these tags (typically 8-12 amino acids) the affinity of antibodies to detect these tags can be low, which makes it difficult to detect weakly expressed proteins. To address this issue, a spaghetti monster fluorescent protein (smFP) tag could be used for the generation of an ExM-compatible organelle marker. SmFPs have 10-15 copies of single epitope tags strategically inserted into a fluorescent protein scaffold which have either an intact or darkened chromophore[55]. This provides many antibody binding sites within a single tag that remain preserved after the ExM denaturation step, resulting in a much higher fluorescent signal compared to single or triple epitope tags. SmFPs tags recently been used successfully in combination with ExM in *P. falciparum*[40]. We have successfully generated parasites lines harboring a CPN60 apicoplast marker with smMyc and a HSP70 mitochondrial marker with smV5, although the visualization of these markers with ExM still needs to be confirmed. Further development of these ExM-compatible organelle markers could provide the molecular malaria research field with a valuable tool to study organelle biology, protein localization, and knockout/knockdown or drug phenotypes, with the increased effective resolution gained from ExM.

Mitochondrial and apicoplast division

The apicoplast and mitochondrion both form intricate, branched network structures, prior to their division in *P. falciparum*. Although it has been shown that apicoplast fission occurs prior to mitochondrial division[2], it was previously unclear how these seemingly disorganized network structures are divided and distributed

over daughter cells. Therefore, one of the main aims of this thesis was to visualize mitochondrial and apicoplast division in *P. falciparum* to better understand these processes. In **chapter 2**, we propose three possible division scenarios: synchronous fission (simultaneous division of the complete organelle), outside-in fission (fission occurs at the ends of the organelle), and branching point fission (fission occurs in a stepwise process starting at the branching points of the network). Recent work from Liffner *et al.* visualized the mitochondrion and apicoplast during different stages of schizogony, using ExM[40]. This study showed that both the mitochondrion and apicoplast do not divide synchronously and that division occurs in a stepwise manner, supporting the branching point fission model. However, it is difficult to determine whether a break in the staining of the organelle marker that they use represents a complete fission of the apicoplast and mitochondrion. Therefore, further studies are needed to confirm the fission model of these organelles. In **chapter 3**, we describe in detail the mitochondrial dynamics during ABS schizogony, using high-resolution confocal microscopy and a new fluorescent mitochondrial marker. We found that the mitochondrion organizes itself in a cartwheel structure, with branches pointing into the forming merozoites. This cartwheel structure is divided into smaller fragments in a stepwise, non-geometrical progression during the final stage of merozoite segmentation. These mitochondrial division steps were confirmed by FIB-SEM image analysis. This also allowed us to visualize the apicoplast division during schizont development. Apicoplast division happens when IMC formation has started, and nuclear division is still ongoing. In contrast to the central cartwheel organization of the mitochondrion, the apicoplast organizes itself to the periphery of the cell prior to its division, while interacting with the CPs. However, similarly to mitochondrial division, the apicoplast divides in a stepwise, non-geometrical progression. During apicoplast division, each ending of an apicoplast branch interacts with a CP, as shown in **chapter 3**. This observation strongly supports the branching point fission model, where each individual apicoplast branch interacts with a CP and is divided in a stepwise manner at the branching points. Interestingly, recent work from James Blauwkamp and Sabrina Absalon shows that in late stage schizonts that fail to divide their apicoplast due to a knockdown of a protein called Anchor, the apicoplast orients in a very similar cartwheel orientation as the mitochondrion (unpublished data, personal communication). This suggests that the cartwheel structure is merely a consequence of merozoite segmentation, rather than active organization process.

Mitochondrial and apicoplast division in other apicomplexan parasites

Three distinct replication forms have been described in apicomplexan parasites: schizogony, endodyogeny, and endopolygeny[56]. While these replication forms differ

in timing and the extend of nuclear division before cytokinesis, they are similar in their fundamental organization. All apicomplexan replication forms rely on self-assembly of daughter cells within the parental cell, coordinated by centrosomes or CPs (centrosome equivalent in *P. falciparum*). *T. gondii* parasites replicate through endodyogeny, where a single round of DNA replication and mitosis is followed by the assembly of two daughter cells. In **chapter 2**, we describe the organelle dynamics during endodyogeny in *T. gondii*. Similarly to our observations of schizogony in *P. falciparum* in **chapter 3**, the endings of the single apicoplast in *T. gondii* associate with the centrosome prior to its division and the apicoplast divides prior to completion of nuclear division[57]. In contrast to the mitochondrion in *P. falciparum*, the mitochondrion in *T. gondii* has a distinct lasso shape that associates with the IMC[57,58]. Branches of the mitochondrion reach into the forming daughter cells. Thereafter, the lasso-shape is reestablished within the daughter cells, but the mitochondria remain attached at their basal ends[59]. Similarly to *P. falciparum* schizogony, mitochondrial division in *T. gondii* is one of the final steps of daughter cell formation. Parasites such as *Sarcocystis neurona* replicate through endopolygeny, where the genome is replicated several times within one nucleus before the last round of mitosis and packaging of haploid nuclei into the daughter cells[60]. Although very little is known about mitochondrial division in this parasite, work from Vaishnava *et al*. shows that similarly to *P. falciparum*, the apicoplast of *S. neurona* associates with the centrosomes at the periphery of the polyploid nucleus[60]. In the last round of mitosis, daughter cells are formed by budding while the apicoplast still associates with the centrosomes and is divided and segregated into the forming daughter cells.

These observations show that although there are some clear differences, there is also striking overlap between timing and organization of organelle division in Apicomplexa. Some apicomplexan parasites undergo more than one form of replication to adapt to their environment and the size of their host cell as they progress through their complex life cycles. This allows the parasites to adapt the timing and scale of offspring production in different life-cycle stages[56]. *T. gondii* for example divides through schizogony in the intestinal epithelium of the cat, while it divides by endodyogeny in its intermediate hosts. While *Plasmodium* parasites replicate through schizogony in blood and liver stages, FIB-SEM analysis revealed that they divided through endopolygeny-like mechanism in oocyst stages[61]. Therefore, it makes sense for these parasites to have overlapping organelle division mechanisms in different replication stages that facilitate these life-cycle transitions, adapting to the different host environments. In **chapter 3**, we show mitochondrial dynamics in different stages of oocyst development in *P. falciparum*. In late-stage oocysts (day 13

after infection), the parasite mitochondrion is organized in so called mitochondrial organization centers (MOCs). These MOCs are analogous to the cartwheel structure observed in asexual blood stages. Very similar mitochondrial organization was also found in *P. berghei* liver stages in sub-compartments created by large membrane invaginations[8]. In both oocyst- and liver-stage sub-compartments, the apicoplast localizes to the periphery of the sub-compartment prior to its division, while closely associating with the nuclei[8,62,63]. The apicoplast divides before completion of nuclear division during early stages of daughter cell segmentation. The mitochondrion then orients in a radial, cartwheel-like fashion within these sub-compartments, prior to its division during the final stages of oocyst- or liver-stage development[8]. These observations are strikingly similar to mitochondrial and apicoplast division in ABS schizogony described in **chapter 3**. These similarities in timing and organization of organelle division suggest that organelle division and segregation mechanisms may be shared between different life-cycle stages of *P. falciparum* as well as different apicomplexan parasites. Therefore, these could potentially provide interesting multi-stage or multi-parasite drug targets.

Organelle division mechanism

The division mechanism for membranous organelles relies on the recruitment and oligomerization of GTPases to form a constrictive ring. In **chapter 2**, we discuss both the ancestral FtsZ-based division machinery and the eukaryotic dynamin-based division machinery. Some early-branching eukaryotes, such as Amoebozoa and red algae still use the bacterial division system for fission of their mitochondria[64]. However, *Plasmodium* parasites lack homology to this ancestral division machinery (**chapter 2**). Plants and algae use a combination of the FtsZ- and dynamin-based machinery for division of the chloroplast[65]. A similar machinery is used by some heterokonts for division of their four-membrane plastids acquired via secondary endosymbiosis[66]. However, apicomplexan parasites lack homology to all components of this division mechanism, indicating that they developed a different division machinery compared to previously studied plastids[67,68].

Humans and yeast also utilize a dynamin division machinery for mitochondrial fission. The first step of mitochondrial division in humans is the wrapping of an ER branch around the mitochondrial fission site[69] (Figure 2). Calcium from the ER transfers to the mitochondrion at the ER-mitochondrial contact sites, which causes constriction of the inner mitochondrial membrane (IMM) in a dynamin related protein 1 (Drp1)-independent manner[70]. Drp1 is then recruited to the fission site

by adaptor proteins and forms an oligomeric ring around the organelle. Upon GTP hydrolysis a conformational change induces constriction of the Drp1 ring, leading to constriction of the organelle[71]. Although the exact mechanism of IMM fission is unknown, it is thought that YME1 and OMA1 mediated cleavage of OPA1 leads to increased levels of short OPA1, which is correlated with increased mitochondrial fission[72]. Another dynamin, dynamin 2, has been indicated to play a role in final scission of the mitochondrion, although this is still under debate[73,74].

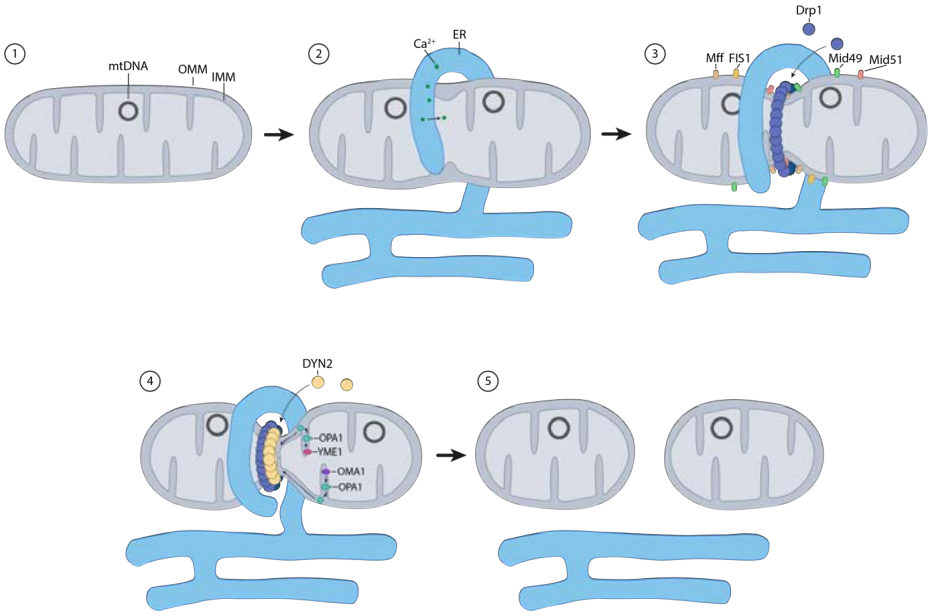

Figure 2. Schematic illustration of mitochondrial division mechanism of human mitochondria. 1) mitochondrion with mitochondrial DNA (mtDNA), inner mitochondrial membrane (IMM) and outer mitochondrial membrane (OMM). 2) ER-mediated pre-constriction of the mitochondrion and replication of mtDNA. 3) Recruitment of Drp1 by adaptor proteins FIS1, MFF, Mid49 and Mid51 to the fission site. Recruited Drp1 forms constrictive ring around the organelle. 4) Constriction of the Drp1 ring causing further organelle constriction. Hypothetical mechanism of IMM fission, mediated by short OPA1, cleaved by YME1 and OMA1 proteases. Hypothetical recruitment of dynamin 2 (DYN2) to mediate final step of mitochondrial division. 5) Completely divided mitochondria.

Mitochondrial-ER contact sites are crucial for lipid homeostasis and calcium transport[75]. Close apposition of the ER and mitochondrion have been reported in early-stage *P. falciparum* schizonts and stage V gametocytes[76]. Complexome profiling experiments identified a potential mitochondrial interactor, TOM7, of the ER membrane complex (EMC) in *P. falciparum*, which may form a tethering complex[76]. However, we did not observe mitochondrial-ER appositions in our

FIB-SEM images of late-stage schizonts. So far, we have not found direct evidence that the ER wraps around the mitochondrial division site or is directly involved in mitochondrial division.

Plasmodium parasites harbor three dynamin proteins (DYN1, -2, and -3), similarly to *Toxoplasma*. *Pf*DYN1 is essential for parasite survival and is suggested to play a role in vesicle budding during hemoglobin uptake[77,78]. *Pf*DYN2 and its homolog in *T. gondii Tg*DrpA cluster together phylogenetically with other dynamin related proteins, such as human Drp1 which mediates mitochondrial fission[68]. In *T. gondii*, *Tg*DrpA has been indicated to be involved in apicoplast division[67], while the non-canonical *Tg*DrpC (*Pf*DYN3 homolog) has been indicated to play a role in mitochondrial division[59]. *Tg*DrpC and *Pf*DYN3 are apicomplexan-specific and lack the GTPase effector domain and middle domain[79,80]. However, in contrast to *Tg*DrpC, *Pf*DYN3 is likely not involved in mitochondrial division (data unpublished, personal communication with Emma McHugh and Stuart Ralph). In **chapter 3**, we speculate about possibility of a shared division mechanism between the apicoplast and the mitochondrion, given their sequential division. Supporting this speculation, a recent preprint from Morano *et al.*[81] shows that *Pf*DYN2 is involved in both apicoplast and mitochondrial division. *Pf*DYN2 localizes to both the mitochondrion and apicoplast and knockdown of *Pf*DYN2 causes parasite death and defective division of both the apicoplast and mitochondrion. Another preprint from Thakur *et al.* shows an essential role of *Pf*DYN2 in mitochondrial function and division, while the role of *Pf*DYN2 in apicoplast division is not assessed[82]. *P. falciparum* is the first known organism in which a single dynamin facilitates division of two different endosymbiotic organelles, highlighting its unique biology.

Dynamins are recruited to the fission site by adaptor proteins. In contrast to dynamins, adaptor proteins are highly variable between different eukaryotes and are not preserved in terms of amino acid sequence, secondary structure, or domain composition[83]. FIS1 is the only known adaptor protein that is highly conserved among mitochondrial-containing eukaryotes. In yeast, FIS1 is the only known membrane bound adaptor protein that is essential for the recruitment of other fission proteins Mdv1 and Caf4, which recruit the yeast dynamin, Dnm1[84,85]. In contrast, human FIS1 is redundant and its role of Drp1 recruitment can be facilitated by other adaptor proteins Mff, MiD49 and MiD51[86,87]. Knockdown or knockout of FIS1 *T. gondii* and *P. falciparum* did not result in a growth defect or affected mitochondrial morphology, suggesting a dispensable role in these ABS parasites[59,88]. However, mislocalization of FIS1 in *T. gondii* to the cytoplasm by truncation of the protein caused significant mitochondrial morphology changes,

suggesting that FIS1 has a function in mitochondrial morphology[89]. During this PhD, I also generated a FIS1 knockout *P. falciparum* parasite line and found that FIS1 was not essential for gametocyte development and exflagellation (data not shown). One preliminary experiment showed that FIS1 knockout parasites could transmit to mosquitoes but did not develop to sporozoites. Future studies could explore if FIS1 plays a role in mitochondrial fission during sporogony, e.g. by studying mitochondrial morphology in different stages of FIS1 knockout oocyst development.

Recent work from James Blauwkamp and Sabrina Absalon found a potential apicoplast adaptor protein, Anchor, which localizes around the apicoplast and is essential for parasite survival in *P. falciparum* (data unpublished, personal communication with James Blauwkamp and Sabrina Absalon). Knockdown of Anchor causes impaired apicoplast division and merozoites stay attached to the residual body after egress, while mitochondrial division and segregation is unaffected. Parasite growth can be rescued by isopentenyl pyrophosphate (IPP) supplementation, indicating an apicoplast-specific role. A pulldown experiment with Anchor identified *Pf*DYN2 as interaction partner. These results strongly indicate that Anchor is an apicoplast adaptor protein that recruits *Pf*DYN2 to the apicoplast fission site, while the mitochondrion likely uses other adaptor proteins for *Pf*DYN2-mediated fission (Figure 3). Future studies could include *Pf*DYN2 co-immunoprecipitation on the Anchor knockdown line to identify mitochondrial adaptor proteins. By removal of Anchor, you might be able to specifically find interactions of *Pf*DYN2 with potential mitochondrial adaptor proteins.

T. gondii parasites that are depleted of *Tg*MORN1, an essential component of the basal complex, fail to constrict the basal complex and divide their apicoplast[90]. *Tg*MORN1 knockout had much milder segregation defect for the mitochondrion, suggesting different involvement of the basal complex in division of each organelle. However, *P. falciparum* parasites lacking the basal complex protein *Pf*CINCH still divide their apicoplast and mitochondrion, despite their inability to form merozoites[91]. This suggests that in contrast to *T. gondii*, the basal complex does not seem to play a direct role in organelle division in ABS *Plasmodium* parasites.

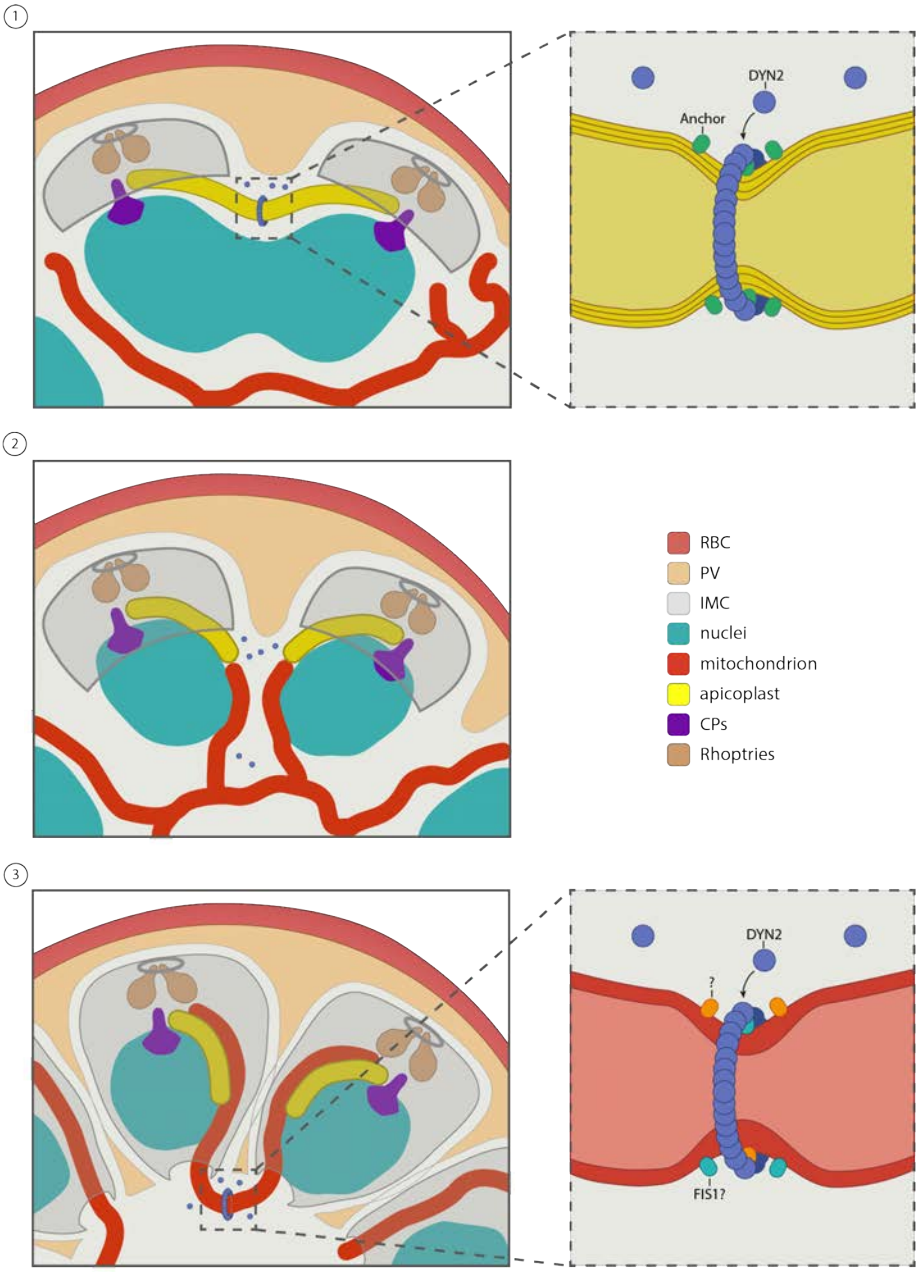

Figure 3. Hypothetical apicoplast and mitochondrial division machinery in *P. falciparum*. 1) PfDYN2 is recruited to the apicoplast fission site by Anchor, where it oligomerizes to form a constrictive ring around the organelle which mediates fission. 2) After apicoplast division, PfDYN2 is released back into the cytoplasm. 3) Thereafter, PfDYN2 is recruited to the mitochondrial fission site, possibly by the redundant FIS1 protein and by other, unknown, adaptor proteins, where it mediates mitochondrial fission by forming a constrictive ring around the organelle.

Organelle segregation mechanisms

The segregation of organelles during cell division is crucial to ensure that daughter cells inherit the necessary components for survival and function. The mechanisms of organelle segregation vary depending on the type of organelle and the organism, but generally involve motor proteins and the coordinated remodeling of the cytoskeleton. In budding yeast, mitochondrial segregation during cell division is mediated by active transport of the mitochondrion by the type V myosin, Myo2, along actin filaments[92]. In mammalian cells, mitochondria are transported along microtubules by kinesins to the plus-end direction and by dyneins to the minus end direction[93] (Figure 4A). The cargo-binding domain of kinesin-1 interacts with an adaptor protein called Milton, which binds to Mitochondrial Rho GTPase (Miro) that localizes to the outer mitochondrial membrane (OMM)[93]. During cell division, mitochondria are transported to the cleavage furrow and cell periphery along astral microtubules of the mitotic spindles mediated by kinesin-1[94]. Mitochondria are released from the microtubules and anchored to actin cables by myosin 19, ensuring uniform distribution of mitochondria[95,96]. In plants, transport of the mitochondria and chloroplasts depends on both actin and tubulin cytoskeleton, although the exact molecular mechanisms of organelle transport during cell division remain to be elucidated[97].

In **chapter 3**, the FIB-SEM visualization of different *P. falciparum* schizont stages reveals new insights into apicoplast and mitochondrial segregation. In the following paragraphs, potential apicoplast and mitochondrial segregation mechanisms will be discussed in more detail.

Recruitment of apicoplast branches to the CPs

In **chapter 3**, FIB-SEM images show that branches of the apicoplast network are recruited to the CPs at the start of merozoite segmentation. Prior to apicoplast division, all apicoplast branch-endings associate with all the CPs in the parasite over the entire length of the organelle. The CP-apicoplast association continues after apicoplast division. These observations suggest that CPs play a central role in apicoplast segregation in *P. falciparum* through recruitment of the apicoplast branches to ensure each merozoite ends up with a single apicoplast. In the apicomplexan parasite *S. neurona*, apicoplast-centrosome associations have likewise been observed during replication[60]. In *T. gondii*, centrosomes have also been shown to play an important role in apicoplast segregation[98,99]. The actin-myosin system is essential for apicoplast-centrosomes interaction and apicoplast segregation[99,100]. Myosin F (MyoF) is an Apicomplexa-specific myosin that is

crucial for parasite survival[101]. In *T. gondii* parasites lacking *Tg*MyoF, the apicoplast fails to associate with the centrosomes, leading to asymmetric segregation of the apicoplast into a single daughter cell or the residual body[99,101]. Interestingly, mitochondrial morphology and inheritance were not affected by *Tg*MyoF depletion[101]. F-actin localizes to the proximity of the apicoplast in both *T. gondii* and *P. falciparum*[100]. Conditional knockout of actin-1 in *P. falciparum* leads to defective apicoplast segregation, while mitochondrial segregation is unaffected[100,102]. In *P. falciparum*, formin-2, an actin nucleator, localizes to the apicoplast and CPs[103]. Formin-2 is also essential for apicoplast inheritance and daughter cell formation in both *T. gondii* and *P. falciparum*[100]. Taken together, these studies show that actin dynamics are essential for apicoplast segregation and its interaction with CPs in *P. falciparum*. Therefore, I hypothesize that apicoplast branches might be recruited to the CPs by myosin-mediated transport along actin filaments (Figure 4B). Formin-2 is an essential actin nucleator that facilitates actin polymerization. To further investigate this hypothesis, super-resolution imaging approaches, such as SIM or STED, could be used to visualize actin filaments with the actin chromobody during merozoite development. Visualization of actin filaments using ExM could also be considered, using the actin chromobody with an ExM-compatible tag, such as an HA- or spaghetti monster-tag. The effect of disruption of actin dynamics (e.g. through formin-2 knockdown or actin-targeted compounds) on these filaments and actin recruitment could be studied. The role of MyoF in apicoplast segregation in *P. falciparum* could be investigated by conditional knockout or knockdown of MyoF in parasites with a fluorescent apicoplast marker. To identify potential adaptor proteins that bind the apicoplast to the cargo domain of MyoF motor protein, a pulldown approach could be used.

Mitochondrial segregation mechanisms

In contrast to the apicoplast, the mitochondrion does not associate with the CPs during its segregation process, as shown in **chapter 3**. Moreover, disruption of actin dynamics by conditional knockout of actin-1 or formin-2 does not affect mitochondrial division and segregation[100,102]. This indicates that mitochondrial segregation is likely facilitated by a distinct mechanism that does not rely on the recruitment of the organelle to the CPs via actin-myosin motors. In **chapter 3**, we show that in schizonts that have completed apicoplast division, the mitochondrial branches extend towards the basal ends of the divided apicoplast. In more developed schizonts, each mitochondrial branch aligns with a divided apicoplast branch over the complete length of this organelle. This association persists during and after mitochondrial division. The timing and organization of these organelle interactions suggest a potential role of the apicoplast in mitochondrial segregation. Nevertheless,

doxycycline-treated apicoplast-negative parasites rescued by IPP supplementation are still able to grow normally, suggesting that the apicoplast is not essential for mitochondrial segregation[104]. However, recent evidence suggests that while these parasites do lose apicoplast DNA and normal apicoplast structure, function of several apicoplast enzymes is still intact, suggesting the presence of apicoplast remnants[105]. Possibly, these remnants would be sufficient to facilitate mitochondrial recruitment and segregation. Nevertheless, the membranous nature of the apicoplast makes it unlikely to facilitate the pulling force required to draw the mitochondrion into the merozoite. Cytoskeletal structures are likely necessary to generate these pulling forces. In *T. gondii*, tethering between the mitochondrion and the IMC is crucial for mitochondrial morphology and mitochondrial distribution during cell division. The tethering is facilitated by the interaction between the mitochondrial membrane-associated protein lasso maintenance factor 1 (LMF1) and inner membrane complex protein 10 (IMC10)[58]. However, this IMC-mitochondrial interaction has not been observed in *Plasmodium* parasites which lack a homolog of LMF1.

Organelle transport in human cells is facilitated by kinesin and dynein motor proteins along microtubules. *Plasmodium* parasites rely on a scaffold of subpellicular microtubules (SPMTs) as the main cytoskeletal structure. These SPMTs are anchored to the apical ring and locate below the IMC but their number and organization varies between different life-cycle stages[106]. *Plasmodium* merozoites harbor 2-3 subpellicular microtubules, a structure that is also referred to as the f-MAST. Depolymerization of the f-MAST by dinitroaniline induction on post-mitotic schizonts reduced invasion rates[107]. EM-studies have shown that the mitochondrion and apicoplast locate directly beneath the f-MAST in free merozoites[108–110]. A study from Fowler *et al*. has tested the effect of a tubulin depolymerization compound, pendimethalin, on mitochondrial segregation[107]. No difference was found between number of mitochondria per merozoite in control and pendimethalin treated cultures, suggesting that SPMTs do not play an essential role in mitochondrial segregation. However, the percentage of merozoites with mitochondria in fully segmented schizonts are lower (60%) than those in observed in our FIB-SEM images (100%). Additionally, it is not clear in the paper what the exact timing is of the induced tubulin depolymerization, and it would be possible that mitochondrial branches have already entered merozoites when tubulin depolymerization is induced. It would therefore be interesting to repeat these experiments, using better high-resolution imaging techniques, ExM or even FIB-SEM to re-test this hypothesis. The results from **chapter 3** also give a much better understanding of the exact timing of mitochondrial recruitment into the forming merozoites and would allow more precise timing of tubulin depolymerization in this experiment.

This would give us a better understanding of the role of SPMTs in mitochondrial segregation during merozoite formation.

Plasmodium parasites harbor 9 kinesin genes but they lack genes for the three classical kinesins (kinesin-1, kinesin-2, kinesin-3) normally involved in intracellular transport[111]. Only one *Plasmodium* kinesin, kinesin-13, is essential in ABS. Kinesin-13 localizes to both the cytoplasm and nucleus in ABS schizonts. However, it's exact localization during mitochondrial segregation stages has not yet been studied. SPMTs in merozoites have their minus end at the apical pole and their plus end reaching toward the basal cell pole[106]. Since kinesins move cargo to the plus end of microtubules (anterograde transport), it is unlikely that they could pull mitochondrial branches into the merozoites via the SPMTs. Dynein on the other hand transport cargo to the minus end of the microtubules (retrograde transport). The cytoplasmic dynein motor complex usually consists of two heavy identical heavy chain subunits, which contain ATPase hydrolysis sites and is responsible for the "walking" movement along the microtubules[112]. The long N-terminal stem interacts with intermediate chains, light intermediate chains and light chains to form the carbo-binding domain of the complex[113]. *P. falciparum* encodes 17 genes, which include 7 dynein heavy chains, 2 dynein intermediate chains, 1 dynein intermediate light chain, and 7 dynein light chains[114]. Monoclonal antibodies against dynein heavy and intermediate chains purified from chicken brain, showed that cross-reactive dyneins are only expressed in late stage schizonts and purified merozoites[115]. However, very little is known about the function of these proteins in *P. falciparum*. Future studies could use targeted genetic strategies, such as conditional knockout or knockdown, to study the role of *P. falciparum* dynein. Nevertheless, the timing of dynein expression and their retrograde transport function leaves room to speculate on a role for dynein motors in transport of mitochondrial branches into the forming merozoites along SPMTs, perhaps guided by contact with the apicoplast (Figure 4C).

Figure 4. Organelle segregation mechanisms. A) Mitochondrial transport mechanisms in human cells. Kinesins transport mitochondria along microtubules towards the plus end, while dyneins transport mitochondria towards the minus end. Miro is anchored into the OMM and interacts with Milton, which binds to the cargo domain of kinesins or dynein. Myosin-19 anchors mitochondria to actin filaments. B) Hypothetical apicoplast segregation mechanism in *P. falciparum*. Myosin-F and a potentially unidentified adaptor protein recruit the apicoplast branches along actin filaments towards the centriolar plaques (CPs). Actin filaments are nucleated by formin-2. C) Hypothetical mitochondrial segregation mechanism in *P. falciparum*. Mitochondrial branches are recruited along actin filaments by dynein along the subpellicular microtubules (SPMTs) towards the apical minus end. Unidentified adaptor proteins attach the dynein to the OMM. The apicoplast might have a role in guiding the mitochondrion into the merozoite and their contact might be mediated by unknown proteins. >

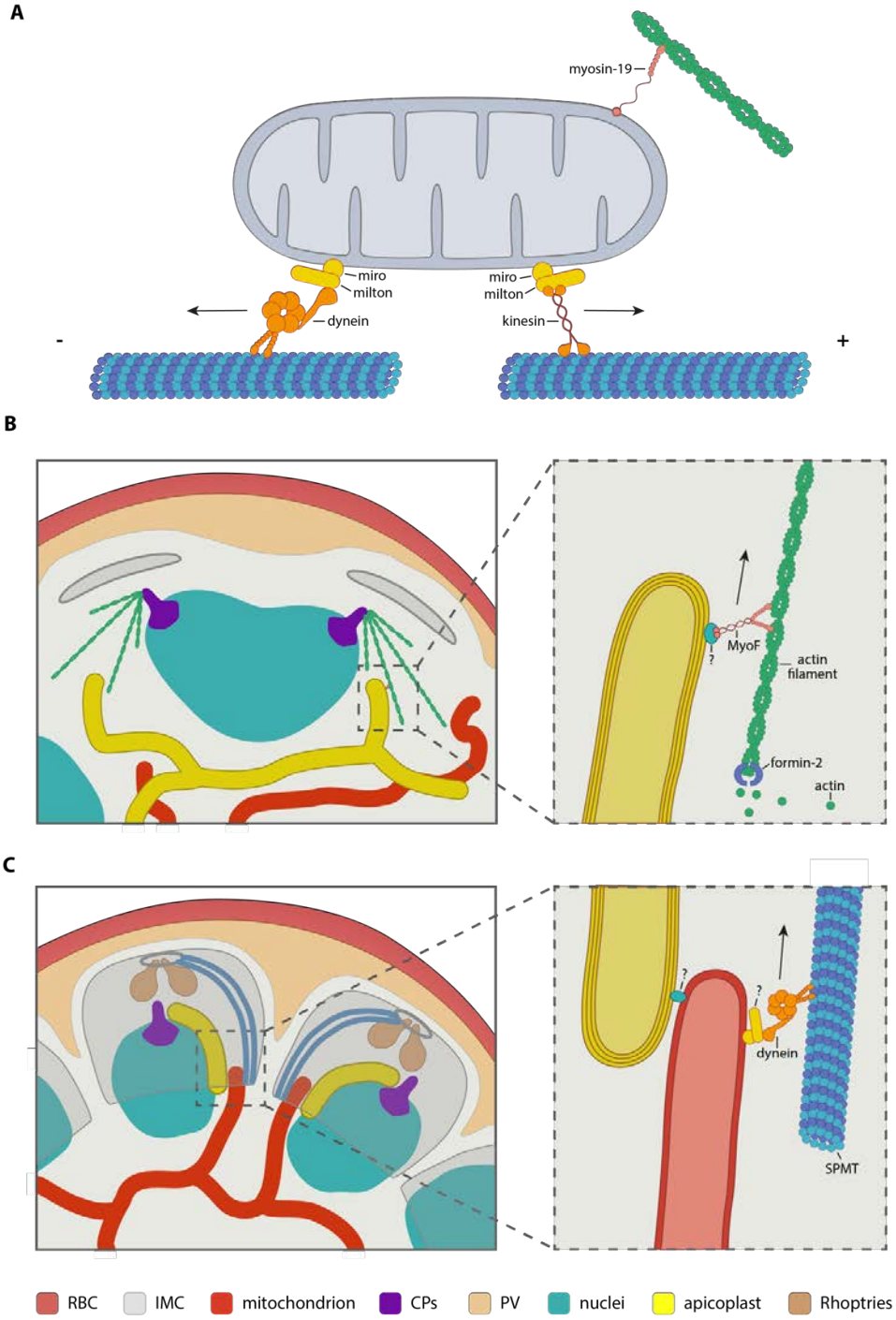
A
myosin-19
miro
milton
dynein
miro
milton
kinesin
-
+
B
MyoF
?
actin
filament
formin-2
actin
C
?
?
dynein
SPMT
RBC
IMC
mitochondrion
CPs
PV
nuclei
apicoplast
Rhoptries

Organelle division and segregation as drug target

Organelle fission during cell division in *Plasmodium* parasites is fundamentally different from this process in their human host. In contrast to the binary division in human cells where a large number of organelles are distributed over two daughter cells during division, *Plasmodium* parasites harbor only a single copy of many of their organelles, which needs to be distributed over a large number of daughter cells. Although we have yet to learn the exact molecular mechanisms that underly this division process, it might present an interesting landscape for the search for new parasite-specific drug targets. Similar timing and organization of mitochondrial and apicoplast division between different life-cycle stages suggests an overlapping division and segregation mechanism between different life-cycle stages. Novel compounds targeting this process could therefore potentially target multiple life-cycle stages. In this paragraph, I will discuss which components of the organelle division and segregation mechanisms could potentially be interesting as novel anti-malarial drug targets.

Mitochondrial dysfunction during inflammatory cell stress has been shown to be an important driver of various diseases, such as sepsis and neurodegeneration[116,117]. Inhibition of mitochondrial fission provides a promising strategy to suppress inflammation and prevent diseases[118,119]. Recently developed peptide and small molecule inhibitors prevent Drp1 recruitment by FIS1 and prevents mitochondrial fission under pathological conditions[120]. Although FIS1 is not essential for mitochondrial division in *P. falciparum*, inhibition of binding of *Pf*DYN2 to other anchor proteins could provide an interesting strategy to target apicoplast and mitochondrial division. Dynasore is a dynamin inhibitor that prevents dynamin-mediated endocytosis[121]. In *P. falciparum*, dynasore has been used to prove involvement of PfDYN1 in hemoglobin uptake[77]. Another recent study shows that dynasore and mitochondrial division inhibitor 1 (Mdivi-1) inhibit mitochondrial segregation and induce ROS production, possibly through *Pf*DYN2 inhibition[82]. Although this shows the potential for dynamin inhibitors to kill the parasite, it also shows that there is a chance of cross-reactivity between dynamins from different species and caution is required when dynamin inhibitors would be developed as anti-malarial compounds to prevent off-target effects.

In the previous paragraphs we discussed the important role of actin in apicoplast segregation. Actin is essential in all life-cycle stages and besides its central role in cell division, it also plays a crucial role in deformation of the host RBC and parasite motility during invasion[102]. Actin inhibitors, such as jasplakinolide, cytochalasin D, truncated latrunculins, and sulfonylpiperazine compounds, inhibit parasite

motility and host-cell invasion[122–125]. Disruption of actin dynamics might therefore present a good opportunity for multi-stage parasite drugs. The small molecule inhibitor SMIFH2 targets formin-2 and kills ABS parasites and results in abnormal gametocytes[103]. However, this inhibitor is not parasite-specific and also affects the actin cytoskeletal structures in animal and yeast cells[126,127]. Further studies are needed to test if parasite-specific inhibitors that target actin dynamics can be generated. Myosin inhibitors have recently been developed as treatment for cardiomyopathy in humans[128]. A recently developed compound targeting MyoA blocks invasion in *P. falciparum*[129]. However, compounds targeting MyoF, crucial for apicoplast segregation, have not yet been identified.

Microtubules play a central role in cell division and are established drug targets in a variety of cancers[130,131]. They are an important component of the cytoskeleton and therefore also important for invasion and parasite growth throughout the complete life cycle. The amino acid sequences of alpha and beta tubulin are highly conserved between humans and *P. falciparum*. However, *Plasmodium* tubulin is more similar to plant than to mammalian tubulin. A study from Hirst *et al.* has identified two compounds that specifically target parasite tubulin, without affecting human microtubules[132]. This indicates that microtubules might present an interesting opportunity for the development of parasite-specific antimalarials.

The role of SPFH proteins in mitochondrial dynamics

The Stomatin/Prohibitin/Flotillin/HflKC (SPFH) protein family is a highly conserved family of proteins, which all contain an SPFH domain. Proteins belonging to this family have been indicated in a diverse set of functions, and play a role in several disease pathologies, such as cancer and Alzheimer's disease[133,134]. Despite the large variety of functions of SPFH proteins, it is thought that one structural principle underlies their function[135]. All SPFH proteins are oligomeric and form ring structures in cholesterol-rich membranes. It is thought that these ring structures form membrane microdomains of specific protein and lipid content. A subset of SPFH proteins, including prohibitins (PHBs) and stomatin-like protein 2 (SLP2) localize to the IMM. These proteins have been indicated in various mitochondrial functions, such as cristae morphogenesis, mitochondrial dynamics, protein degradation, cell cycle regulation, and apoptosis[136–141].

Plasmodium parasites harbor four SPFH proteins, including two canonical prohibitins (PHB1, PHB2), stomatin-like protein (STOML) and an unusual myzozoan-

specific prohibitin-like protein (PHBL)[5]. All four *Plasmodium* SPFH proteins are thought to be mitochondrial. STOML is of particular interest, since it localizes to punctate foci at the parasite mitochondrion during oocyst growth, specifically at organelle branching points[5]. As this is a stage during which mitochondrial division is happening, we hypothesized that STOML might have a function in mitochondrial division or segregation. Additionally, it is shown that the STOML homolog in humans, SLP2, forms a complex with *i*-AAA protease YME1L, which is involved in processing of OPA1, regulating mitochondrial dynamics. In the absence of SLP2, the long OPA1 isoform is lost, and stress-induced mitochondrial hyper fusion is prevented[142]. Although *Plasmodium* lacks a clear OPA1 homolog, we were still curious to study if STOML has a function in mitochondrial dynamics.

Characterization of STOML in *P. falciparum*

In **chapter 4**, we explored the function of STOML in *P. falciparum*. Live imaging was used to study the localization of STOML tagged with mNeonGreen in ABS parasites. We found that STOML-mNG localizes to punctate foci on the mitochondria and the number of STOML-mNG foci per parasite increases during ABS development. In trophozoite and schizont stages, STOML-mNG foci localize to mitochondrial branching points and endings of mitochondrial branches. In a late schizont where the mitochondrion orients in a cartwheel structure prior to its division, STOML-mNG localizes to the endings of each mitochondrial branch. This specific localization fits well with a localization that can be expected from a protein that is involved in mitochondrial division or segregation. To further explore the function of STOML, *STOML* knockout parasites were generated. *STOML* knockout caused a significant growth defect, caused by slower development of the parasites throughout the life cycle. There were no obvious differences in mitochondrial morphology between $stoml^{-}_{mito}$ and wild-type parasites, and there was no evidence that mitochondrial division or segregation in $stoml^{-}_{mito}$ parasites was affected. Therefore, it is unlikely that STOML has a direct function in mitochondrial division and segregation, despite its suggestive localization. However, a redundant function of STOML in these processes cannot be completely ruled out.

The human STOML homolog SLP2, is found in cardiolipin rich mitochondrial membrane domains, which are important for the stability of respiratory chain complexes[143]. Decreased levels of SLP2 in T cells caused a decreased activity of respiratory chain complexes, probably due to deficient respiratory chain supercomplex formation. A recent preprint from Sparkes *et al.* has shown that

mitochondrial respiration is essential for ATP production during gametogenesis[144]. We hypothesized that if STOML would have a function in ETC chain assembly, *stoml*$^{-}_{mito}$ parasites would not be able to form gametes. However, *stoml*$^{-}_{mito}$ parasites were able to form healthy-looking gametocytes and male gametocytes were exflagellating. To further investigate this hypothesis, we tested if *stoml*$^{-}$ parasites had an increased sensitivity for drugs targeting the respiratory chain, such as atovaquone. However, there was no difference in drug sensitivity between *stoml*$^{-}$ and wild-type parasites, indicating that STOML does not have a direct function in respiratory chain assembly. Nevertheless, it is important to realize that this assay is not a direct readout of ETC protein complex assembly. A recent preprint shows that inducible knockdown of the complex III subunit *Pf*Rieske, which is essential in ABS, does cause hypersensitivity to ETC targeting drugs[145], indicating that the readout of this assay indeed reflects if ETC is intact. Alternatively, future studies could use complexome profiling in *stoml*$^{-}$ parasites to test if ETC supercomplex formation is affected. The effect of *STOML* knockout on transmission to the mosquito and mosquito stage development could also be tested.

Complexome profiling data showed that STOML resides in a large ~2 MDa protein complex[146]. To further explore the function of STOML, two independent pulldown experiments were performed to identify potential interaction partners. A protein of unknown function (PF3D7_1306200) and FtsH ATP-dependent zinc metalloprotease (PF3D7_1464900) were significantly enriched in both pulldown experiments. While complexome profiling data showed that PF3D7_1306200 did not co-migrate with STOML on a native-page gel, FtsH showed co-migration on a native-page gel in gametocyte stages. PF3D7_1306200 contains an AB-hydrolase domain and is predicted to be essential[22]. A recently characterized AB-hydrolase domain containing protein, ABHD16A, has been shown to localize to the ER-mitochondrial contact sites and regulates the recruitment of the fission and fusion machineries, by altering phospholipid composition[147]. However, AB-hydrolase containing proteins belong to one of the largest superfamilies and include proteases, lipases, peroxidases, esterase, epoxide hydrolyses, and dehalogenases. Therefore, it is hard to predict the function of PF3D7_1306200 based on this domain. It's predicted apicoplast targeting sequence[148] and lack of comigration with STOML on a native gel shown by complexomics data[146] make it unlikely that PF3D7_1306200 forms a complex with STOML at the IMM. However, the consistent pulldown could be explained by a potential mitochondrial localization of PF3D7_1306200, as it ranks at place 126 out of the 445 predicted mitochondrial proteins, with a mitochondrial score of 4.72[149]. If PF3D7_1306200 is indeed a mitochondrial protein, it would be possible that it interacts with STOML. To further verify interaction between

FtsH or PF3D7_1306200 and STOML, tagged parasites lines could be generated and reciprocal pulldown and co-localization experiments could be performed. Additionally, the roles of FtsH and PF3D7_1306200 could be investigated by generation of conditional knockout or knockdown parasite lines.

SPFH proteins are known to form large protein complexes with metalloproteases, regulating their protease activity[136,150,151]. The human, *Arabidopsis thaliana*, and *Trypanosma brucei* homologs of *Pf*STOML, form a large proteolytic complex with YME1L/FTSH4, which are FtsH homologs[151–153]. This indicates that FtsH is a very likely interaction partner of STOML, since the STOML-FtsH complex is conserved across different eukaryotes.

The role of FtsH/AAA metalloproteases

FtsH metalloproteases are present in bacteria, as well as organelles of bacterial origin, such as chloroplasts and mitochondria (in mitochondria they are often referred to as AAA proteases). Most bacteria harbor only a single FtsH gene, while yeast and humans have three genes, and higher plants can have up to 12 FtsH genes[154–156]. FtsH/AAA proteases are highly conserved and contain three functional domains: one or two N-terminal transmembrane domains (TMDs), an ATPase domain of the AAA superfamily, and a C-terminal metallopeptidase domain[157] (Figure 5). The presence of one or two TMDs determines the topology of the protease in the membrane. *i*-AAA proteases have one TMD and have their proteolytic domain exposed to the intermembrane space in mitochondria, while *m*-AAA proteases have two TMDs and have their active site exposed to the mitochondrial matrix. Six subunits assemble into a functional *m*-AAA or *i*-AAA protease[158].

Optimal functioning of mitochondria depends on the accurate composition and quality of the mitochondrial proteome[159,160]. AAA proteases have a central role in mitochondrial quality control, by selective degradation of damaged, unassembled, and excessive mitochondrial proteins[157,158]. One of the greatest threats in mitochondria that necessitates tight monitoring and regulation is the ROS-generating oxidative phosphorylation (OXPHOS) system. Rapid removal of defective OXPHOS components is essential to prevent accumulation of aggregation-prone polypeptides that can lead to uncontrolled ROS formation and mitochondrial dysfunction[160–162]. AAA proteases play a central role in this task. In mammals, yeast, and plants both *m*-AAA and *i*-AAA proteases have been shown to remove aberrant components of the respiratory chain complexes or ATP synthase at both sides of the

IMM[160,161,163–165]. Oxidatively damaged mitochondrial proteins that arise as a result of imbalanced OXPHOS functioning are also degraded by AAA proteases[152,161,166]. AAA proteases also contributed to the formation and maintenance of other IMM complexes, such as mitochondrial calcium uniporter (MCU) and mitochondrial cristae organizing system (MICOS)[167–171].

More and more studies have indicated a role of AAA proteases outside of protein quality control. AAA proteases are capable of highly specific proteolytic processing. The best-known example of this is *m*-AAA mediated processing of the nuclear-encoded subunit of the mitochondrial ribosome, MrpL32[172–174]. This mechanism is highly conserved in yeast, mammals, and plants. The mammalian and yeast *i*-AAA protease Yme1L influences mitochondrial protein import during stress by removal of TIM17 subunit of TIM23 translocase[175,176]. This downregulation of the import pathway leads to a substantial reduction of unfolded polypeptides entering the organelle[177]. Additionally, yeast and mammalian *i*-AAA proteases control the turnover of Ups1, Ups2 and PRELID1 respectively, which regulate biogenesis of cardiolipin and phosphatidylethanolamine, two mitochondria-specific phospholipids[178,179].

Plasmodium parasites harbor three FtsH proteins, including one predicted *m*-AAA protease (PF3D7_1119600) and two *i*-AAA proteases (PF3D7_1464900, PF3D7_1239700)[180]. The *Pf*FtsH identified as potential STOML interaction partner clusters together with *i*-AAA proteases at the IMM, which have their proteolytic domain exposed to the intermembrane space. The function of the other *i*-AAA protease FtsH1 (PF3D7_1239700) has been studied in *P. falciparum*. *Pf*FtsH1 is shown to form higher order oligomers and exhibits zinc- and ATP-dependent protease activity. Expression of *Pf*FtsH1 in *E. coli* causes defective cytokinesis, suggesting a potential role in organelle division. While one study localizes FtsH1 to foci on the mitochondrion[180], other evidence suggests a function in apicoplast biogenesis and FtsH1 has been localized to the apicoplast in *T. gondii*[181,182]. Knockdown of *Pf*FtsH1 caused a gradual loss of the apicoplast genome and a significant growth defect, which could be rescued by IPP supplementation, indicating a potential role of FtsH1 in apicoplast biogenesis or segregation[181]. Future studies could use a microscopy approach to study apicoplast division and segregation in *Pf*FtsH1 knockdown parasites to confirm this role of *Pf*FtsH1. The roles of the other two FtsH proteins in *P. falciparum*, remain to be investigated. Unfortunately, attempts to generate endogenously tagged knockdown parasites to study localization and function of these FtsH proteins were unsuccessful[181].

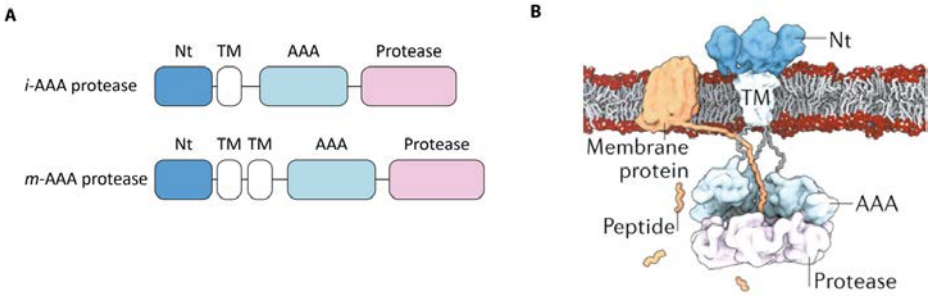

Figure 5. General domain structure of FtsH/AAA proteases. A) Protein domains of i-AAA and m-AAA proteases with N-terminal domain (Nt), transmembrane domain (TM), ATPase domain of AAA superfamily (AAA), protease domain (Protease). B) General structure of AAA+ protease and substrate membrane protein at the inner mitochondrial membrane, with permission adapted from Puchades et al.[183].

The role of the STOML-FtsH supercomplex

Cryo-electron microscopy has demonstrated that the bacterial HflK/C form a large oligomeric structure around membrane-anchored FtsH hexamers[150,184]. This barrel-like HflK/C complex surrounds FtsH proteases and likely serves to prevent other membrane proteins from approaching FtsH, thereby avoiding the unwanted degradation of functional membrane proteins. Additionally, the HflK/C enclosure facilitates the identification of defective membrane proteins. Damaged or misfolded proteins, which tend to have flexible, unfolded termini, can be selectively recognized by this complex. In **chapter 4**, we showed that AlphaFold multimer predicts STOML to form a similar oligomeric barrel structure. These results indicate that STOML might form an analogous supercomplex with FtsH in *P. falciparum*, possibly regulating FtsH accessibility. Depletion of STOML would lead to more accessible FtsH and therefore possibly higher FtsH-mediated mitochondrial protein degradation. This would disturb normal mitochondrial function and could explain why STOML knockout caused slower parasite development throughout the ABS. The bacterial HflK and HflC are also not essential, but their role becomes more important under stress conditions when there is a higher chance of protein damage or misfolding[185]. Knockout of HflK or HflC cause hypersensitivity to aminoglycoside antibiotics, which induce mistranslation leading to disassembled or misfolded membrane proteins[185,186]. It would therefore be interesting to study the effect of stress-induced conditions on *stoml*$^-$ parasites. Future studies could test the effect of mitochondrial stress (e.g. by starvation conditions, usage of a mitochondrial-protease inhibitor, or induction of oxidative stress by H_2O_2) on parasite survival and mitochondrial function in *stoml*$^-$ and wild-type parasites.

The function of the FtsH-STOML complex could also be explored through characterization of FtsH function. Inducible knockout or knockdown lines could be generated to study the effect of FtsH depletion on parasite growth, mitochondrial morphology and function, and protein degradation. A proteomics approach could be used to investigate the changes in mitochondrial protein levels upon STOML of FtsH depletion. Additionally, a complexomics approach can be used to study the effect of FtsH depletion on mitochondrial complex formation.

Apicomplexan evolution might be able to reveal more insights into the function of the FtsH-STOML complex. For instance, *Cryptosporidium* parasites lack a canonical mitochondrion but instead harbor a mitochondrial remnant referred to as the mitosome[187]. Mitosomes have lost mtDNA and lack most mitochondrial functions. All *Cryptosporidium* species harbor components for iron-sulfur cluster biogenesis, while complex III and IV of the respiratory chain are replaced by an alternative oxidase[188,189]. However, there are also some striking differences between *Cryptosporidium* species (Table 2). While the gastric-type parasites *Cryptosporidium muris* and *Cryptosporidium andersoni* still harbor components of the TCA cycle, as well as complex II and V of the respiratory chain, the intestinal-type parasites *Cryptosporidium parvum* and *Cryptosporidium hominis* lack all these components and merely harbor an alternative complex I[188]. Interestingly, a BLAST search revealed that a STOML homolog is present in *C. muris* and *C. andersoni*, while it is absent in *C. parvum* and *C. hominis* (Table 2). However, all *Cryptosporidium* species lack an FtsH (*i*-AAA protease) homolog, while *C. muris*, *C. andersoni*, and *C. parvum* have a *m*-AAA protease homolog. *C. hominis* lacks an FtsH/AAA protease homolog. These findings indicate that STOML is likely not involved in iron-sulfur cluster biogenesis or maintenance of mtDNA. As STOML can be found in species that lack *i*-AAA proteases, it is possible that STOML has additional functions besides its role in protein quality control in the STOML-FtsH complex. The presence of STOML specifically in *Cryptosporidium* species that harbor TCA cycle components and truncated ETC indicate that the function of STOML might be linked to the expression or function of these pathways. Future studies could perform a more detailed bioinformatic analysis to study the presence of STOML and FtsH proteases across apicomplexan species with different mitochondrial components. This could give new insights into their potential function as well as the potential function of the STOML-FtsH complex.

Table 2. Distribution of SPFH and mitochondrial metabolic proteins across Apicomplexa.

species	STOML	Prohibitin	PHBL	FtsH /AAA	TCA cycle	I	II	III, IV	V
Plasmodium falciparum	🟢	🟢	🔴	i,i,m	🟢	🟢	🟢	🟢	🟢
Toxoplasma gondii	🟢	🟢	🔴	i,i,m	🟢	🟢	🟢	🟢	🟢
Cryptosporidium muris	🟢	🟢	🔴	m	🟢	🟢	🟢	🔴	🟢
Cryptosporidium andersoni	🟢	🟢	🔴	m	🟢	🟢	🟢	🔴	🟢
Cryptosporidium parvum	🔴	🟢	🔴	m	🔴	🟢	🔴	🔴	🔴
Cryptosporidium hominis	🔴	🟢	🔴	-	🔴	🟢	🔴	🔴	🔴

A BLAST search was performed to identify homologs to Plasmodium SPFH proteins and FtsH/AAA proteases in other apicomplexan species. The presence of a homolog is indicated by a green circle and the absence by a red circle. The presence of and number of i-AAA proteases is indicated by "i", while the presence and number of m-AAA proteases is indicated by "m". The presence of TCA cycle proteins, alternative complex I (I), and other electron transport chain complexes (complex II, complex III and IV, and complex V) are indicated.

SPFH proteins and FtsH/AAA proteases as drug target

SPFH proteins have been shown to regulate the activity FtsH/AAA proteases in bacteria and eukaryotes through the formation of supercomplexes[150,151,190,191]. These complexes play a crucial role the protein quality control mechanism in bacteria and endosymbiotic organelles[150,151,184,192]. The mitochondrion and apicoplast of *Plasmodium* parasites provide attractive drug targets, as discussed in previous paragraphs. In the next paragraph, I will explore if mitochondrial SPFH proteins and AAA proteases have a potential as novel anti-malarial drug targets.

Prohibitins are overexpressed in various cancers. Several compounds, including fluorizoline and Rocaglamide (Roc-A), can be used as anti-cancer compound by targeting PHB1 and PHB2, preventing CRAF activation and sensitizing cancer cells to apoptosis[193,194]. A recent study showed that Roc-A interacts with *Pf*PHBs and inhibits growth of yeast mutants that were functionally complemented with *Pf*PHBs, validating them as a Roc-A target[195]. Roc-A treatment of parasites inhibited growth at nanomolar concentrations in ABS and gametocyte stages and significantly reduces parasite transmission. These results validated RocA as an efficient antimalarial compound through targeting of *Pf*PHBs.

The other two SPFH proteins in *Plasmodium* parasites, STOML and PHBL, are not essential for parasite survival and might therefore be less interesting drug targets. Nevertheless, in **chapter 4**, we showed that knockout of STOML causes a significant growth defect in *P. falciparum*. Inhibition of STOML by a small-molecule inhibitor could therefore potentially reduce parasite replication rates. Additionally, it is possible that the potential function of STOML in mitochondrial protein quality control becomes more important during stress conditions when there is a higher chance of protein damage and misfolding, as discussed in the previous paragraph. STOML impaired parasites might therefore become more sensitive to oxidative damage and potentially also to antimalarials that act through increased oxidative stress. Therefore, STOML targeting compounds could be interesting as a combination therapy with other compounds by increasing parasite sensitivity to compounds that act through via increasing of oxidative stress. Quinolones, such as chloroquine, increase oxidative stress in *Plasmodium* parasites by inhibiting the conversion of free heme to hemozoin[196]. It is thought that artemisinins, such as dihydroartemisinin (DHA), execute their antimalarial function through interaction with iron, leading to the production of free radicals and oxidative stress[197]. However, in **chapter 4**, we showed that *stoml*$^{-}$ parasites did not have an increased sensitivity to chloroquine and DHA. Therefore, it is unlikely STOML targeting compounds could increase drug sensitivity to oxidative stress-inducing compounds.

FtsH/AAA proteases might provide promising antimalarial drug target, given their likely essential role in protein quality control in the mitochondrion and apicoplast. All three FtsH proteins in *P. falciparum* are predicted to be essential[22], and depletion of FtsH1 has been shown to significantly inhibit parasite growth[181]. Several unsuccessful attempts to generate endogenously-tagged knockdown lines of the other two FtsH proteins suggests their likely essential role[181]. Furthermore, it has been shown that Actinonin, a small molecule inhibitor, is able to kill parasites at low µM concentrations by targeting *Pf*FtsH1 and inhibiting apicoplast biogenesis[181]. Future studies could further explore the promising potential of these proteases as drug targets.

Concluding remarks

Although great progress has been made the past century in our understanding of the malaria parasite, there are still many aspects of its molecular biology that we do not understand. Rapid rise of resistance to current antimalarials requires the continuous development of novel drugs. The unique parasite mitochondrion and apicoplast provide excellent parasite-specific drug targets. Understanding

the intricate mechanisms of their division and segregation could expose new vulnerabilities of the parasite. This thesis has provided many new mechanistic insights in the timing and orchestration of mitochondrial and apicoplast division and segregation. Our findings also highlighted the close interaction between the mitochondrion and apicoplast during parasite replication and revealed the role of the CPs in apicoplast but not mitochondrial segregation. Although the localization of STOML suggested a potential role in mitochondrial division or segregation, knockout of the protein did not seem to affect mitochondrial morphology or division. We showed the potential interaction of STOML with the *i*-AAA protease, FtsH. AlphaFold predictions of the STOML multimeric structure highlight the potential role of STOML in regulating accessibility of FtsH, and therefore mitochondrial protein quality control. This knowledge is not only fundamental to better understand the molecular biology of the parasite but paves the way for future exploration of these mechanisms as potential antimalarial drug targets.

References

1. Boualam, M. A., Pradines, B., Drancourt, M. & Barbieri, R. Malaria in Europe: A Historical Perspective. *Front. Med.* **8**, 7–9 (2021).
2. van Dooren, G. G. *et al.* Development of the endoplasmic reticulum, mitochondrion and apicoplast during the asexual life cycle of Plasmodium falciparum. *Mol. Microbiol.* **57**, 405–419 (2005).
3. Jackson, K. E. *et al.* Dual targeting of aminoacyl-tRNA synthetases to the apicoplast and cytosol in Plasmodium falciparum. *Int. J. Parasitol.* **42**, 177–186 (2012).
4. Okamoto, N., Spurck, T. P., Goodman, C. D. & McFadden, G. I. Apicoplast and mitochondrion in gametocytogenesis of Plasmodium falciparum. *Eukaryot. Cell* **8**, 128–132 (2009).
5. Matz, J. M., Goosmann, C., Matuschewski, K. & Kooij, T. W. A. An Unusual Prohibitin Regulates Malaria Parasite Mitochondrial Membrane Potential. *Cell Rep.* **23**, 756–767 (2018).
6. Vega-Rodríguez, J. *et al.* The glutathione biosynthetic pathway of Plasmodium is essential for mosquito transmission. *PLoS Pathog.* **5**, 16–18 (2009).
7. Sturm, A., Mollard, V., Cozijnsen, A., Goodman, C. D. & McFadden, G. I. Mitochondrial ATP synthase is dispensable in blood-stage Plasmodium berghei rodent malaria but essential in the mosquito phase. *Proc. Natl. Acad. Sci. U. S. A.* **112**, 10216–10223 (2015).
8. Stanway, R. R. *et al.* Organelle segregation into Plasmodium liver stage merozoites. *Cell. Microbiol.* **13**, 1768–1782 (2011).
9. Ngotho, P. *et al.* Revisiting gametocyte biology in malaria parasites. *FEMS Microbiol. Rev.* **43**, 401–414 (2019).
10. Boltryk, S. D. *et al.* CRISPR/Cas9-engineered inducible gametocyte producer lines as a valuable tool for Plasmodium falciparum malaria transmission research. *Nat. Commun.* **12**, 1–16 (2021).
11. Ponnudurai, T., Lensen, A. H. W., Meis, J. F. G. M. & Meuwissen, J. H. E. Synchronization of Plasmodium falciparum gametocytes using an automated suspension culture system. *Parasitology* **93**, 263–274 (1986).
12. Graumans, W. *et al.* AlbuMAX supplemented media induces the formation of transmission-competent P. falciparum gametocytes. *bioRxiv* 1–9 (2024).
13. Eappen, A. G. *et al.* In vitro production of infectious Plasmodium falciparum sporozoites. *Nature* **612**, 534–539 (2022).
14. Valenciano, A. L., Gomez-Lorenzo, M. G., Vega-Rodríguez, J., Adams, J. H. & Roth, A. In vitro models for human malaria: targeting the liver stage. *Trends Parasitol.* **38**, 758–774 (2022).
15. Roth, A. *et al.* A comprehensive model for assessment of liver stage therapies targeting Plasmodium vivax and Plasmodium falciparum. *Nat. Commun.* **9**, 1–16 (2018).
16. Collins, C. R. *et al.* Robust inducible Cre recombinase activity in the human malaria parasite Plasmodium falciparum enables efficient gene deletion within a single asexual erythrocytic growth cycle. *Mol. Microbiol.* **88**, 687–701 (2013).
17. Ghorbal, M. *et al.* Genome editing in the human malaria parasite Plasmodium falciparum using the CRISPR-Cas9 system. *Nat. Biotechnol.* **32**, 819–821 (2014).
18. Gardner, M. J. *et al.* Genome sequence of the human malaria parasite Plasmodium falciparum. *Nature* **419**, 498–511 (2002).
19. Lee, M. C. S. & Fidock, D. A. CRISPR-mediated genome editing of Plasmodium falciparum malaria parasites. *Genome Med.* **6**, 1–4 (2014).

20. Lee, A. H., Symington, L. S. & Fidock, D. A. DNA Repair Mechanisms and Their Biological Roles in the Malaria Parasite Plasmodium falciparum. *Microbiol. Mol. Biol. Rev.* **78**, 469–486 (2014).
21. Bushell, E. *et al.* Functional Profiling of a Plasmodium Genome Reveals an Abundance of Essential Genes. *Cell* **170**, 260-272.e8 (2017).
22. Zhang, M. *et al.* Uncovering the essential genes of the human malaria parasite Plasmodium falciparum by saturation mutagenesis. *Science* **360**, eaap7847 (2018).
23. Skinner-Adams, T. S., Lawrie, P. M., Hawthorne, P. L., Gardiner, D. L. & Trenholme, K. R. Comparison of Plasmodium falciparum transfection methods. *Malar. J.* **2**, 1–4 (2003).
24. Wu, Y., Sifri, C. D., Lei, H. H., Su, X. Z. & Wellems, T. E. Transfection of Plasmodium falciparum within human red blood cells. *Proc. Natl. Acad. Sci. U. S. A.* **92**, 973–977 (1995).
25. ThermoFisher. *Transfecting Plasmid DNA into HEK 293 Cells Using Lipofectamine LTX Reagent*. (2006).
26. Aravind, L., Iyer, L. M., Wellems, T. E. & Miller, L. H. Plasmodium Biology: Genomic Gleanings. *Cell* **115**, 771–785 (2003).
27. Kudyba, H. M., Cobb, D. W., Vega-Rodríguez, J. & Muralidharan, V. Some conditions apply: Systems for studying Plasmodium falciparum protein function. *PLoS Pathog.* **17**, 1–16 (2021).
28. Verhoef, J. M. J., Meissner, M. & Kooij, T. W. A. Organelle dynamics in apicomplexan parasites. *MBio* **12**, (2021).
29. Ramaprasad, A. & Blackman, M. J. A scaleable inducible knockout system for studying essential gene function in the malaria parasite. *bioRxiv* 2024.01.14.575607 (2024).
30. Durrant, M. G. *et al.* Bridge RNAs direct modular and programmable recombination of target and donor DNA. *Nature* **630**, 984–993 (2024).
31. Hiraizumi, M. *et al.* Structural mechanism of bridge RNA-guided recombination. *Nature* **630**, 994–1002 (2024).
32. Karathanasis, C., Sanchez, C. P., Heilemann, M. & Lanzer, M. Assessing Antigen Presentation on the Surface of Plasmodium falciparum-Infected Erythrocytes by Photoactivated Localization Microscopy (PALM). *Methods Mol. Biol.* **2470**, 457–466 (2022).
33. Schloetel, J. G., Heine, J., Cowman, A. F. & Pasternak, M. Guided STED nanoscopy enables super-resolution imaging of blood stage malaria parasites. *Sci. Rep.* **9**, 1–10 (2019).
34. Woodland, J. G., Hunter, R., Smith, P. J. & Egan, T. J. Chemical Proteomics and Super-resolution Imaging Reveal That Chloroquine Interacts with Plasmodium falciparum Multidrug Resistance-Associated Protein and Lipids. *ACS Chem. Biol.* **13**, 2939–2948 (2018).
35. Tilley, L. *et al.* Super-resolution optical imaging of malaria parasites. *Opt. InfoBase Conf. Pap.* 368–369 (2011).
36. Wolpers, C. Zur elektronoptischen Darstellung der Malaria tertiana. *Klin. Wochenschr.* **18**, (1942).
37. Collinson, L. M. *et al.* Volume EM: a quiet revolution takes shape. *Nat. Methods* **20**, 777–782 (2023).
38. Chen, F., Tillberg, P. W. & Boyden, E. S. Expansion microscopy. *Science (80-.).* **347**, 543–548 (2015).
39. Gambarotto, D. *et al.* Imaging cellular ultrastructures using expansion microscopy (U-ExM). *Nat. Methods* **16**, 71–74 (2019).
40. Liffner, B. *et al.* Atlas of Plasmodium falciparum intraerythrocytic development using expansion microscopy. *Elife* 1–39 (2023) doi:10.1101/2023.03.22.533773.
41. Louvel, V. *et al.* iU-ExM: nanoscopy of organelles and tissues with iterative ultrastructure expansion microscopy. *Nat. Commun.* **14**, (2023).
42. Laporte, M. H., Klena, N., Hamel, V. & Guichard, P. Visualizing the native cellular organization by coupling cryofixation with expansion microscopy (Cryo-ExM). *Nat. Methods* **19**, 216–222 (2022).

43. Molina-Cruz, A., Canepa, G. E. & Barillas-Mury, C. Plasmodium P47: a key gene for malaria transmission by mosquito vectors. *Curr. Opin. Microbiol.* **40**, 168–174 (2017).

44. Molina-Cruz, A. *et al.* Plasmodium falciparum evades immunity of anopheline mosquitoes by interacting with a Pfs47 midgut receptor. *Proc. Natl. Acad. Sci. U. S. A.* **117**, 2597–2605 (2020).

45. Vaughan, A. M. *et al.* A transgenic Plasmodium falciparum NF54 strain that expresses GFP-luciferase throughout the parasite life cycle. *Mol. Biochem. Parasitol.* **186**, 143–147 (2012).

46. Wilde, M. L. *et al.* Protein kinase A is essential for invasion of Plasmodium falciparum into human erythrocytes. *MBio* **10**, (2019).

47. Carrasquilla, M. *et al.* Barcoding Genetically Distinct Plasmodium falciparum Strains for Comparative Assessment of Fitness and Antimalarial Drug Resistance. *MBio* **13**, (2022).

48. Taylor, H. M. *et al.* Plasmodium falciparum homologue of the genes for plasmodium vivax and Plasmodium yoelii adhesive proteins, which is transcribed but not translated. *Infect. Immun.* **69**, 3635–3645 (2001).

49. Florens, L. *et al.* A proteomic view of the malaria parasite life cycle. *Proc. 50th ASMS Conf. Mass Spectrom. Allied Top.* **419**, 59–60 (2002).

50. Kooij, T. W. A., Rauch, M. M. & Matuschewski, K. Expansion of experimental genetics approaches for Plasmodium berghei with versatile transfection vectors. *Mol. Biochem. Parasitol.* **185**, 19–26 (2012).

51. Ribeiro, J. M. *et al.* Guide RNA selection for CRISPR-Cas9 transfections in Plasmodium falciparum. *Int. J. Parasitol.* **48**, 825–832 (2018).

52. Sato, S. & Wilson, R. J. M. Organelle-specific cochaperonins in apicomplexan parasites. *Mol. Biochem. Parasitol.* **141**, 133–143 (2005).

53. Tonkin, C. J. *et al.* Localization of organellar proteins in Plasmodium falciparum using a novel set of transfection vectors and a new immunofluorescence fixation method. *Mol. Biochem. Parasitol.* **137**, 13–21 (2004).

54. Bindels, D. S. *et al.* MScarlet: A bright monomeric red fluorescent protein for cellular imaging. *Nat. Methods* **14**, 53–56 (2016).

55. Viswanathan, S. *et al.* High-performance probes for light and electron microscopy. *Nat. Methods* **12**, 568–576 (2015).

56. Francia, M. E. & Striepen, B. Cell division in apicomplexan parasites. *Nat. Rev. Microbiol.* **12**, 125–136 (2014).

57. Nishi, M., Hu, K., Murray, J. M. & Roos, D. S. Organellar dynamics during the cell cycle of Toxoplasma gondii. *J. Cell Sci.* **121**, 1559–1568 (2008).

58. Ornitz, R. *et al.* IMC10 and LMF1 mediate mitochondrial morphology by mitochondrion-pellicle contact sites in Toxoplasma gondii. *J. Cell Sci.* (2022).

59. Melatti, C. *et al.* A unique dynamin-related protein is essential for mitochondrial fission in Toxoplasma gondii. *PLoS Pathog.* **15**, e1007512 (2019).

60. Vaishnava, S. *et al.* Plastid segregation and cell division in the apicomplexan parasite Sarcocystis neurona. *J. Cell Sci.* **118**, 3397–3407 (2005).

61. Araki, T. *et al.* Three-dimensional electron microscopy analysis reveals endopolygeny-like nuclear architecture segregation in Plasmodium oocyst development. *Parasitol. Int.* **76**, 102034 (2020).

62. Stanway, R. R., Witt, T., Zobiak, B., Aepfelbacher, M. & Heussler, V. T. GFP-targeting allows visualization of the apicoplast throughout the life cycle of live malaria parasites. *Biol. cell* **101**, 415–430 (2009).

63. Burda, P.-C. *et al.* A Plasmodium plasma membrane reporter reveals membrane dynamics by live-cell microscopy. *Sci. Rep.* **7**, 9740 (2017).

64. Leger, M. M. *et al.* An ancestral bacterial division system is widespread in eukaryotic mitochondria. *Proc. Natl. Acad. Sci. U. S. A.* **112**, 10239–10246 (2015).

65. Yoshida, Y. Insights into the Mechanisms of Chloroplast Division. *Int. J. Mol. Sci.* **19**, (2018).

66. Miyagishima, S. Mechanism of plastid division: from a bacterium to an organelle. *Plant Physiol.* **155**, 1533–1544 (2011).

67. van Dooren, G. G. *et al.* A novel dynamin-related protein has been recruited for apicoplast fission in Toxoplasma gondii. *Curr. Biol.* **19**, 267–276 (2009).

68. Charneau, S. *et al.* Characterization of PfDYN2, a dynamin-like protein of Plasmodium falciparum expressed in schizonts. *Microbes Infect.* **9**, 797–805 (2007).

69. Friedman, J. R. *et al.* ER tubules mark sites of mitochondrial division. *Science (80-.).* **334**, 358–362 (2011).

70. Chakrabarti, R. *et al.* INF2-mediated actin polymerization at the ER stimulates mitochondrial calcium uptake, inner membrane constriction, and division. *J. Cell Biol.* **217**, 251–268 (2018).

71. Mears, J. A. *et al.* Conformational changes in Dnm1 support a contractile mechanism for mitochondrial fission. *Nat. Struct. Mol. Biol.* **18**, 20–26 (2011).

72. Anand, R. *et al.* The i-AAA protease YME1L and OMA1 cleave OPA1 to balance mitochondrial fusion and fission. *J. Cell Biol.* **204**, 919–929 (2014).

73. Lee, J. E., Westrate, L. M., Wu, H., Page, C. & Voeltz, G. K. Multiple dynamin family members collaborate to drive mitochondrial division. *Nature* **540**, 139–143 (2016).

74. Fonseca, T. B., Sánchez-Guerrero, Á., Milosevic, I. & Raimundo, N. Mitochondrial fission requires DRP1 but not dynamins. *Nature* **570**, E34–E42 (2019).

75. Wu, H., Carvalho, P. & Voeltz, G. K. Here, there, and everywhere: The importance of ER membrane contact sites. *Science* **361**, (2018).

76. Evers, F. *et al.* Comparative 3D ultrastructure of Plasmodium falciparum gametocytes. *bioRxiv* 2023.03.10.531920 (2023).

77. Zhou, H., Gao, Y., Zhong, X. & Wang, H. Dynamin like protein 1 participated in the hemoglobin uptake pathway of Plasmodium falciparum. *Chin. Med. J. (Engl).* **122**, 1686–1691 (2009).

78. Milani, K. J., Schneider, T. G. & Taraschi, T. F. Defining the morphology and mechanism of the hemoglobin transport pathway in Plasmodium falciparum-infected erythrocytes. *Eukaryot. Cell* **14**, 415–426 (2015).

79. Fukushima, N. H., Brisch, E., Keegan, B. R., Bleazard, W. & Shaw, J. M. The GTPase effector domain sequence of the Dnm1p GTPase regulates self-assembly and controls a rate-limiting step in mitochondrial fission. *Mol. Biol. Cell* **12**, 2756–2766 (2001).

80. Breinich, M. S. *et al.* A dynamin is required for the biogenesis of secretory organelles in Toxoplasma gondii. *Curr. Biol.* **19**, 277–286 (2009).

81. Morano, A. A., Xu, W., Shadija, N., Dvorin, J. D. & Ke, H. The dynamin-related protein Dyn2 is essential for both apicoplast and mitochondrial fission in Plasmodium falciparum. *bioRxiv* (2024).

82. Thakur, V. *et al.* A dynamin-like protein in the human malaria parasite plays an essential role in mitochondrial homeostasis and fission during asexual blood stages. *bioRxiv* 1–42 (2024).

83. Bui, H. T. & Shaw, J. M. Dynamin assembly strategies and adaptor proteins in mitochondrial fission. *Curr. Biol.* **23**, 891–899 (2013).

84. Mozdy, A. D., McCaffery, J. M. & Shaw, J. M. Dnm1p GTPase-mediated mitochondrial fission is a multi-step process requiring the novel integral membrane component Fis1p. *J. Cell Biol.* **151**, 367–380 (2000).

85. Koppenol-Raab, M. *et al.* A targeted mutation identified through pKa measurements indicates a postrecruitment role for Fis1 in yeast mitochondrial fission. *J. Biol. Chem.* **291**, 20329–20344 (2016).

86. Palmer, C. S. *et al.* Adaptor proteins MiD49 and MiD51 can act independently of Mff and Fis1 in Drp1 recruitment and are specific for mitochondrial fission. *J. Biol. Chem.* **288**, 27584–27593 (2013).

87. Koirala, S. *et al.* Interchangeable adaptors regulate mitochondrial dynamin assembly for membrane scission. *Proc. Natl. Acad. Sci. U. S. A.* **110**, E1342–E1351 (2013).

88. Maruthi, M., Ling, L., Zhou, J. & Ke, H. Dispensable role of mitochondrial fission protein 1 (Fis1) in the erythrocytic development of Plasmodium falciparum. *mSphere* **5**, e00579-20 (2020).

89. Jacobs, K., Charvat, R. & Arrizabalaga, G. Identification of Fis1 interactors in Toxoplasma gondii reveals a novel protein required for peripheral distribution of the mitochondrion. *MBio* **11**, e02732-19 (2020).

90. Lorestani, A. *et al.* A Toxoplasma MORN1 null mutant undergoes repeated divisions but is defective in basal assembly, apicoplast division and cytokinesis. *PLoS One* **5**, e12302 (2010).

91. Rudlaff, R. M., Kraemer, S., Streva, V. A. & Dvorin, J. D. An essential contractile ring protein controls cell division in Plasmodium falciparum. *Nat. Commun.* **10**, 2181 (2019).

92. Pruyne, D., Legesse-Miller, A., Gao, L., Dong, Y. & Bretscher, A. Mechanisms of polarized growth and organelle segregation in yeast. *Annu. Rev. Cell Dev. Biol.* **20**, 559–591 (2004).

93. Mishra, P. & Chan, D. C. Mitochondrial dynamics and inheritance during cell division, development and disease. *Nat. Rev. Mol. Cell Biol.* **15**, 634–646 (2014).

94. Lawrence, E. J., Boucher, E. & Mandato, C. A. Mitochondria-cytoskeleton associations in mammalian cytokinesis. *Cell Div.* **11**, (2016).

95. Rohn, J. L. *et al.* Myo19 ensures symmetric partitioning of mitochondria and coupling of mitochondrial segregation to cell division. *Curr. Biol.* **24**, 2598–2605 (2014).

96. Fung, T. S., Chakrabarti, R. & Higgs, H. N. The multiple links between actin and mitochondria. *Nat. Rev. Mol. Cell Biol.* **24**, 651–667 (2023).

97. Koç, A. & De Storme, N. Structural regulation and dynamic behaviour of organelles during plant meiosis. *Front. Cell Dev. Biol.* **10**, 1–19 (2022).

98. Striepen, B. *et al.* The plastid of Toxoplasma gondii is divided by association with the centrosomes. *J. Cell Biol.* **151**, 1423–1434 (2000).

99. Devarakonda, P. M., Sarmiento, V. & Heaslip, A. T. F-actin and myosin F control apicoplast elongation dynamics which drive apicoplast-centrosome association in Toxoplasma gondii. *MBio* **14**, (2023).

100. Stortz, J. F. *et al.* Formin-2 drives polymerisation of actin filaments enabling segregation of apicoplasts and cytokinesis in Plasmodium falciparum. *Elife* **8**, e49030 (2019).

101. Jacot, D., Daher, W. & Soldati-Favre, D. Toxoplasma gondii myosin F, an essential motor for centrosomes positioning and apicoplast inheritance. *EMBO J.* **32**, 1702–1716 (2013).

102. Das, S., Lemgruber, L., Tay, C. L., Baum, J. & Meissner, M. Multiple essential functions of Plasmodium falciparum actin-1 during malaria blood-stage development. *BMC Biol.* **15**, 1–16 (2017).

103. Collier, S. *et al.* Plasmodium falciparum formins are essential for invasion and sexual stage development. *Commun. Biol.* **6**, 1–15 (2023).

104. Yeh, E. & DeRisi, J. L. Chemical rescue of malaria parasites lacking an apicoplast defines organelle function in blood-stage Plasmodium falciparum. *PLoS Biol.* **9**, e1001138 (2011).

105. Swift, R. P., Rajaram, K., Liu, H. B. & Prigge, S. T. Dephospho-CoA kinase, a nuclear-encoded apicoplast protein, remains active and essential after Plasmodium falciparum apicoplast disruption. *EMBO J.* **40**, 1–15 (2021).

106. Ferreira, J. L. *et al.* Variable microtubule architecture in the malaria parasite. *Nat. Commun.* **14**, 1–17 (2023).

107. Fowler, R. E., Fookes, R. E., Lavin, F., Bannister, L. H. & Mitchell, G. H. Microtubules in Plasmodium falciparum merozoites and their importance for invasion of erythrocytes. *Parasitology* **117**, 425–433 (1998).

108. Bannister, L. H. *et al.* Plasmodium falciparum apical membrane antigen 1 (PfAMA-1) is translocated within micronemes along subpellicular microtubules during merozoite development. *J. Cell Sci.* **116**, 3825–3834 (2003).

109. Bannister, L. H., Hopkins, J. M., Fowler, R. E., Krishna, S. & Mitchell, G. H. A brief illustrated guide to the ultrastructure of Plasmodium falciparum asexual blood stages. *Parasitol. Today* **16**, 427–433 (2000).

110. Hopkins, J. *et al.* The plastid in Plasmodium falciparum asexual blood stages: A three-dimensional ultrastructural analysis. *Protist* **150**, 283–295 (1999).

111. Zeeshan, M. *et al. Genome-wide functional analysis reveals key roles for kinesins in the mammalian and mosquito stages of the malaria parasite life cycle*. *PLoS Biology* vol. 20 (2022).

112. Schmidt, H. & Carter, A. P. Review: Structure and mechanism of the dynein motor ATPase. *Biopolymers* **105**, 557–567 (2016).

113. DiBella, L. M. *et al.* The Tctex1/Tctex2 class of dynein light chains. Dimerization, differential expression, and interaction with the LC8 protein family. *J. Biol. Chem.* **276**, 14366–14373 (2001).

114. Githui, E. K., De Villiers, E. P. & McArthur, A. G. Plasmodium possesses dynein light chain classes that are unique and conserved across species. *Infect. Genet. Evol.* **9**, 337–343 (2009).

115. Fowler, R. E. *et al.* Microtubule associated motor proteins of Plasmodium falciparum merozoites. *Mol. Biochem. Parasitol.* **117**, 187–200 (2001).

116. Carré, J. E. *et al.* Survival in critical illness is associated with early activation of mitochondrial biogenesis. *Am. J. Respir. Crit. Care Med.* **182**, 745–751 (2010).

117. Itoh, K., Nakamura, K., Iijima, M. & Sesaki, H. Mitochondrial dynamics in neurodegeneration. *Trends Cell Biol.* **23**, 64–71 (2013).

118. Guo, X. *et al.* Inhibition of mitochondrial fragmentation diminishes Huntington's disease-associated neurodegeneration. *J. Clin. Invest.* **123**, 5371–5388 (2013).

119. Joshi, A. U. *et al.* Fragmented mitochondria released from microglia trigger A1 astrocytic response and propagate inflammatory neurodegeneration. *Nat. Neurosci.* **22**, 1635–1648 (2019).

120. Rios, L. *et al.* Targeting an allosteric site in dynamin-related protein 1 to inhibit Fis1-mediated mitochondrial dysfunction. *Nat. Commun.* **14**, (2023).

121. Preta, G., Cronin, J. G. & Sheldon, I. M. Dynasore - Not just a dynamin inhibitor. *Cell Commun. Signal.* **13**, 1–7 (2015).

122. Münter, S. *et al.* Plasmodium Sporozoite Motility Is Modulated by the Turnover of Discrete Adhesion Sites. *Cell Host Microbe* **6**, 551–562 (2009).

123. Siden-Kiamos, I., Pinder, J. C. & Louis, C. Involvement of actin and myosins in Plasmodium berghei ookinete motility. *Mol. Biochem. Parasitol.* **150**, 308–317 (2006).

124. Dans, M. G. *et al. Sulfonylpiperazine compounds prevent Plasmodium falciparum invasion of red blood cells through interference with actin-1/profilin dynamics*. *PLoS Biology* vol. 21 (2023).

125. Johnson, S. *et al.* Truncated Latrunculins as Actin Inhibitors Targeting Plasmodium falciparum Motility and Host Cell Invasion. *J. Med. Chem.* **59**, 10994–11005 (2016).

126. Rizvi, S. A. *et al.* Identification and Characterization of a Small Molecule Inhibitor of Formin-Mediated Actin Assembly. *Chem. Biol.* **16**, 1158–1168 (2009).

127. Isogai, T., Van Der Kammen, R. & Innocenti, M. SMIFH2 has effects on Formins and p53 that perturb the cell cytoskeleton. *Sci. Rep.* **5**, (2015).

128. Braunwald, E., Saberi, S., Abraham, T. P., Elliott, P. M. & Olivotto, I. Mavacamten: a first-in-class myosin inhibitor for obstructive hypertrophic cardiomyopathy. *Eur. Heart J.* **44**, 4622–4633 (2023).

129. Moussaoui, D. *et al.* Mechanism of small molecule inhibition of Plasmodium falciparum myosin A informs antimalarial drug design. *Nat. Commun.* **14**, (2023).

130. Florian, S. & Mitchison, T. J. Anti-microtubule drugs. *Methods Mol. Biol.* **1413**, 403–421 (2016).

131. Steinmetz, M. O. & Prota, A. E. Microtubule-Targeting Agents: Strategies To Hijack the Cytoskeleton. *Trends Cell Biol.* **28**, 776–792 (2018).

132. Hirst, W. G. *et al.* Purification of functional Plasmodium falciparum tubulin allows for the identification of parasite-specific microtubule inhibitors. *Curr. Biol.* **32**, 919-926.e6 (2022).

133. Bartolome, A., Boskovic, S., Paunovic, I., Bozic, V. & Cvejic, D. Stomatin-like protein 2 overexpression in papillary thyroid carcinoma is significantly associated with high-risk clinicopathological parameters and BRAFV600E mutation. *Apmis* **124**, 271–277 (2016).

134. Signorile, A., Sgaramella, G., Bellomo, F. & De Rasmo, D. Prohibitins: A Critical Role in Mitochondrial Functions and Implication in Diseases. *Cells* **8**, 71 (2019).

135. Daumke, O. & Lewin, G. R. SPFH protein cage — one ring to rule them all. *Cell Res.* **32**, 117–118 (2022).

136. Steglich, G., Neupert, W. & Langer, T. Prohibitins regulate membrane protein degradation by the m-AAA protease in mitochondria. *Mol. Cell. Biol.* **19**, 3435–3442 (1999).

137. Merkwirth, C. & Langer, T. Prohibitin function within mitochondria: Essential roles for cell proliferation and cristae morphogenesis. *Biochim. Biophys. Acta - Mol. Cell Res.* **1793**, 27–32 (2009).

138. Merkwirth, C. *et al.* Prohibitins control cell proliferation and apoptosis by regulating OPA1-dependent cristae morphogenesis in mitochondria. *Genes Dev.* **22**, 476–488 (2008).

139. Da Cruz, S. *et al.* SLP-2 interacts with prohibitins in the mitochondrial inner membrane and contributes to their stability. *Biochim. Biophys. Acta - Mol. Cell Res.* **1783**, 904–911 (2008).

140. Christie, D. A. *et al.* Stomatin-Like Protein 2 Binds Cardiolipin and Regulates Mitochondrial Biogenesis and Function. *Mol. Cell. Biol.* **31**, 3845–3856 (2011).

141. Mitsopoulos, P. *et al.* Stomatin-like protein 2 deficiency results in impaired mitochondrial translation. *PLoS One* **12**, 1–13 (2017).

142. Tondera, D. *et al.* SIP-2 is required for stress-induced mitochondrial hyperfusion. *EMBO J.* **28**, 1589–1600 (2009).

143. Mitsopoulos, P. *et al.* Stomatin-Like Protein 2 Is Required for In Vivo Mitochondrial Respiratory Chain Supercomplex Formation and Optimal Cell Function. *Mol. Cell. Biol.* **35**, 1838–1847 (2015).

144. Sparkes, P. C. *et al.* Mitochondrial ATP synthesis is essential for efficient gametogenesis in Plasmodium falciparum. *bioRxiv* (2024).

145. Sheokand, P., Mühleip, A. & Sheiner, L. Plasmodium falciparum mitochondrial complex III, the target of atovaquone, is essential for progression to the transmissible sexual stages. *bioRxiv* (2024).

146. Evers, F. *et al.* Composition and stage dynamics of mitochondrial complexes in Plasmodium falciparum. *Nat. Commun.* **12**, 3820 (2021).

147. Nguyen, T. T. & Voeltz, G. K. An ER phospholipid hydrolase drives ER-associated mitochondrial constriction for fission and fusion. *Elife* **11**, 1–30 (2022).

148. Boucher, M. J. *et al.* Integrative proteomics and bioinformatic prediction enable a high-confidence apicoplast proteome in malaria parasites. *PLoS Biol.* **16**, 1–29 (2018).

149. Esveld, S. L. Van *et al.* A Prioritized and Validated Resource of Mitochondrial Proteins in Plasmodium Identifies Unique Biology. *mSphere* **6**, e00614-21 (2021).

150. Ma, C. *et al.* Structural insights into the membrane microdomain organization by SPFH family proteins. *Cell Res.* **32**, 176–189 (2022).

151. Wai, T. *et al.* The membrane scaffold SLP2 anchors a proteolytic hub in mitochondria containing PARL and the i -AAA protease YME1L. *EMBO Rep.* **17**, 1844–1856 (2016).

152. Opalińska, M., Parys, K. & Jańska, H. Identification of physiological substrates and binding partners of the plant mitochondrial protease FTSH4 by the trapping approach. *Int. J. Mol. Sci.* **18**, 1–11 (2017).

153. Serricchio, M. & Bütikofer, P. A Conserved Mitochondrial Chaperone-Protease Complex Involved in Protein Homeostasis. *Front. Mol. Biosci.* **8**, 767088 (2021).

154. Akiyama, Y., Yoshihisa, T. & Ito, K. FtsH, a membrane-bound ATPase, forms a complex in the cytoplasmic membrane of Escherichia coli. *J. Biol. Chem.* **270**, 23485–23490 (1995).

155. Leonhard, K. *et al.* Membrane protein degradation by AAA proteases in mitochondria: Extraction of substrates from either membrane surface. *Mol. Cell* **5**, 629–638 (2000).

156. Sokolenko, A. *et al.* The gene complement for proteolysis in the cyanobacterium Synechocystis sp. PCC 6803 and Arabidopsis thaliana chlorophlasts. *Curr. Genet.* **41**, 291–310 (2002).

157. Opalińska, M. & Jańska, H. AAA proteases: Guardians of mitochondrial function and homeostasis. *Cells* **7**, 1–15 (2018).

158. Janska, H., Kwasniak, M. & Szczepanowska, J. Protein quality control in organelles - AAA/FtsH story. *Biochim. Biophys. Acta - Mol. Cell Res.* **1833**, 381–387 (2013).

159. Pickles, S., Vigié, P. & Youle, R. J. Mitophagy and Quality Control Mechanisms in Mitochondrial Maintenance. *Curr. Biol.* **28**, R170–R185 (2018).

160. Bohovych, I., Chan, S. S. L. & Khalimonchuk, O. Mitochondrial Protein Quality Control: The Mechanisms Guarding Mitochondrial Health. *Antioxidants Redox Signal.* **22**, 977–994 (2015).

161. Stiburek, L. *et al.* YME1L controls the accumulation of respiratory chain subunits and is required for apoptotic resistance, cristae morphogenesis, and cell proliferation. *Mol. Biol. Cell* **23**, 1010–1023 (2012).

162. Leonhard, K. *et al.* AAA proteases with catalytic sites on apposite membrane surfaces comprise a proteolytic system for the ATP-dependent degradation of inner membrane proteins in mitochondria. *EMBO J.* **15**, 4218–4229 (1996).

163. Atorino, L. *et al.* Loss of m-AAA protease in mitochondria causes complex I deficiency and increased sensitivity to oxidative stress in hereditary spastic paraplegia. *J. Cell Biol.* **163**, 777–787 (2003).

164. Arlt, H. *et al.* The formation of respiratory chain complexes in mitochondria is under the proteolytic control of the m-AAA protease. *EMBO J.* **17**, 4837–4847 (1998).

165. Weber, E. R., Hanekamp, T. & Thorsness, P. E. Biochemical and functional analysis of the YME1 gene product, an ATP and zinc-dependent mitochondrial protease from S. cerevisiae. *Mol. Biol. Cell* **7**, 307–317 (1996).

166. Kicia, M., Gola, E. M. & Janska, H. Mitochondrial protease AtFtsH4 protects ageing Arabidopsis rosettes. **5**, 126–128 (2010).

167. Quirós, P. M., Langer, T. & López-Otín, C. New roles for mitochondrial proteases in health, ageing and disease. *Nat. Rev. Mol. Cell Biol.* **16**, 345–359 (2015).

168. Gerdes, F., Tatsuta, T. & Langer, T. Mitochondrial AAA proteases - Towards a molecular understanding of membrane-bound proteolytic machines. *Biochim. Biophys. Acta - Mol. Cell Res.* **1823**, 49–55 (2012).

169. Glynn, S. E. Multifunctional mitochondrial AAA proteases. *Front. Mol. Biosci.* **4**, (2017).

170. König, T. *et al.* The m-AAA Protease Associated with Neurodegeneration Limits MCU Activity in Mitochondria. *Mol. Cell* **64**, 148–162 (2016).

171. Li, H. *et al.* Mic60/Mitofilin determines MICOS assembly essential for mitochondrial dynamics and mtDNA nucleoid organization. *Cell Death Differ.* **23**, 380–392 (2016).

172. Bonn, F., Tatsuta, T., Petrungaro, C., Riemer, J. & Langer, T. Presequence-dependent folding ensures MrpL32 processing by the m-AAA protease in mitochondria. *EMBO J.* **30**, 2545–2556 (2011).

173. Nolden, M. *et al.* The m-AAA protease defective in hereditary spastic paraplegia controls ribosome assembly in mitochondria. *Cell* **123**, 277–289 (2005).

174. Woellhaf, M. W., Hansen, K. G., Garth, C. & Herrmann, J. M. Import of ribosomal proteins into yeast mitochondria. *Biochem. Cell Biol.* 1–30 (2014).

175. Rampello, A. J. & Glynn, S. E. Identification of a Degradation Signal Sequence within Substrates of the Mitochondrial i-AAA Protease. *J. Mol. Biol.* **429**, 873–885 (2017).

176. Rainbolt, T. K., Atanassova, N., Genereux, J. C. & Wiseman, R. L. Stress-regulated translational attenuation adapts mitochondrial protein import through Tim17A degradation. *Cell Metab.* **18**, 908–919 (2013).

177. Schulz, C., Schendzielorz, A. & Rehling, P. Unlocking the presequence import pathway. *Trends Cell Biol.* **25**, 265–275 (2015).

178. Potting, C., Wilmes, C., Engmann, T., Osman, C. & Langer, T. Regulation of mitochondrial phospholipids by Ups1/PRELI-like proteins depends on proteolysis and Mdm35. *EMBO J.* **29**, 2888–2898 (2010).

179. Potting, C. *et al.* TRIAP1/PRELI complexes prevent apoptosis by mediating intramitochondrial transport of phosphatidic acid. *Cell Metab.* **18**, 287–295 (2013).

180. Tanveer, A. *et al.* An FtsH protease is recruited to the mitochondrion of Plasmodium falciparum. *PLoS One* **8**, e74408 (2013).

181. Amberg-Johnson, K. *et al.* Small molecule inhibition of apicomplexan FtsH1 disrupts plastid biogenesis in human pathogens. *Elife* **6**, (2017).

182. Karnataki, A., DeRocher, A. E., Feagin, J. E. & Parsons, M. Sequential processing of the Toxoplasma apicoplast membrane protein FtsH1 in topologically distinct domains during intracellular trafficking. *Mol. Biochem. Parasitol.* **166**, 126–133 (2009).

183. Puchades, C., Sandate, C. R. & Lander, G. C. The molecular principles governing the activity and functional diversity of AAA+ proteins. *Nat. Rev. Mol. Cell Biol.* **21**, 43–58 (2020).

184. Qiao, Z. *et al.* Cryo-EM structure of the entire FtsH-HflKC AAA protease complex. *Cell Rep.* **39**, 110890 (2022).

185. Wessel, A. K. *et al.* Escherichia coli SPFH Membrane Microdomain Proteins HflKC Contribute to Aminoglycoside and Oxidative Stress Tolerance. *Microbiol. Spectr.* **11**, 1–11 (2023).

186. Kohanski, M. A., Dwyer, D. J., Wierzbowski, J., Cottarel, G. & Collins, J. J. Mistranslation of Membrane Proteins and Two-Component System Activation Trigger Antibiotic-Mediated Cell Death. *Cell* **135**, 679–690 (2008).

187. Keithly, J. S., Langreth, S. G., Buttle, K. F. & Mannella, C. A. Electron tomographic and ultrastructural analysis of the Cryptosporidium parvum relict mitochondrion, its associated membranes, and organelles. *J. Eukaryot. Microbiol.* **52**, 132–140 (2005).

188. Mathur, V., Wakeman, K. C. & Keeling, P. J. Parallel functional reduction in the mitochondria of apicomplexan parasites. *Curr. Biol.* **31**, 2920-2928.e4 (2021).

189. Putignani, L. *et al.* Characterization of a mitochondrion-like organelle in Cryptosporidium parvum. *Parasitology* **129**, 1–18 (2004).

190. Kihara, A., Akiyama, Y. & Ito, K. A protease complex in the Escherichia coli plasma membrane: HflKC (HflA) forms a complex with FtsH (HflB), regulating its proteolytic activity against SecY. *EMBO J.* **15**, 6122–6131 (1996).

191. Gehl, B. & Sweetlove, L. J. Mitochondrial Band-7 family proteins: Scaffolds for respiratory chain assembly? *Front. Plant Sci.* **5**, 1–6 (2014).

192. Hernando-Rodríguez, B. & Artal-Sanz, M. Mitochondrial quality control mechanisms and the PHB (Prohibitin) complex. *Cells* **7**, 1–19 (2018).

193. Polier, G. *et al.* The natural anticancer compounds rocaglamides inhibit the Raf-MEK-ERK pathway by targeting prohibitin 1 and 2. *Chem. Biol.* **19**, 1093–1104 (2012).

194. Sánchez-Vera, I. *et al.* The prohibitin-binding compound fluorizoline induces the pro-inflammatory cytokines interleukin-8 and interleukin-6 through the activation of JNK and p38 MAP kinases. *Biochem. Pharmacol.* **218**, (2023).

195. Saini, M. *et al.* Characterization of Plasmodium falciparum prohibitins as novel targets to block infection in humans by impairing the growth and transmission of the parasite. *Biochem. Pharmacol.* **212**, 115567 (2023).

196. Kavishe, R. A., Koenderink, J. B. & Alifrangis, M. Oxidative stress in malaria and artemisinin combination therapy: Pros and Cons. *FEBS J.* **284**, 2579–2591 (2017).

197. Cui, L. & Su, X. Discovery, mechanisms of action and combination therapy of artemisinin. *Expert Rev. Anti. Infect. Ther.* **7**, 999–1013 (2009).

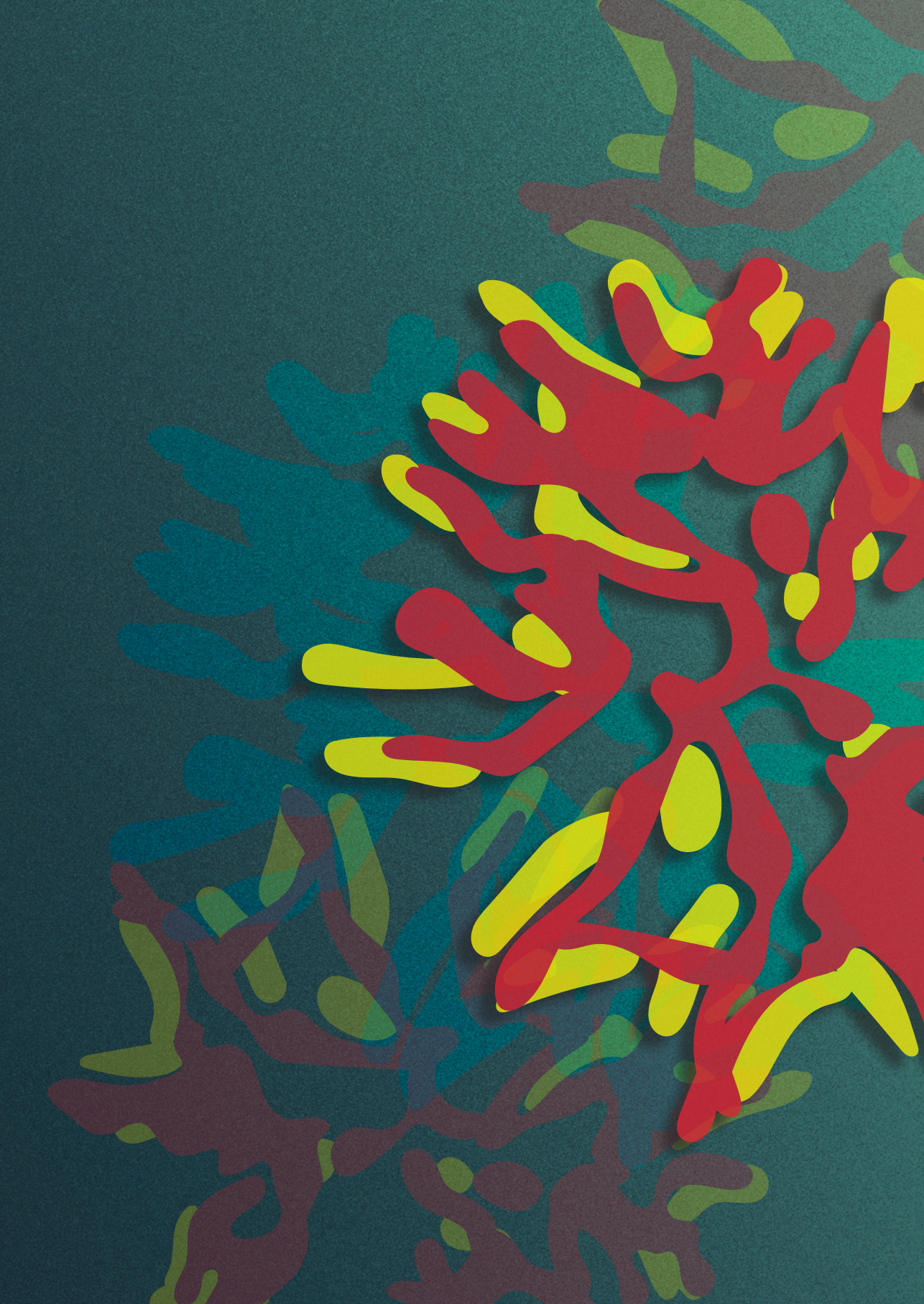

Chapter 6

Summary
Samenvatting
Research Data Management
List of publications
Acknowledgements
About the author
Portfolio

Summary

Malaria is a devastating parasitic disease causing 249 million cases and 608,000 deaths in 2022, predominantly in children below 5 years old. *Plasmodium falciparum* is the most deadly species responsible for malaria. The rapid emergence of resistance to current antimalarials emphasize the urgent need for the development of novel antimalarial drugs.

The two so-called endosymbiotic organelles of the parasite present promising drug targets due to their unique biology. One of these, the mitochondrion, is best known as the powerhouse of the cell. The parasite mitochondrion differs greatly from human mitochondria on a molecular and functional level and is a validated drug target of several antimalarial compounds, such as atovaquone, ELQ300, and DSM265. The apicoplast is a plastid organelle of red algal origin that is exclusive to malaria parasites and a wide variety of close and distant single-cell relatives. This organelle houses several important metabolic pathways which are the targeted of various antimalarial compounds, such as fosmidomycin and thiolactomycin. *Plasmodium* parasites go through a complicated life cycle, which includes several stages of asexual replication in the human and mosquito hosts. During replication in the human red blood cell, one parasite is segmented in up to 40 daughter cells through a process called schizogony. Parasite replication happens on a much larger scale in mosquito and liver stages, where thousands or tens of thousands of daughter cells are formed within a single parental parasite. It is crucial for the parasite to properly divide and distribute the singular mitochondrion and apicoplast to ensure each daughter parasite receives a complete set of organelles. However, how these processes exactly happen, and which proteins are involved remained unknown.

In this thesis, the current knowledge on organelle division in malaria parasites and closely related species is summarized and different division mechanisms are proposed (**chapter 2**). We developed a novel mitochondrial marker in *P. falciparum*, which was used to visualize mitochondrial dynamics during blood and mosquito stages in great detail (**chapter 3**). Using high-resolution fluorescent microscopy, we demonstrated that the mitochondrion orients in a cartwheel structure prior to its division, which happens in a non-geometrical progression during the final stages of daughter-cell formation. Focused-Ion Beam Scanning Electron Microscopy (FIB-SEM) imaging is a technique that allows the three-dimensional reconstruction of cells at nanometer resolution providing much more detail than can be achieved with light microscopy-based approaches. Exploiting FIB-SEM generated images,

we confirmed the mitochondrial division steps and revealed new details on the timing and progression of apicoplast division. The close interaction between the mitochondrion and apicoplast during parasite replication was highlighted and the potential role in apicoplast segregation of so-called centriolar plaques, the centrosome equivalent of the parasite, was revealed. These results contributed to a new, detailed model for apicoplast and mitochondrial division and segregation in *P. falciparum*.

Plasmodium parasites harbor four mitochondrial proteins belonging to the SPFH (Stomatin, Prohibitin, Flotillin and HflK/C) family. SPFH proteins form membrane-spanning or membrane-anchored complexes and are involved in various functions. We characterized the role of stomatin-like protein (STOML) in *P. falciparum* (**chapter 4**). Although the localization of STOML to the mitochondrial branching points and endings of mitochondrial branches during schizogony suggests a potential role of this protein in mitochondrial dynamics, deletion of the *STOML* gene did not lead to obvious differences in mitochondrial morphology in asexual blood-stage parasites. Deletion of *STOML* caused slower development of the parasite throughout asexual blood-stage development but did not affect gametocyte development and exflagellation. Sensitivity to drugs targeting the electron transport chain, one of the central functions of mitochondria, did not change in parasites lacking *STOML*, suggesting that STOML is not directly involved in the assembly of the protein complexes involved in the electron transport chain. Complexome profiling data gives an indication about the consistency and size of protein complexes in the parasite and showed that STOML resides in a large protein complex. We also purified STOML demonstrating that it likely interacts with FtsH, a zinc-dependent metalloprotease. Structure predictions using the computer-based tool AlphaFold and comparison with the cryo-EM structure of a related bacterial protein complex suggested that STOML forms a vault-like structure consisting of multiple copies of the protein around FtsH, possibly regulating accessibility this protease, and therefore have a function in mitochondrial protein quality control.

In this thesis, I used cutting-edge imaging techniques to reveal novel insights into the division and segregation of the singular mitochondrion and apicoplast in *Plasmodium* parasites. Furthermore, we characterized the function of STOML in these parasites, and found a potential role in regulation of mitochondrial protein quality control through the FtsH metalloprotease. These new insights into the fundamental biology of the parasites contribute to a better understanding of these crucial processes and pave the way for future studies to explore their potential as antimalarial drug targets.

Samenvatting

Malaria is een parasitaire ziekte die in 2022 zorgde voor 249 miljoen besmettingen en meer dan 600,000 doden, voornamelijk bij kinderen jonger dan 5 jaar oud. *Plasmodium falciparum* is de meest dodelijke malariaparasiet soort. De snelle opkomst van resistentie tegen de huidige antimalariamiddelen benadrukt de dringende behoefte aan de ontwikkeling van nieuwe malariamedicijnen.

De twee zogeheten endosymbiotische organellen van de parasiet vormen veelbelovende doelwitten voor geneesmiddelen vanwege hun unieke biologie. Een van deze organellen, het mitochondrion, is bekend van zijn functie in energieproductie. Het mitochondrion van de parasiet verschilt sterk van menselijke mitochondriën op moleculair en functioneel niveau. Het is een gevalideerd doelwit van verschillende malariamedicijnen, zoals atovaquone, ELQ300 en DSM265. De apicoplast is een plastide organel dat afkomstig is uit een rode alg en exclusief voorkomt in malariaparasieten en verwante, eencellige soorten. De apicoplast huist verschillende belangrijke stofwisselingsprocessen die het doelwit zijn van medicijnen zoals fosmidomycine en thiolactomycine. *Plasmodium* parasieten doorlopen een ingewikkelde levenscyclus, met verschillende momenten van aseksuele vermenigvuldiging in de mens en de mug. Tijdens vermenigvuldiging in de rode bloedcellen wordt één parasiet gesegmenteerd in maximaal 40 dochterparasieten via een proces dat schizogonie wordt genoemd. Parasietvermenigvuldiging vindt op veel grotere schaal plaats in muggen- en leverstadia, waarbij duizenden tot tienduizenden dochtercellen worden gevormd in een enkele ouderparasiet. Het is cruciaal voor de parasiet om de enkele mitochondrion en apicoplast correct te delen en te distribueren om ervoor te zorgen dat elke dochterparasiet een complete set organellen ontvangt. Tot voor kort was er weinig bekend over hoe deze processen precies plaatsvinden en welke eiwitten hierbij betrokken zijn.

In dit proefschrift wordt de huidige kennis over organeldeling in malaria-parasieten en nauwverwante soorten samengevat en worden verschillende delingsmechanismen voorgesteld (**hoofdstuk 2**). We hebben een nieuwe mitochondriële marker ontwikkeld in *P. falciparum*, die werd gebruikt om de dynamische ontwikkeling van het mitochondrion tijdens bloed- en mugstadia in detail te visualiseren (**hoofdstuk 3**). Met behulp van fluorescentiemicroscopie hebben we aangetoond dat het mitochondrion zich in een wielstructuur oriënteert voordat het zich deelt, wat gebeurt in een niet-geometrische progressie tijdens de laatste stadia van parasietdeling. Focused-Ion Beam Scanning Electron

Microscopy (FIB-SEM) is een techniek die driedimensionale reconstructie van cellen op nanometerschaal mogelijk maakt, waardoor veel meer details zichtbaar worden dan met lichtmicroscopie. Visualisatie met behulp van FIB-SEM bevestigde de mitochondriële delingsstappen en onthulde nieuwe details over de timing en progressie van apicoplastdeling. Ook hebben we de nauwe interactie tussen het mitochondrion en de apicoplast tijdens parasietvermenigvuldiging laten zien en vonden we een mogelijke rol van centriolar plaques, het equivalent van de centrosomen in de parasiet, in verdeling van de gedeelde apicoplast over dochtercellen. Deze resultaten hebben bijgedragen aan een nieuw, gedetailleerd model voor apicoplast- en mitochondriële deling en verdeling in *P. falciparum*.

Plasmodium parasieten hebben vier mitochondriële eiwitten die behoren tot de SPFH (Stomatin, Prohibitin, Flotillin en HflK/C) eiwitfamilie. SPFH-eiwitten vormen membraangebonden complexen en zijn betrokken bij verschillende functies. We hebben de rol van stomatin-like eiwit (STOML) in *P. falciparum* gekarakteriseerd (**hoofdstuk 4**). Hoewel de lokalisatie van STOML naar de vertakkingspunten en uiteinden van mitochondriële vertakkingen tijdens schizogonie een potentiële rol van dit eiwit in mitochondriële dynamiek suggereert, leidde het verwijderen van *STOML* niet tot duidelijke mitochondriële structuurverschillen in aseksuele bloedstadiumparasieten. De ontwikkeling van parasieten zonder *STOML* verliep aanmerkelijk langzamer gedurende het aseksuele bloedstadium, maar de ontwikkeling en activatie van de seksuele stadia werd niet beïnvloed. De gevoeligheid voor medicijnen die de elektronentransportketen aanvallen, veranderde niet in parasieten zonder *STOML*, wat suggereert dat *STOML* niet direct betrokken is bij de vorming van de betrokken eiwitcomplexen. Complexome profiling data geeft een indicatie samenstelling van de aanwezige eiwitcomplexen in de parasiet en liet zien dat STOML voorkomt in een groot eiwitcomplex. We hebben STOML gepurificeerd en lieten zien dat het een interactie heeft met FtsH, een zink-afhankelijke metalloprotease. We hebben de structuur van het STOML-complex voorspeld met de computer tool AlphaFold en hebben deze vergeleken met de cryo-EM structuur van een gerelateerd eiwitcomplex in bacteriën. We vonden dat het STOML-eiwitcomplex waarschijnlijk een gewelf-achtige structuur vormt rondom FtsH en hiermee waarschijnlijk de toegankelijkheid van FtsH reguleert en een functie heeft in de kwaliteitscontrole van mitochondriële eiwitten.

In dit proefschrift heb ik vooruitstrevende microscopietechnieken gebruikt om nieuwe inzichten te krijgen in de deling en verdeling van het mitochondrion en de apicoplast in *Plasmodium* parasieten. Bovendien hebben we de functie van STOML in deze parasieten gekarakteriseerd en een potentiële rol gevonden in de regulatie

van mitochondriële eiwitkwaliteitscontrole via de FtsH metalloprotease. Deze nieuwe inzichten in de fundamentele biologie van de parasieten dragen bij aan een beter begrip van deze cruciale processen en banen de weg voor toekomstige studies om hun potentieel als malariamedicijndoelwitten te verkennen.

Research Data Management

The research data described in this thesis have been obtained during my PhD at the Department of Medical Microbiology, Radboud University Medical Center (Radboudumc). The reuse of research data is facilitated by the guidelines to enhance to Findability, Accessibility, Interoperability and Reuse of research data (FAIR principle). Data for the experimental chapters 3 and 4 was obtained through laboratory experiments, which did not involve animals and human red blood cells and serum used for malaria parasite culture were anonymized and untraceable. All experiments performed during the PhD trajectory are documented in the digital lab book Labguru, which is backed-up daily on the Radboudumc server. Storage locations of plasmids, bacterial and parasite stocks that are generated during this PhD are documented in communal excel files on the Radboudumc MMB department, which is backed up monthly and accessible for other department members. The experimental data from chapter 3 and 4 are published in Data Sharing Collections in the Radboud Data Repository and openly accessible for reuse (https://doi.org/10.34973/1wef-re42, https://doi.org/10.34973/kknj-an72). Data Sharing Collections remain available for 15 years. The Focused-Ion Beam Scanning Electron Microscopy (FIB-SEM) data in chapter 3 was obtained from Evers et al. 2023 (*BioRxiv*) and available for reuse through the EMPIAR database (EMPIAR-12160) once the manuscript has been published.

List of publications

Verhoef JMJ, Bekkering E, Boshoven C, et al. The role of stomatin-like protein (STOML) in Plasmodium falciparum. *Review Commons.* (under review)

Longley RJ, Malinga J, Hesping E, Sutanto E, DonVito SM, Kucharski M, Oyong DA, **Verhoef JMJ**, et al. MAM 2024: Malaria in a changing world. *Trends in Parasitology* (2024).

Verhoef JMJ, Boshoven C, Evers F, et al. Detailing organelle division and segregation in Plasmodium falciparum. *Journal of Cell Biology* (2024).

Evers F, Roverts R, Boshoven C, Kea-te Lindert M, **Verhoef JMJ**, et al. Comparative 3D ultrastructure of Plasmodium falciparum gametocytes. *Nature Communications* (2024). (in press)

de Vries LE, Jansen PA, Barcelo C, Munro J, **Verhoef JMJ**, et al. Preclinical characterization and target validation of the antimalarial pantothenamide MMV693183. *Nature Communications* (2022).

Pasternak M, **Verhoef JMJ**, et al. RhopH2 and RhopH3 export enables assembly of the RhopH complex on the *P. falciparum*-infected erythrocyte membrane. *Communications Biology* (2022).

Verhoef JMJ, Meissner M, and Kooij TWA. Organelle dynamics in apicomplexan parasites. *Mbio* (2021). (Literature review)

Schalkwijk J*, Allman EL*, Jansen PAM*, de Vries LE*, **Verhoef JMJ**, et al. Antimalarial pantothenamide metabolites target acetyl–coenzyme A biosynthesis in Plasmodium falciparum. *Science Translational Medicine* 11.510 (2019). (* these authors contributed equally)

Acknowledgements

The End. For so long the end seemed unreachable far away. But the time has finally come that I can truly say that my PhD is finished. It has been an amazing 4.5 years, with many ups and downs. There were times when I questioned why I was doing this and whether it was worth the effort, but through it all, I have grown and developed in countless ways. What made this journey truly special, however, were the incredible people who supported me along the way. I am truly grateful for all the support, and I consider myself extremely lucky to have so many amazing people around me.

Taco, I want to thank you for everything you have done for me the last years. I came to you as a master student, asking for an internship position. I already had an internship position in a different department but decided last minute to change it and do my internship with you and Laura. That was a great decision. Not only did I learn so much under your and Laura's supervision, but you also nominated me for several awards for my internship report that extremely boosted my CV. With your help I got a second internship position in the lab of Prof. Alan Cowman in Melbourne. I am very grateful that you wanted to write a PhD project together, and that you gave me all the freedom to design the project exactly as I liked it. You have always supported me in all my ambitions and wishes, and the freedom you gave me made me into an independent researcher. Thanks again for all your support.

Teun, although you have not been heavily involved in my project, I do want to thank you for all your support, especially during the more difficult times. You were always willing to meet or think along when I asked for your help. I did greatly enjoy working together with you on sustainability projects, such as the freezer challenge.

Akhil, I am incredibly grateful for your advisory role during my PhD. Your endless experience and knowledge of the parasite mitochondrion led to insightful discussions and guided me to focus on the right experiments during crucial junctions in my PhD trajectory. I'm extremely grateful for my time in Philadelphia, visiting your lab and later the MPM conference in Woods Hole. Even though we had never met in person, you and Sheila were so kind to invite me to stay with you during my visit. I had an amazing time in the US, and I couldn't have felt more welcome. Thanks again for all your support and for your recommendation letter that helped me to get my postdoc position in Julian Rayner's lab. If you are ever close to the Netherlands (or the coming three years the UK), I hope we will be able to meet again. Otherwise, I hope we see each other at another malaria conference.

Rick, I want to thank you for your mentoring role the last years. We met during the minor Medical Biotechnology, in the third year of my bachelor and I was very happy that I could secure a bachelor internship position in your lab. I greatly enjoyed my internship, and it stimulated me to continue in molecular research. It was therefore not difficult for me to choose a mentor when I started my PhD. I greatly value the meetings that we had and always felt more motivated afterwards. Your recommendation letter also contributed to be getting the new postdoc position in Cambridge. Thank you for all the support.

I want to thank everyone from the **Kooij pond**. It has been absolutely great working together with all of you and I couldn't have wished for nicer colleagues. I do greatly appreciate how we worked together as a group and how everyone would always be willing to help each other out. I'm truly grateful for the friendships that we build, and I hope we will stay in touch.

Nick, it was a great pleasure to work with you. Thank you for all your advice and help with the mosquito experiments. I do greatly appreciate your unlimited interest and enthusiasm for science. However, besides 4 years of exposure, I still don't like your taste of music, I'm sorry.

Felix, thanks for the great collaborations that we had, resulting in three papers together. I think you are an amazing scientist and greatly value our discussions. You have become a very good friend over the last years, and I hope we will still go to many festivals together.

Alex, it was a great pleasure to sit next to you in the lab for a few years. Thanks for organizing the amazing lab retreat with the Kooij group! We have had a lot of fun together and I was incredibly sad to see you leave. However, I'm very happy that we still see each other every now and again and that we stay in touch.

Laura, the amazing work that you did as my first master student has now resulted in a very nice publication in JCB. It was a great pleasure to work together with you, and I'm very happy that you came back to start your own PhD in the lab. I cherish all the fun things we did together, and I hope you and Ez will come and visit us in Cambridge.

Ezra, I want to thank you for your great work with setting up the STOML pulldown experiments. Because of these experiments and the AlphaFold modelling, the

STOML paper became something to be proud of. Thanks for all the great times in and out of the lab and I hope we will stay in touch.

Silvia, it is so great to see how you have developed the last year, from a student to a confident, independent researcher supervising your own students. I do really value that you are always up to do something fun together! I wish you best of luck with the rest of your PhD and hope we will be able to visit Venice together one day.

I'm extremely grateful to all my colleagues from the **parasitology** group. Everyone has been a great support, and I really enjoyed my time with all of you. I would like to give some special thanks to **Karina** and **Kjerstin**. You are both the foundation of the lab and were always willing to help me with any of my questions. **Annemieke**, I want to thank you for helping me with all the administrative business and answering all my questions. **Annie**, thank you so much for bringing me in contact with Michal from the Cowman lab, which resulted in my second internship position. You were always willing to help me with any questions or issues during my PhD, and I was very sad to see you leave. I hope I will be able to visit you in Leiden soon and meet little Hiro. Thanks **Renate**, for being such a nice person and for always making me laugh. **Carolina,** thank you for being an inspiring feminist and for your kind heart. I also want to thank everyone from the **malaria unit**, especially **Geert-Jan, Marga, Wouter, and Rianne**, for always helping me with any questions and with the mosquito experiments. Thanks to the whole **virology** group. It has been a great pleasure to work next to you and do fun things together. **Milou**, thanks for your happy spirit, it was great to get to know you and I hope we stay in touch. **Oscar**, thanks for the nice mountain bike sessions and your optimistic and chill view on life. I would also like to thank the **Aesculaaf**, for hosting us when we needed a beer. I want to thank the **Spar**, for having an unlimited supply of Nocco energy drink during the thesis writing period and **Blommers**, for having the best cinnamon buns and friendly people.

I also want to thank the whole **Lowlands crew**, including **Felix H, Maartje, Sara, Felix, Saskia, Michelle, Carolina, Merel, Ezra, Zhong, Geert-Jan**. The research project at Lowlands was one of the most fun things I did during my PhD. It was amazing to see that so many people were interested in testing their mosquito attractiveness and we worked extremely well as a team. Thanks for this incredible experience.

Many thanks to all the people from the **RTC microscopy**, especially **Marieke** and **Ben**, for helping me with all my microscopy issues and questions.

I would like to thank my internship supervisors, for teaching me all the lab techniques and skills that I needed for my PhD. **Walther van den Broek**, my bachelor internship supervisor, you thought me how to do cell culture, cloning, transfections, microscopy and more. Thanks to you I discovered that I loved to do lab research. **Laura de Vries**, my master internship with you was great in so many ways. You are such a patient and good teacher, and I feel like I've learned parasite culture and experiments from the best. It was a great pleasure to work with you, and I'm very happy that you can continue your research now at the Radboud with your Veni! **Michal Pasternak**, thank you so much for your support and supervision during my master internship in Melbourne. You really nourished my love for microscopy, and I think we were a great team together. I hope we stay in touch!

I would like to thank **Barend**. It was a great pleasure to supervise your master internship. Your contributions were the foundation for some of the figures in this thesis and resulted in your co-authorship on the paper. I felt extremely honored to speak on your graduation I wish you all the best for the rest of your career. **Aleksandra**, thank you so much for all your hard work during your master internship. I really appreciate your deep interest in science, your enthusiasm that goes much further than only your own research topic, and your never-ending stream of questions. Your bright mind and ambition are a perfect combination for a beautiful career. I wish you all the best with your PhD in Utrecht.

I would like to give a special thanks to my dear friends **Roos** and **Maartje**. I'm extremely grateful that you were my constant companions throughout this PhD journey. Your support and the many fun moments that we shared made all the difference and kept me going. Thanks for all the Aesculaaf sessions, which were sometimes more of a PhD therapy session, but also a lot of fun. Thanks for all the nice dinners, festivals, nights out and so much more.

Daarnaast wil ik graag nog een aantal mensen buiten het lab bedanken. **Anna** en **Dalidah**, al vriendinnen sinds de middelbare school (voor Anna zelfs al vanaf de basisschool). Bedankt voor alle fijne momenten die we samen hebben gehad afgelopen jaren. Ik keek er altijd enorm naar uit om lekker met jullie bij te kletsen, leuke dingen te doen, en met scooters door weilanden te rijden. Jullie kunnen me altijd aan het lachen maken en ik ben erg dankbaar voor onze vriendschap. **Rens** en **Marike**, heel erg bedankt voor alle leuke momenten afgelopen jaar en jullie onophoudelijke steun. Ons fietsclubje was erg belangrijk voor mijn mentale gezondheid en het was heerlijk om samen grote rondes te fietsen in het weekend om weer op te laden voor de week. De reis die we samen naar Guatemala hebben

gemaakt was een van de tofste vakanties ooit, en ik hoop dat we in de toekomst nog meer mooie reizen gaan maken samen. **Maarten, Kiri, Floor, Daniek** en **Sam**, jullie vriendschap gaat het verst terug van allemaal. Eigenlijk zou ik jullie meer omschrijven als familie. Bedankt voor jullie onvoorwaardelijke vriendschap en ik hoop dat we over 50 jaar nog steeds samen op kampeerweekendjes gaan. **Thijmen, Denise, Olivier** en **Jessica**, bedankt voor alle fijne momenten samen. De bruiloft vorig jaar in Italië was een van de mooiste en leukste ervaringen van de afgelopen jaren. Bedankt voor jullie vriendschap, en ik hoop dat jullie ons snel een keertje in Cambridge komen opzoeken. **Lea**, thank you for always making me laugh and for all the great moments we had the last years. Our road trip in Australia was one of the highlights. I also hope to see you in Cambridge soon.

Maartje en **Marike**, bedankt dat jullie naast me staan als mijn paranimfen tijdens de laatste stap van mijn PhD. Ik ben erg dankbaar voor jullie support en vriendschap.

Nicole en **Marcel**, bedankt voor al jullie steun en support de afgelopen jaren. Jullie stonden altijd voor ons klaar en hebben ons op zo veel manieren geholpen en gesteund. Ik kan me geen fijnere schoonouders voorstellen.

Marc en **Caroline**, mijn ouders, ik wil jullie graag bedanken voor jullie grenzeloze liefde en steun. Jullie hebben me gevormd tot de persoon die ik vandaag de dag ben. Dankzij jullie heb ik altijd de vrijheid gehad om mijn passies na te streven en mezelf te ontwikkelen op creatief, muzikaal, sportief, en educatief gebied. De prachtige reizen die we samen hebben gemaakt, waren onvergetelijk en hebben mijn blik op de wereld verruimd. Ik ben diep dankbaar voor alles wat jullie voor mij hebben gedaan en de onvoorwaardelijke liefde die ik van jullie heb mogen ontvangen. Ik had me geen betere ouders kunnen wensen. Dankjewel voor alles.

Cas, mijn kersverse echtgenoot, mijn beste vriend, mijn fietsmaatje, mijn collega, en nog zo veel meer. De afgelopen jaren hebben we samen zoveel mooie momenten beleefd. Hoewel sommigen hun twijfels hadden toen we vertelden dat we in hetzelfde lab zouden gaan werken, was het voor mij geen moment vervelend. Integendeel, het was juist erg tof om onze passie samen te kunnen delen. Ik wil je enorm bedanken voor je onvoorwaardelijke steun en support in de afgelopen jaren. Ik kon altijd op je rekenen—of het nu ging om hulp in het lab of mentale steun tijdens moeilijke momenten. Jij was degene die me keer op keer hielp om de motivatie te vinden en door te zetten. Nu beginnen we aan een nieuw avontuur, eerst op de fiets en daarna in Engeland. Ik kijk ernaar uit om samen nog veel meer mooie en fijne momenten te beleven. I love you.

About the Author

Julie Mily Jansje Verhoef was born in on 30th of April in 1996 in Eindhoven, the Netherlands. She lived in Curaçao with her parents from one to four years old, after which they moved back to Eindhoven. Here, she grew up and finished high school in 2014. In the same year, she moved to Nijmegen to start the bachelor Biomedical Sciences at the Radboud University. Her bachelor internship was in the lab of Dr. Rick Wansink, where she studied the molecular mechanism of myotonic dystrophy in muscle cells under the daily supervision of Walther van den Broek. This fueled her interest in molecular and cell biology and drove her to start the Molecular Mechanisms of Diseases (MMD) master at Radboud University. Her first master internship was in the lab of Dr. Taco Kooij at the Radboudumc, under the daily supervision of Laura de Vries. This internship sparked her interest in malaria research and drove her to do her second internship in the same topic in the lab of Prof. Alan Cowman at Walter and Eliza Hall Institute in Melbourne, under the daily supervision of Dr. Michal Pasternak. Together with Taco, she successfully applied for an individual PhD grant from the Radboudumc. In December 2019 she started this PhD trajectory under the supervision of Dr. Taco Kooij and Prof. Teun Bousema. Besides her research activities, she was also a member and co-founder of the Radboudumc Green Lab Initiative, and she was involved in the organization of the New Frontiers symposium on Translational Glycoscience. Julie will join the lab of Prof. Julian Rayner as a postdoctoral researcher at the University of Cambridge.

PhD portfolio of Julie Verhoef

Department: **Medical Microbiology**
PhD period: 01/**12/2019 – 31/03/2024**
PhD Supervisor(s): **Prof. J.T. Bousema**
PhD Co-supervisor(s): **Dr T.W.A. Kooij**

Training activities	Hours
Courses	
• Radboudumc - Introduction day (2020)	6.00
• RIMLS - Introduction course "In the lead of my PhD" (2020)	15.00
• MIC FIJI course (2021)	20.00
• Radboudumc - Scientific integrity (2021)	20.00
• Student supervision course (2022)	2.00
• Next step in your career (2023)	16.00
Seminars	
• Webinar VuePathDB (2020)	1.00
• Meet the expert Adobe Illustrator (2020)	2.00
• Webinar freezer challenge (2020)	1.00
• Labguru seminar (2021)	1.00
• Seminar from Markus Ganter, visiting scientist (2021)	3.00
• Meeting Green Labs Netherlands (2021)	3.00
• Organization Radboud Research Round on sustainable research (2021)	14.00
• Organization New Frontiers publieksavond (2021)	14.00
• Radboud Research Round (2022)	1.00
• Presenting at Radboud Impact Festival (2022) – oral presentation	4.00
• MIC user meeting (2022)	1.00
• Guest speaker Micheal Delves (2022)	2.00
• Lab visit with talk to my co-promotors lab in Philadelphia (2022) – oral presentation	8.00
• Guest speaker Mikha Gabriela (2022)	1.00
• Guest speaker Tobias Spielmann (2022)	1.00
• Talk from Novartis at TropIQ (2022)	1.00
• Present a workshop for the Green Lab Initiative (2022) – oral presentation	6.00
• Lecture series on entrepreneurship (2022)	6.00
• Talk from Cees Dekker (2022)	1.00
• Presenting at MIC user meeting (2022) – oral presentation	6.00
• Monthly electron microscopy seminars (2022)	12.00
• Guest speaker Victoria Ingham (2023)	1.00
• Guest speaker Wai Hong Tham (2023)	1.00

Training activities	Hours
Conferences	
• BioMalPar (2020)	14.00
• PhD retreat online (2020) – poster presentation	8.00
• Symposium on parasite and vector biology (2021)	8.00
• BioMalPar (2021)	21.00
• Being jury member on MMD internship symposium (2021)	6.00
• PhD retreat (2021) – poster presentation	8.00
• New Frontiers Symposium (2021) – poster presentation	14.00
• Presenting Pub quiz at New Frontiers Symposium (2021)	14.00
• Co-organization New Frontiers symposium (2021)	96.00
• RCI Science day (2022)	8.00
• KNP Spring meeting (2022) – oral presentation	14.00
• Molecular Parasitology Meeting in the Woods Hole, USA (2022) – oral presentation	14.00
• PhD retreat 2023 (2023) – oral presentation	16.00
• Virtual symposium Advances in Malaria (2023)	6.00
• Dutch Malaria day (2023) – oral presentation	8.00
• Molecular Approaches to Malaria in Lorne, Australia (2024) – Flash talk and poster presentation	40.00
Other	
• Co-organization Radboudumc freezer challenge (2020)	14.00
• Make Radboudumc Freezer Challenge after movie (2021)	14.00
• Journal club (monthly) (2019-2024)	100.00
• Chair of Radboudumc Green Lab Initiative (2021)	48.00
• Member of Green Lab Initiative with monthly meetings (2022)	28.00
Teaching activities	
Supervision of internships / other	
• Supervision Internship (6 months) – MSc student MMD (2021)	52.00
• Supervision Internship (10 weeks) – MSc student MMD (2021)	20.00
• Supervision Internship (6 months) – MSc student Human Biology (2022)	52.00
• Supervision Internship (6 months) – MSc student MMD (2023)	52.00
Total	**845.00**

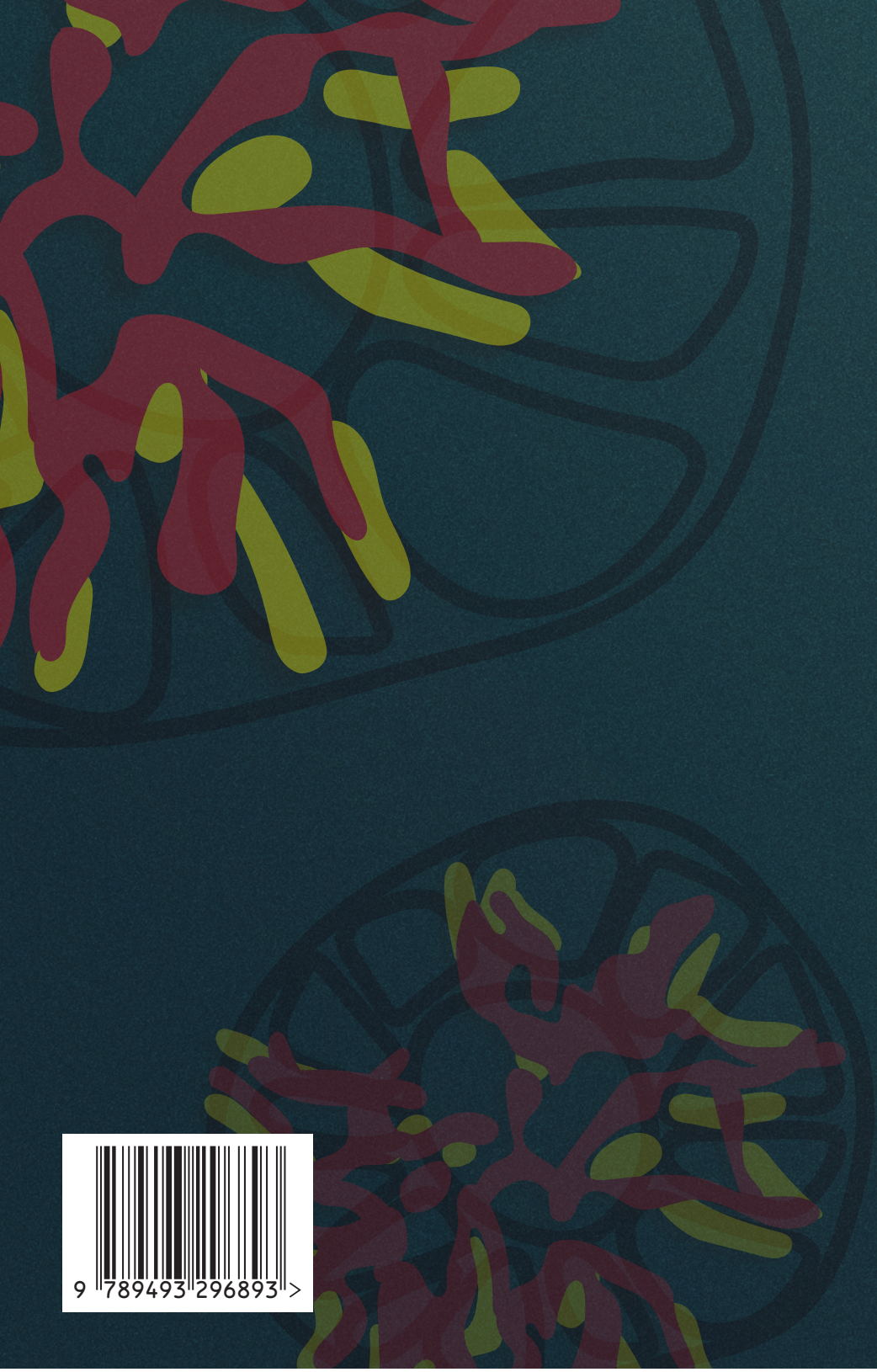

9 789493 296893 >

Radboudumc
university medical center

IN DEI NOMINE FELICITER

Radboud University